THE MOLECULAR ROLE OF NON-CANONICAL NOTCH SIGNALING VIA DELTEX-1 IN HIGH GRADE GLIOMA

Inauguraldissertation

zur

Erlangung der Würde eines Doktors der Philosophie

vorgelegt der

Philosophisch-Naturwissenschaftlichen Fakultät

der Universität Basel

von

Roland Martin Huber

aus Siegershausen TG

Basel, 2011

Genehmigt von der Philosophisch-Naturwissenschaftlichen Fakultät auf Antrag von:

Prof. Dr. Markus A. Rüegg
(Fakultätsverantwortlicher)

Prof. Dr. Adrian Merlo
(Dissertationsleiter)

Dr. Brian A. Hemmings, FRS
(Korreferent)

Basel, den 21.06.2011

Prof. Dr. Martin Spiess
Dekan

"It's not enough to say we are doing our best. We must succeed in doing what is necessary."

Winston Spencer Churchill

Acknowledgement

My first and outmost thanks go to my family for raising me to become a curious, independent and critical person interested in the beauty of nature and natural sciences. All I am today roots in my family.

I am deeply grateful to Prof. Adrian Merlo for his trust in me and my work, his well measured guidance and help, his willingness to share his views and thoughts on science but also philosophy, and for his critical and thorough supervision of my thesis.

Many people were involved in this piece of work in some way or the other and I would like to take the time to say thank you to all the members of the lab who were an invaluable help and also good friends; to Dr. Brian A. Hemmings for his generosity of giving me a place to work in difficult times as well as for his scientific support; to all the members of the CCRP glioma group for help, reagents and valuable comments and discussions; to all the members of my thesis committee for their help and valuable time; to Prof. Markus Rüegg for presenting this thesis to the faculty of science; to Oncosuisse, the SNF and the regional cancer league of Basel for financial support; to all my friends, fellow officers and colleagues who helped, supported, and shaped me to become who I am.

Anita, thank you for your love, your support, your patience and your help…

Table of Contents

Summary

Glioblastoma Multiforme is a WHO grade IV brain tumor with glial characteristics leading to more years of life lost than any other cancer. A better understanding of GBM biology and valid animal models are the two key elements to improved therapeutic results. We found Deltex1, which is part of an alternative Notch pathway, to activate both the PI3K/PKB and the MAPK/ERK pathway and to induce anti-apoptotic Mcl-1. DTX1 over-expression resulted in increased clonogenic and growth potential and also induced cell migration and invasion. Microarray gene expression analysis identified a DTX1-specific transcriptional program related to the changes in phenotype observed. Patients with low *DTX1* levels have a favorable prognosis. Therefore, we propose the alternative Notch pathway via DTX1 as an oncogenic factor in glioblastoma. This could partially explain previous findings linking Notch status to prognosis wherein high Notch2 levels correlated with reduced patient survival. We found activated Notch2 in neural stem cells to induce glioma-inducing-cell features including increased proliferation, reduced apoptosis and astrocytic lineage commitment. These observations were found both *in vitro* and *in vivo* using a conditional mouse model. Together, these findings indicate an important role for Notch signaling (both canonical and non-canocical) in high grade glioma, offering a potential treatment target. We have also established an *in vivo* model of GBM which allowed us to analyze the efficacy of novel treatment regimens. Short term treatment of orthotopic xenograft gliomas in nude mice with histone deacetylase inhibitors and 2-deoxy-D-glucose resulted in prolonged survival, reduced tumor growth and induction of cancer cell apoptosis. Therefore, epigenetic reprogramming in combination with energy deprivation was found to have anti-tumor activity *in vivo*. In an independent project we identified GSK3β as a downstream target of Bmi1. GSK3β maintains a more stem cell like characteristic in GBM cells, potentially also in the glioma inducing cells. Several inhibitors to GSK3β exist and LiCl, which is often used in the clinic, correlates with reduced glioma incidence. Altogether, we believe we have added considerable knowledge on the biology of gliomas thereby helping to characterize the underlying events of gliomagenesis. Furthermore, we have established proof of principle for a novel treatment strategy *in vivo*.

Introduction

The human body consists of roughly 50 trillion ($50*10^{12}$) cells. Each one contains the full genetic information, but only uses a small fraction thereof to exert its biological function. The number of biological processes taking place in these cells is indicative of the likelihood of mistakes. While many, if not most processes are quenched by control mechanisms or redundant systems, some of them manifest and may cause malignant aberrations. A biological organism will be exposed to harmful effects *ab initio*. Internal effects like DNA replication errors, chromosomal dislocations or miss-segregations can occur throughout development or later in life. On top of that, an organism is exposed to a wide array of chemical, physical and biological influences potentially harmful to the genetic information. These errors accumulate over time in a growth selective process [1] eventually leaving the cell with a significantly altered genome which can ultimately cause uncontrolled growth and neoplastic disorders. Cancer is projected to become – and in the European Union it already is – the leading cause of death worldwide (Figure 1). The average age of the world population and the overall life expectancy is steadily increasing, giving mutations ever more time to accumulate in individual cells. Therefore, this trend appears to become even more sustained over the coming decades.

Basically every human tissue can develop neoplastic disorders and usually there are several forms of tumors per tissue type, leaving a plethora of different diseases which all carry the inherent genetic variability of the individual. Currently we are still unable to determine individualized cancer profiles for patients due to technical and financial limits. However, with the rise of fast throughput and large scale analysis tools like microarrays or on-chip proteomics, there is hope to get closer to this approach. Fortunately there seem to be few, generally applicable concepts inherent to specific cancer subclasses offering a unifying understanding of the particular disease and indicating possible routes of treatment.

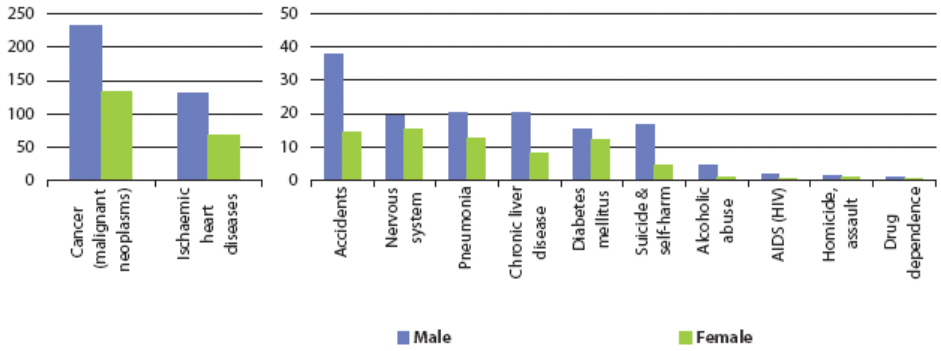

(1) Note the differences in the scales employed between the two parts of the figure; the figure is ranked on the average of male and female; EU-27 averages calculated on the basis of the latest year available for each Member State.

Source: Eurostat (tps00116, tps00119, tps00125, tps00134, tps00128, tps00131, tps00137, tps00122, tps00140, tps00143, tps00146 and tps00149)

Figure 1. Causes of death in the EU in 2006 (adapted from EUROSTAT survey 2006).

In the EU-27 malignant neoplastic disorders were the leading cause of death in 2006. Y-axis shows related deaths per 100'000 inhabitants.

Independent of the tumor type or location, several characteristic traits are found in all neoplastic disorders and are key features of cancer. Although the resulting feature may be the same, the underlying cause can be different. Several genotypes can lead to the same clinical phenotype. An overview of such traits and their underlying causes in general and in high grade gliomas (HGG) in particular are stated below.

A Brief History of Cancer Cell Biology

Seven features distinguish tumors and cancer cells from normal tissue [2]. They can be grouped into features which enable the cell to proliferate and grow even when not intended to, the ability to circumvent internal and external control mechanisms (e.g. immune evasion and neutralization of intrinsic apoptotic clearance), to ensure sufficient supply of nutrients and ultimately to disseminate. These traits can be related to malignant changes in seven distinct cellular mechanisms:

Cell Growth. A normal cell cannot grow in the absence of specific, growth promoting signals. These signals are usually external – either soluble factors or extracellular matrix components – and are detected and usually conveyed by membrane bound receptors. The signal is then transmitted via intracellular signaling cascades. A cancer cell can acquire self-sufficiency of growth signals at all three levels of such cascades. Mutations can lead to the aberrant expression of growth factors which then act in an autocrine fashion back on the cell itself providing the necessary growth-stimulus. The productions of PDGF in HGGs or TGFα in sarcomas are examples thereof [3]. Over-expression of receptors can render the cell independent of ligand through ligand-independent dimerization or make it hyper-responsive to ambient levels of growth factors. Alternatively, mutations can yield constitutively active versions of receptors making the down stream signal transmission independent of ligands or receptor amounts. For example, a truncated version of the EGFR lacking most of the cytoplasmic receptor fires constitutively due to the lack of regulatory domains. Complex down stream signaling networks conveying these receptor signals offer manifold options for alterations. Ectopic expression of proteins, hyper-activating mutations of kinases or loss-of-function in inhibitors and phosphatases are commonly found in cancer cells.

Insensitivity to Growth Inhibiting Signals. Soluble or localized ligands activate cell surface receptors and this signal is then conveyed by signaling cascades blocking cell growth and proliferation usually arresting cells in the G_1-phase of the cell cycle. The main gatekeeper or integrator of this signaling is the Rb protein which blocks proliferation if hypo-phosphorylated. It is therefore not surprising that mutations in the Rb protein are commonly found in various cancer types [3]. Mutations again occur at all levels of this circuitry: loss of

integrins and other cell surface receptors, mutations in the signaling mediators or in intermediate and final targets like Smad4 or Rb itself are related to insensitivity to anti-growth signals of cancer cells [4]. A tumor can only proliferate if the anti-growth circuitry is circumvented independent of the cell of origin.

Evasion of Apoptosis. The cell intrinsic program of cell death – apoptosis – is present in all tissues and cell types. Activation of apoptosis leads to the controlled disintegration of the cell within hours. The induction of apoptosis is one of the main causes of tumor attrition and therefore has to be overcome by cancer cells. The apoptotic machinery can be divided into two major components: sensors and effectors. Sensors probe the cell environment (e.g. extra-cellular matrix, plasma, cell-cell contacts, etc.) as well as the cell interior for the lack of survival signals or the presence of death signals. TNFα binding to TNFα-R1 is an example of a death signal inducing apoptosis [5]. The main effectors are the Bcl-2 protein family members which integrate the signals onto the mitochondria inducing the release of cytochrome C into the cell plasma. This activates a series of Caspases ultimately leading to the controlled disassembling of the cell. However, other members of the Bcl-2 family have anti-apoptotic functions balancing the system [2]. Approximately 50% of all human cancers and the majority of high grade glioma (HGG) have mutations in the tumor suppressor p53 which is part of the apoptotic signaling cascade [6]. The precise control of growth and apoptosis are a prerequisite to multi-cellular life. Therefore it is not surprising that redundant pathways and control mechanisms exist. It is noteworthy that the mutations most commonly found in tumors are affecting signaling nodes integrating several of these pathways leaving no or only limited control mechanisms intact.

Abnormal Replicative Potential. All of the above traits affect signaling pathways which integrate signals from the cell environment and the cell intrinsic state. However, cells contain an independent program limiting their overall replicative potential irrespective of the signaling input. Therefore, cultured primary cells have a finite replicative potential and hyper-activation of proliferation signals does not suffice to override this limit [7]. Loss-of-function of Rb and p53 can disable this block – leaving the cell in a state called senescence – leading to a state of genome instability, called crisis. About one out of 10 million cells will survive crisis and will have become immortalized [8]. Most cancer cell lines derive exactly

from such cells and a similar mechanism is likely to take place in the tumor itself. Normally, the gradual loss of telomeric DNA at the ends of the chromosomes will induce cellular senescence and crisis, limiting the number of cell divisions to about 60-70. 85-90% of all tumors have up-regulated telomerase enzyme activity preventing the gradual loss of telomeres and thereby circumventing this limiting effect [9].

Angiogenesis. A human tumor cell – like any other cell – needs O_2 and nutrients for survival and growth. Therefore, all cells have to reside within approx. 100µm of a capillary vessel providing these pivotal elements. Angiogenesis is tightly regulated during morphogenesis and organogenesis and regulatory effects are mainly mediated by cell surface proteins [10]. Initiation of vascularization is triggered by the soluble factors VEGF or FGF which are detected by cell surface receptors on endothelial cells. Tumors induce neo-vascularization through the ectopic expression of VEGF and FGFs and/or through the loss of inhibitory cell surface proteins like Thrombospondin-1. Angiogenesis is related to tumor progression and usually occurs in mid to late stage tumors. Angiogenesis offers an appealing therapeutic target. Bevacizumab (Roche), a humanized monoclonal antibody against VEGF, has become the first-in-line treatment for several cancers worldwide (eg. high grade and metastasizing lung, colon and breast cancer). Although highly effective in preventing further angiogenesis and therefore further tumor growth, anti-angiogenic therapies will not suffice to kill tumors. Pre-existing vasculature will always provide the outer layers of the tumor with sufficient nutrients leaving a pool of cancer cells under the selective pressure of blocked angiogenesis. Therefore, anti-angiogenic therapies are most appealing in combination with cytotoxic agents rather than as a mono-therapy.

Invasion and Metastasis. Metastases account for ~90% of all cancer related deaths. Gliomas represent a special case given that they do not form metastases. However, they are highly invasive. In order to leave the original location of the tumor, cells have to acquire several traits. First, cell adhesion has to be reduced. This usually occurs by changing the expression pattern of intergrins and CAMs to variants with lower binding capacity or even repulsive character. The change of the cell-cell or cell-ECM binding also leads to alterations in the signaling networks of the cells [2]. Next, the cells have to survive in a different micro-environment. Again the changes in the cell surface proteins enable this step. To leave the

original niche and invade into any other tissue, the cells have to be able to loosen the ECM with the help of proteases. Therefore, invasive and metastatic cells express high levels of proteases digesting the connective tissue by which they are engulfed or at the site of invasion. Finally, the cells need to actively migrate over certain distances driven by intracellular cytoskeleton rearrangements in coordination with the binding strength to the ECM (avoid “slipping or sticking”).

Evasion of Immunosurveilance. The human body is under constant surveillance of the immune system not only wading off pathogens, but also attacking and eliminating cells with destructive potential to the body. Cytotoxic T-cells and NK-cells specifically kill cells which display abnormal or non-self peptides and molecular fragments on their MHC-I proteins or MHC-like ligands, respectively. Therefore, cancer cells which display their mutated proteins on their cell surface have to evade this clearance mechanism. This can occur through the generation of an inflammatory micro-environment which changes the response of leucocytes to given cues or through insensitivity to apoptosis promoting signals (see above: Evasion of Apoptosis). The down regulation of MHC proteins or other markers is also frequently found.

The Case of *Gliblastoma Multiforme*

Glioblastoma multiforme (GBM) is the most common primary brain tumor in adults. It is of glial origin and is graded by the WHO as stage IV tumor (Figure 2). The prognosis is particularly poor with cancer related death in almost all cases. Treatment includes surgical resection, radio- and chemo-therapy. However, average survival has not improved substantially over the past decades and remains between 8-14 months after diagnosis [11]. Currently there is no cure available and even the most aggressive treatment regimens only expand the survival time by weeks [12]. GBM incidence ranges from 2.9 to 3.5 per 100'000 in Europe and North America [13]. No clear risk factors are known except for the exposure to high doses of ionizing radiation. Males are 1.7 times more often affected than women and the prevalence for GBM is higher in Caucasians than in African Americans. The average age at diagnosis is 64 years of age. GBM in children are rare. GBMs are usually spontaneous diseases; however, rare families with a history of Li-Fraumeni- or Turcot-Syndrom have an increased risk of developing GBM [14].

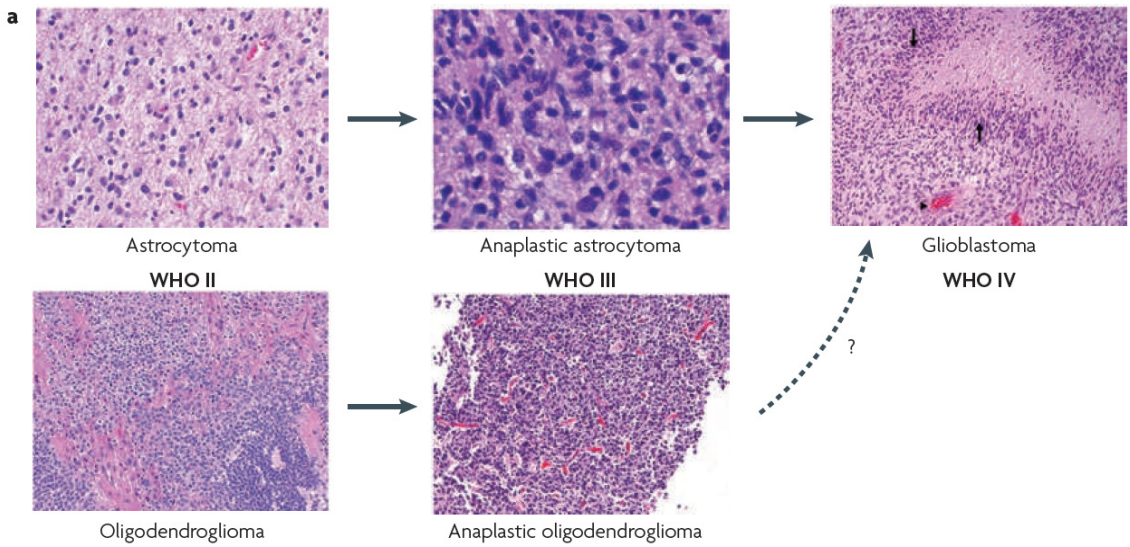

Figure 2. Current World Health Organization (WHO) classifications for diffuse glioma and medulloblastoma [15].

(a) Schematic showing the classification of diffuse gliomas of astrocytic and oligodendroglial lineages. Representative micrographs of histological HE stainings for each tumor class are given. The hallmark histological features of glioblastoma, microvascular proliferation (black arrowhead) and pseudopalisading necrosis (black arrows) are also indicated.

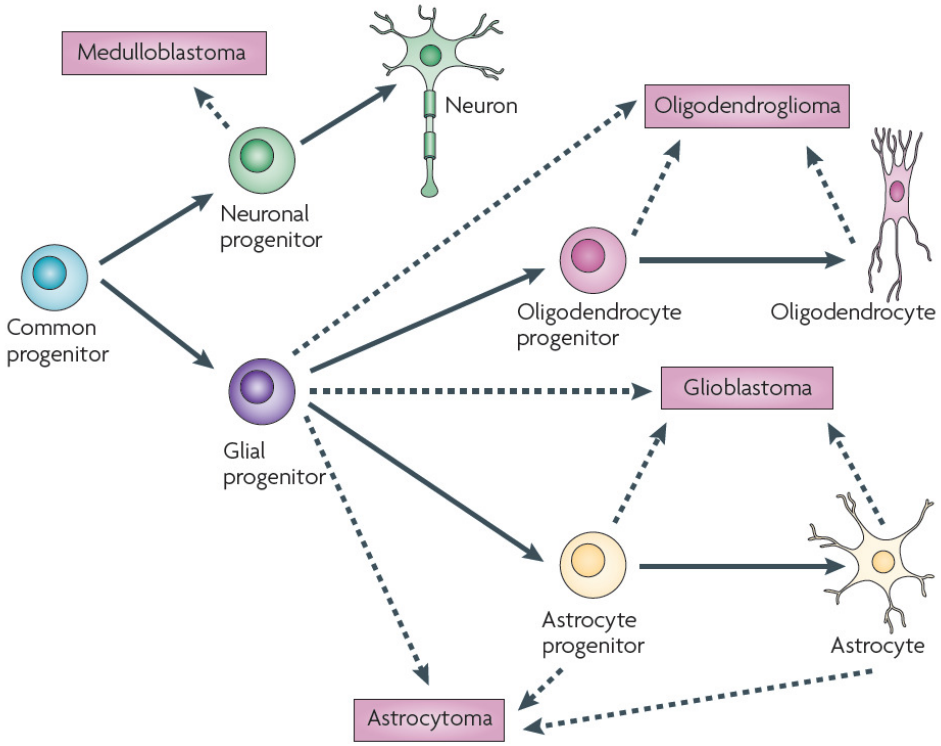

Figure 3. The neuro-glial cell lineage tree [15].

Self-renewing, common progenitors are thought to produce committed neuronal and glial progenitors that eventually differentiate into mature neurons, astrocytes and oligodendrocytes. Although the precise cells of origin for diffuse glioma variants and medulloblastoma remain largely unknown, a selection of likely candidates for each (dashed arrows) is indicated.

Glioblastoma usually arise *de novo* with no history of previous brain neoplasias. Only ~5% of all GBM are secondary lesions progressing from lower grade astrocytomas [13]. Primary and secondary GBM show distinct patterns of mutations, but the prognosis is not significantly different. If the tumors arise from dedifferentiated glial cells or from stem- or precursor-cells with accumulated mutations is still under debate. However, recent findings point toward precursor cells as cells-of-origin for astro-glial tumors (Figure 3) [16-19]. GBMs mostly originate in the white matter of the brain, but then massively infiltrate adjacent areas. Most GBMs are located in the frontal and temporal lobe. GBMs are rarely found in the cerebellum, brain stem or spinal cord, but can expand through the *corpus callosum* to the contralateral hemisphere. They are highly invasive with no clear demarcation between tumor tissue and healthy brain. The clinical presentations of GBM are manifold and depend mostly on the tumor location. General symptoms can develop rapidly through the high

proliferative rate and can include head ache, epileptic seizures, localized neurological deficits based on the tumor location and changes of the patient's personality. Signs of increased intra cranial pressure like nausea or even coma develop later and indicate a poor prognosis. Histologically, GBMs can be distinguished from anaplastic astrocytomas (AA) through the presence of necrotic areas, micro-vasculature and pseudo-palisading cells around necrotic areas (Figure 2) [14]. The cells are mostly GFAP positive and often more than 20% are positive for the proliferation marker Ki-67. Tumors with mutated p53 show aberrant aggregation of p53 protein in the nucleus [20].

GBM pose several exceptional problems during treatment: i) It is located in the central nervous system. This makes both detection and accessibility particularly difficult. ii) GBMs grow rapidly leaving only a small time window for treatment. Even considerable tumor resection will be overridden by the rapid proliferation within months. iii) Well-proven principles of tumor treatment, e.g. respecting a safe resection margin of 2 cm, can not be applied due to the location in the CNS. For example, tumor resection is limited to the neoplastic tissue and does not include adjacent areas in order to minimize brain damage. This leads to incomplete resection or even tumor cell dissemination.

Molecular Genetics of GBM. GBM – a heterogenic group of primary brain neoplasias – can be grouped according to their genetic changes and clinical history. Secondary GBM, meaning GBMs which arise through continuous progression from lower grade gliomas, show distinct mutational patterns from primary GBM. Grade II astrocytomas often have mutated p53 and PDGFR over-expression. Through additional mutations like CDK4/6 amplification, RB mutation or loss of chromosome 19q or 1p, these tumors become more aggressive and develop into grade III anaplastic-astrocytomas. Additional loss of chromosome 10q, or in rare cases (~10%) PTEN mutations, lead to the progression to grade IV GBMs. This process takes 5-10 years and is typically found in younger patients (<45 years of age). The prognosis is around 9-14 months. Secondary GBM account for ~5-10% of all GBM cases [21].

Primary GBM are the rule (~90%) and these tumors normally have different genetic alterations. Mutations are often found in $INK4a^{ARF}$, EGFR and PTEN (~40%) and over-expression of EGFR, Cyclin D and MDM2. Loss of heterozygosity (LOH) is commonly found in

10p and 10q and even total loss of chromosome 10 occurs. Average survival is 9-12 months [21]. Since these alterations only describe the most common mutations in primary or secondary GBM and do not offer a functional classification, a more recent analysis of 206 GBM offers a signaling pathway based classification [3]. These classes are functionally related and offer a rational for targeted therapies although they are significantly overlapping (Figure 4).

The RTK/RAS/PI3K pathway is affected in 88% of GBM (Figure 4). Gain-of-function alterations are mostly found in EGFR, PDGFRa, PI3K and ErbB2. Loss-of-function changes in this pathway are found in PTEN and NF1. The hyper-activation of this pathway induces cell proliferation, survival and translation. It is also linked to cell migration and invasion. 87% of GBM have frequent genetic alterations in the p53 pathway. Gain of function of MDM2 or loss of function of $INK4a^{ARF}$ and p53 make glioma cells more apoptosis resistant and prevent cellular senescence. Cell cycle control is affected in 78% by alterations of the RB pathway thereby releasing the G_1/S-phase block of normal cells regulated by this system. Gain of function mutations are found in the CDK4 gene but are relatively rare. However, loss of function mutations which affect the CDKN2 locus are about 50% [22]. RB itself is mutated in ~10% of GBM [3].

The RTK/RAS/PI3K group can be further subdivided into three distinct subclasses by the activity among signal transduction pathways and associated genomic alterations [23]. These three classes associate with EGFR over-expression, PDGFB over-expression, and loss of NF1 (Figure 5).

These three distinct patterns were revealed by proteomic analysis of protein expression and activation in glioma-relevant signaling pathways. The EGFR signaling class has significant Notch signaling activation measured by elevated expression of Notch ligands, cleaved Notch receptors and down-stream target Hes1 [23]. The PDGFRA class shares features with the ‘proneural’ group of gliomas previously identified using transcriptional analysis [24], and is characterized by genes expressed during normal cortical oligodendrocyte development such as Olig2, Sox2 and doublecortin and signaling pathways involved in that process as well, such as PDGF and SHH. Initial data show no relevant clinical

or histological differences between these three groups. However, other studies did identify Notch signaling and its genetic status as a prognostic marker in gliomas [25]. Although the alternative classification into 'proneural', 'proliferative', or 'mesenchymal' gliomas does have predictive value it does not offer refined strategies for treatment. The prognostically most favorable sub-class 'proneural' includes also lower grade gliomas and stereotypic alterations of GBM like PTEN loss, however EGFR activation or amplification are not found in this group. Therefore, a classification system based on pathway activity rather than transcription level seems to be more informative.

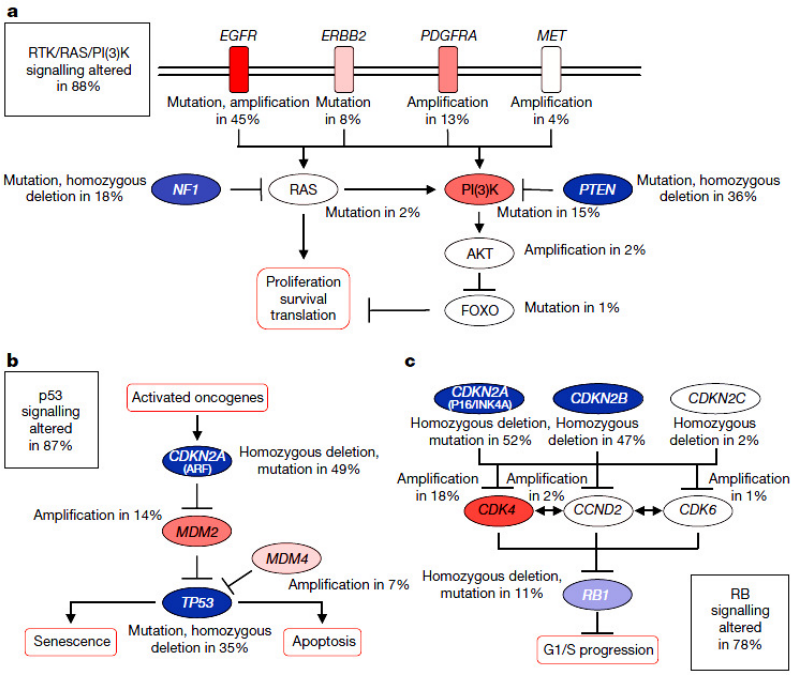

Figure 4. Frequent genetic alterations in three critical signaling pathways [3].

Primary sequence alterations and significant copy number changes for components of the RTK/RAS/PI(3)K (a), p53 (b) and RB (c) signalling pathways are shown. Red indicates activating genetic alterations, with frequently altered genes showing deeper shades of red. Conversely, blue indicates inactivating alterations, with darker shades corresponding to a higher percentage of alteration. For each altered component of a particular pathway, the nature of the alteration and the percentage of tumours affected are indicated. Boxes contain the final percentages of glioblastomas with alterations in at least one known component gene of the designated pathway.

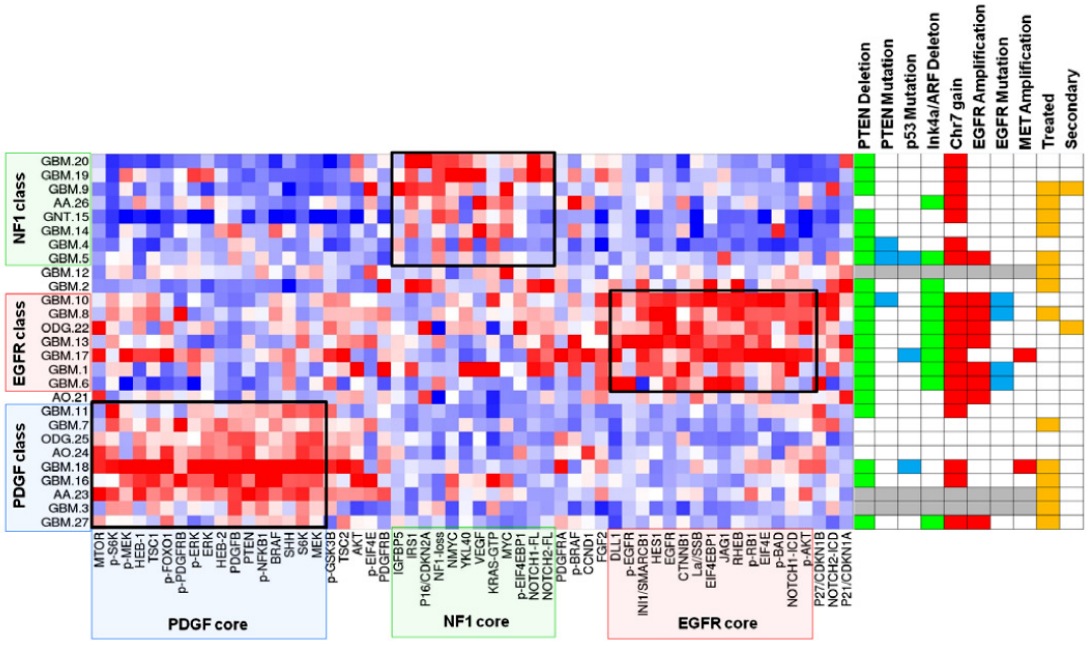

Figure 5. Clustering of gliomas by signature-defining proteins [23].

Unsupervised k-means clustering of 27 gliomas by 44 core proteins. 3-way clustering was determined to be the best fit by consensus matrix stability and cophenetic correlation. Right: summary of array-CGH, sequencing and clinical information is given for each tumor. Red denotes copy number gain or focal amplification as specified; green marks deletion of at least one copy. Blue denotes mutations. Gray marks samples for which DNA was unavailable.

Notch receptors in GBM. Notch receptors are evolutionary conserved trans-membrane receptors conveying cell to cell signals (Figure 6). They play a key role in developmental processes regulating proliferation, cell fate decisions and survival in various tissues and species, including neural stem cells [23, 24]. In mammals, a total of four Notch receptors are known (Notch1-4) having partially redundant functions. Five ligands (Dll1, 3, 4 and Jagged1, 2) bind to the receptors inducing proteolytic cleavage of the intracellular domain by gamma-secretase to the active form Notch-ICD (Notch-intracellular domain). Notch-ICD translocates to the nucleus and forms a protein complex with RPBJk, MAML1 and other co-factors. This complex leads to the activation of Notch activator genes like *Hairy and Enhancer of Split* homologs (eg. Hes1 and Hes5). Hes genes counteract bHLH genes and thereby act as transcriptional repressors. For example, Hes genes counteract the transcription factor Mash-1 and thereby block neuronal differentiation in neural precursor cells [26]. Deregulation of Notch signaling is implicated in various neoplastic disorders [16, 27, 28]. It can either act as

an oncogene, like in T-ALL (T-cell acute lymphoblastic leukemia) where translocation of Notch1 and its aberrant activation leads to the uncontrolled expansion of immature T-cells and subsequently to leukemia, or as a tumor suppressor as in the mammalian skin where Notch loss-of-function leads to the development of basal-call-carcinoma-like tumors [29]. Interestingly, different Notch receptor variants can have opposing effects on cancer development. For example, in the childhood brain tumor medulloblastoma, Notch2 clearly promoted tumorigenesis whereas Notch1 had an inhibitory effect on tumor growth [30].

There is accumulating evidence for Notch-signaling through RBPJκ but independent of Hes or Hey factors. Potential targets which all contain RBPJκ binding sites in their promoter regions are CyclinD1, p21 and GFAP [31-33]. The RBPJκ independent Notch signaling through Deltex will be further described below (Introduction and Chapter 1). The down stream signaling of Notch receptors is highly cell context dependent. During brain development Notch has been described in glial specification as well as progenitor-cell self renewal. Hereby, active Notch signaling drives astrocytic differentiation and inhibits neuronal and oligodendroglial development. Furthermore, Notch signaling is known to be involved in cellular responses to hypoxia and angiogenesis, two processes which are characteristic for human gliomas and HGG in particular [34].

Primary GBM display elevated levels of Hes1 expression indicating active Notch signaling whereas low grade astrocytoma and secondary GBM show high levels of Hash-1, a sign of inactive Notch signalling [35, 36]. Both Hash-1 and Dll-1 expression (which is controlled by Hash-1) also correlated with lower grade gliomas and secondary GBM in an independent study [24]. Given the role of Notch signaling in maintaining an undifferentiated and proliferative state in NSC this is indicative of an oncogenic role of Notch in gliomas and primary GBM in particular [37]. Loss of Notch2 in oligodendrogliomas and GBMs was associated with favorable patient prognosis in a cohort of 26 OG and 118 GBM patients [25]. siRNA against Notch1 induced cell death, decreased proliferation and blocked cell cycle progression in transfected glioma cell lines. Mice orthotopically injected with siRNA-Notch1 cells survived significantly longer than animals injected with control cells. Both these results indicate an oncogenic role for Notch in gliomas by maintaining an undifferentiated and proliferative state in cancer cells. A proteomic study emphasized such a function in Ras-

mediated GBM [38]. However, other surveys could not link the functional role of Notch in gliomas to other genetic alterations. The Notch downstream genes Hey-1 and Deltex1 nevertheless correlate with worse patient prognosis [39].

Notch signaling interacts with other signaling pathways known to be altered in GBM. For example, the RTK/RAS/PI3K pathway via EGFR cross talks with Notch signaling [37]. Different studies indicate a tight coupling of both pathways and down-stream targets in normal development and cancer; particularly well studied is this link in tumor angiogenesis [40-44]. Ras transformed astrocytes express more Notch and were more sensitive to GSI treatment. Over-expression of K-Ras together with Notch-ICD leads to periventricular brain lesions with active proliferation and elevated Nestin expression [38]. Notch was activated by Ras and PKB in a mouse glioma model. In addition, the stem cell marker Nestin was under direct transcriptional control of Notch [45, 46]. Together these findings indicate a direct link of EGFR/Ras, Notch, and Nestin. Furthermore, Notch can also induce the expression of EGFR in glial cells potentially pointing to a vicious circle of cross stimulation.

The mechanism by which quiescent cells, including adult stem cells, preserve their ability to resume proliferation after weeks or even years of cell cycle arrest are not known. This reversibility is not a passive property of non-dividing cells since forced cell cycle arrest of only 4 days induces premature and irreversible cell senescence. The Notch down-stream target Hes-1 is required for cellular quiescence to be reversible by preventing cell senescence or terminal differentiation. Therefore, active Notch signaling in GBM via Hes-1 was suggested to safeguard against irreversible cell cycle exit both during normal cellular quiescence and pathologically in the setting of tumorigenesis [47].

Non-canonical Notch signaling through Deltex1. Deltex is a Notch interacting protein which contains a basic region at the N-terminus which binds to the Ankyrin repeats of the intracellular domain of Notch in Drosophila. Deltex has been proposed to regulate Notch activity by antagonizing the interaction between Notch and Suppressor of Hairless [48]. In mammalian cells, *DTX1* has been shown to be a transcription target of Notch itself suggesting a positive feedback loop between Notch and DTX1. However, Deltex protein family members contain a RING finger domain at their C-terminus with E3 ubiquitin ligase

activity. Deltex forms part of a three protein complex (containing Notch, Deltex and non-visual beta-arrestin) mediating the degradation of intracellular Notch through a ubiquitination-dependent pathway [49]. Loss-of-function mutations provided *in vivo* evidence for the functional relation of Deltex, Notch and non-visual beta-arrestin in Drosophila wing development. Therefore, Deltex appears to act as a signal repressor or as negative feedback regulator of Notch signaling in mammalian cells.

Deltex also exerts its function on Notch independent targets. DTX1 exerts E3 ubiquitin ligase activity on other protein substrates, such as the mitogen-activated protein kinase signaling component MAP kinase kinase kinase (MEKK1). Targeted MEKK1 degradation by Deltex suppresses the activation of T-cells [50]. In mouse, three novel ligands to the Notch receptor family have been identified which signal specifically through the DTX1 pathway [51-53] independently of RBPJκ and MAML1. However, the genes involved in this pathway are still ill defined [54, 55]. In summary, Deltex constitutes a distinct, cell context-dependent Notch signaling pathway working in parallel or independently of canonical Notch signaling via RBPJκ.

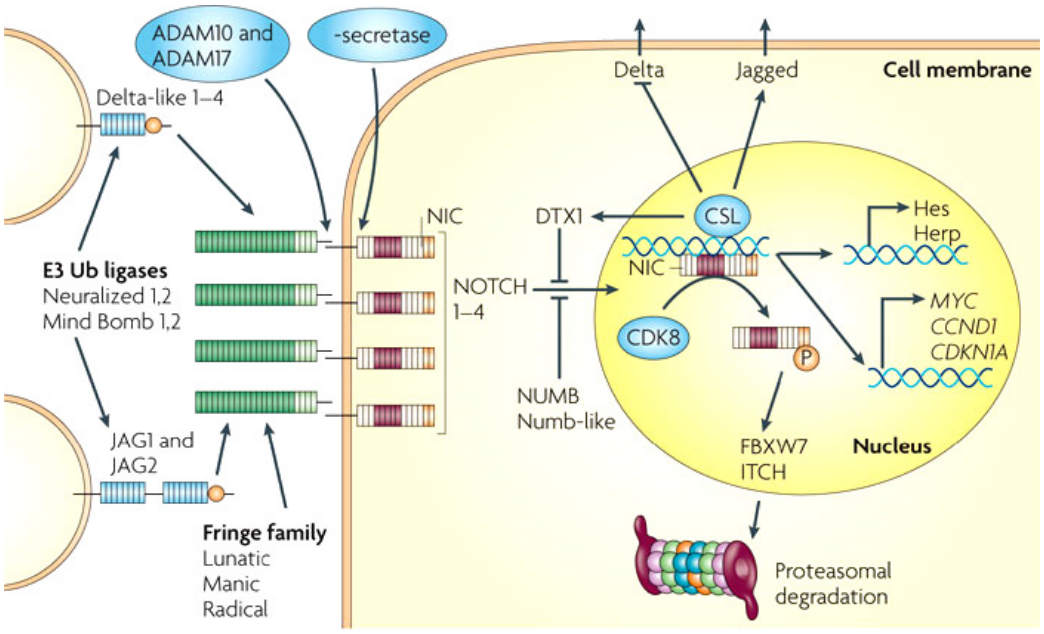

Figure 6. Notch signaling in mammalian cell [56].

Two families of transmembrane ligands and four Notch receptors exist in mammals. After ligand binding, Notch receptors are cleaved first by an ADAM metalloproteinase and then by the presenilin-γ-secretase complex. The resulting Notch intracellular domain (NICD) translocates to the nucleus, where it associates with the DNA

binding protein RBPJk (also known as CSL), converting it from a repressor to an activator of transcription. This induces the transcription of Hes family genes, which encode basic helix–loop–helix transcriptional repressors, and genes of the Herp family. Cell cycle regulatory genes, such as MYC, CCND1 (which encodes cyclin D1) and CDKN1A (which encodes p21) are induced in a cell type-specific manner. The Notch transcription-activating complex is terminated by phosphorylation of NICD by cyclin-dependent kinase 8 (CDK8), with subsequent recognition by ubiquitin ligases and proteasomal degradation. Negative regulatory mechanisms are also provided by the E3 ubiquitin ligases Deltex 1 (DTX1), ITCH, and NUMB.

Animal Models of High Grade Gliomas (HGG)

In vitro cancer studies are limited in their informative value due to the fact that they consist of isolated cancer cells without tissue context or micro-environment. Metabolic processes, the blood-brain-barrier, or the interaction of tumor cells with the tumor stroma are missing. Animal models are powerful tools to investigate tumors in complex biological settings and enable the analysis of processes which do not take place in a culture dish (eg. angiogenesis, tissue invasion, metastasis, cancer-stroma interaction, etc.). Archetypical mutations in gliomas are known and through the help of animal models it is possible to identify the functional role of any such mutation and to probe for potential counter-measures. Animal glioma models will hopefully provide methods for identifying promising therapeutic strategies and insight into basic biological processes of gliomas *in vivo*. Furthermore, the question of the cell of origin of high grade glioma (HGG) has not been resolved yet. The genetic profiles of gliomas are quite well established [3]. Mimicking the glioma specific mutations in different cell types could clarify the cell of origin question and thereby would identify the most reliable model for gliomagenesis. Several strategies are used to obtain such *in vivo* models and are summarized below (Table 1) [57].

Table 1. Summary of strategies used to model gliomas *in vivo* (adapted from [57])

Strategy	**Principles**	**Primary genetic modifications**	**Cell-of-origin**	**Secondary mutations**
Mutagens	DNA alkylation	unknown	unknown	likely
Transplantation	xeno- or allografts into immunocompromised animals	unknown / known	unknown	less likely
GM (germline)	transgene or gene targeting	known	depending unknown or known	more likely
GM (somatic)	replication competent virus	known	unknown	more likely
GM (somatic)	replication deficient virus	known	known	less likely

Table 1. Listed above are the mechanisms that have been used to generate experimental gliomas in animals. All entail modulation of gene expression by one method or another.

All of these four (Table 1) methods have their specific advantages and disadvantages, and are utilized depending on the specific question at hand. Below, the different principles and methods are discussed according to their individual strengths and weaknesses.

Gliomas can be induced by DNA damaging agents (eg. nitrosurea derivates) which induce mutations in the host DNA. Although the lesions induced by such procedures bear similarities with gliomas, they are poor experimental instruments [58]. First of all, the mutations in the lesion are unknown as is the cell of origin. Secondly, the mutagens often induce additional neoplasms which compromise the analysis of the brain lesion. Thirdly, tumors have to be genetically characterized at the end of the experiment, making this model extremely time- and labor-intensive. Therefore, the value of such a model remains rather limited.

Orthotopic and ectopic xeno- and allografts of glioma cells in *nude* or SCID mice are the most commonly used *in vivo* models of HGG. Compared to the above model using mutagens, this method offers several important advantages. The cells used for the implantation are often genetically characterized (mutations, LOH, over-expression of proteins etc.) and can be modified prior to the implantation. Standardized conditions make it possible to compare results. The use of different cell lines also gives insights into the effects of individual mutations compared to the genetic background of the cells. However, this model is also handicapped by several disadvantages: the recipient animal normally has no adaptive immune system. Adaptive immune reactions taking place in the tumor stroma are therefore absent and may compromise the entire study. Cells routinely used in these models are usually cultured for hundreds of passages selecting clones most competent of growing under culture conditions rather than reflecting the multi-clonal character of original tumors. Additionally, most of these grafts are dissimilar to human gliomas in respect of their histology as well as in their infiltrative behavior.

Several large scale studies have characterized the mutation patterns in GBM [3, 24]. Although the cell of origin is not clearly identified yet, these patterns can be used to generate glioma models with defined genetic backgrounds. These genetic modifications (GM) can either be applied locally by means of virus injections or using a germline strategy. The later offers several options: oncogenes – in the case of HGG this could be EGFR, PDGFRA or constitutively active PI3K – can be over-expressed in general or even in a tissue specific manner. The same applies for loss of function of tumor suppressors which can be deleted by

gene targeting strategies or blocked in their function through the expression of dominant-negative proteins. A combination of gain and loss of function give the possibility to generate almost any desired genotype in a specific tissue or cell type. However, it is often not sufficient to introduce such alterations to induce glioma growth but additional, spontaneous mutations are needed in the altered but still functional cells [57]. The last strategy for modeling gliomas is somatic cell genetic modification using retroviral vectors using either replication competent or incompetent viruses. When replication competent viruses are used a large number of cells are infected. This increases the probability to induce a glioma, however, it makes it also very difficult to control and analyze. More sophisticated systems use viruses which can only infect cells expressing a specific receptor (eg. avian leukosis virus which needs the tv-a receptor). The receptor can be expressed through tissue or cell type specific promoters defining the cell type which will be infected [57].

In summary, the orthotopic implantation of glioma xenografts into immuno-deficient rodents is the only method available which gives reproducible results to date. Unfortunately, these models have proven to be poor predictors of therapeutic efficacy in humans [59]. Therefore, a model with better predictive power is urgently needed.

Different allo- and xenograft models. Several graft models of HGG use allogenic material where gliomas have been induced through administration of mutagens to induce glial neoplasms. These are then cultured, analyzed and evaluated for experimental use. Due to the bigger body size, most of these models have been established in rats. These models include the C6, F98, 9L/LacZ and RG2 rat glioma cell lines which can be implanted into recipient animal brains. Although these cell lines are used for allo-transplantation, the animals usually receive a choline-deficient diet to reduce their immune-response [60]. The mouse glioma cell line GL261 and the human U87MG cell line can either be injected into immuno-compromised mice (eg. nude or SCID) or into inbred mice (eg. C57BL/6) fed with a choline-deficient diet. Additionally, low passage cultures can be xeno-transplanted from patient biopsies into immuno-compromised animals which give highly related pheno-copies of the initial lesion.

The question of the appropriate cell line for a glioma model relies on two main factors: which genetic background and which mutations should be present? If potential treatments are to be tested, most researchers favor human cell lines. Established cell lines are mostly genetically defined and specific mutations can be taken into account. Low passage *ex vivo* implants give pheno-copies of the original lesions and show a pronounced phenotype of infiltration, a trait often reduced in cell lines. However, these cell lines can neither be genetically modified (over-expression of a certain gene, for example) nor are the results comparable to other studies. Established cell lines on the other hand enable genetic modifications prior to implantation but often lack some of the glioma specific characteristics in the recipient animal (infiltration, ev. neo-vascularization).

Work on the orthotopic brain tumor model established at the FMI and the evaluation of different anit-cancer drugs will be presented in chapter 2 of this thesis.

The Cell of Origin – A Stem Cell gone Awry?

Totipotent embryonic or multipotent adult (or somatic) stem cells have several defining key features: i) they have a limitless replicative potential and telomerase activity, ii) they can self-renew and give rise to more committed progenitor cells in what is known as a stem cell division, and iii) they can give rise to all (embryonic) or several (adult) different cell types. Somatic stem cells are committed to a defined set of tissues their progenitor cells can differentiate into. In the brain the Neuronal Stem Cells (NCS) produce both neuronal progenitors which give rise to neurons as well as glial precursors which give rise to oligodendrocytes and astrocytes (Figure 3). These NSC are mostly localized in the sub-ventricular zone (SVZ) or the Dentate Gyrus (DG) of the hippocampus. The NSC, like all somatic stem cells, are tightly regulated and controlled by their cellular niche. More recently, the principle of stem cells has been applied to cancer biology in what is referred to as "the cancer stem cell hypothesis". The central tenet of this hypothesis is that solid and liquid tumors alike are composed of i) a relatively small subset of slowly cycling cells that undergo self renewal for an indefinite period of time and ii) a larger population of cells that have committed to a particular fate and have finite division capacity [16]. It is often speculated that unsuccessful therapies are related to a lack of effectiveness towards these Cancer Stem Cells (CSC) [61].

Table 2: Milestones in the History of the Glioma Stem Cell Hypothesis (adapted from [16])**.**

mid 19th century	Lobstein, Cohnheim, and others comment on similarities between embryogenesis and the biology of cancer cells.
1926	Bailey and Cushing develop the brain tumor classification system from which modern taxonomies derive. The system emphasizes the histological resemblance of brain tumor cells to cells of the developing CNS.
mid 1960s	Metcalf, Sachs, and others develop *in vitro* clonogenic assays to display the cellular progenitors of blood.
1966	Altman and Das describe postnatal neurogenesis in rats.
1988	Weissman et al. isolate the multipotent hematopoetic stem cell.
1992	Reynolds and Weiss identify postnatal neural progenitors (in neurosphere cultures).
1994	Dick et al. isolate malignant stem cells from human acute myeloid leukemia.
2000	Prospective isolation of human CNS stem cells.
2002 – 2004	Cancer stem cells isolated from adult and pediatric astrocytomas.

Although the similarities in embryogenesis and the biology of cancer have been described as early as the mid 19th century, it was in the late 1980s when the discovery of adult stem cells offered a functional link between the two (Table 2). The concept of stem-like cells in neoplastic diseases was first proposed in 1994 for leukemia [62]. After the discovery of adult NSC this model was then tested in gliomas identifying sub-populations of glioma cells with stem-like characteristics and elevated tumorigenic potential [63-66]. These findings suggest that a small fraction of the glioma cells are the driving force behind HGG. They are believed to – just as their adult stem cell counterparts – have the ability to proliferate infinitely, cycle slowly and additionally to be the mediators of both chemo- and radio-resistance. However, they significantly differ from normal SC in the way that they can only give rise to genetically abnormal progeny. An operational definition of glioma stem cell is a tumor cell sub-population that can self-renew in culture, perpetuate a tumor in orthotopic transplantation *in vivo*, and generate diversified neuron-like and glia-like postmitotic progeny *in vivo* or *in vitro* [16].

However, important questions concerning this hypothesis remain elusive. Different studies use different methods to identify glioma stem-like cells rendering unclear if the same cell population was analyzed [66, 67]. Furthermore, most studies use the cell surface marker CD-133 to identify GSC form fresh surgical isolates. However, it has been demonstrated that CD-133 negative cell populations can have a more stem-like phenotype than their CD133+ counterparts challenging the idea of using a single cell surface marker to indentify glioma stem-like cells [68]. Also, endothelial cells and endothelial precursor cells express CD133. These cells are radio-resistant and could explain some of the features attributed to glioma stem-like cells if the samples were contaminated with such cells particularly in studies using fresh tumor biopsies. Thirdly, experiments with tumor xenograft models may lead to underestimation of the percentage of glioma stem-like cells due to interspecies barriers, questioning the idea of only few, tumor perpetuating cells [69].

Experimental analysis of GSC could be further distorted when using neurosphere cultures. Free floating neurospheres are highly mobile and readily fuse with other spheres as shown by time lapse microscopy. This mechanism could account for some of the heterogeneity of cells derived from single spheres under differentiating conditions rather

than the pluripotency of the neurosphere cells [70]. A similar kind of contamination with differentiated cells has, at least to some extent, to be expected in surgical isolates. Adjacent cells or tumor infiltrating cells could be co-cultured or even co-injected in xeno-transplantation experiments which could account for the heterogeneity found in the resulting tumor. Together, these caveats show that there are important technical questions to be resolved before the CSC hypothesis can be further transferred to gliomas. It appears rather peculiar to apply the concept of stem cells – probably the most strictly regulated and most heavily shielded cell type of all – to cancer biology, unless the actual source of gliomas was a malignant adult stem cell. However, the cell of origin of gliomas remains unknown. Several possible cells of origins are currently debated in the literature and shall be briefly resumed below.

Mature Glia Cells. Prior to the discovery of adult neural stem cells, mature astrocytes and astrocyte precursors were believed to be the only proliferation competent cells in the adult brain and therefore the most likely, if not the only possible source of gliomas. The fact that these cells would have to de-differentiate in order to produce the GBM specific histology presented a major question to this model. More recently it was shown that only a few transcription factors ectopically expressed in differentiated cells can lead to de-differentiation into cells with ESC characteristics [71-73]. Targeting early cortical astrocytes *in vitro* and *in vivo* with oncogenes or activated signal generating proteins (eg. EGFRvIII or PDGFRA) can produce tumors in animal models with reliable glioma histology [74, 75]. However, the astrocyte marker used in these targeting experiments was GFAP, a protein expressed in various other types of progenitor cells as well. Therefore, the results obtained leave open the possibility that cells other than mature astrocytes had been targeted. Furthermore, this glioma inducing capacity has not been shown for mature astrocytes derived from adult brains suggesting that the intrinsic proliferation potential of the cells is a key determinant, at least in this experimental setup. In order to reach more reliable data on the de-differentiation hypothesis genetic methods which exclusively target adult astrocytes need to be developed.

Neural Progenitor Cells. These cells are actively proliferating or at least have the intrinsic potential to do so. Therefore, less mutational ‘hits’ are needed to generate a glioma cell of

origin. NPC are usually cell lineage restricted and proliferate only at low rates. Activation of Sox2 in oligodendroglial precursors is sufficient to induce stem-like characteristics [76]. Similar mechanisms could also be involved in gliomagenesis. The NG2 progenitor cell population is the most actively cycling cell type in the adult brain. They have been reported to have multipotent qualities [77]. Furthermore, they can undergo epigenetic reprogramming in culture to produce neurons and astrocytes rather than oligodendrocytes [78]. Therefore, several modes of transformation are possible which require only few mutational alterations to give rise to a glioma initiating cell. Again, the lack of precise experimental tools allowing targeting precisely defined progenitor cell populations at a defined time point restricts the experimental design to cells manipulated *in vitro*.

Multipotent Neural Progenitors. Adult stem cells and multipotent progenitors hold all traits required to become a glioma initiating cell in case of malignant transformation. Although there are important differences among the different classes of these cells (for review see [79]), they are all capable to proliferate and to give rise to glioma-histology-like tumors. In fact, several lines of evidence currently hint to these cells as the most likely cell of origin of gliomas without ruling out retrograde de-differentiation as an occasional way of CNS tumor development [19].

Both NSCs as well as GSCs are driven by the same signaling pathways. For example, the Notch signaling regulates the proliferation and differentiation of precursor cells during development. Several studies have shown now that Notch is constitutively active in high grade gliomas and that blocking it might have a positive effect on patient prognosis. Furthermore, other mitogens, such as PDGF, EGF, FGF etc., promote the growth of NPC and are often found to be active in glioma cells. Loss of PTEN, amplification of EGFR or mutations rendering this receptor constitutively active, and LoF of NF1 are frequently found in gliomas. However, these pathways are widely used even in the adult brain. Cell cycle regulating proteins like p16/p19, p53, or Rb are mutated in the majority of gliomas. Again, this does not indicate adult stem cells as source of gliomas since these proteins are also present in adult astrocytes. However, the transcription factor Olig2, which is not expressed in astrocytes, is often found in all types of glial tumors [27].

At first clinical presentation gliomas are found in almost all brain regions, but most typically in the subcortical white matter, along blood vessels and in subpial collections [16]. Both glioma cells and NPC are highly motile and both white matter as well as blood vessels are established lines of migration for these cells. Clinical observations of GBM patients treated with brachy-therapy show a necrotic trail from the tumor towards the SVC along suspected migratory routes (A. Merlo, personal communication). It is appealing to suggest that this area indicates the general migratory behavior of glioma cells indicating cells in the SVC as cell of origin.

In summary, the current data favors the hypothesis of an adult stem or progenitor cell as source of gliomas. Mutations disrupt the tight control mechanisms usually in place ultimately leading to uncontrolled growth. However, this model does not answer the question why individual cells within a tumor (often referred to as cancer stem cells) have different tumorigenic potentials. Work on the function, signaling and targeting of such cells will be presented in chapters 1, 3, and 4.

Results

Part 1

The alternative Notch pathway via Deltex-1 is an oncogenic factor in malignant glioma.

article manuscript, 2011

Roland M. Huber[1,3]; Balasubramanian Sivasankaran[1,4]; Michal Rajski[2]; Maria Maddalena Lino[1]; Brian A. Hemmings[3] ; Adrian Merlo[1*]

1: Laboratory of Molecular Neuro-Oncology, Department of Biomedicine, University Hospital Basel, Hebelstarsse 20, CH-4031 Basel, Switzerland

2: Institute of Physiology, University of Zürich, Winterthurerstrasse 190, CH-8057 Zürich, Switzerland

3: Friedrich Miescher Institute for Biomedical Research, Maulbeerstrasse 66, CH-4058 Basel, Switzerland

4: current address: Hepatology Laboratory, Department of Biomedicine, University Hospital Basel, Hebelstrasse 20, CH-4031 Basel, Switzerland

Summary

Glioblastoma multiforme is the most malignant tumor of the central nervous system and results in more years of life lost than any other cancer type. Deltex1 is part of an alternative Notch pathway distinct from the canonical cascade. We show that DTX1 activates the RTK/PI3K/PKB and the MAPK/ERK pathway and induces anti-apoptotic Mcl-1. The clonogenic and growth potential of glioma cells correlated with DTX1 levels. DTX1 controlled the tumorigenic potential *in vivo*, and over-expression of DTX1 increased cell migration and invasion. Microarray gene expression analysis identified a DTX1-specific, MAML1-independent transcriptional program - including *microRNA-21*. Patients with low *DTX1* levels have a favorable prognosis. Therefore, we propose the alternative Notch pathway via DTX1 as an oncogenic factor in glioblastoma.

Significance

Glioblastoma multiforme (GBM) is a primary brain tumor of glial origin with poor prognosis and cancer related death in almost all patients. Low levels of Notch receptor expression correlate with prolonged survival in GBM and other gliomas. Different down stream pathways of Notch receptors are known; however, research has mainly focused on the canonical RBPJκ/MAML1-pathway. Here we show the alternative, or non-canonical, pathway functioning through Deltex1 (DTX1) to mediate key features of tumor aggressiveness. Proliferation, invasion, clonogenic potential and patient survival correlate with DTX1 levels. We identify a DTX1 specific gene expression profile which is functionally linked to the changes in tumor aggressiveness. These findings describe the role of NOTCH/DTX1 signaling in glial tumors and offer potential therapeutic targets.

Introduction

Glioblastoma multiforme (GBM) is the most common primary tumor of the central nervous system. This malignant neoplasm occurs with an incidence of 3-7 cases per 100'000 inhabitants per year in Western Europe and North America [1]. Despite continuing efforts to improve treatment over the last two decades and considerable advances in microsurgery, radio- and chemotherapy, median survival of patients remained limited around 14 months after diagnosis [2]. GBM is a highly aggressive tumor characterized by rapid growth and extensive infiltration of adjacent brain areas. Overall, GBM results in more years of life lost than any other cancer type as cancer related death is the case in nearly all patients.

Notch receptors are evolutionary conserved transmembrane receptors which convey extracellular signals across the cell membrane and trigger signal cascades regulating gene expression. Best known for their role in development, Notch signaling has also become a major field of interest in cancer research. Notch activation has been implicated as a positive determinant of cancer formation in T cell acute lymphoblastic leukemias (T-ALL), primary melanomas, breast cancer and gliomas [3]. Furthermore, loss-of-function and gain-of-function mutations of Notch receptors and their ligands have been related to the pathogenesis of various diseases [4] and Notch1 signaling was shown to control proliferation and apoptosis in gliomas [5]. Previous studies have also shown that loss of Notch2 positively predicts patient survival in subgroups of high grade glial brain tumors, including GBM [6]. A possible mechanism by which Notch mediates tumor aggressiveness is by the induction of Tenascin-C – an extracellular glycoprotein which correlates with malignancy in glioblastoma and other cancers [7] – by the Notch canonical co-activator RBPJκ. This indicates a mechanism by which Notch signaling modulates tumor invasiveness, one of the hallmarks of GBM [8, 9]. The role of canonical Notch signaling in cancer development, progression and metastasis is intensively studied. However, the role of the non-canonical signaling pathway via Deltex is still unknown.

Deltex is a Notch interacting protein which contains a basic region at the N-terminus where it binds to the ankryn repeats of the intracellular domain of Notch in Drosophila. Deltex has been proposed to regulate Notch activity by antagonizing the interaction

between Notch and Suppressor of Hairless [10]. In mammalian cells, *DTX1* has been shown to be a transcription target of Notch itself suggesting a positive feedback loop between Notch and DTX1. However, Deltex protein family members contain a RING finger domain at their C-terminus with E3 ubiquitin ligase activity. Deltex has been shown to be part of a three protein complex (containing Notch, Deltex and non-visual beta-arrestin) mediating the degradation of the intracellular Notch receptor through a ubiquitination-dependent pathway [11]. Loss-of-function mutations provided *in vivo* evidence for the functional relation of Deltex, Notch and non-visual beta-arrestin in Drosophila wing development. Therefore, Deltex appears to act as a signal repressor or as negative feedback of Notch signaling in mammals.

Deltex also exerts its function on Notch independent targets. DTX1 has been shown to exert E3 ubiquitin ligase activity on other protein substrates, such as the mitogen-activated protein kinase signaling component MAP kinase kinase kinase (MEKK1). Targeted MEKK1 degradation by Deltex suppresses the activation of T-cells [12]. In mouse, three new ligands to the Notch receptor family have been identified which signal specifically through the DTX1 pathway [13-15] independently of RBPJκ and MAML1. However, the genes involved in this pathway are ill defined [16, 17]. In summary, Deltex constitutes a distinct, cell context-dependent Notch signaling pathway.

Regarding the cellular origin of gliomagenesis, several findings suggest progenitor or adult stem cells as possible founder cells of intracranial neoplasms. Most interestingly, Deltex has been shown to block the transcription factor MASH1 in neural progenitor cells by binding to p300 and thereby blocking differentiation of these cells. This differentiation block was shown to be independent of canonical Notch signaling via RBPJκ [18]. Furthermore, a Deltex mediated block of neural differentiation has been shown in microchaetae sensory precursors in Dorsophila indicating a conserved role for Deltex as a regulator of differentiation [19].

In this study we provide evidence that DTX1 has an oncogenic role in high grade gliomas. We provide molecular insight in how a modulation of DTX1 levels changes the signaling network in cancer cells and relate this finding to changes in the proliferative,

migratory and clonogenic potential. We identify a set of genes specifically controlled by this non-canonical Notch signaling and its impact on the *in vitro* and *in vivo* tumor phenotype.

Results

Deltex 1 is expressed in primary gliomas and glioma-derived cell lines

We analyzed *Deltex1* (*DTX1)* expression both at the transcript and at the protein level in tumor biopsies and glioma-derived cell lines. First, we performed semi-quantitative RT-PCR with cDNA derived from established glioma cell lines, tumor biopsies directly derived from the operating room and with low passage *ex vivo* glioma cell lines generated in our laboratory. All established cell lines showed *DTX1* expression at varying levels. All tumor biopsies and all *ex vivo* cell lines showed robust *DTX1* expression at the transcript level (Figure 1, A). We performed RT-PCR based transcript mapping, confirming in all probes full length transcripts by the presence of exon 1, 2, 3-5, 6-8, and 9 as well as of the 3'UTR of the mRNA with individual primer sets (data not shown). We found expression of DTX1 at varying levels in all glioma cell lines, tumor biopsies and *ex vivo* cell lines expressed by western blotting (Figure 1, B), confirming transcript analysis.

To further validate our results, total RNA was isolated from two normal human brain controls, three normal human astrocyte cultures, 15 glioblastoma multiforme, seven astrocytomas (grade II-III) and six oligodendrogliomas, and processed for gene expression analysis by microarrays [20]. Two independent probes detecting *DTX1* mRNA (1559618_at and 227336_at, Affymetrix) confirmed *DTX1* expression in all samples analyzed. Most glioma samples with different histologies showed elevated levels of *DTX1* expression ($p=0.094$) compared to controls (Figure 1, C). Altogether, we found DTX1 to be expressed in glioma biopsies and cell lines both at the transcript and protein level.

To further investigate the role of DTX1 in gliomas, we generated cell lines over-expressing DTX1 (pcDNA3-DTX1-myc) and glioma cells with reduced levels of DTX1 through shRNA interference (pLKO.1-shRNA-DTX1) (Figure 1, D). Cell line U373 expresses high endogenous levels of Notch1 and Notch2, whereas cell line LN18 shows low expression levels for these two receptors [8]. Furthermore, U373 and LN18 differ in their p16/p14 status thereby representing the two major subclasses of GBM (U373: *p16/p14* wild type; LN18: *p16/p14* homozygous deletion) [21].

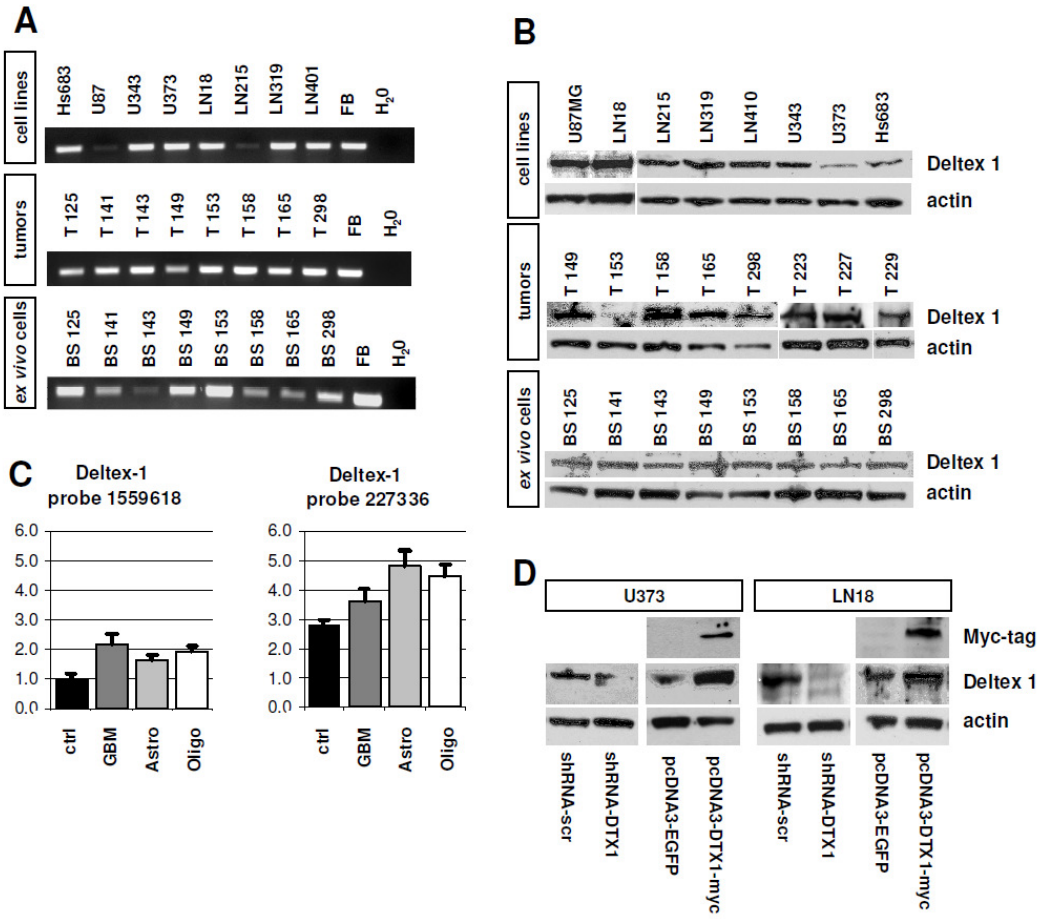

Figure 1. DTX1 is expressed in gliomas, *ex vivo* cell lines and established glioma derived cell lines.

(A) Semi-quantitative RT-PCR probing for exon 1 of DTX1 in established glioma derived cell lines, glioma tumor biopsies and *ex vivo* cell lines. *Ex vivo* cell lines were derived from tumor biopsies as indicated by the numbering and were maintained as low passage cultures. Fetal brain (FB) was used as positive control. (B) Western Blot analysis of glioma derived cell lines, glioma tumor biopsies and *ex vivo* cell lines probing for DTX1 and β-actin. (C) Microarray gene expression analysis of tumors and control tissue. Two non diseased normal brain samples and three normal human astrocyte cultures were used as control (ctrl), 15 GBMs, seven astrocytomas and six oligodendrogliomas were analyzed. Bars represent average expression values per group ±SEM. Results for both probes on the chip detecting DTX1 mRNA are shown. (D) Western blot analysis of transfected cell lines U373 and LN18 probing for DTX1, Myc-tag and β-actin demonstrating DTX1 over-expression and down regulation as indicated according to the genotype.

Deltex 1 regulates signaling pathways of cell growth and survival.

Unlimited replicative potential of tumor cells is a hallmark of aggressive cancers. Notch acts as a switch-like signaling mechanism controlling the transition from proliferation to differentiation and vice versa depending on the cellular context. We therefore analyzed several signaling pathways in relation to the DTX1 status of the cell which are known to control proliferation and are often altered in GBM.

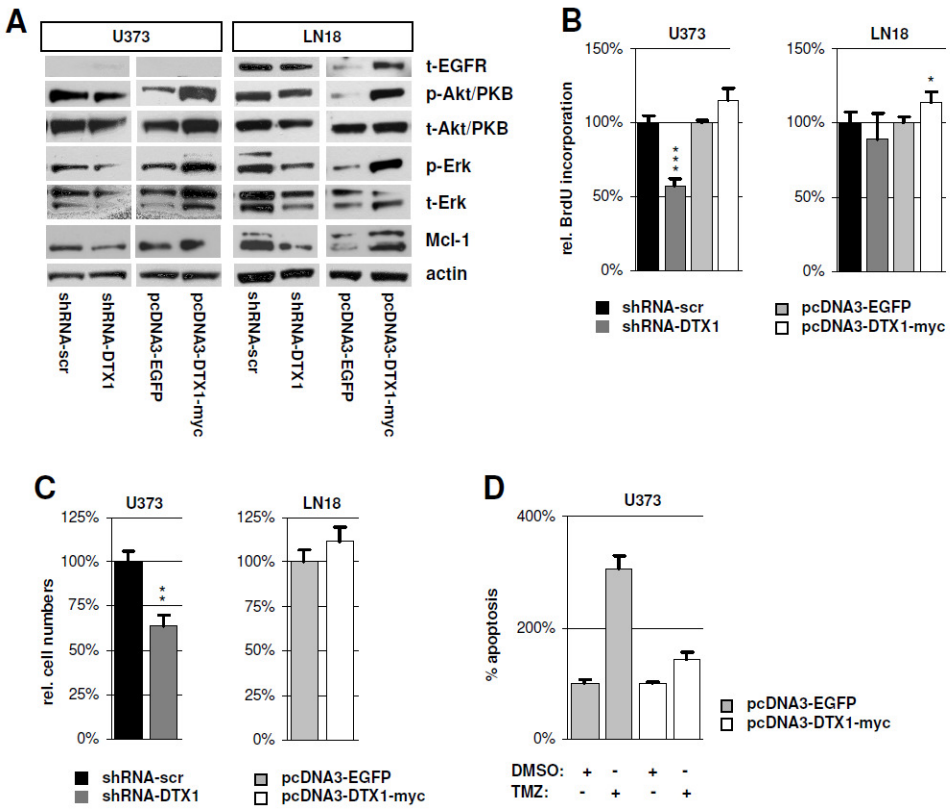

Figure 2. Proliferation and signaling pathways are modified by DTX1 in glioma cell lines.

(A) Western blot analysis of signaling proteins. Blots for total EGFR (t-EGFR), phosphorylated Akt/PKB (p-Akt/PKB), total Akt/PKB (t-Akt/PKB), phosphorylated Erk (p-Erk), total Erk (t-Erk), Mcl-1 and beta actin (actin) are shown. (B) Proliferation analysis by BrdU incorporation assay. Relative average values of 5 individual experiments are shown per genotype. (C) Proliferation analysis by cell counting. Equal numbers of cells were seeded, grown for 3d under standard conditions and counted afterwards. (D) Apoptosis in U373 cells after treatment with 100µM temozolomide (TMZ) or DMSO vector control. Relative values of sub-G_1 cells are shown normalized to control cells treated with vector control. Averages of at least three independent experiments are shown. Values are normalized to controls. Error bars: ±SEM. * $p<0.05$, ** $p<0.01$, *** $p<0.001$.

In gliomas, the PI3K/PKB/mTOR and the MAPK/ERK pathways are upregulated by specific mutations [22]. We analyzed the effect of DTX1 on the expression level of EGF receptor (EGFR), a receptor tyrosine kinase frequently over-expressed in gliomas. In the EGFR-expressing glioma cell line LN18, DTX1 over-expression increased EGFR protein levels. However, shRNA-DTX1 only marginally reduced EGFR levels (Figure 2, A). In the U373 cell line that does not express EGFR, we could not induce *de novo* expression of EGFR by DTX1 (Figure 2, A). In both LN18-DTX1-myc and U373-DTX1-myc we observed a massive increase of the phospho-Akt/PKB (p-Akt/PKB) levels. In contrast, we detected a moderate reduction of p-Akt/PKB levels in the LN18-shRNA-DTX1 and U373-shRNA-DTX1 cells. In both glioma cell lines analyzed, down-regulation of DTX1 reduced the levels of phosphorylated Erk (p-Erk). On the other hand, DTX1 over-expression induced p-Erk (Figure 2, A). The changes observed for p-Akt/PKB and p-Erk levels were paralleled by changes in the total amounts of the proteins. The anti-apoptotic protein Mcl-1 was reduced by shRNA-mediated DTX1 down-regulation and induced in DTX1-myc over-expressing cells in both cell lines (Figure 2, A).

To determine how these changes in MAPK and PI3K/PKB signaling affect proliferation, we performed BrdU incorporation assays to detect alterations in tumor cell proliferation in relation to DTX1 levels. U373-DTX1-myc cells showed a slight increase in proliferation of 15% ($p=0.15$) whereas U373-shRNA-DTX1 cells displayed a significant reduction by 35% ($p<0.001$, ***) (Figure 2, B). In LN18 cells, over-expression of DTX1 increased proliferation by 14% ($p<0.01$, **). However, down-regulation did not significantly change the proliferative behavior of LN18 cells (Figure 2, B). In accordance with the results obtained in the BrdU incorporation assay, we observed a reduction by 35% ($p<0.01$, **) when analyzing cell numbers after 3 days of unchallenged growth in U373-shRNA-DTX1 cells (Figure 2, C). In LN18-DTX-myc cells, we observed 14% more cells compared to controls after 3 days of growth ($p=0.26$) (Figure 2, C). Background apoptosis was not changed in any of the cell lines compared to controls as analyzed by sub-G_1 cell content (data not shown). When challenged with 100µM temozolomide relative apoptosis in U373-EGFP increased to 305% of control but only to 143% in U373-DTX1-myc cells ($p < 0.01$, **) (Figure 2, D). There was no significant difference between U373-shRNA-scr and U373-shRNA-DTX1 cells regarding TMZ sensitivity (data not shown).

These results show that two major survival and growth promoting signaling pathways and the anti-apoptotic protein Mcl-1 are positively regulated by DTX1 in glioma cell lines. Proliferation and drug resistance correlated with these findings. A direct link between DTX1 and the MAPK and PI3K/PKB pathways has so far not been described, we therefore wanted to identify the molecular mediators involved.

Deltex 1 controls gene expression in glioma cells and regulates genes independently of the canonical Notch signaling cascade

We compared U373-EGFP GBM control cells to U373-DTX1 cells by microarray gene expression experiments that allow the identification of genes controlled by non-canonical Notch signaling. Given the tight interaction of DTX1 with Notch and the proposed negative feedback loop on the canonical pathway, we aimed to exclude genes which are altered due to a secondary inhibitory effect of DTX1 on the canonical pathway. Therefore, we compared the first dataset to the gene expression profiles of U373 cells expressing a dominant negative form of MAML1 (MAML1-dn) mimicking the negative feedback of DTX1 on canonical Notch signaling.

We identified 763 annotated genes to be differentially expressed in U373-DTX1 cells (665 up, 98 down) and 991 in U373-MAML1-dn (872 up, 119 down) when compared to EGFP control cells (Supplementary Table 1; Supplementary Figure 1, A). 572 genes were commonly affected in both cell lines compared to U373-EGFP control cells, 419 uniquely in U373-MAML1-dn and 191 uniquely in U373-DTX1 cells (Supplementary Figure 1, B). Out of the 191 annotated transcripts unique to U373-DTX1 cells (Supplementary Table 3), 121 were significantly up-regulated and 70 were significantly down regulated more than 2 fold compared to EGFP cells (Supplementary Table 1).

Unsupervised clustering based on overall gene expression profiles pointed towards a high similarity between MAML1-dn and DTX1 transcriptomes. This indicates a negative feedback role for DTX1 on canonical Notch signaling resulting in correlated effects ($p<0.05$) on overall gene expression (Supplementary Figure 1, A and 2, A). Unsupervised clustering based on the annotated 191 genes specifically altered in U373-DTX1 cells showed

high specificity for this DTX1 gene set compared to both EGFP and MAML1-dn expressing cells ($p<0.05$; Supplementary Figure 2, B). To confirm the validity of these two clusters, we assessed the uncertainty in hierarchical cluster analysis. For each cluster, *p*-values were calculated via multiscale bootstrap resampling [23]. These results confirmed that both clusters (Supplementary Figure 2, A, B) are strongly supported by data ($p < 0.05$).

Table 1

Accession ID	Gene Symbol	Protein Name	fold change
examples of genes up regultated >2-fold and related to cancer			
NM_004416	*DTX1*	*deltex homolog 1* [1)]	*47.20*
NM_005264	GFRA1	GDNF family receptor alpha 1	3.00
AY699265	MIRN21	microRNA 21	2.85
NM_001018159	NAE1	NEDD8 activating enzyme E1 subunit 1	2.54
NM_018131	CEP55	centrosomal protein 55kDa	2.49
NM_012096	APPL1	adaptor protein, phosphotyrosine interaction, PH domain and leucine zipper containing 1	2.37
NM_003238	TGFB2	transforming growth factor, beta 2	2.16
NM_001025366	VEGFA	vascular endothelial growth factor A	2.14
NM_005921	MAP3K1	mitogen-activated protein kinase kinase kinase 1	2.05
ENST00000321331	HIGD1A	HIG1 domain family, member 1A	2.04
NM_175866	UHMK1	U2AF homology motif (UHM) kinase 1	2.02
examples of genes down regulated >2-fold and related to cancer			
NM_001040058	SPP1	secreted phosphoprotein 1	0.27
NM_003811	TNFSF9	tumor necrosis factor (ligand) superfamily, member 9	0.28
NM_002346	LY6E	lymphocyte antigen 6 complex, locus E	0.30
NM_001946	DUSP6	dual specificity phosphatase 6	0.41
NM_020645	NRIP3	nuclear receptor interacting protein 3	0.43
NM_016086	STYXL1	serine/threonine/tyrosine interacting-like 1	0.45
NM_002231	CD82	CD82 molecule	0.46
NM_030964	SPRY4	sprouty homolog 4	0.47
NM_001964	EGR1	early growth response 1	0.48

1) DTX1 over-expressing cell line

Next we analyzed the functional groups of DTX1-specific genes according to their gene ontology (GO). Most genes belong to metabolic (23 genes) or signal transduction (22 genes) networks. Among others, the GO categories cell cycle control, cell motion, extracellular matrix and apoptosis also contained 30 genes controlled by DTX1 suggesting a

direct mechanistic link between the phenotypes observed and gene expression (Supplementary Table 2). We next performed an extensive literature search for all 191 genes specific for DTX1 with respect to their functional role in cancer and GBM in particular. Some 20 genes with described functions in cancer specifically controlled by DTX1 are shown in Table 1. Interestingly, we observed an induction of *miR-21*, a microRNA which has previously been shown to target a network of tumor suppressive pathways in GBM cells [24]. Taken together these results identify a set of genes specifically controlled by non-canonical Notch signaling through DTX1 including known oncogenes and oncomirs.

miR-21 expression is controlled by DTX1 and is p300 dependent

To evaluate the results obtained by microarray analysis, we performed quantitative PCR measurements of miR-21 levels. We found a reduction of miR-21 in U373-shRNA-DTX1 to only 30% of the control levels ($p < 0.001$, ***) whereas over-expression of DTX1 resulted in an increase of miR-21 to 951% of the control ($p < 0.001$, ***) (Figure 3, A).

Previous studies have identified the histone acetyl-transferase p300 as a binding partner of DTX1 which in turn modulates p300's co-activator activity in various contexts [18]. Therefore, we analyzed the effect of p300 knock down on the DTX1 induced miR-21 expression. We transiently transfected U373-DTX1-myc cells with siRNAs targeting p300 (sip300) or scrambled control siRNAs (siCTRL) alongside a GFP vector. After 2 days, >80% of the cells showed GFP expression indicating high transfection efficiency (data not shown). p300 levels were analyzed by qPCR showing effective targeting of p300 (Figure 3, B). DTX1-myc cells transfected with sip300 showed reduced miR-21 expression remaining with 23% of DTX1-myc control or 31% of siCTRL levels ($p < 0.001$, ***) (Figure 3, C). Transfection of U373-DTX1-myc cells with miR-21 inhibitor (α-miR-21) reduced miR-21 levels to 25% compared to DTX1-myc cells (Figure 3, D) ($p < 0.001$, ***) and to 32% compared to cells treated with an inhibitor control (α-CTRL) (Figure 3, D) ($p < 0.01$, **).

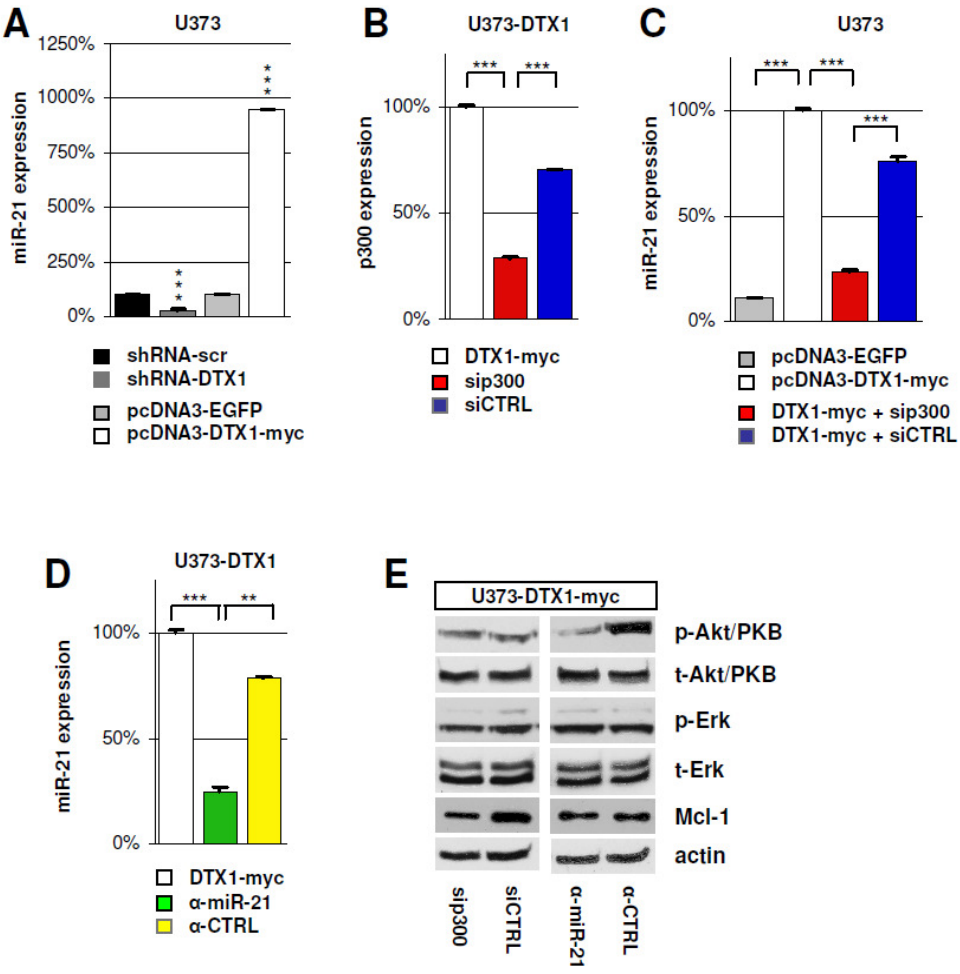

Figure 3. DTX1 controls miR-21 expression in glioma cells in a p300 dependent manner.

(A) Real time quantitative PCR analysis of miR-21 expression in U373 cells with modified DTX1 levels. (B) p300 and (C) miR-21 expression levels in U373-DTX1-myc cells transfected with siRNA targeting p300 (sip300, red) or control siRNA (siCTRL, blue) analyzed by qPCR. (D) miR-21 expression in U373-DTX1-myc cells treated with miR-21 inhibitor (α-miR-21, green) or an inhibitor control (α-CTRL, yellow). Average relative expression values of at least four independent experiments are shown. Error bars: ±SEM. * $p<0.05$, ** $p<0.01$, *** $p<0.001$. (E) Western blot analysis of signaling cascades in U373-DTX1-myc cells transfected with sip300 or siCTRL. Blots were probed for phosphorylated and total Akt/PKB, phosphorylated and total Erk, Mcl-1 and actin.

Inhibition of miR-21 resulted in a reduction of p-Akt/PKB levels in DTX1-myc cells whereas the down-regulation of p300 did neither affect phosphorylation nor total Akt/PKB protein levels (Figure 3, E). Similarly, Erk phosphorylation and total amounts were not affected either upon inhibition of miR-21 (Figure 3, E). Mcl-1 expression was reduced in U373-DTX1-myc cells treated with sip300 but was unchanged in α-miR-21 treated cells

(Figure 3, E). Taken together, these data demonstrate that miR-21 expression is controlled by DTX1. The induction of miR-21 and Mcl-1 is p300-dependent while activation of Akt/PKB depends on miR-21.

The clonogenic potential of glioma cells is regulated by Deltex 1

The ability to initiate clonogenic growth – a determinant of tumorigenicity – is reflected by the potential to form colonies *in vitro* when seeded at very low density, minimizing cell-cell contact or when grown in an anchorage independent manner in low density soft agar or as floating spheres. We therefore analyzed the clonogenic potential of glioma cell lines with modified DTX1 expression.

Cells transfected either with EGFP, DTX1-myc, shRNA-DTX1 or shRNA-scr were seeded, grown for 3 weeks, fixed and stained with Cresyl violet. Over-expression of DTX1 significantly increased the number of colonies compared to the EGFP control. We observed 43% more colonies and 358% more colonies in U373 and LN18, respectively ($p<0.001$, ***) (Figure 4, A, B). U373-shRNA-DTX1 cells showed a significant reduction in colony formation by 42% ($p<0.001$, ***). Down regulation of DTX1 in LN18 cells resulted in a reduction by 73% ($p<0.001$, ***). The overall area covered by individual colonies appeared smaller in DTX1 over-expressing LN18 cells. However, cell density was massively increased in these colonies. Furthermore, LN18-DTX1 cells showed a pronounced phenotype of aggregation and grew in multiple layers, which was not observed in control cells (Supplementary Figure 3).

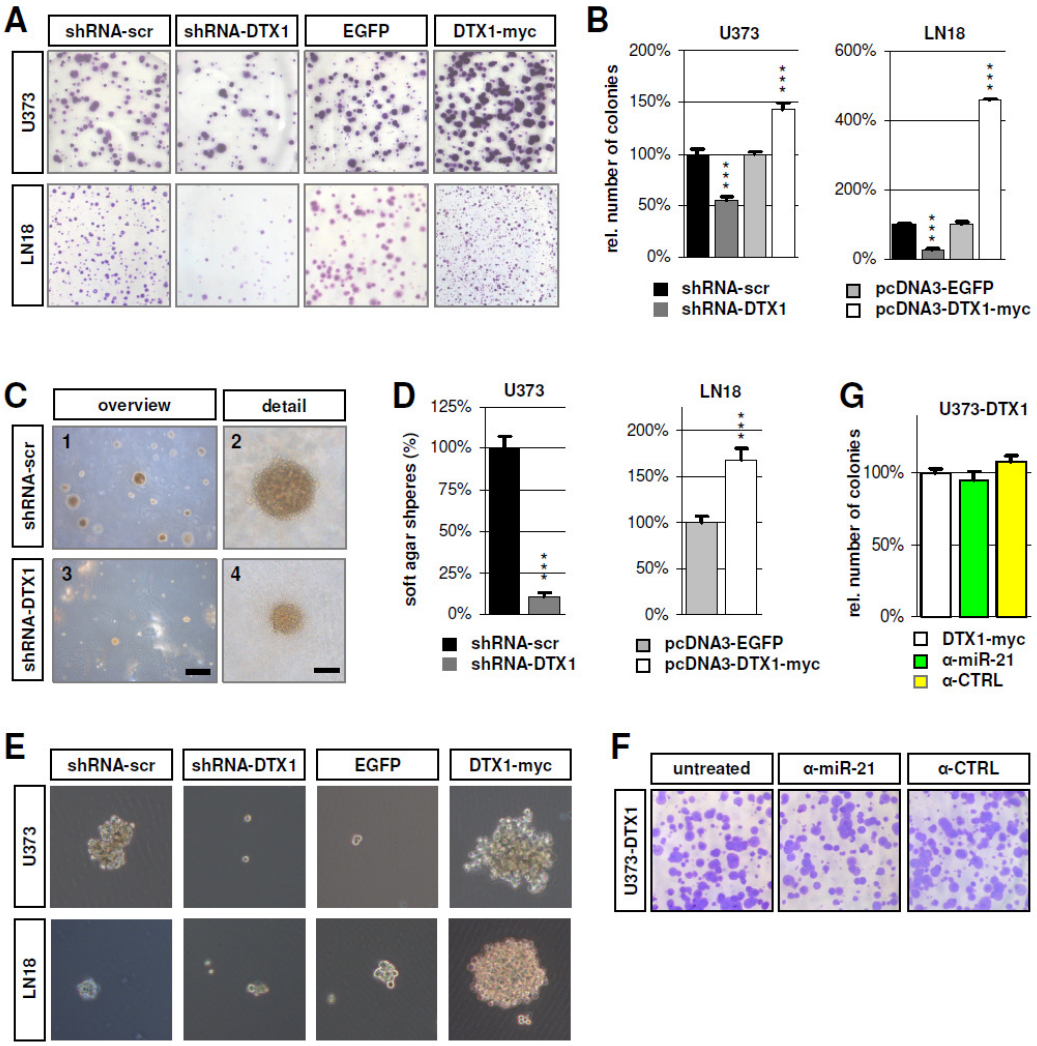

Figure 4. DTX1 regulates the clonogenic capacity of glioma cells.

(A) Low density cell seeding of glioma cells with showing positive correlation between colony formation potential and DTX1 levels in glioma cell lines U373 and LN18. (B) Quantification of colonies formed in the low density seeding assay after 21d. All colonies were included irrespective of size. (C) Soft agar colony formation assay shown as light microscopic overview images (1, 3) or detailed close up images (2, 4) of a representative individual colony showing surface independent growth in 0.3% agar. Scale bars: overview 400µm; detailed view 80µm. (D) Quantitative analysis of the number of colonies formed after 15d of incubation in soft agar shown in (C). (E) Floating cancer spheres grown in NBE medium for 24d (shRNA-scr and shRNA-DTX1) or 15d (EGFP and DTX1-myc) shown as light microscopic images. (F) Low density seeding of U373-DTX1-myc cells treated with miR-21 inhibitor (α-miR-21) or control inhibitor (α-CTRL). (G) Quantification of low density seeding shown in (F). Average values are shown. Error bars: ±SEM. *** p<0.001.

Anchorage-independent cell growth was also dependent on the DTX1 status. While the shRNA-scr control cells readily formed spheres with considerable density, the shRNA-DTX1 cells only formed very few colonies. On average, these colonies were also smaller than the control spheres (Figure 4, C). In total, a reduction of around 90% of growing spheres was observed in the case of DTX1 down regulation in U373 ($p < 0.001$, ***) (Figure 4, D). Over-expression of DTX1 in LN18 cells resulted in a 68% increase in colony number ($p < 0.001$, ***) (Figure 4, D). Over-expression of DTX1 in U373 or shRNA-DTX1 in LN18 did not significantly change sphere formation. miR-21 inhibition did not change the clonogenic potential of glioma cells when plated at low density (Figure 4, F, G).

Cells were seeded in serum-free neurobasal medium to check for differences in floating cancer sphere formation as an additional measure for the oncogenic effect of DTX1. Down-regulation of DTX1 reduced both colony numbers and size in both cell lines. U373-DTX1-myc cells formed more and larger spheres when compared to EGFP control cells. Likewise, LN18-DTX1-myc cells formed larger spheres while control cells did only form few and small spheres (Figure 4, E). Taken together, these results show a significantly reduced aggressiveness of glioma cells with down regulated DTX1 as shown by the reduced ability to give rise to cell colonies or spheres in all assays performed. This effect was insensitive to miR-21 inhibition.

Deltex 1 controls cell migration and invasiveness in glioma cells

GBM are highly invasive neoplasms. We have previously shown that Notch signaling induces Tenascin C (TnC), a marker for tumor malignancy which stimulates glioma cell migration and invasion through the canonical Notch pathway. This induction was RBPJκ-dependent and could be blocked by using a dominant negative form of the Notch canonical co-activator MAML1 (Sivasankaran et al., 2009). However, it remained unanswered if the non-canonical Notch pathway also has a regulatory role in cell migration and invasiveness.

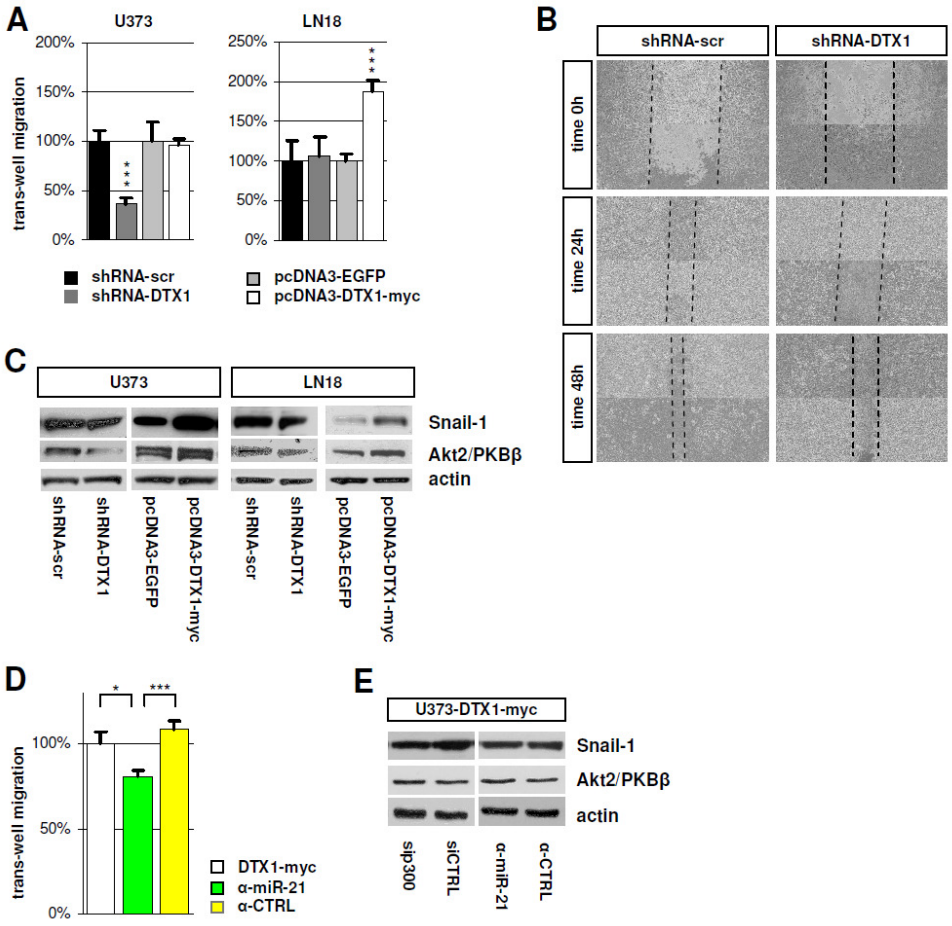

Figure 5. Migration and invasion potential of glioma cells is regulated by DTX1.

(A) Boyden chamber trans-well migration assay with U373 and LN18 glioma cells on collagen coated membranes with 8µm porosity. Counts were performed after 24h. (B) Scratch test wound healing assay. A scratch wound was inflicted and immediately imaged (time 0h). Follow up images were taken after 24 and 48 hours. Dashed lines indicated border of cell layer. (C) Western blot analysis of known pro-migratory factors in glioma probing for Snail-1, Akt2/PKBβ, and beta-actin. (D) Boyden chamber trans-well migration assay with U373-DTX1-myc cells not treated (white), treated with a miR-21 inhibitor (α-miR-21, green) or an inhibitor control (α-CTRL , yellow). (E) Western blot analysis of known pro-migratory factors in glioma probing for Snail-1, Akt2/PKBβ, and beta-actin after transfection with siRNA targeting p300 (sip300) or control construct (siCTRL) and after miR-21 inhibition (α-miR-21) or application of control inhibitor (α-CTRL). Average values are shown from at least three individual experiments. Error bars: ±SEM. * $p<0.05$, *** $p<0.001$.

To determine this role, we performed transmembrane invasion assays with the two GBM cell lines U373 and LN18 by modifying DTX1 expression. DTX1 over-expression did not significantly alter the invasive behavior of U373 cells whereas the U373-shRNA-DTX1 cells showed an average reduction of invasion by 63% compared to control cells ($p < 0.001$, ***) (Figure 5, A). Cell invasion was elevated in LN18-DTX1 cells to 188% of the EGFP controls ($p <$

0.001, ***) whereas shRNA-mediated knock-down of DTX1 did not influence the invasive potential of LN18 cells (Figure 5, A). Again we observed a strong effect upon down-regulation of DTX1 in the U373 cell line with high endogenous Notch levels. Similarly, up-regulation of DTX1 in LN18 cells with low endogenous Notch levels increased migration.

To confirm these results in an independent experimental setup, we performed scratch test wound healing assays. Wounds were imaged immediately after the scratch wound was inflicted as well as 24 and 48 hours later. Wound closing, which is a measure for cell motility, was massively reduced in U373-shRNA-DTX1 cells compared to controls (Figure 5, B) confirming the initial finding of the transwell migration assay.

Elevated levels of p-Akt/PKB have been shown to positively correlate with migrating glioma cells, and reduction of total Akt2/PKBβ has been shown to inhibit the migratory as well as the invasive potential of glioma cells [25, 26]. To determine if the alterations in the invasive and migratory potential observed could be explained by these mechanisms, we analyzed the expression pattern of Akt2/PKBβ in our cell lines. We found a positive correlation of Akt2/PKBβ and DTX1 in both cell lines analyzed (Figure 5, C). The elevated levels of p-Erk in DTX1 over-expressing cells (Figure 2, C) pointed towards pathway know to regulate the migratory potential of cells through an Erk/NFκB/Snail1 pathway controlling epithelial to mesenchymal transition (EMT) in primary human mesothelial cells [27]. We therefore analyzed the levels of Snail1 in our glioma cell lines and found a positive correlation with DTX1 which is in accordance to the observed increase in p-Erk levels (Figure 2, C).

Besides targeting a network of tumor suppressor genes, miR-21 has also been described as a migration and invasion promoting factor in gliomas [28]. Therefore we aimed at determining the effect of miR-21 on migration in DTX1 over-expressing cells. DTX1-myc cells treated with miR-21 inhibitors migrated 19% less than DTX1-myc cells ($p < 0.05$, *) and 28% less than DTX1-myc cells treated with a control inhibitor ($p < 0.001$, ***) (Figure 5, D). Snail-1 upregulation was slightly p300, but not miR-21 dependent (Figure 5, E). Akt2/PKBβ induction through DTX1 was neither affected in cells with sip300 nor in cells treated with a miR-21 inhibitor (Figure 5, E). Taken together, we have demonstrated that DTX1 positively

correlates with glioma cell migration and invasiveness. Furthermore, we have shown that this effect could be mediated by alterations in known pro-migratory signaling pathways in GBM.

Deltex 1 controls the tumorigenic potential of glioma *in vivo*

We analyzed the data publicly available at the REMBRANDT database (REpository of Molecular BRAin Neoplasia DaTa, NCI, NIH, USA) to determine if the *in vitro* findings could be brought forward to tumor behavior in patients. GBM patients with intermediate DTX1 expression levels had a median survival time of 402 days. Patients with low levels (reduced by 2 fold or more of intermediate) had a median survival time of 544 days, an increase of more than 35%. Furthermore, the expression of *DTX1*, *PKBβ*, *Snail-1* and *EGR1* significantly correlated with patient survival in GBM patients (Supplementary Figure 4) ($p < 0.05$, *). To assess whether this finding was conferrable to other cancers, we analyzed a data set of early breast cancer samples [29] for the correlation of *DTX1* expression levels and patient survival. Again, prolonged survival in the group with sub-reference *DTX1* expression was detected throughout the period of observation (data not shown).

In summary, we found *DTX1* expression levels to correlate with patient survival. Low *DTX1* expression favors better prognosis in GBM patients. This is in accordance with our *in vitro* data and identifies DTX1 as an oncogenic factor in HGG.

Discussion

The functional role of Notch has been intensively studied in human gliomas over the last years. Notch-signaling through distinct receptors regulates critical aspects of glioma biology such as differentiation, proliferation, tumor stroma and angiogenesis [30]. For example, Notch2 status has been identified as a highly significant prognostic marker in GBM and oligodendroglioma independent of other mutation patterns [6]. The role of DTX1, the mediator of non-canonical Notch signaling, has not been elucidated yet in cancer. DTX1 has been linked to invasiveness in osteosarcoma [31], however, its role in glioma remains elusive.

In this study we demonstrated an oncogenic role of DTX1 in high grade glioma. DTX1 increased tumor aggressiveness, seen by elevated clonogenicity, increased the migratory and invasive potential of glioma cells and induced several signaling pathways protecting cancer cells form apoptosis and stimulating survival and proliferation. These effects are linked to a set of genes whose expression is specifically controlled by DTX1. We will discuss our results in the context of DTX1 as a regulator of gene expression, the regulation of DTX1 itself and of DTX1 as a novel oncogenic factor.

DTX1 has an oncogenic role in glioma

Oncogenes have the potential to induce malignant growth by conveying uncontrolled proliferation, insensitivity to growth limiting and pro-apoptotic signals, by inducing cell migration, invasion and neo-vascularisation. DTX1 aggravates several of these mechanisms in glioma cells. The ability to grow when seeded at low density, as floating spheres or in soft agar indicates abnormal growth potential and increased resistance to anoikis. These phenotypes are enhanced in glioma cells by high DTX1 levels. Our *in vivo* data further demonstrate that growth is enhanced in tumors with DTX1 over-expression. Furthermore, GBM patients with low *DTX1* expression levels have a better prognosis and have a >35% longer median survival than controls. The increased levels of RTK/PI3K/PKB and MAPK/ERK activation observed in DTX1-myc cells offer a mechanistic explanation for this enhanced tumorigenic potential. The elevated protein levels of the anti-apoptotic factor Mcl-1 point to

a second mode of action. Interestingly, a link between Notch receptors and Mcl-1 had been demonstrated [32]. However, this effect could not be assigned to the canonical factors MAML1 and RBPJκ. Taken together, these findings suggest that Mcl-1 is specifically controlled through the non-canonical Notch pathway. DTX1 mediated effects may be conferrable to other solid tumors. For example, the better prognosis of early breast cancer patients with low *DTX1* expression levels points in this direction.

Massive tumor cell migration and brain invasion are hallmarks of GBM. These migrating cells pose a major obstacle to any successful therapy, thwarting complete surgical resection. DTX1 positively correlates with the migratory and invasive potential of glioma cells. This effect is depending on the levels of endogenous Notch. For example, in U373 cells, which have high levels of endogenous Notch, DTX1 only alters the migratory behavior upon down-regulation. In low Notch expressing LN18 cells the opposite is true. Although the pro-migratory factors Snail-1 and Akt2/PKBβ are influenced by DTX1 in both lines, high Notch activity appears to saturate the migratory behavior and cannot be further induced by over-expressing DTX1 whereas low Notch levels readily induce migration. The MAPK/ERK pathway has previously been linked to proliferation and migration in glioblastoma [33]. DTX1 levels strongly correlate with the levels of p-Erk in all cell lines analyzed independent of Notch levels. Furthermore, MMP-9, an endopeptidase that digests basement membrane type IV collagen, is induced by p-Erk in glioma cells [34]. Therefore, elevated levels of p-Erk could explain the increased invasive potential while the elevated levels of Akt2/PKBβ act on cell adhesion and cytoskeleton rearrangement [26] leaving the cells with significantly aggravated invasive and migratory behavior as observed in our experiments.

DTX1 controls the expression of oncogenes, tumor suppressors and oncomirs in glioma

Deltex has been shown to be a negative regulator of Notch signaling in cancer cells by targeting the Notch-ICD for ubiquitination and degradation [31]. Notch signaling itself induces Deltex which thereby leads to a negative feedback loop. The high degree of similarity in our overall gene expression profiles between MAML1-dn and DTX1-myc cells further supports this model. However, DTX1 also controls genes which are not regulated by the canonical Notch pathway and have a direct impact on cancer progression, e.g. miR-21

which has a well established role as an oncomir through several modes of action [24, 35, 36]. Our results demonstrate miR-21 activation through non-canonical Notch signaling to depend on p300 levels. In *C. elegans* LIN-12/Notch signaling has previously been linked to microRNA expression [37]. The two Notch signaling pathways may represent an evolutionary conserved mechanism of microRNA regulation.

DUSP6, a gene down regulated in DTX1 over-expressing cells, belongs to a class of dual-specificity phosphatases which dephosphorylate MAPK pathway proteins ERK, JNK, and p38 [38]. This offers a direct functional link between DTX1 specific gene expression and p-Erk levels. Additionally, we found APPL1, a co-activator of Akt2/PKBβ [39], to be up-regulated by DTX1. Both have a similar activating effect on cell migration in glioma cells. It is not clear to which extent the change in the invasive potential of the cells is mediated by these pathways or by miR-21, which also has been described as a regulator of invasiveness. However, inhibition of miR-21 alone did not reduce migration as much as down regulation of DTX1 did, indicating an additive, combinatorial effect of several mechanisms controlled by DTX1.

Altogether, DTX1 activates a set of transcripts with oncogenic functions and down regulates tumor suppressors in parallel. How these different aspects interact and to which extent the changes in expression are direct or indirect remain to be established. An additional layer of complexity is added by the fact that not all changes in gene expression or signaling are p300 dependent in our experiments. Whereas miR-21, Snail-1 or Mcl-1 expression was reduced in cells with diminished p300 levels this was not the case for Akt2/PKBβ or Erk. Several modes of action could explain this finding. DTX1 has been shown to bind to p300 and thereby sequester it from its previous binding partners. This effect leads to the inhibition of the transcription factor MASH1 which controls differentiation in neural progenitor cells [18]. If the change induced by DTX1 is caused by reducing p300 availability at a certain site, a further reduction of p300 by siRNA would not further enhance the initial alteration. Non-canonical Notch signaling also inhibits E47, a widely expressed transcription factor [40]. Therefore, DTX1 could regulate gene expression directly by forming a DNA binding complex with p300 and thereby reducing its availability and/or by changing the activity of other transcription factors.

Deltex can be activated by Notch and other signaling cascades

If the DTX1 specific transcriptional program is activated by specific ligands of Notch receptors as it was shown for oligodendrocyte maturation which is induced by F3/Contactin [13], remains to be determined. The NB-3/Notch1 pathway also has been reported to signal specifically through DTX1 but not through the canonical pathway [41].

Although Notch receptors are the best established activators of Deltex, there are also other mechanisms described. The transcription factor NFAT (nuclear factor of activated T cells) was shown to induce DTX1 expression in T cells where DTX1 then acted as a transcriptional regulator independently of Notch [42]. Granule cell precursors of the cerebellum increase *DTX1* expression when stimulated with Shh [43]. If this induction of Deltex occurred directly or if this was a secondary effect due to overall changes in gene expression remained unaddressed. Regarding GBM, DTX1 is induced by Notch signaling, however, alternative pathways like SHH may also contribute to direct activation of DTX1. It remains to be shown in glioma if NB3, F3/contactin and other specific ligands to Notch receptors exclusively signal through the non-canonical pathway. In conclusion, we propose the alternative Notch pathway via DTX1 as an oncogenic factor in malignant glioma. We found low *DTX1* expression levels to correlate with prolonged survival in solid tumor patients.

Experimental Procedures

Cell culture and cell lines

Glioma cell lines (LN18, U373) with defined genetic status for TP53, p16/p14 and PTEN were cultured in Eagle's medium supplemented with 25mM glucose, glutamine, standard antibiotics, and 10% fetal calf serum. All cells were maintained at 37°C in 5% CO_2 in a humified chamber (standard conditions). If not stated otherwise in the figure legends, cells were seeded at 5'000-10'000 cells/cm^2 in 94mm culture dishes (Sarsted, Nümbrecht, Germany). For cell counting, the cells were cultured and treated as stated in the figure legends and counted using a 'Neubauer'-chamber (hemacytometer).

Plasmids and transfections

The lentiviral vectors pLKO.1-puro-scrambled-shRNA (Addgene, Cambridge, MA, USA) and pLKO.1-puro-shRNA (Sigma, sh1938: CCGGC CACTG CTATC TACCC AACAA CTCGA GTTGT TGGGT AGATA GCAGT GGTTT TT) targeting DTX1 were transfected into HEK293 cells together with plasmids encoding the packaging (pCMV_dr8_91) and envelope proteins (pMD2-VSV-G) using $CaCl_2$ precipitation. The concentration of infectious particles in the supernatant was titrated using HeLa cells. Glioma cells were transduced with infectious viral particles. Stably transfected clones were selected with 2 µg/ml puromycin. DTX1 over-expression was obtained with pcDNA3-IRES-EGFP as control and pcDNA3-DTX1-myc-IRES-EGFP (kind gift form Prof. Kimie Ohta, Keio University, Japan) using $CaCl_2$ precipitation for 8 hours. Stably transfected clones were selected with 100 µg/ml geniticin (Gibco, Invitrogen, San Diego CA, USA).

RT-PCR and qPCR

RNA was extracted using TRI-Reagent (Sigma, St.Louis MO, USA), phenol/chloroform extraction and were purified with RNeasy spin column kit (Qiagen, Venlo, The Netherlands). cDNA synthesis was performed using the 'Thermo Script RT-PCR System' and random primer hexameres (Invitrogen, San Diego CA, USA). DTX1 primers: fwd (5'- GGGCT GATGC CTGTG

AATG-3'), rev (5'- CCTGG CGAAA CTGGT GC-3'). RNA and cDNA amounts were measured on a NanoDrop ND-1000 Spectrophotometer and equalized prior to synthesis reactions. qPCR for p300 was performed as described elsewhere [44]. microRNAs were isolated using miRNeasy Mini Kit (Qiagen) according to manufacturer's instructions. Taqman MicroRNA Reverse Transcription Kit and Megaplex RT Primers human pool A v 2.1 (Applied Biosystems) were used for cDNA synthesis of microRNAs and Taqman Pri-miRNA Assay for the measurement of miR-21 levels according to manufacturer's instructions (Applied Biosystems).

Cell proliferation analysis

Cell proliferation was analyzed using the 'Amersham Cell Proliferation Biotrak ELISA, version 2' system (GE Helathcare, UK) according to manufacturer's instructions. In short, 5'000 cells were seeded in the well of a 96-well plate and grown for two days, labeled with BrdU for 3-4h, fixed and labeled with a peroxidase-labeled anti-BrdU antibody. After coloring reaction the optical density was measured with a 'SpectraMAX 250' plate reader and analyzed with accompanying 'Soft Max Pro' software (Molecular Devices, MDS Analytical Technologies, Toronto, Canada). For cell counting, equal amounts of cells were seeded in triplicates and grown under standard conditions. Cells were then harvested and each biological replicate was counted ≥8 times using a 'Neubauer'-chamber (hemacytometer).

Colony formation, shpere and soft agar assay

In colony formation experiments for each cell line 1'000 cells were plated in triplicates into 94-mm Petri dishes containing 10 ml of standard culture medium. Cells were then fixed with 4% formaldehyde in 1x PBS and stained with crystal violet. For sphere formation, cells were seeded in Neurobasal medium (Invitrogen) supplemented with basic FGF (20 ng/ml, Invitrogen), EGF (20 ng/ml, R&D Systems), B27 supplement (1x) and N_2 supplement (0.5x) (Invitrogen) and grown under standard conditions for different times: shRNA-scr and shRNA-DTX1 for 24d, EGFP and DTX1-myc cells for 15d. In soft agar experiments for each cell line 1'000 cells were seeded in 0.3% agar (Nobel Agar, Becton Dickinson, USA) in DMEM supplemented with 10% FCS without phenol red (Gibco, Invitrogen, San Diego CA, USA) and grown for 15 days under standard conditions. All spheres

were documented with an 'Olympus IX50' microscope using the 'Color View Soft Image System' controlled by 'cell^P' software (Olympus, Tokio, Japan).

Transwell migration and scratch test assay

Transwell migration assays were performed using modified Boyden chamber units with polycarbonate filters of 8µm porosity (Costar, Vitaris, Switzerland). The lower side of the filter was coated with 25 µg/ml collagen 1 (Sigma, St.Louis, USA) for 2h at 37°C. The bottom chamber was filled with DMEM containing 10% FCS. Cells ($2x10^4$ per well in serum-free DMEM) were plated in the upper chamber in 100µl medium and incubated for 24h in standard conditions. After removal of the remaining cells from the upper surface of the filter insert, migrated cells at the bottom of the filter were fixed with 3.7% formaldehyde in PBS and stained with 0.1% crystal violet. For every individual filter, the cells in 9 fields of view were counted. Every experiment was conducted in triplicates.

For scratch test analysis, cells were grown to ~90% confluency under standard conditions. A wound was inflicted by scratching a 200µl pipette tip (Starlab, Milton Keynes, UK) over the surface of the culture flask. The wounds were documented as described above for the soft agar immediately after scratching, after 24 and 48 hours.

Western blot analysis and antibodies

Cells were grown to 80-90% confluency, washed twice with 1x PBS, lysed in buffer containing 2% sodium dodecyl sulfate (SDS), 50mM Tris pH 6.8, 0.1M dithiothreitol (DTT), boiled at 95°C for 5min and used either immediately or frozen at -20°C. Protein lysates were resolved on denaturing 8-12% SDS-polyacrylamide gels and transferred to nitrocellulose membranes (iBlot Gel transfer stacks, Invitrogen). The following primary antibodies were used: anti-Actin (Sigma-Aldrich, St. Louis, USA), anti-phospho-Akt/PKB and anti-total-Akt/PKB (Ser-473) (Millipore), anti-Akt2/PKBβ (Cell Signaling), anti-DTX1 (ABBiotech), anti-EGFR (Santa Cruz Biotechnology), anti-phospho-Erk and anti-total-Erk (Santa Cruz Biotechnology), anti-Mcl-1 (Santa Cruz Biotechnology), anti-Myc Tag (Millipore) and anti-Snail1 (Abcam). Decorated proteins were revealed using horseradish peroxidase-conjugated anti-mouse, anti-rabbit, anti-rat (New England Biolabs) or anti-goat (Pierce) secondary antibodies and

visualized by the chemoluminescence detection system SuperSignal West Pico (Thermo Scientific).

Microarray analysis of patient biopsies and cell lines

Microarray gene expression analysis of patient biopsies has been reported earlier [20]. This data set was reanalyzed in respect of *DTX1* expression. For cell lines, total RNA was extracted from U373-EGFP, U373-DTX1-myc and U373-MAML1-dn cells in triplicates and amplified once. Samples were hybridized to Affymetrix chips HuGene 1.0 ST v1. The data analysis and gene filtering was performed using R/Bioconductor [45]. Signal condensation was performed using only the RMA from the Bioconductor Affy package. Differentially expressed genes were indentified using the empirical Bayes method (F-test) implemented in the LIMMA package and adjusted with the False Discovery Rate (FDR) method [46]. We selected those probe sets with a log2 average contrast signal of at least 4, an adjusted p value <0.01 and an absolute linear fold change of >2. The gene expression data has been deposited at the Gene Expression Omnibus Databank (accession ID: GSE22772) according to MIAME standards. Hierarchical clustering and visualization was performed in R software. The scripts are available upon request. Assessment of the uncertainty in hierarchical cluster analysis was performed with “pvclust” package as described elsewhere [23] based on all annotated genes or 191 annotated genes specifically alerted by DTX1 as described in the text.

Supplementary Material

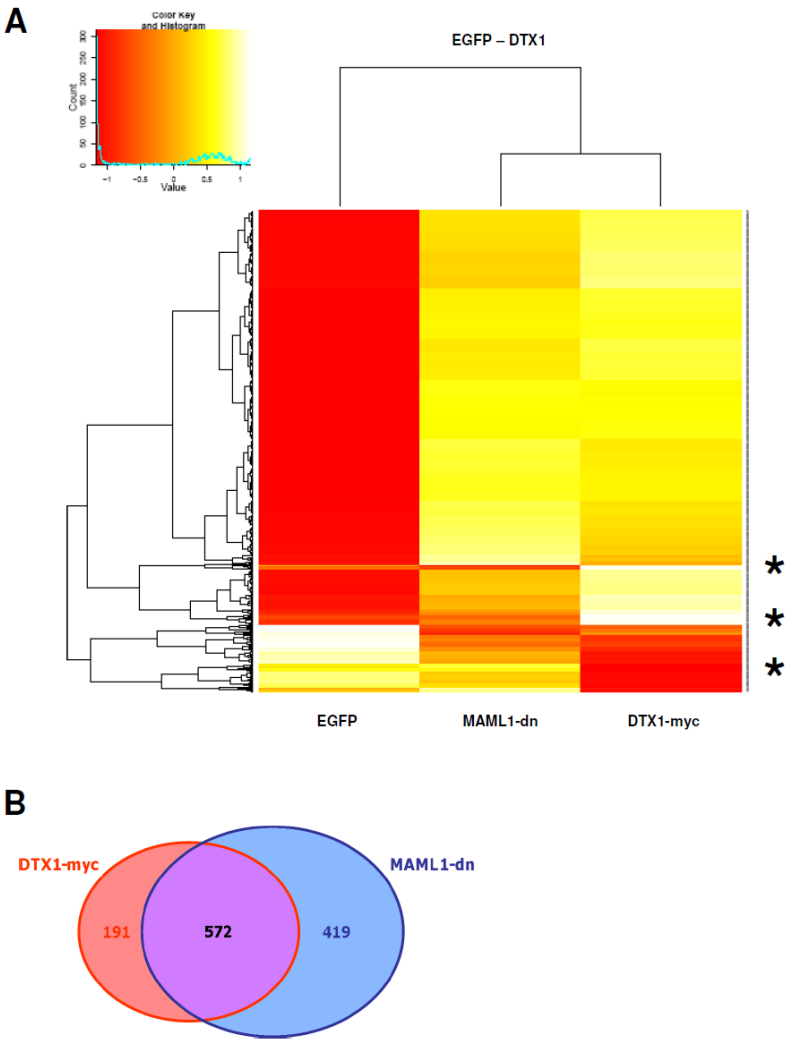

Supplementary Figure 1. Heat map of differential gene expression in glioma cell lines with modified Notch canonical and non-canonical signaling.

(A) Gene expression values are shown as color coded heat map with red representing low and white representing high expression values. The three samples are listed on the x-axis, individual genes on the y-axis. Gene clustering was performed according to similarity in expression pattern. All genes shown are differentially expressed in at least one sample (fold change of expression >2, p-value < 0.01). Asterisks indicate example areas with unique expression patterns in DTX1-myc cells. (B) Venn-Diagram of gene expression analysis. Genes differentially expressed in U373-DTX1-myc are shown in red, genes differentially expressed in U373-MAML1-dn are shown in blue, genes altered in both cell lines are shown in purple.

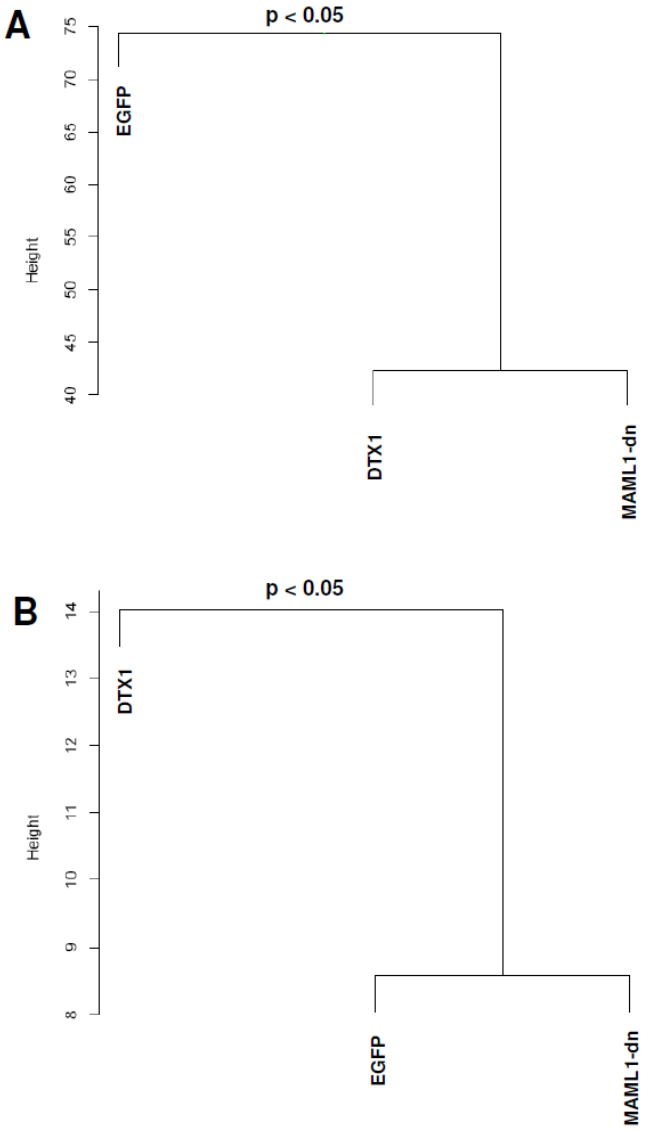

Supplementary Figure 2. Dendrograms based on gene expression profiles of glioma cell lines.

Dendrograms based on the gene expression profiles of the glioma cell lines used visualizing relatedness of samples based on (A) overall gene expression pattern including all 22'000 genes annotated on the microarray and (B) based on the 191 genes indentified to be specifically controlled by DTX1. *p*-values were calculated via multiscale bootstrap resampling.

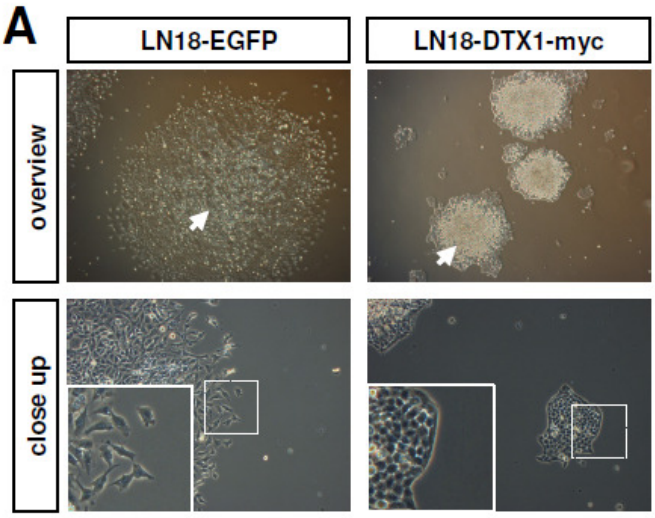

Supplementary Figure 3. Colony size and cell density are changed in LN18-DTX1-myc cells.

(A) Low density seeding colonies shown as light microscopic pictures demonstrating the aggregation phenotype in LN18-DTX1-myc cells. Arrows point to the center of individual colonies indicating the area of aggregation in LN18-DTX1-myc cells. Close up images show borders of colonies at higher magnification.

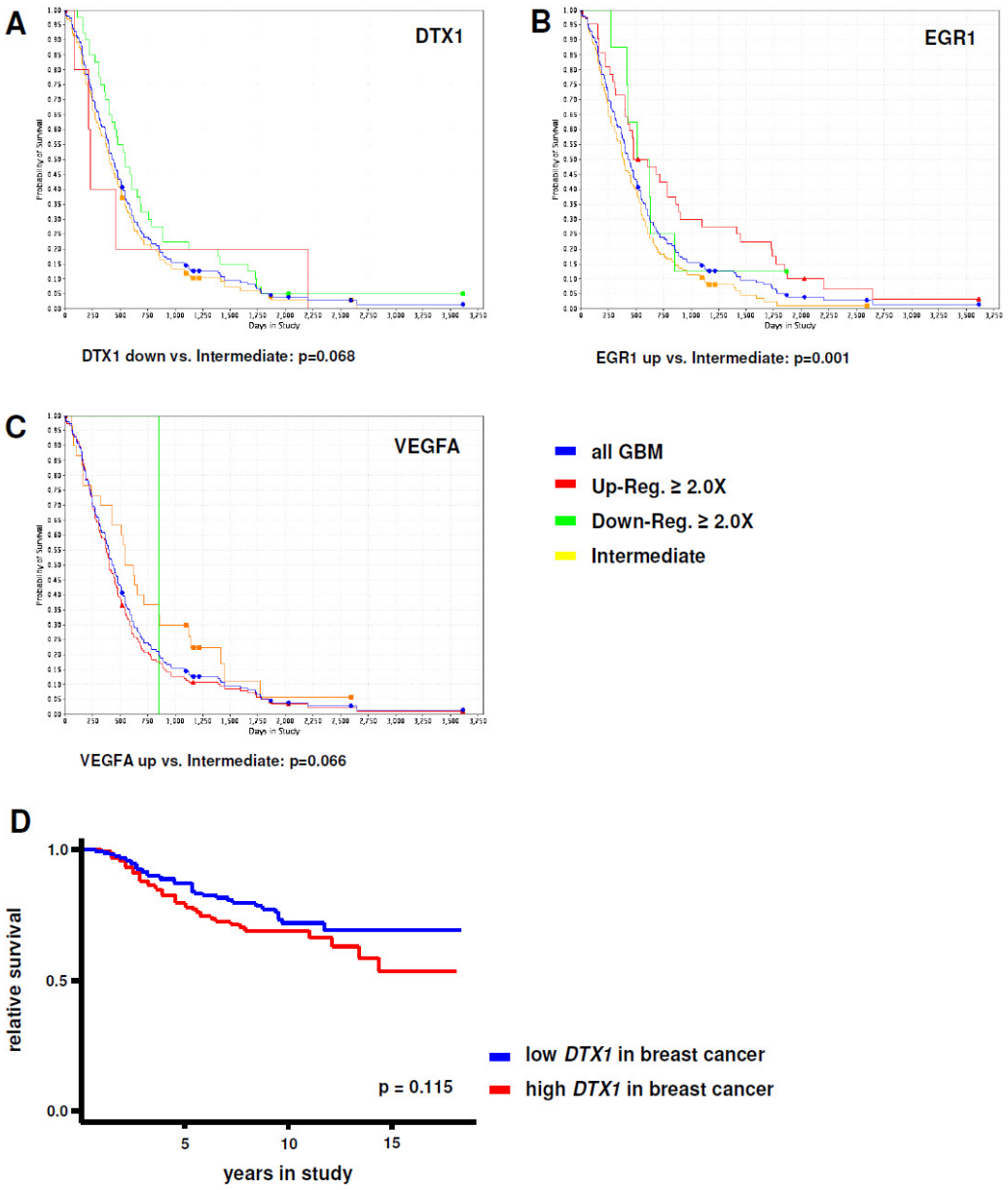

Supplementary Figure 4. Kaplan-Meier survival plots for samples with differential gene expression in GBM and early breast cancer.

Survival plots based on the expression levels of *DTX1*, *PKBβ*, *Snail-1*, and *EGR1* in color coded graphs. Red: up regulated by 2 fold or more; green: down regulated by 2 fold or more; yellow: intermediate gene expression. P-values for all four samples up to 1'500 days in study are below 0.05 . Data derived form the Repository for Molecular Brain Neoplasia Data, NCI, NIH.

SupplementaryTable 1

number of genes changed in DTX1-myc cells	
up regulated in DTX1 vs. EGFP	665
down regulated in DTX1 vs. EGFP	98
number of genes changed in MAML1-dn cells	
up regulated in MAML1-dn vs. EGFP	872
down regulated in MAML1-dn vs. EGFP	119
number of genes commonly changed in both cell lines	
up regulated in DTX1 and MAML1-dn vs. EGFP	542
down regulated in DTX1 and MAML1-dn vs. EGFP	30
number of genes uniquely changed in DTX1-myc cells	
up regulated in DTX1 vs. EGFP and MAML1-dn	121
down regulated in DTX1 vs. EGFP and MAML1-dn	70

Supplementary Table 2

number of genes per gene onthology class		
metabolic process	23	12%
signal transduction	22	12%
cell cycle	15	8%
transcription	14	7%
intracellular transport	14	7%
protein modification process	13	7%
cell motion	6	3%
cell adhesion / extra cellular matrix	5	3%
cell homeostasis	5	3%
apoptosis	4	2%
immune response	3	2%
translation	3	2%
others	41	21%
n/a	23	12%

Supplementary Table 3

Accession ID	Gene Symbol	Protein Name	log FC
NM_004416	*DTX1*	*deltex homolog 1*	*5.56*
NM_001305	CLDN4	claudin 4	4.49
NM_006988	ADAMTS1	ADAM metallopeptidase with thrombospondin type 1 motif, 1	2.16
NM_016542	RP6-213H19.1	serine/threonine protein kinase MST4	2.02
NM_000465	BARD1	BRCA1 associated RING domain 1	1.91
NM_000047	ARSE	arylsulfatase E (chondrodysplasia punctata 1)	1.80
NM_018165	PBRM1	polybromo 1	1.68
NM_153020	RBM24	RNA binding motif protein 24	1.62
NM_000339	SLC12A3	solute carrier family 12 (sodium/chloride transporters), member 3	1.62
NM_005264	GFRA1	GDNF family receptor alpha 1	1.58
NM_001992	F2R	coagulation factor II (thrombin) receptor	1.57
NM_001786	CDC2	cell division cycle 2, G1 to S and G2 to M	1.56
NM_024639	ZNF322A	zinc finger protein 322A	1.54
NM_006625	FUSIP1	FUS interacting protein (serine/arginine-rich) 1	1.54
NM_016816	OAS1	2',5'-oligoadenylate synthetase 1, 40/46kDa	1.54
NM_004523	KIF11	kinesin family member 11	1.53
NM_018303	EXOC2	exocyst complex component 2	1.53
NM_000138	FBN1	fibrillin 1	1.52
AY699265	MIRN21	microRNA 21	1.51
NM_198098	AQP1	aquaporin 1 (Colton blood group)	1.51
NM_019054	FAM35A	family with sequence similarity 35, member A	1.49
NM_012334	MYO10	myosin X	1.44
BC010491	C2orf59	chromosome 2 open reading frame 59	1.43
NM_007112	THBS3	thrombospondin 3	1.41
NM_007027	TOPBP1	topoisomerase (DNA) II binding protein 1	1.41
NM_013352	DSE	dermatan sulfate epimerase	1.39
NM_006317	BASP1	brain abundant, membrane attached signal protein 1	1.38
NM_053276	VIT	vitrin	1.37
NM_001018159	NAE1	NEDD8 activating enzyme E1 subunit 1	1.35
NM_015446	AHCTF1	AT hook containing transcription factor 1	1.34
NM_015255	UBR2	ubiquitin protein ligase E3 component n-recognin 2	1.33
NM_014333	CADM1	cell adhesion molecule 1	1.32
NM_014363	SACS	spastic ataxia of Charlevoix-Saguenay (sacsin)	1.32
NM_018131	CEP55	centrosomal protein 55kDa	1.31
NM_007296	BRCA1	breast cancer 1, early onset	1.31
NM_002806	PSMC6	proteasome (prosome, macropain) 26S subunit, ATPase, 6	1.31
NM_005124	NUP153	nucleoporin 153kDa	1.30
NM_022113	KIF13A	kinesin family member 13A	1.29
NM_018243	SEPT11	septin 11	1.27
NM_005559	LAMA1	laminin, alpha 1	1.26
NM_014783	ARHGAP11A	Rho GTPase activating protein 11A	1.26
NM_003358	UGCG	UDP-glucose ceramide glucosyltransferase	1.25
NM_015382	HECTD1	HECT domain containing 1	1.25
NM_015295	SMCHD1	structural maintenance of chromosomes flexible hinge domain containing 1	1.25
NM_012096	APPL1	adaptor protein, phosphotyrosine interaction, PH domain and leucine zipper containing 1	1.24

NM_024776	SGK269	NKF3 kinase family member	1.24
NM_133265	AMOT	angiomotin	1.23
NM_032485	MCM8	minichromosome maintenance complex component 8	1.23
NM_003107	SOX4	SRY (sex determining region Y)-box 4	1.22
NM_002806	PSMC6	proteasome (prosome, macropain) 26S subunit, ATPase, 6	1.22
NM_014969	WDR47	WD repeat domain 47	1.22
NM_005385	NKTR	natural killer-tumor recognition sequence	1.20
NM_001204	BMPR2	bone morphogenetic protein receptor, type II (serine/threonine kinase)	1.19
NM_080927	DCBLD2	discoidin, CUB and LCCL domain containing 2	1.19
NM_007235	XPOT	exportin, tRNA (nuclear export receptor for tRNAs)	1.18
NM_012124	CHORDC1	cysteine and histidine-rich domain (CHORD)-containing 1	1.18
NM_006638	RPP40	ribonuclease P/MRP 40kDa subunit	1.18
NM_001797	CDH11	cadherin 11, type 2, OB-cadherin (osteoblast)	1.17
NM_001128205	SULF1	sulfatase 1	1.17
NM_005160	ADRBK2	adrenergic, beta, receptor kinase 2	1.17
NM_016513	ICK	intestinal cell (MAK-like) kinase	1.16
NM_020319	ANKMY2	ankyrin repeat and MYND domain containing 2	1.16
NM_001821	CHML	choroideremia-like (Rab escort protein 2)	1.16
NM_022841	RFX7	regulatory factor X, 7	1.16
NM_019054	FAM35A	family with sequence similarity 35, member A	1.16
NM_138771	CCDC126	coiled-coil domain containing 126	1.15
NM_015199	ANKRD28	ankyrin repeat domain 28	1.15
NM_015446	AHCTF1	AT hook containing transcription factor 1	1.15
NM_004162	RAB5A	RAB5A, member RAS oncogene family	1.15
NM_017437	CPSF2	cleavage and polyadenylation specific factor 2, 100kDa	1.14
NM_001042517	DIAPH3	diaphanous homolog 3 (Drosophila)	1.14
NM_015384	NIPBL	Nipped-B homolog (Drosophila)	1.13
NM_001624	AIM1	absent in melanoma 1	1.12
NM_005246	FER	fer (fps/fes related) tyrosine kinase	1.12
NM_007159	SLMAP	sarcolemma associated protein	1.11
NM_003238	TGFB2	transforming growth factor, beta 2	1.11
NM_006708	GLO1	glyoxalase I	1.11
NM_178862	STT3B	STT3, subunit of the oligosaccharyltransferase complex, homolog B	1.10
NM_001025366	VEGFA	vascular endothelial growth factor A	1.10
NM_013296	GPSM2	G-protein signaling modulator 2 (AGS3-like, C. elegans)	1.09
NM_002759	EIF2AK2	eukaryotic translation initiation factor 2-alpha kinase 2	1.09
NM_003341	UBE2E1	ubiquitin-conjugating enzyme E2E 1 (UBC4/5 homolog, yeast)	1.08
NM_080546	SLC44A1	solute carrier family 44, member 1	1.08
NM_015092	SMG1	PI-3-kinase-related kinase SMG-1	1.08
NM_003368	USP1	ubiquitin specific peptidase 1	1.08
NM_022459	XPO4	exportin 4	1.07
NM_003798	CTNNAL1	catenin (cadherin-associated protein), alpha-like 1	1.06
NM_199132	ZNF468	zinc finger protein 468	1.06
NM_005746	NAMPT	nicotinamide phosphoribosyltransferase	1.06
NM_003162	STRN	striatin, calmodulin binding protein	1.06
NM_003659	AGPS	alkylglycerone phosphate synthase	1.05
NM_024769	ASAM	adipocyte-specific adhesion molecule	1.05
AK295862	KIAA0528	KIAA 0528	1.05
NM_021038	MBNL1	muscleblind-like (Drosophila)	1.04
NM_007085	FSTL1	follistatin-like 1	1.04
NM_012158	FBXL3	F-box and leucine-rich repeat protein 3	1.04
NM_001123390	TBC1D3H	TBC1 domain family, member 3H	1.04
NM_005921	MAP3K1	mitogen-activated protein kinase kinase kinase 1	1.04

NM_019024	HEATR5B	HEAT repeat containing 5B	1.04
NM_012253	TKTL1	transketolase-like 1	1.04
NM_018010	IFT57	intraflagellar transport 57 homolog (Chlamydomonas)	1.03
NM_006101	NDC80	NDC80 homolog, kinetochore complex component	1.03
NM_020165	RAD18	RAD18 homolog (S. cerevisiae)	1.03
NM_020923	ZDBF2	zinc finger, DBF-type containing 2	1.03
ENST00000321331	HIGD1A	HIG1 domain family, member 1A	1.03
NM_015054	UHRF1BP1L	UHRF1 binding protein 1-like	1.03
NM_153362	PRSS35	protease, serine, 35	1.02
NM_000213	ITGB4	integrin, beta 4	1.02
NM_006355	TRIM38	tripartite motif-containing 38	1.02
AK094159	FLJ36840	hypothetical LOC645524	1.02
NM_015097	CLASP2	cytoplasmic linker associated protein 2	1.02
NM_206855	QKI	quaking homolog, KH domain RNA binding (mouse)	1.01
ENST00000379607	EIF1AX	eukaryotic translation initiation factor 1A, X-linked	1.01
NM_001113546	LIMA1	LIM domain and actin binding 1	1.01
NM_175866	UHMK1	U2AF homology motif (UHM) kinase 1	1.01
ENST00000308482	LRRFIP1	leucine rich repeat (in FLII) interacting protein 1	1.01
NM_017801	CMTM6	CKLF-like MARVEL transmembrane domain containing 6	1.01
NM_001024457	RGPD1	RANBP2-like and GRIP domain containing 1	1.01
NM_001257	CDH13	cadherin 13, H-cadherin (heart)	1.01
NM_020748	INTS2	integrator complex subunit 2	1.00
NM_174942	GAS2L3	growth arrest-specific 2 like 3	1.00
NM_000693	ALDH1A3	aldehyde dehydrogenase 1 family, member A3	-1.00
NM_000014	A2M	alpha-2-macroglobulin	-1.01
BC043250	LOC732275	similar to hCG1645603	-1.02
NM_016234	ACSL5	acyl-CoA synthetase long-chain family member 5	-1.02
NM_001114618	MGAT1	mannosyl (alpha-1,3-)-glycoprotein beta-1,2-N-acetylglucosaminyltransferase	-1.04
NM_014365	HSPB8	heat shock 22kDa protein 8	-1.04
NM_005252	FOS	v-fos FBJ murine osteosarcoma viral oncogene homolog	-1.04
NM_001772	CD33	CD33 molecule	-1.05
NM_033549	TRIM41	tripartite motif-containing 41	-1.05
NM_012410	SEZ6L2	seizure related 6 homolog (mouse)-like 2	-1.05
NM_001964	EGR1	early growth response 1	-1.06
NM_001217	CA11	carbonic anhydrase XI	-1.06
NM_003009	SEPW1	selenoprotein W, 1	-1.07
NM_022170	EIF4H	eukaryotic translation initiation factor 4H	-1.08
NM_006598	SLC12A7	solute carrier family 12 (potassium/chloride transporters), member 7	-1.08
NM_000155	GALT	galactose-1-phosphate uridylyltransferase	-1.09
NM_030964	SPRY4	sprouty homolog 4 (Drosophila)	-1.10
NM_004041	ARRB1	arrestin, beta 1	-1.10
NM_018192	LEPREL1	leprecan-like 1	-1.11
NM_000358	TGFBI	transforming growth factor, beta-induced, 68kDa	-1.12
NM_012306	FAIM2	Fas apoptotic inhibitory molecule 2	-1.12
NM_002231	CD82	CD82 molecule	-1.13
AK302783	LOC728212	hypothetical LOC728212	-1.14
NM_024615	PARP8	poly (ADP-ribose) polymerase family, member 8	-1.14
NM_018044	NSUN5	NOL1/NOP2/Sun domain family, member 5	-1.15
NM_016086	STYXL1	serine/threonine/tyrosine interacting-like 1	-1.15
NM_032564	DGAT2	diacylglycerol O-acyltransferase homolog 2 (mouse)	-1.17
NM_006435	IFITM2	interferon induced transmembrane protein 2 (1-8D)	-1.17
NM_004283	RAB3D	RAB3D, member RAS oncogene family	-1.17
NM_198282	TMEM173	transmembrane protein 173	-1.18

NM_018110	DOK4	docking protein 4	-1.18
NM_020645	NRIP3	nuclear receptor interacting protein 3	-1.22
NM_002607	PDGFA	platelet-derived growth factor alpha polypeptide	-1.23
NM_173619	MGC34761	hypothetical protein MGC34761	-1.23
NM_145662	SPANXA2	SPANX family, member A2	-1.26
NM_001036	RYR3	ryanodine receptor 3	-1.26
NM_015253	WSCD1	WSC domain containing 1	-1.27
NM_001946	DUSP6	dual specificity phosphatase 6	-1.28
NM_005582	CD180	CD180 molecule	-1.30
NM_000170	GLDC	glycine dehydrogenase (decarboxylating)	-1.30
NM_001164	APBB1	amyloid beta (A4) precursor protein-binding, family B, member 1 (Fe65)	-1.32
BC033537	KIAA1576	KIAA1576 protein	-1.34
NM_001020818	MYADM	myeloid-associated differentiation marker	-1.35
NM_024022	TMPRSS3	transmembrane protease, serine 3	-1.37
NM_003283	TNNT1	troponin T type 1 (skeletal, slow)	-1.38
NM_021939	FKBP10	FK506 binding protein 10, 65 kDa	-1.38
NM_002065	GLUL	glutamate-ammonia ligase (glutamine synthetase)	-1.39
NM_173357	SSX6	synovial sarcoma, X breakpoint 6	-1.45
NM_020826	SYT13	synaptotagmin XIII	-1.45
AK058065	LOC100128840	hypothetical protein LOC100128840	-1.50
NM_001089	ABCA3	ATP-binding cassette, sub-family A (ABC1), member 3	-1.51
NM_000852	GSTP1	glutathione S-transferase pi 1	-1.51
AF503509	C1orf32	chromosome 1 open reading frame 32	-1.52
NM_052896	CSMD2	CUB and Sushi multiple domains 2	-1.52
NM_004530	MMP2	matrix metallopeptidase 2 (gelatinase A, 72kDa gelatinase, 72kDa type IV collagenase)	-1.54
NM_005330	HBE1	hemoglobin, epsilon 1	-1.58
NM_002606	PDE9A	phosphodiesterase 9A	-1.60
NM_014244	ADAMTS2	ADAM metallopeptidase with thrombospondin type 1 motif, 2	-1.70
NM_002346	LY6E	lymphocyte antigen 6 complex, locus E	-1.72
NM_020422	TMEM159	transmembrane protein 159	-1.72
NM_003811	TNFSF9	tumor necrosis factor (ligand) superfamily, member 9	-1.82
NR_002223	TPRXL	tetra-peptide repeat homeobox-like	-1.84
NM_001040058	SPP1	secreted phosphoprotein 1	-1.90
NM_001354	AKR1C2	aldo-keto reductase family 1, member C2	-2.05
AY513283	GLUL	glutamate-ammonia ligase (glutamine synthetase)	-2.12
NM_012188	FOXI1	forkhead box I1	-2.39
NM_001958	EEF1A2	eukaryotic translation elongation factor 1 alpha 2	-2.48
NM_003835	RGS9	regulator of G-protein signaling 9	-2.65
NM_001175	ARHGDIB	Rho GDP dissociation inhibitor (GDI) beta	-2.75
NM_001025195	CES1	carboxylesterase 1 (monocyte/macrophage serine esterase 1)	-3.06

Acknowledgement

We thank Beatrice Dolder, Jacqueline Rauch, Marie-Christine Müller and Elisabeth Taylor for excellent technical assistance; Prof. Kimie Ohta for valuable reagents; Tim Roloff for microarray analysis and bioinformatics; Jan Tchorz, Michal Grzmil and Gerald Moncayo for helpful comments throughout the project. This work was supported by Oncosuisse (grant # KFP OCS-01613-12-2004).

References

1. Ohgaki, H. and P. Kleihues, *Epidemiology and etiology of gliomas.* Acta Neuropathol, 2005. **109**(1): p. 93-108.
2. Stupp, R. and D.C. Weber, *The role of radio- and chemotherapy in glioblastoma.* Onkologie, 2005. **28**(6-7): p. 315-7.
3. Dotto, G.P., *Crosstalk of Notch with p53 and p63 in cancer growth control.* Nat Rev Cancer, 2009. **9**(8): p. 587-95.
4. Artavanis-Tsakonas, S., M.D. Rand, and R.J. Lake, *Notch signaling: cell fate control and signal integration in development.* Science, 1999. **284**(5415): p. 770-6.
5. Purow, B.W., et al., *Expression of Notch-1 and its ligands, Delta-like-1 and Jagged-1, is critical for glioma cell survival and proliferation.* Cancer Res, 2005. **65**(6): p. 2353-63.
6. Boulay, J.L., et al., *Loss of NOTCH2 positively predicts survival in subgroups of human glial brain tumors.* PLoS One, 2007. **2**(6): p. e576.
7. Zamecnik, J., *The extracellular space and matrix of gliomas.* Acta Neuropathol, 2005. **110**(5): p. 435-42.
8. Sivasankaran, B., et al., *Tenascin-C is a novel RBPJkappa-induced target gene for Notch signaling in gliomas.* Cancer Res, 2009. **69**(2): p. 458-65.
9. Lino, M. and A. Merlo, *Translating biology into clinic: the case of glioblastoma.* Curr Opin Cell Biol, 2009. **21**(2): p. 311-6.
10. Matsuno, K., et al., *Deltex acts as a positive regulator of Notch signaling through interactions with the Notch ankyrin repeats.* Development, 1995. **121**(8): p. 2633-44.
11. Mukherjee, A., et al., *Regulation of Notch signalling by non-visual beta-arrestin.* Nat Cell Biol, 2005. **7**(12): p. 1191-201.
12. Liu, W.H. and M.Z. Lai, *Deltex regulates T-cell activation by targeted degradation of active MEKK1.* Mol Cell Biol, 2005. **25**(4): p. 1367-78.
13. Hu, Q.D., et al., *F3/contactin acts as a functional ligand for Notch during oligodendrocyte maturation.* Cell, 2003. **115**(2): p. 163-75.
14. Hu, Q.D., et al., *Axoglial interaction via the notch receptor in oligodendrocyte differentiation.* Ann Acad Med Singapore, 2004. **33**(5): p. 581-8.
15. Eiraku, M., et al., *DNER acts as a neuron-specific Notch ligand during Bergmann glial development.* Nat Neurosci, 2005. **8**(7): p. 873-80.
16. Brennan, K. and P. Gardner, *Notching up another pathway.* Bioessays, 2002. **24**(5): p. 405-10.
17. Martinez Arias, A., V. Zecchini, and K. Brennan, *CSL-independent Notch signalling: a checkpoint in cell fate decisions during development?* Curr Opin Genet Dev, 2002. **12**(5): p. 524-33.
18. Yamamoto, N., et al., *Role of Deltex-1 as a transcriptional regulator downstream of the Notch receptor.* J Biol Chem, 2001. **276**(48): p. 45031-40.
19. Ramain, P., et al., *Novel Notch alleles reveal a Deltex-dependent pathway repressing neural fate.* Curr Biol, 2001. **11**(22): p. 1729-38.
20. Korur, S., et al., *GSK3beta regulates differentiation and growth arrest in glioblastoma.* PLoS One, 2009. **4**(10): p. e7443.
21. Ishii, N., et al., *Frequent co-alterations of TP53, p16/CDKN2A, p14ARF, PTEN tumor suppressor genes in human glioma cell lines.* Brain Pathol, 1999. **9**(3): p. 469-79.

22. Grzmil, M. and B.A. Hemmings, *Deregulated signalling networks in human brain tumours.* Biochim Biophys Acta, 2010. **1804**(3): p. 476-83.
23. Suzuki, R. and H. Shimodaira, *Pvclust: an R package for assessing the uncertainty in hierarchical clustering.* Bioinformatics, 2006. **22**(12): p. 1540-2.
24. Papagiannakopoulos, T., A. Shapiro, and K.S. Kosik, *MicroRNA-21 targets a network of key tumor-suppressive pathways in glioblastoma cells.* Cancer Res, 2008. **68**(19): p. 8164-72.
25. Joy, A.M., et al., *Migrating glioma cells activate the PI3-K pathway and display decreased susceptibility to apoptosis.* J Cell Sci, 2003. **116**(Pt 21): p. 4409-17.
26. Zhang, B., et al., *Reduction of Akt2 inhibits migration and invasion of glioma cells.* Int J Cancer, 2009. **125**(3): p. 585-95.
27. Strippoli, R., et al., *Epithelial-to-mesenchymal transition of peritoneal mesothelial cells is regulated by an ERK/NF-kappaB/Snail1 pathway.* Dis Model Mech, 2008. **1**(4-5): p. 264-74.
28. Gabriely, G., et al., *MicroRNA 21 promotes glioma invasion by targeting matrix metalloproteinase regulators.* Mol Cell Biol, 2008. **28**(17): p. 5369-80.
29. van de Vijver, M.J., et al., *A gene-expression signature as a predictor of survival in breast cancer.* N Engl J Med, 2002. **347**(25): p. 1999-2009.
30. Stockhausen, M.T., K. Kristoffersen, and H.S. Poulsen, *The functional role of Notch signaling in human gliomas.* Neuro Oncol, 2010. **12**(2): p. 199-211.
31. Zhang, P., et al., *Regulation of NOTCH signaling by reciprocal inhibition of HES1 and Deltex 1 and its role in osteosarcoma invasiveness.* Oncogene, 2010. **29**(20): p. 2916-26.
32. Oishi, K., et al., *Notch promotes survival of neural precursor cells via mechanisms distinct from those regulating neurogenesis.* Dev Biol, 2004. **276**(1): p. 172-84.
33. Zohrabian, V.M., et al., *Rho/ROCK and MAPK signaling pathways are involved in glioblastoma cell migration and proliferation.* Anticancer Res, 2009. **29**(1): p. 119-23.
34. Lakka, S.S., et al., *Downregulation of MMP-9 in ERK-mutated stable transfectants inhibits glioma invasion in vitro.* Oncogene, 2002. **21**(36): p. 5601-8.
35. Selcuklu, S.D., M.T. Donoghue, and C. Spillane, *miR-21 as a key regulator of oncogenic processes.* Biochem Soc Trans, 2009. **37**(Pt 4): p. 918-25.
36. Huang, T.H., et al., *Up-regulation of miR-21 by HER2/neu signaling promotes cell invasion.* J Biol Chem, 2009. **284**(27): p. 18515-24.
37. Yoo, A.S. and I. Greenwald, *LIN-12/Notch activation leads to microRNA-mediated down-regulation of Vav in C. elegans.* Science, 2005. **310**(5752): p. 1330-3.
38. Patterson, K.I., et al., *Dual-specificity phosphatases: critical regulators with diverse cellular targets.* Biochem J, 2009. **418**(3): p. 475-89.
39. Mitsuuchi, Y., et al., *Identification of a chromosome 3p14.3-21.1 gene, APPL, encoding an adaptor molecule that interacts with the oncoprotein-serine/threonine kinase AKT2.* Oncogene, 1999. **18**(35): p. 4891-8.
40. Ordentlich, P., et al., *Notch inhibition of E47 supports the existence of a novel signaling pathway.* Mol Cell Biol, 1998. **18**(4): p. 2230-9.
41. Cui, X.Y., et al., *NB-3/Notch1 pathway via Deltex1 promotes neural progenitor cell differentiation into oligodendrocytes.* J Biol Chem, 2004. **279**(24): p. 25858-65.
42. Hsiao, H.W., et al., *Deltex1 is a target of the transcription factor NFAT that promotes T cell anergy.* Immunity, 2009. **31**(1): p. 72-83.

43. Oliver, T.G., et al., *Transcriptional profiling of the Sonic hedgehog response: a critical role for N-myc in proliferation of neuronal precursors.* Proc Natl Acad Sci U S A, 2003. **100**(12): p. 7331-6.
44. Suzuki, K., et al., *Napthalimidobenzamide DB-51630: a novel DNA binding agent inducing p300 gene expression and exerting a potent anti-cancer activity.* Bioorg Med Chem, 2005. **13**(12): p. 4014-21.
45. Gentleman, R.C., et al., *Bioconductor: open software development for computational biology and bioinformatics.* Genome Biol, 2004. **5**(10): p. R80.
46. Wettenhall, J.M. and G.K. Smyth, *limmaGUI: a graphical user interface for linear modeling of microarray data.* Bioinformatics, 2004. **20**(18): p. 3705-6.

Part 2

In vivo evaluation of targeted glioma therapies in orthotopic and ectopic glioma models.

thesis chapter, 2011

Roland M. Huber[1,2], Deborah Hynx[2], Brian A. Hemmings[2], Adrian Merlo[1]

1) Laboratory of Molecular Neuro-Oncology, University Hospital Basel, Basel, Switzerland

2) Friedrich Miescher Institute for Biomedical Research, Basel, Switzerland

Summary

High grade gliomas (HGG) are tumors of the central nervous system with unmet medical needs. Grade IV HGG, known as *glioblastoma multiforme* (GBM), are rapidly growing and highly infiltrative, making large volume tumor resection and irradiation impossible. Effective chemo/bio-therapeutic strategies which can be applied systemically and reach all tumor cells irrespective of their localization are therefore urgently needed. Previous work in our lab has identified a combination of histone deacetylase inhibitors (HDI) and glycolysis inhibitor 2-deoxy-D-glucose (2DG) as potent strategy inducing cell death in glioma and other cancer cell lines *in vitro*. The synergistic effects of epigenetic remodulation of cancer cells paralleled by energy deprivation induced apoptosis at high levels without negative effects on control cells. Here we report the evaluation of this combination therapy in an *in vivo* model of GBM. Treatment of orthotopic glioma in nude mice with high levels of 2DG in combination with the HDI sodium butyrate (NaB) significantly reduced tumor growth without detectable side effects. Treated tumors displayed areas of necrosis not found in control tumors and increased levels of apoptosis. In contrast, these were not found in control tumors. Overall, the combinatorial use of HDIs and 2DG has anti-tumor properties *in vivo*. We suggest this therapy to be evaluated in a clinical setting in order to determine the efficacy in HGG patients.

Introduction

The treatment of malignant high grade gliomas consists of three major lines of attack. The late detection of most gliomas and the fast growth rate make surgical resection of the tumor bulk, which leads to increased intracranial pressure, imperative in basically all cases. Removal of the tumor mass alleviates neurological symptoms. However, given the highly infiltrative phenotype of gliomas and GBMs in particular, a complete surgical resection is not possible and recurrence is usually the case within a 2 cm margin of the original tumor edge in 95% of cases [1]. The second line of attack is radiotherapy, which can be applied both before (experimental) and after surgery (standard). Preoperative irradiation helps to demarcate the tumor-brain border and facilitates surgical resection. Postoperative irradiation mainly aims at eradicating residual tumor cells adjacent to the resection site or even in whole brain applications. The side effects of whole brain irradiation can be substantial, particularly in young patients. Radio-sensitizers, such as temozolomide, and occasionally 2-deoxy-D-glucose, are applied to increase the effectiveness of radiotherapy [2]. Thirdly, glioma patients are treated with chemotherapy aiming at eliminating residual tumor cells. The drug most commonly used is the DNA-alkylating agent Temozolomide, which is also used as a radio-sensitizer. However, the effectiveness of this compound is under intense debate [3].

Numerous potential drug targets and therapeutic compounds targeting GBM cells have been published. However, no therapy which improved patient prognosis by more than a few weeks has been reported up to date [3]. A major bottleneck hampering progress is the translation of *in vitro* into *in vivo* results. This still is a prerequisite for any clinical trial although *in vivo* models of GBM have proven to be of poor prognostic value for the effectiveness in patients [4]. We aimed at establishing an *in vivo* GBM model enabling us to evaluate our previous *in vitro* data and to potentially provide *in vivo* data for subsequent clinical trials. We choose a model of human glioma cells (U87MG) transfected with firefly luciferase which can be implanted into immuno-compromised nude mice [6]. The tumor can be visualized by injecting luciferin which will be cleaved by the luciferase enzyme in a luminescent reaction. The cleaving of luciferin sets photons free which can be recorded with super-sensitive digital cameras. It was shown, that tumor size is reliably represented by the bioluminescence of the implant, making tumor measurement very quick and comparatively

easy [5]. Furthermore, the treatment effects can be evaluated in human tumor cells, however in an artificial environment without an operative adaptive immune system. Immunological effects are therefore absent in this setting. On the other hand, using a model well established in the field make the results comparable to other studies.

We previously reported a study on the use of Histone Deacetylase Inhibitors (HDI) in combination with 2-deoxy-D-glucose as a potential cancer therapy [6]. Because HDIs induce re-expression of tumor suppressor genes in several distinct pathways [6] and cancer cells critically depend upon continuous energy supply, we explored the therapeutic potential of a combination of these two compounds that simultaneously target the epigenetic status and the energy demand of cancer cells. Synergistic effects may even allow reducing the drug dosage of potentially toxic HDIs [7] although HDIs of the new generation are well tolerated [11]. We found that the combination of 2-DG and HDIs lead to a strong synergistic effect resulting in widespread apoptosis of tumor cells of the brain, breast, and cervix, while sparing normal rat astrocytes *in vitro* [6].

The aim of the study reported here was: i) to evaluate the *in vivo* efficacy of the HDI + 2DG combination therapy as chemo-therapeutic approach targeting gliomas *in vivo*, ii) asses the toxic effects of the combination therapy on the host animal, and iii) compare the anti-tumor potential of selected dosing regimens and drug concentrations. We show that HDI (sodium butyrate) in combination with 2DG applied at high concentration for 4 consecutive days significantly reduces tumor growth *in vivo* without having acute toxic effects. We suggested the treatment of high grade gliomas with the HDI + 2DG combination therapy as a novel strategy which should be evaluated in a clinical setting.

Results

Bioluminescence of different glioma cell lines expressing firefly luciferase analyzed for *in vivo* suitability

A bioluminescent cell line used for tumor growth analysis needs to meet several criteria: i) the cell line has to be tumorigenic in the host animal, particularly at the site of implantation (subcutaneous, in the brain, etc.), ii) BL has to be a reliable representation of tumor size, and iii) the generated tumor should closely reproduce the original tumor histologically, anatomically, and biochemically. The well established cell line U87-luc [7] routinely used in orthotopic *in vivo* GBM models meets most of these requirements, except that it does not generate a tumor with particular GBM-like histology. We therefore aimed at generating luciferase expressing cell lines derived from GBMs attempting to generate a model which would reflect the clinical situation more precisely. We transfected U373 and LN18 cells with a luciferase expression vector, and analyzed individual, stable clones in respect of their suitability as an orthotopic glioma model.

U87-luc cells show linear correlation of BL and cell number (Figure 1, A) and a linear correlation of signal intensity and tumor size *in vivo* was reported previously [5]. This cell line was used as reference in the subsequent analysis. Stable U373-luc and LN18-luc clones were analyzed for luciferase expression by Western blot analysis (Figure 1, B) and clones with high Luc-protein levels were evaluated in a luminometer (Figure 1, C). Four clones showed linear correlation over a wide concentration range and were therefore used in pilot orthotopic *in vivo* experiments. Only one clone (U373-pLuc) resulted in detectable tumors. However, BL was only significantly above background levels 5-8 days prior to the onset of illness in the host animal; a time period which does not allow to perform adequate experiments. In comparison, U87-luc cells are detectable 5-7 days post implantation with an observation period of up to 35 days prior to the onset of symptoms. The late signal detection could be explained by the lower Luc activity in the newly generated cell lines (Figure 1, D). The subsequent experiments were therefore performed with the reference cell line U87-luc.

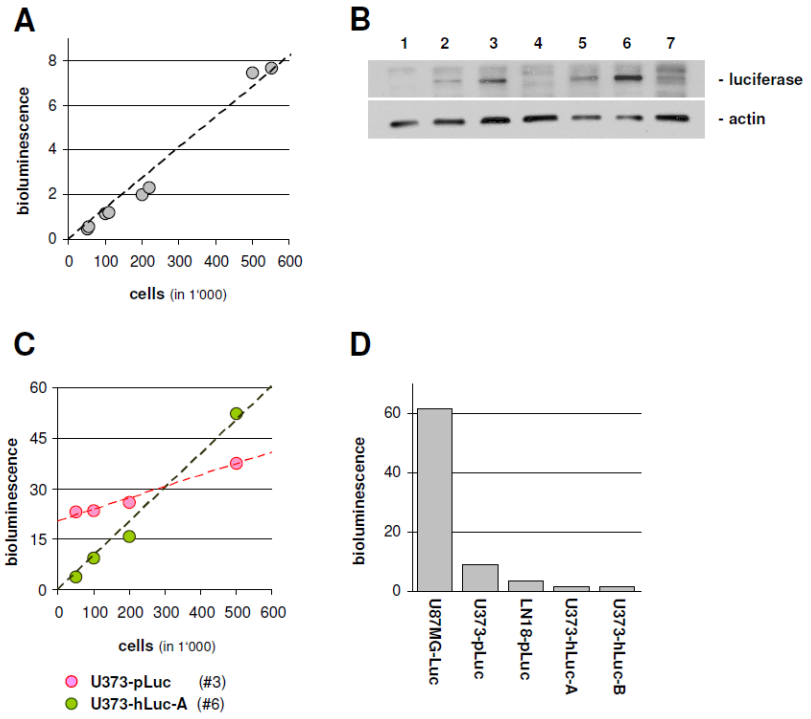

Figure 1. Bioluminescence of different luciferase transfected glioma cell lines

(A) BL of U87-luc cells. Dashed line shows best-fit curve (R^2 = 0.9744) demonstrating linear proportionality of BL and cell numbers. (B) Western blot probing for luciferase in transfected U373 cells. Seven stable clones are shown. (C) BL of clones #3 and #6 from (B) are shown. Dashed lines show best fit curve (R^2 > 0.98) indicating direct proportionality between BL and cell numbers. (D) BL of different glioma cell lines transfected with luciferase compared to U87-luc reference cell line. 5x10^5 cells were measured each. BL is shown on an arbitrary scale corresponding to photons/time in panels (A), (C) and (D).

Orthotopic U87-luc tumors show exponential growth in the brains of *Foxn1^{nu}* nude mice

Nude mice (Crl:Nu) were implanted with 5*10^5 U87-luc cells in 10µl of sterile PBS 3mm caudal and 2mm lateral to the bregma of the scull and 3mm below the dura. After 7 days of recovery, the animals were injected with the luciferin substrate and analyzed in an *in vivo* bioluminescence imager (Figure S1, A-E). Unchallenged growth resulted in exponential signal increase in asymptomatic host animals for up to 4 weeks (Figure 2, A). A signal intensity of more than 10^8 photons per second (ph/s) for a given tumor was soon paralleled by pain related behavior. In a pilot group we found that animals with tumors above this threshold did not survive for more than 3-4 days during which they showed overt signs of pain and uneasiness. Therefore, 10^8 ph/s was defined as termination criteria for all following

experiments. Following this rule, untreated control animals reached a median survival of 28 days post implantation (Figure 2, B).

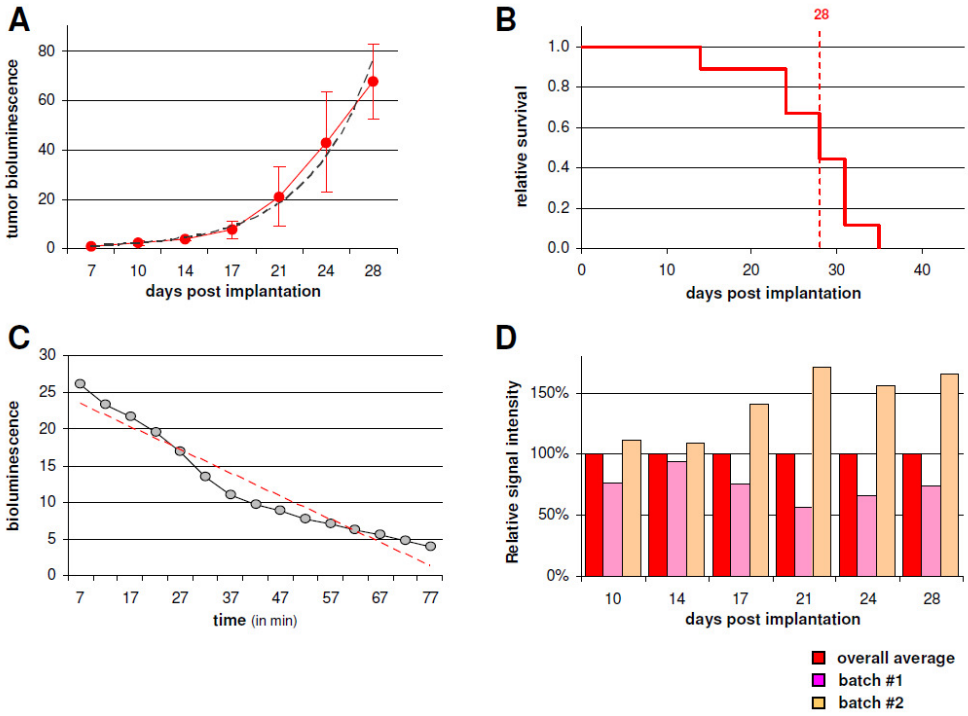

Figure 2. Bioluminescence of control tumors

(A) BL of untreated control U87-tumors. Error bars: ±SD. Dashed line shows best-fit curve (R^2 = 0.9918) indicating exponential growth. (B) Kaplan-Meier plot of animals with control tumors shown in (A). Dashed line at 50% survival: 28 days. (C) BL of a single U87-luc tumor measured over time after luciferin administration. Dashed line shows best-fit curve (R^2 = 0.933) indicating approx. linear decay of BL. (D) Relative tumor signal intensities of different experimental batches normalized to the overall average per time point. BL is shown on an arbitrary scale in panels (A) and (C).

To determine the optimal time point for luminescence imaging, we performed time lapse imaging experiments. Individual tumors were imaged every 5 min after a single dose of luciferin. The first 5 min resulted in highly variable luminescence kinetics, but from 7 min up to 77 min an almost linear decay of the signal intensity was observed (Figure 2, C). To avoid the variable start phase but to use the signal at high intensity, animals were routinely

imaged 10min after the substrate was injected. A control study comparing imaging results at 10 and 20 min post substrate injection showed, that the signal was proportionally the same after 20 min but overall intensity, and therefore also sensitivity, was markedly reduced (data not shown). Different tumor batches (tumors implanted at the same time) showed considerable variation (Figure 2, D). Therefore, tumors were always compared to batch matched control tumors rather than to an overall average. This batch matched approach yielded highly reproducible results.

Sodium Butyrate (NaB) and 2-deoxy-D-glucose reduce tumor growth *in vivo*

The histone deacetylase inhibitor NaB in combination with the glycolysis inhibitor 2DG has been shown to synergistically induce apoptosis in glioma and other cancer cells [9]. We analyzed the effect of a combinatorial treatment with NaB (1 mg/g) + 2DG (0.8 mg/g) administered daily by i.p. injection. Treated tumors showed a non-significant signal increase compared to control from day 10 to 24 (end of observation), but no difference in survival time could be observed (Figure 3, A-B). Although the signal variance was considerable and intermittent signal-loss was observed in the treatment group, we were unable to find any signs of tumor reduction or necrosis (Figure 3, C and data not shown). However, histological analysis showed ~3% apoptotic cells in the treated tumors versus <1% in the controls. All tumors were highly positive for the proliferation marker Ki67 with 35-45% actively proliferating cells in all tumors analyzed.

The finding of accelerated tumor growth in the treatment group could not be related to batch differences, differences in proliferation rates or changes in body weight due to 2DG treatment. Therefore, we analyzed the effect NaB and 2DG had on the bioluminescence of U87-luc cells *in vitro*. When treated with 2DG, a slight drop in relative BL was observed (Figure 4, A-B). This is in accordance with the observation that glioma cells treated with 2DG have reduced levels of ATP [9] which is needed for the luminescence reaction. Therefore, a reduction of the relative BL was to be expected. However, U87-luc cells treated with NaB showed a highly significant increase of relative BL by >2-fold (Figure 4, A-B). A panel of additional compounds was analyzed in respect to their impact on relative BL. The mTOR inhibitor Rapamycin reduced relative BL significantly to ~60% of the control whereas

RAD001, an alternative mTOR inhibitor, did not affect BL (Figure 4, C). The Mnk inhibitor CGP57380 and the Syk inhibitor QAB205 did not significantly change BL although there was a trend towards reduced signal intensity (Figure 4, C). The alterations in the relative BL could not be related to changes in luciferase expression since the protein levels of the enzyme were not affected in any of the treatment groups (Figure 4, D). It therefore appears likely that the observed increase in BL is related to a change of enzymatic activity of the luciferase rather than an actual increase in tumor growth. This is further supported by the unchanged survival time of the experimental animals and the histological tumor presentation, which is indiscriminate between treated and control tumors.

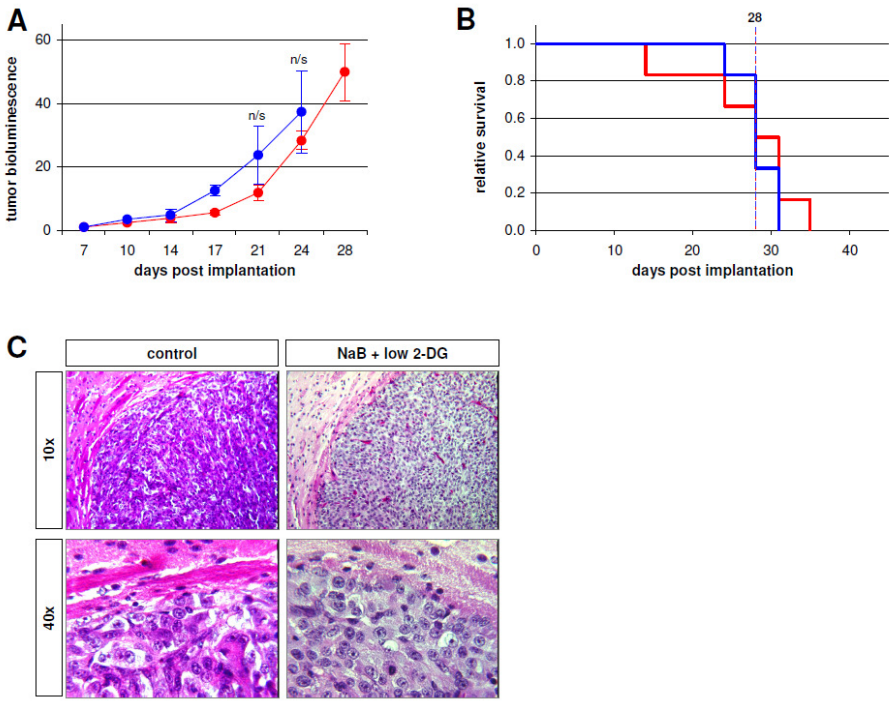

Figure 3. Treatment of U87-tumors with NaB and 2-DG

(A) BL of control (red) and treated (blue; NaB + 2-DG) U87-tumors. Error bars: ±SD. (B) Kaplan-Meier survival curve of control mice (red) and treated mice (blue). 50% survival: 28 days for both groups. (C) H&E staining of ortotopic tumor implants (U87-luc) with (NaB + low 2DG) or w/o treatment (control) indicating absence of tumor necrosis.

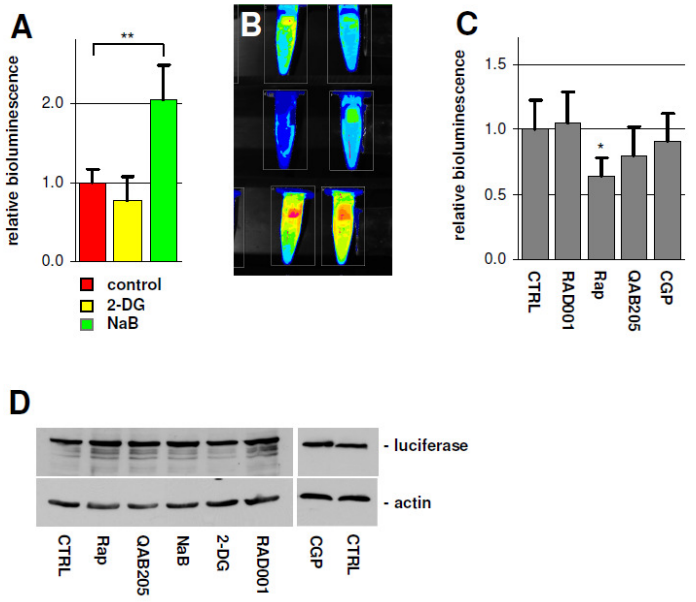

Figure 4. Bioluminescence of U87-luc cells is changes by NaB and 2-DG

(A) Relative BL of U87-luc cells treated as indicated for 24h and normalized to control. Error bars: ± SD. ** $p<0.01$. (B) Color coded BL image of $5*10^5$ living U87-luc cells per tube treated as follows: top row: control cells; middle row: treated with 2-DG (2.4 mg/kg); bottom row: treated with NaB (1 mg/kg). (C) Relative BL of U87-luc cells treated with additional compounds: RAD001 (10nM); Rapamycin (10nM); QAB205 (1ug/ml); CGP (10µM). Error bars : ± SD. * $p<0.05$. (D) WB analysis of luciferase expression in U87-luc cells treated as indicated and actin as loading control.

To determine if the percentage of apoptotic cells in the treated tumors could be further increased, we performed a dose escalation study showing that short term treatment with a maximum of NaB (1 mg/g) + 2DG (2.4 mg/g) during 4 consecutive days was well tolerated by the animals. Higher concentrations of either drug were not tolerated, particularly if administered in combination. Treatment of tumor bearing animals from day 7-10 post implantation with this regimen resulted in a significant reduction of tumor growth (Figure 5, A). Treated animals showed stable disease from day 10 to 17 and tumor size was reduced to approximately one third of the control afterwards. Control animals had a median survival of 28 days whereas treated animals had a median survival of 31 days (Figure 5, D). NaB (1mg/g) alone did not significantly reduce implant growth (Figure 5, B) although there was a reduction of BL in the second half of the observation period. The survival time was not affected with a median of 28 days. 2DG (2.4 mg/g) alone resulted in increased BL compared to control from day 17 onwards (Figure 5, C). This group showed the strongest signal variation and overall health was greatly reduced (weight loss, reduced nesting behavior,

etc.). A link between 2DG and the increased signal intensity could not be found (Figure 4, A-B, D). Histological analysis of tumors treated with NaB (1 mg/kg) and 2DG (2.4 mg/kg) in combination revealed increased apoptosis and areas of tumor necrosis which was never observed in control or single compound treated samples (Figure 5, E) indicating a pro-apoptotic effect *in vivo* and offering a possible mode of action for reducing tumor growth as observed (Figure 5, A).

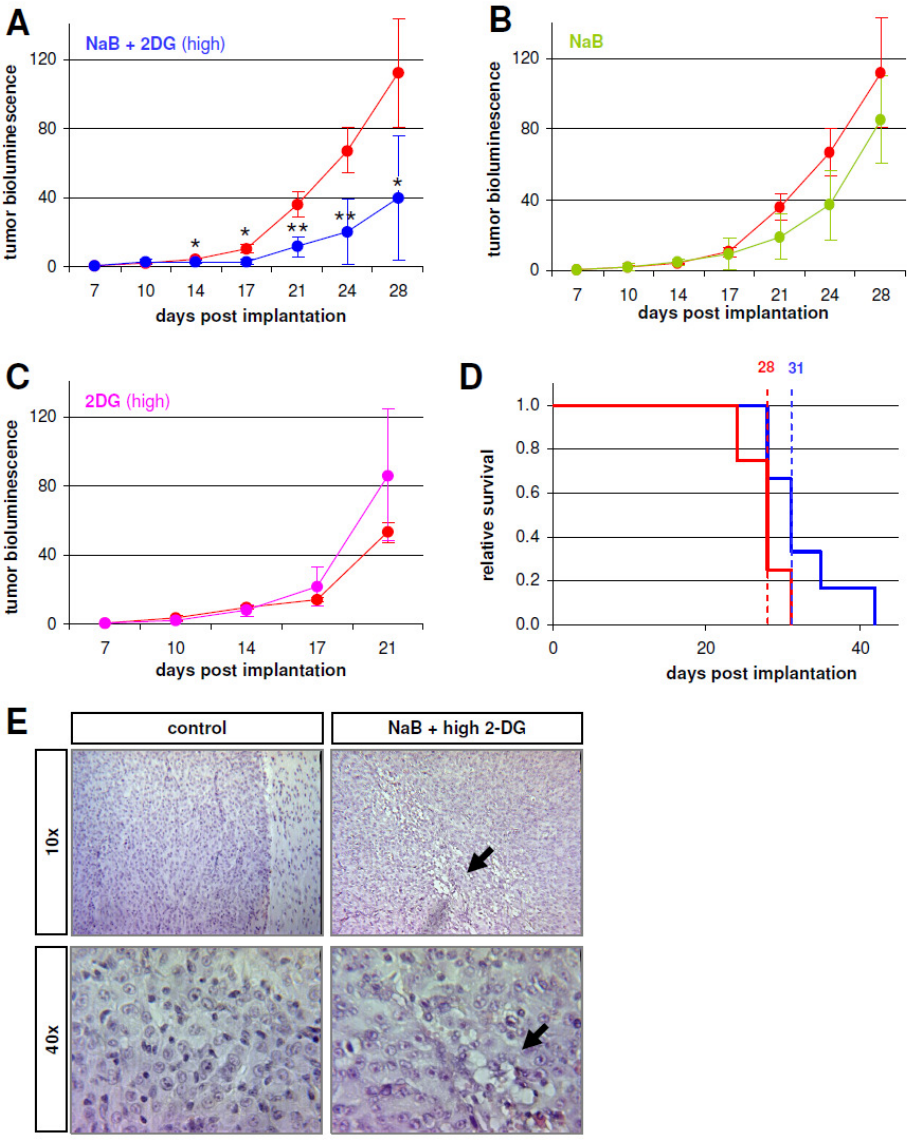

Figure 5. Treatment of U87-tumors with NaB and high 2-DG

U87-tumors BL: control (red) and (A) treated (blue; NaB + high 2-DG), (B) NaB alone, and (C) 2DG alone. Error bars: ±SD. * $p < 0.05$; ** $p < 0.01$. (D) Kaplan-Meier survival curve of control mice (red) and treated mice (blue). 50% survival: control 28 days, treated 31 days. (E) H&E staining of U87-luc tumors shown as light microscopic images treated as indicated. Arrows indicate necrotic areas.

Evaluation of genetically modified glioma cell lines *in vivo* in different genetic mouse backgrounds

Not all molecules of interest can be evaluated in the orthotopic model due to limitations in the experimental set-up. In short, transfection and stable expression of additional genetic constructs to study their role in tumor growth within the U87-Luc cell lines has proven to be difficult, particularly because the different clones have varying luminescence efficiencies. In addition, U87-luc cells do not express all proteins currently under investigation. Thus the use of corresponding inhibitors is not always possible. Therefore, we evaluated several genetically modified cell lines in an alternative *in vivo* model, wherein cells are implanted subcutaneous and growth is monitored by measuring the palpable tumor nodule rather than by BL. As a control, U87-Luc cells, which readily grow in the brains of nude mice, were injected s.c. at the body flanks. The cells formed large, fast growing nodules after 10-14 days post inoculation (data not shown). Genetically modified U373 and LN18 cells, two cell lines reported to be tumorigenic in nude mice [13], did not give any detectable tumor nodules in Crl:Nu mice (Swiss Webster background) over an observation period of >9 weeks. Even the parental cell lines which were not transfected or genetically modified did not form tumors. Increased cell number per implant or the additional use of extracellular matrix proteins to facilitate tumor initiation did not change these results. Therefore, we aimed at evaluating the growth behavior in two alternative mouse lines. The Hsd:Nu (Hsd:Nu-Foxn1^{nu}, athymic BALB/c, Harlan) which have the alternative BALB/c genetic background was recommended by Novartis having used this particular line in their brain tumor studies. Furthermore, these mice seem to be less sensitive to anesthesia, which was a major problem of the orthotopic brain tumor model. Additionally, we aimed at evaluating s.c. tumor growth in Hsd:BNX mice (Hsd:NIHS-*Lyst*^{bg}*Foxn1*^{nu}*Btk*^{xid}, Harlan). These triple mutant animals have neither adaptive nor innate immune cells (no NK-, B- or T-cells) and have been recommended to be used in studies with cells not growing in other immuno-compromised mice (eg *nude*, NOD-Scid, etc.). The growth behavior of all GBM cell lines evaluated in the different mouse lines is summarized in Table 1.

Table 1. Tumorigenic potential of glioma cell lines in different mouse lines.						
	Crl:Nu-Foxn1^{nu} (Swiss)		Hsd:Nu-Foxn1^{nu} (athymic)		Hsd:BNX (NIH-III)	
	brain	flank	brain	flank	brain	flank
U87-Luc	+	+	+	*n/a*		
U373	*n/a*	-	*n/a*	-	*n/a*	*n/a*
U373-pLuc	+	*n/a*	*n/a*	*n/a*	*n/a*	*n/a*
U373-shRNA-scr	*n/a*	-	*n/a*	-	*n/a*	+
U373-shRNA-DTX1	*n/a*	-	*n/a*	-	*n/a*	+
U373-shRNA-MerTK	*n/a*	-	*n/a*	-	*n/a*	
LN18-EGFP	*n/a*	-	*n/a*	-	*n/a*	-
LN18-DTX1-myc	*n/a*	-	*n/a*	-	*n/a*	-

Table 1. 8 glioma derived cell lines were evaluated for their tumorigenic potential in three different immuno-compromised mouse lines. Implants were either orthotopic (brain) or subcutaneous on the flank of the animal (flank). (+) tumor formed growing nodules; (-) no tumor nodule was detectable after prolonged observation; n/a not assessed; blank fields indicate cell line/mouse combinations which are still pending. Tumor growth was assessed by bioluminescence in the brain and palpable nodule size in the flank.

Discussion

Previous work in our lab identified HDIs in combination with 2DG as an effective, pro-apoptotic cancer therapy *in vitro*. Epigenetically reprogrammed glioma cells were more sensitive to the glycolysis inhibitor 2DG inducing high levels of cell death at concentrations leaving normal rat astrocytes, HEK293 and RASMC cells unaffected [8]. This is in accordance with other studies reporting low toxicity for HDIs even when used in combination strategies in clinical settings [8]. Animals exposed to NaB on a daily basis by i.p. injection did not show overt signs of toxicity, unwanted side effects or behavioral changes in our study. However, *in vivo* efficacy of the HDI/2DG regimen has not been analyzed up to date.

Long term exposure to low concentrations of HDI and 2DG in combination did not reduce tumor growth although it was able to induce apoptosis in a limited number of cells (~3%). Short term exposure to higher concentrations, however, was able to induce both apoptosis and tumor necrosis and reduced tumor growth significantly. Therefore, the combinatorial use of epigenetic modulators and energy deprivation seems a therapeutic approach with considerable potential in clinical settings. Furthermore, the finding of increased BL in U87-luc cells treated with NaB *in vitro* could indicate that the anti-tumor effect of the HDI/2DG combination is underrepresented in our model. This also holds true for the effect the regimen has on the overall survival. Since the termination criteria was defined by BL (at 10^8 ph/s), it is unclear if the animals were not sacrificed prematurely due to the increased BL after NaB treatment. Adding an additional layer of complexity, we found animals treated with NaB only to have similar BL increase and survival times as control animals. If the anti-tumor effect and the increase in BL are just kept in balance in this setting is unclear. However, the control tumor cannot be differentiated from NaB treated samples when analyzed histologically. The question how NaB influences BL *in vivo* can only be addressed in a setting in which animals remain in the experiment until they die spontaneously or until they show overt signs of illness. Without these experiments the primary endpoint of overall survival will remain non-distinctive in our study. Experiments to answer this question are currently ongoing.

NaB, TSA, Depsipeptide, and Apicidin are HDIs from natural sources [8] and NaB has been reported to cross the blood brain barrier in mice [9]. Synthetic HDI, for example AN-9 or FK-228, are currently in clinical phase I/II studies in leukemia patients showing increased HDI activity *in vivo* compared to natural HDIs [10, 11]. The synthetic HDI LAQ824 [9], which is in clinical phase I/II studies for solid tumors, lymphomas and leukemia, has increased HDI activity compared to NaB and also crosses the blood brain barrier [8]. Therefore, it will be interesting to see how HDIs with optimized activity will perform in combination with 2DG in glioma and potentially other cancer models. Optimized bio-availability and target specificity lead to fewer side effects and allow for higher target concentrations. In sum, this should further improve the therapeutic effect of our strategy. In addition, our dosing regimen was constricted to 4 days with an overall observation period of ~31days. The main impact (loss of total BL or reduction thereof) was observed immediately after the therapy followed by an increase in BL at reduced levels after approx. another 7-10 days. Pharmacokinetics are highly variable between species. Therefore such a regimen can not be immediately translated to humans. However, it points to a regimen that should include expanded or recurrent exposures to the combination therapy.

2DG at high concentrations administered as single agent for 4 days did not reduce tumor growth; instead, a slight increase in BL was observed compared to the control group. Our *in vitro* results showed that 2DG does not induce increased BL in U87-luc cells nor did it have a growth promoting effect. To the contrary, 2DG had a cytostatic effect *in vitro*. We cannot exclude the possibility, that 2DG (2.4 mg/kg) acts differently *in vivo*. However, given the fact that 2DG is used in several tumor models without ever being related to increased tumor growth [10, 11], we find it rather unlikely that there is an unknown, growth promoting effect. Furthermore, the increase in BL was not significant and showed huge variation. 2DG by itself can have a negative effect on overall health and body weight in particular due to energy deprivation or reduced metabolism [12]. Therefore, the combined effect of tumor burden and energy reduction may lead to additive effects reducing overall life expectancy. Animals treated with the HDI/2DG combination apparently profit significantly from the anti-tumor effect fully compensating for the adverse effect of 2DG. Combined application of HDI and 2DG has a favorable effect compared to 2DG alone due to epigenetic reprogramming.

The single *Foxn1*^{nu} mutation background did not allow s.c. tumor growth in our experimental set up when using U373 or LN18 parental cells. Orthotopic growth was observed for several cell lines irrespective of subcutaneous growth in all genetic backgrounds analyzed (Table 1). Several reasons could cause this effect: the nude mutation was found to be leaky in our colonies. A fraction of the animals would develop coat hair over time indicating some residual Foxn1 activity or compensatory mechanisms (at least in the hair follicles). Furthermore, this mutation only impairs T-cell maturation rendering the adaptive immune system inactive [13]. The innate immune system is not affected leaving the Natural Killer cells (NK) active. These NK cells (which have the natural ability to kill tumor cells) recognize non-self proteins presented on MHC-I like molecules highly up regulated in tumor cells and kill cells presenting such on the cell surface [14]. Tumor cells and particularly xenogenic tumor cells display a plethora of non-self markers and are therefore prime targets of NK cells. Furthermore, the cell lines used in these experiments were cultured on plastic dishes for hundreds of passages selecting for "on-plastic" growth capacity rather than for tumorigenic potential. The combined effect of long term culturing and the innate immune system of the host animal are likely to explain the lack of xenogenic tumor growth in the nude mutants. The mouse line Hsd:NIHS-*Lyst*^{bg}*Foxn1*^{nu}*Btk*^{xid} is devoid of NK cells (*beige* mutation), T-cells (*nude* mutation), and mature B-cells (*xid* mutation) and therefore lack major components of both the adaptive and the innate immune system [18]. The experiments determining the growth potential of our experimental cell lines described above in these animals are currently ongoing. If the modified cell lines do not form palpable tumor nodules in these immuno-compromised animals, we have to assume that the cells (particularly after repeated transfection and selection) have lost their tumorigenic potential. Strategies to overcome this problem in an *in vivo* setting are currently unclear.

The orthotopic GBM model is currently the only *in vivo* model of HGG we have at hand. Therefore, we aim at analyzing several additional regimens and inhibitors in this experimental setup. The rational of these projects as well as a short scientific introduction are listed below.

Future Perspectives and Outlook

The possibility of continuously monitoring tumor growth in an orthotopic model of high grade gliomas will provide us with the ability to evaluate novel inhibitors and combination therapies. In the near future several such treatments shall be analyzed which have shown promising results *in vitro*. These experiments are focused around three main findings and the corresponding inhibitors:

MNK1 inhibitor CGP57380. MAP kinase-interacting kinase 1 (MNK1), which is downstream of the MAP kinase pathway [16] and which is over-expressed in GBM, was found to have a critical funciton in GBM malignancy. It was shown that MNK1 regulates the SMAD2-dependent TGF-β pathway and also cell motility in glioma cells. In addition, targeting MNK1 with the inhibitor CGP57380 together with an mTOR inhibitor (eg. Rapamycin) induced cell cycle arrest and strongly inhibited global translation and GBM cell proliferation [15]. Based on these findings, we aim at evaluating a combination therapy of CGP57380 and Rapamycin (or its derivative RAD001) in our *in vivo* model. Acute toxicity screening has been completed with no negative effects detected. Therefore, the CGP57380 (25 mg/kg) + RAD001 (3 mg/kg) combination will be evaluated in the next batches of tumor bearing animals. Primary endpoints will be tumor growth (measured by BL) and overall survival. Secondary endpoints will be toxcicity and generalized adverse effects.

Spleen Tyrosine Kinase (SYK) inhibitors. Recently, the spleen tyrosine kinase SYK, SRC kinase LYN and the immunoreceptor molecule CD32 (exclusively activating SYK or ZAP70 through SRC's) were identified to be highly over expressed in GBM [16] and increased expression of these molecues correlates with significantely reduced patient survival time (REMBRANDT). Further investigation confirmed the expression of SYK/LYN/CD32 in GBM derived cancer spheres and cell lines. To study the role of SYK in glioblastoma, cell lines were treated with three small molecule inhibitors of SYK. All of these inhibitors showed a strong inhibition in basal and EGF induced proliferation and migration (Gerald Moncayo, personal comunication). After the acute toxicity screening, upon which at least one compound had to be excluded from this study allready, we aim at evaluating the anti-cancer potential of the remaining SYK inhibitors in the orthotopic glioma model as well as the effect genetic

modification of cell lines (either by over-expressing or down-knocking of SYK) has on their tumorigenic potential in the s.c. flank model. In the orthotopic assay the primary and secondary endpoints are similar to the ones described for CGP57380. In the flank model the primary endpoint is palpable tumor size and the secondary endpoint is ulceration-free progression. Toxicity and generalized adverse effects will be included as third endpoint.

Proto-oncogene tyrosine-protein kinase MER (MerTK). In the same screen as we have identified MNK1 and SYK, we also found MerTK to be elevated in GBM samples when compared to normal brain or human astrocyte controls [18]. MerTK has an anti-apoptotic function in glioma cells but is only consistently expressed in cancer spheres or sphere derived adherent cells (Yuhua Wang, personal communication). Therefore, the experimental set up differs from the two others in several aspects. First, we aim at analyzing the tumor growth in the flank model using cancer spheres transfected either with shRNA-luc (as control) or shRNA-MerTK as implants and to compare growth behavior. Secondly, since U87 cells do not express MerTK, the specific inhibitor 'compound 52' [17] can not be applied to the current orthotopic model. However, cancer spheres could be injected orthotopically [18]. The readout would be asymptomatic survival as well as overall survival of treated versus untreated animals. However, these experiments would require substantial amounts of animals per group to correct for individual variation. Furthermore, only post mortem analysis would give conclusive insight on tumor invasion, growth, vascularization, and apoptosis. Since it is not possible to control for tumor formation prior to necropsy, the evaluation would be even further complicated. The establishment of luciferase expressing cancer spheres (controlled for MerTK expression) therefore appears as a more feasible, however, still difficult approach.

Regimens with a growth inhibiting and life prolonging effect *in vivo* have the potential to induce comparable effects in patients. Although results obtained in rodents are difficult to translate into clinical outcome [5] such results represent the groundwork for any clinical trial. Hopefully we will be able to identify regimens with high anti-tumor efficacy in the GBM model based on drugs which are already safety approved by the EMEA or FDA, making the initiation of a phase I clinical trial comparatively easy.

Materials and Methods

Cell Lines

U87MG-Luc [19], U373 and LN18 cells were grown in Dulbecco's Modified Eagle Medium (DMEM, Invitrogen) supplemented with 10% (v/v) fetal bovine serum (FBS, No: S1810, Labforce, Basel, Switzerland), 1% glutamax solution (v/v) (Invitrogen) and 1% (v/v) penicillin/streptomycin solution (Invitrogen). Cells were suspended by proteolysis with 1x trypsin-EDTA (Invitrogen) for 5 minutes at 37°C and transfected with Firefly Luciferase expression plasmids (pcDNA3.1-Luc-IRES-GFP) using $CaCl_2$ precipitation. Stably transfected cells were maintained in 100µg/ml Geneticin® or G418 (Invitrogen Corporation, California, USA) for U87-luc and 0.2µg/ml Puromycin (Invitrogen) for U373 and LN18.

Western blot analysis and antibodies

Cells were grown to 80-90% confluency, washed twice with 1x PBS, lysed in buffer containing 2% sodium dodecyl sulfate (SDS), 50mM Tris pH 6.8, 0.1M dithiothreitol (DTT), boiled at 95°C for 5min and used either immediately or frozen at -20°C. Protein lysates were resolved on denaturing 8-12% SDS-polyacrylamide gels and transferred to nitrocellulose membranes (iBlot Gel transfer stacks, Invitrogen). The following primary antibody was used: polyclonal goat anti-luciferase Ab (Chemicon). Decorated proteins were revealed using horseradish peroxidase-conjugated anti-goat (Pierce) secondary antibodies and visualized by the chemoluminescence detection system SuperSignal West Pico (Thermo Scientific).

Mouse Lines and Brain Injections

Immuno-compromised mice were used in the orthotopic brain injections: Crl:Nu(loc)-Foxn1^{nu} (CRL, France). The strain was maintained in a Swiss Webster Background as an outbred line by crossing heterozygote females with homozygote males. Hsd:Nu athymic Nude-Foxn1^{nu} (Harlan, Netherlands) generated in a BALB/c background and maintained as an outbred strain were also evaluated in orthotopic injections. Hsd:NIHS-*Lyst*^{bg}*Foxn1*^{nu}*Btk*^{xid} (Hsd:BNX) maintained as an inbred colony were used as indicated above. All animals were

housed in IVC settings with food and water *ad libitum*. For orthotopic injections the mice were anesthetized with Ketamine/Xylozine/Acepromazin (75/13/2 mg/kg) by i.p. injection and kept on a 37°C heating pad. $5*10^5$ U87-luc cells in 10µl sterile PBS were injected 3 mm caudal and 2 mm lateral of the bregma, 3 mm below the dura with a 100µl Hamilton syringe using a 25 Gauge needle mounted in a stereotactic frame. Animals received 0.3 mg/kg Buprenorphine i.p. or s.c. as analgesic treatment post implantation for 3 days.

Bioluminescence Imaging

Mice were injected with 10µl/g (body weight) of D-luciferin in PBS (15mg/ml) i.p. Animals were immobilized with 2.5% Isoflurane via individual face masks. Imaging was performed in a NightOwl BL imager (Berthold Technologies) at 560 nm emission wavelength after 10 min incubation time of the substrate for 30 sec. Integrated signal intensity was normalized to background and calculated for individual tumors. Cell lines were imaged with the same settings and same substrate concentration at 25°C in 1.5 ml tubes (Eppendorf).

Histology

Tumor bearing brains were fixed in 4% Formalin at RT over night, washed and embedded in paraffin. Thin sections (2-4 um) were cut and dried at 37°C o/n. Stainings were performed as indicated in the figure legends.

Supplemental Material

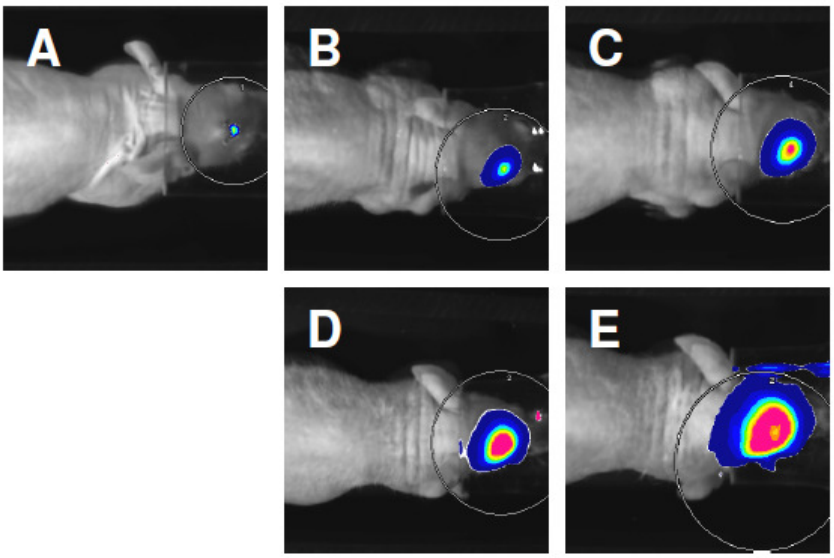

Figure S1. Bioluminescence signal of a defined tumor followed over time

A single U87-tumor was measured at time points (A) 7 days post implantation, (B) 14 days, (C) 21 days, (D) 24 days, and (E) 28 days. All images were taken 10 min after application of 300 µl luciferin solution (15mg/ml) i.p. BL is shown color coded with blue representing low and red high signal density as a heat map.

Acknowledgment

We thank Béatrice Dolder, Jaqcueline Rauch and Marie-Christine Müller for expert technical assiatance; Dr. T. O'Railley for scientific advice and help with data analysis; Drs. Michal Grzmil and Gerald Moncayo as well as Yuhua Wang for scientific discussions, particularly on the future perspectives and valuable comments on the manuscript. This study was supported by a CCRP grant from Oncosuisse to AM, BAH and B. Bettler.

Author Contributions

RMH, AM: designed the study; RMH, DH: performed experiments and analyzed data; AM, BAH: revised the manuscript; RMH: wrote the manuscript.

References

1. Mangiola, A., et al., *Invasive tumor cells and prognosis in a selected population of patients with glioblastoma multiforme.* Cancer, 2008. **113**(4): p. 841-6.
2. Stupp, R., et al., *Effects of radiotherapy with concomitant and adjuvant temozolomide versus radiotherapy alone on survival in glioblastoma in a randomised phase III study: 5-year analysis of the EORTC-NCIC trial.* Lancet Oncol, 2009. **10**(5): p. 459-66.
3. McLendon, R.E. and E.C. Halperin, *Is the long-term survival of patients with intracranial glioblastoma multiforme overstated?* Cancer, 2003. **98**(8): p. 1745-8.
4. Lee, J., et al., *Tumor stem cells derived from glioblastomas cultured in bFGF and EGF more closely mirror the phenotype and genotype of primary tumors than do serum-cultured cell lines.* Cancer Cell, 2006. **9**(5): p. 391-403.
5. Szentirmai, O., et al., *Noninvasive bioluminescence imaging of luciferase expressing intracranial U87 xenografts: correlation with magnetic resonance imaging determined tumor volume and longitudinal use in assessing tumor growth and antiangiogenic treatment effect.* Neurosurgery, 2006. **58**(2): p. 365-72; discussion 365-72.
6. Mei, S., A.D. Ho, and U. Mahlknecht, *Role of histone deacetylase inhibitors in the treatment of cancer (Review).* Int J Oncol, 2004. **25**(6): p. 1509-19.
7. Dai, C. and E.C. Holland, *Glioma models.* Biochim Biophys Acta, 2001. **1551**(1): p. M19-27.
8. Minucci, S. and P.G. Pelicci, *Histone deacetylase inhibitors and the promise of epigenetic (and more) treatments for cancer.* Nat Rev Cancer, 2006. **6**(1): p. 38-51.
9. Atadja, P., et al., *Selective growth inhibition of tumor cells by a novel histone deacetylase inhibitor, NVP-LAQ824.* Cancer Res, 2004. **64**(2): p. 689-95.
10. Jain, V.K., et al., *Effects of 2-deoxy-D-glucose on glycolysis, proliferation kinetics and radiation response of human cancer cells.* Int J Radiat Oncol Biol Phys, 1985. **11**(5): p. 943-50.
11. Maschek, G., et al., *2-deoxy-D-glucose increases the efficacy of adriamycin and paclitaxel in human osteosarcoma and non-small cell lung cancers in vivo.* Cancer Res, 2004. **64**(1): p. 31-4.
12. Dwarakanath, B.S., et al., *Clinical studies for improving radiotherapy with 2-deoxy-D-glucose: present status and future prospects.* J Cancer Res Ther, 2009. **5 Suppl 1**: p. S21-6.
13. Reth, M., *Immunodeficiency. Trapping the nude mouse gene.* Curr Biol, 1995. **5**(1): p. 18-20.
14. Wu, J. and L.L. Lanier, *Natural killer cells and cancer.* Adv Cancer Res, 2003. **90**: p. 127-56.
15. Grzmil, M., et al., *MAP Kinase-Interacting Kinase 1 Regulates SMAD2-Dependent TGF-{beta} Signaling Pathway in Human Glioblastoma.* Cancer Res, 2011. **71**(6): p. 2392-402.
16. Korur, S., et al., *GSK3beta regulates differentiation and growth arrest in glioblastoma.* PLoS One, 2009. **4**(10): p. e7443.
17. Huang, X., et al., *Structural insights into the inhibited states of the Mer receptor tyrosine kinase.* J Struct Biol, 2009. **165**(2): p. 88-96.

18. Shu, Q., et al., *Direct orthotopic transplantation of fresh surgical specimen preserves CD133+ tumor cells in clinically relevant mouse models of medulloblastoma and glioma.* Stem Cells, 2008. **26**(6): p. 1414-24.
19. Rubin, J.B., et al., *A small-molecule antagonist of CXCR4 inhibits intracranial growth of primary brain tumors.* Proc Natl Acad Sci U S A, 2003. **100**(23): p. 13513-8.

Part 3

GSK3β regulates differentiation and growth arrest in glioblastoma.

'PLoS ONE', 2009

Serdar Korur[1], **Roland M. Huber[1]**, Balasubramanian Sivasankaran[1], Michael Petrich[1], Pier Morin, Jr[2], Brian A. Hemmings[2], Adrian Merlo[1], Maria Maddalena Lino[1]

1) Laboratory of Molecular Neuro-Oncology, University Hospital Basel, Basel, Switzerland

2) Friedrich Miescher Institute for Biomedical Research, Basel, Switzerland

Abstract

Cancers are driven by a population of cells with the stem cell properties of self-renewal and unlimited growth. As a subpopulation within the tumor mass, these cells are believed to constitute a tumor cell reservoir. Pathways controlling the renewal of normal stem cells are deregulated in cancer. The polycomb group gene Bmi1, which is required for neural stem cell self-renewal and also controls anti-oxidant defense in neurons, is upregulated in several cancers, including medulloblastoma. We have found that Bmi1 is consistently and highly expressed in GBM. Downregulation of Bmi1 by shRNAs induced a differentiation phenotype and reduced expression of the stem cell markers Sox2 and Nestin. Interestingly, expression of glycogen synthase kinase 3 beta (GSK3β), which was found to be consistently expressed in primary GBM, also declined. This suggests a functional link between Bmi1 and GSK3β. Interference with GSK3β activity by siRNA, the specific inhibitor SB216763, or lithium chloride (LiCl) induced tumor cell differentiation. In addition, tumor cell apoptosis was enhanced, the formation of neurospheres was impaired, and clonogenicity reduced in a dose-dependent manner. GBM cell lines consist mainly of CD133-negative (CD133-) cells. Interestingly, *ex vivo* cells from primary tumor biopsies allowed the identification of a CD133- subpopulation of cells that express stem cell markers and are depleted by inactivation of GSK3β. Drugs that inhibit GSK3, including the psychiatric drug LiCl, may deplete the GBM stem cell reservoir independently of CD133 status.

Introduction

Recent studies suggest that cancer stem cells are the driving force behind tumorigenesis [1]. CD133 (also known as Prominin 1) was identified as a surface marker of cancer stem cells in brain tumors [2]. As few as 100 CD133-positive (CD133+) cells were shown to induce tumors in transplantation experiments giving rise to a phenocopy of the initial neoplasia [2], [3]. CD133+ cells, which express multi-drug resistance and DNA repair proteins [4], are highly resistant to chemo- and radiation therapy. However, stemness is not restricted to the expression of the CD133 marker, since CD133-negative (CD133−) cell populations were also found to be tumorigenic [5]. Cancer stem cells have also been detected in glioblastoma (GBM), the most malignant human brain tumor, with an annual incidence of 36 per million and a mean survival of less than 1 year [6]–[8]. GBM, a highly invasive and proliferative tumor, manifests itself as a *de novo* lesion or progresses from less undifferentiated low-grade astrocytoma.

Bmi1 is a member of the polycomb group of proteins involved in brain development [9]. Polycomb group proteins maintain embryonic and adult stem cells by forming multi-protein complexes that function as transcription repressors [10]–[17]. Bmi1 is also involved in cancer by cooperation with Myc in lymphoma formation [18] and blocking of senescence in immortalized mouse embryonic fibroblasts through repression of the Ink4a/Arf-locus [19]. It is also amplified and/or overexpressed in non-small-cell lung cancer, colorectal carcinoma, nasopharyngeal carcinoma, medulloblastoma, lymphoma, multiple myeloma and primary neuroblastoma [9], [13], [19]–[22]. Whether Bmi1 is expressed in GBM is controversial [9]. In a mouse glioma model, Bmi1 was implicated in tumorigenesis in an Ink4a/Arf-independent manner [23]. Furthermore, it was shown recently that microRNA-128 inhibits proliferation and self-renewal in glioma at least partially by downregulating Bmi1 [24].

Glycogen synthase kinase 3 (GSK3), a serine/threonine kinase, regulates numerous signaling pathways involved in cell cycle control, proliferation, differentiation and apoptosis [25], [26]. The mammalian isoforms GSK3α and GSK3β are functionally independent as GSK3α cannot rescue the embryonically lethal phenotype of GSK3β (−/−) mice [27]. GSK3 has been described as a pro-survival factor in pancreatic cancer [28] and as a pro-apoptotic factor in colorectal cancer [29] and is interconnected with several pathways and implicated

in Alzheimer's disease [30], diabetes [31], bipolar disorder [32], and more recently cancer [33].

We have analyzed the role of GSK3 in malignant gliomas and its links to critical signaling proteins. Downregulation of Bmi1 reduced GSK3β levels and induced the differentiation of malignant glial cells. Direct inhibition of GSK3β by lithium chloride (LiCl), SB216763 and siRNA decreased Nestin and Sox2 levels and induced the cell differentiation markers CNPase, glial fibrillary acidic protein (GFAP) and β-tubulin III. In addition, LiCl and SB216763 depleted cancer stem cells grown as human GBM *ex vivo* cell cultures, induced differentiation and inhibited neurosphere formation. Thus, GSK3 may represent a novel therapeutic target for malignant gliomas.

Results

Bmi1 is overexpressed in GBM, oligodendroglioma and astrocytoma

Bmi1 overexpression has been reported in several different tumor types including medulloblastoma and neuroblastoma. In an analysis of Bmi1 mRNA and protein expression in GBM cell lines and primary brain tumors, all GBM cell lines expressed high Bmi1 levels, with the LN319 line having the highest expression comparable to the reference line DAOY [9] (Figure 1A and data not shown). In primary brain tumor samples, Bmi1 expression was marked in 16/19 (84%) of GBM, 5/7 (71%) of oligodendroglioma and 3/7 (42%) of astrocytoma. In contrast, fully differentiated normal brain tissue had no Bmi1 protein (Figure 1B, C).

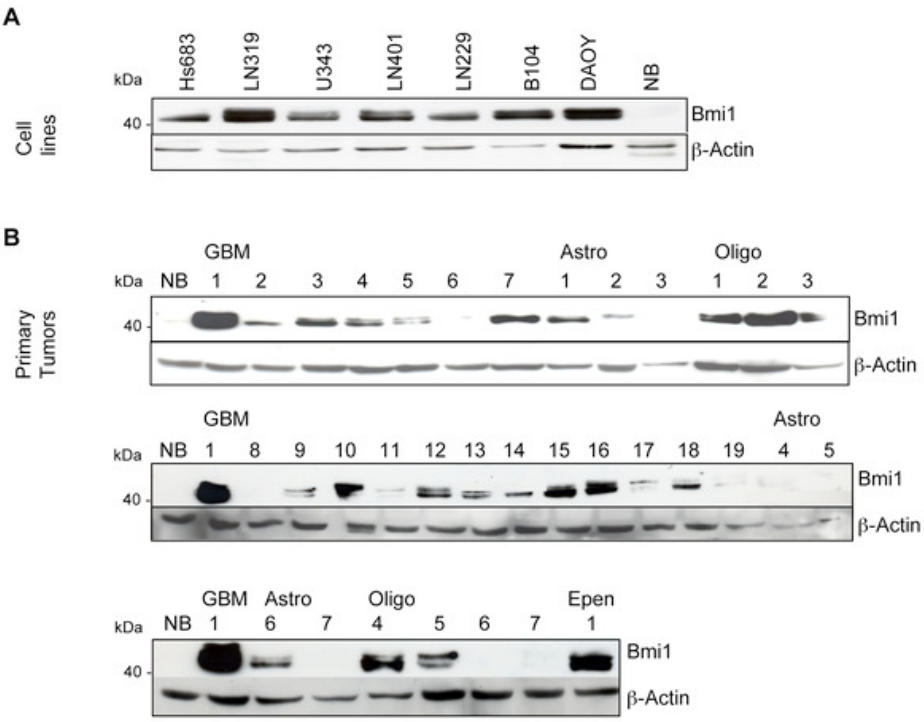

C

Primary tumors

GBM	16/19
Astro	3/7
Oligo	5/7

Figure 1. Bmi1 was highly expressed in GBM.

Bmi1 expression in (A) GBM cell lines and (B) primary brain tumors. (C) Ratio of Bmi1-positive primary tumors. NB: normal brain. EPEN: Ependymoma.

shRNA against Bmi1 downregulates GSK3β

To study the role of Bmi1 in GBM, Bmi1 expression was knocked down using lentiviral-mediated delivery of shRNAs. Bmi1 was efficiently downregulated in the Hs683, U373, U87, and U343 GBM cell lines (Figures 2A and S1A and data not shown) using different shRNA sequences (Figure S1B). Since the Polycomb group gene Bmi1 is involved in the regulation of development and tumorigenesis, the effect of Bmi1 downregulation in GBM cells was screened by analysis of proteins involved in key cellular pathways of the cell cycle, development, metabolism, apoptosis and growth, including Erk, Akt, GSK3β, p16 and p14, Bcl-2, c-Myc, Nestin and Sox2. In contrast to non-neoplastic cells in Bmi1 knockout mice [19], Bmi1 downregulation in GBM cells did not affect Ink4a/Arf protein levels (Figure 2A). Bmi1 downregulation induced cell differentiation associated with morphological changes and decreased expression of the stem cell-related proteins Nestin and Sox2, accompanying induction of an astrocytic fate in U373 glioma cell line, determined by increased levels of the astrocyte-specific marker GFAP, and decreased levels of oligodendrocyte-specific marker CNPase (Figures 2A–D and S2B). In contrast, Bmi1 overexpression accompanied dedifferentiation as shown by increased Nestin expression (Figure S1C). Interestingly, GSK3β levels were markedly reduced (Figures 2A and S1A–B). This raised the question of whether GSK3β mediates the effects observed on cell differentiation. To this end, we used the small molecules LiCl and SB216763 as well as siRNA to interfere with GSK3β activity in GBM cells.

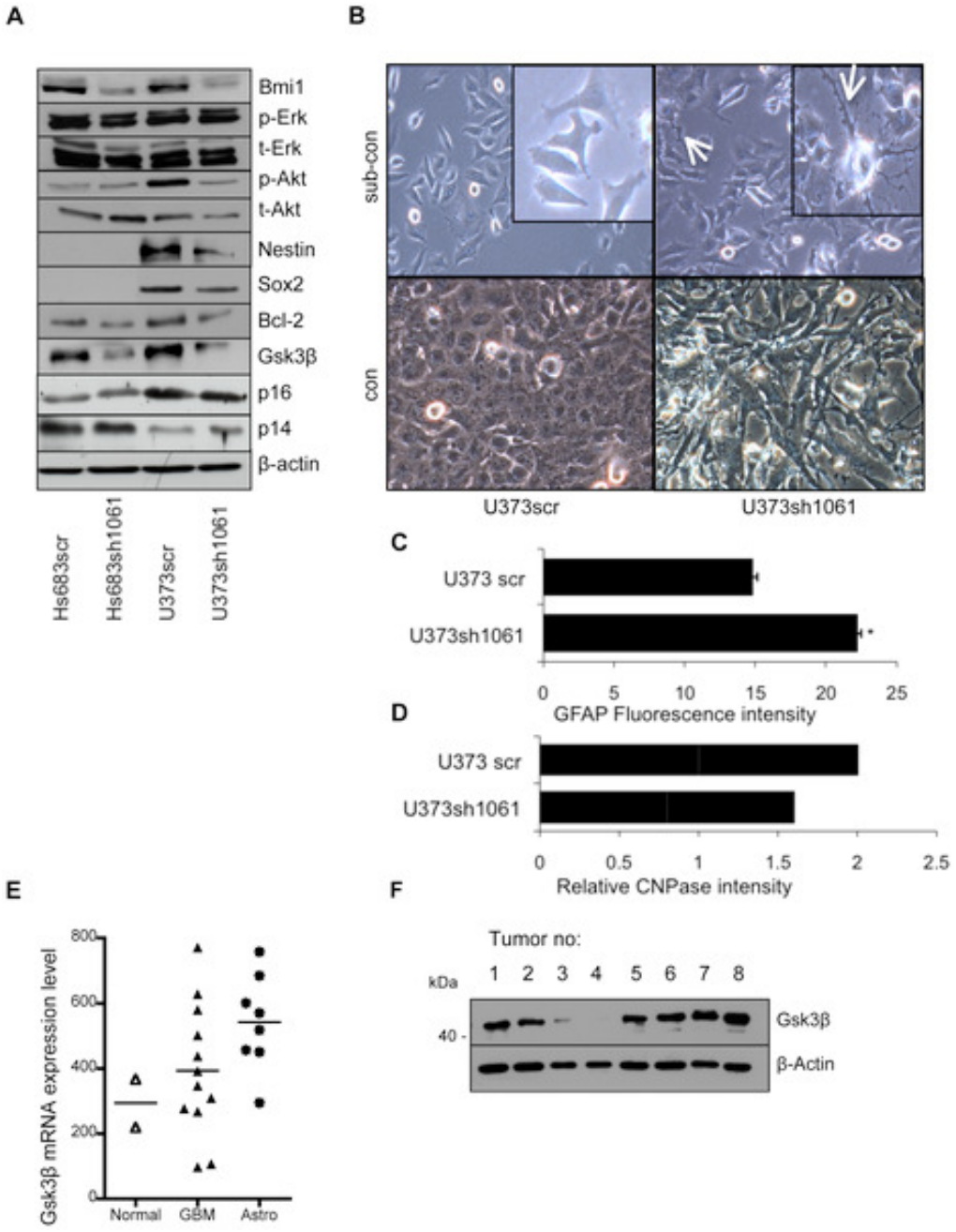

Figure 2. GSK3β was downregulated by reduction of Bmi1 expression.

(A) GBM cell lines U373 and Hs683 transduced with shRNA against Bmi1 (sh1061) or with scrambled shRNA (scr). Bmi1 downregulation induced downregulation of the following proteins: p-AKT, Nestin (in U373), Bcl2, and GSK3β. No effects are evident on the p16/p14^{ARF}, or p-ERK protein levels. (B) Scrambled control or U373 Bmi1-downregulated cells at subconfluency (sub-con) or confluency (con). Bmi1-downregulated cells show differentiated morphology (arrow: long, branched processes). (C) The glial fibrillary acidic protein (GFAP) levels in U373scr and U373sh1061 cells measured by flow cytometry. (D) Relative CNPase protein levels in U373scr and U373sh1061 measured by western blotting, quantified using ImageJ software and normalized to β-actin levels. (E) GSK3β mRNA values from a series of primary brain tumors (GBM and astrocytoma) and normal brain. (F) GSK3β protein is expressed in primary GBM. *P<0.05; one-way ANOVA (Newman-Keuls Multiple Comparison Test).

GSK3β is expressed in GBM

Thirty-two primary tumor tissues obtained from patients diagnosed with GBM were studied using microarray and western blot analysis to measure GSK3β mRNA and protein levels. GSK3β mRNA were higher in GBM and astrocytoma patients compared with the control (Figures 2E, F and S2) and protein was found to be expressed in the majority of the tumors analyzed. The high GSK3β expression in astrocytoma was most probably due to greater necrosis in the GBM, with increased protein degradation (Figure S2B).

siRNA- and drug-induced inhibition of GSK3 increases differentiation markers

The effect of the inhibition of GSK3 on protein levels of progenitor (Nestin and Sox2) and differentiation (CNPase, GFAP, and β-tubulin III) markers in GBM cell lines U373, LN319, BS125 and LN18 was analyzed using the drugs LiCl and SB216763 or siRNAs. β-catenin is targeted for degradation upon phosphorylation by GSK3β [25]. Blocking GSK3β therefore leads to accumulation of β-catenin, which was used as a read-out for the effects of LiCl and SB216763 on GSK3 activity (Figure 3B). After 72 h treatment with LiCl and SB216773, Nestin protein level decreased in the Nestin-expressing U373, LN319 and LN18 cell lines (Figures 3A, B), which was confirmed by immunocytochemistry (Figure 4B). Nestin and Sox2 were not expressed in the "*ex vivo*" BS125 GBM cell line. Sox2 levels were reduced in LN18, U373 and LN319 upon GSK3 inhibition (Figure 3A, B). The oligodendrocyte specific marker 2′, 3′-cyclic nucleotide 3′-phosphodiesterase (CNPase) and the neuronal marker β-tubulin III increased in BS125, LN18 and LN319, (Figure 3A, B). GSK3 inhibition also increased the protein levels of the astrocytic lineage-specific marker GFAP in LN319 and BS125 (Figure 4A). Downregulation of GSK3 activity in LN18 by siRNA reduced Nestin and Sox2 protein levels (Figure 4C), confirming the specificity of the inhibitory drug SB216763 in blocking GSK3β. The effect of the specific GSK3 inhibitor SB216763 was more pronounced and consistent than the effect of LiCl, which is known to target other signaling molecules [26]. Thus GSK3 inhibition specifically decreased the expression of progenitor markers (Nestin and Sox2) and induced the expression of differentiation markers (neuronal marker β-tubulin III, oligodendrocyte-specific marker CNPase and the astrocytic marker GFAP) in a cell line-dependent manner.

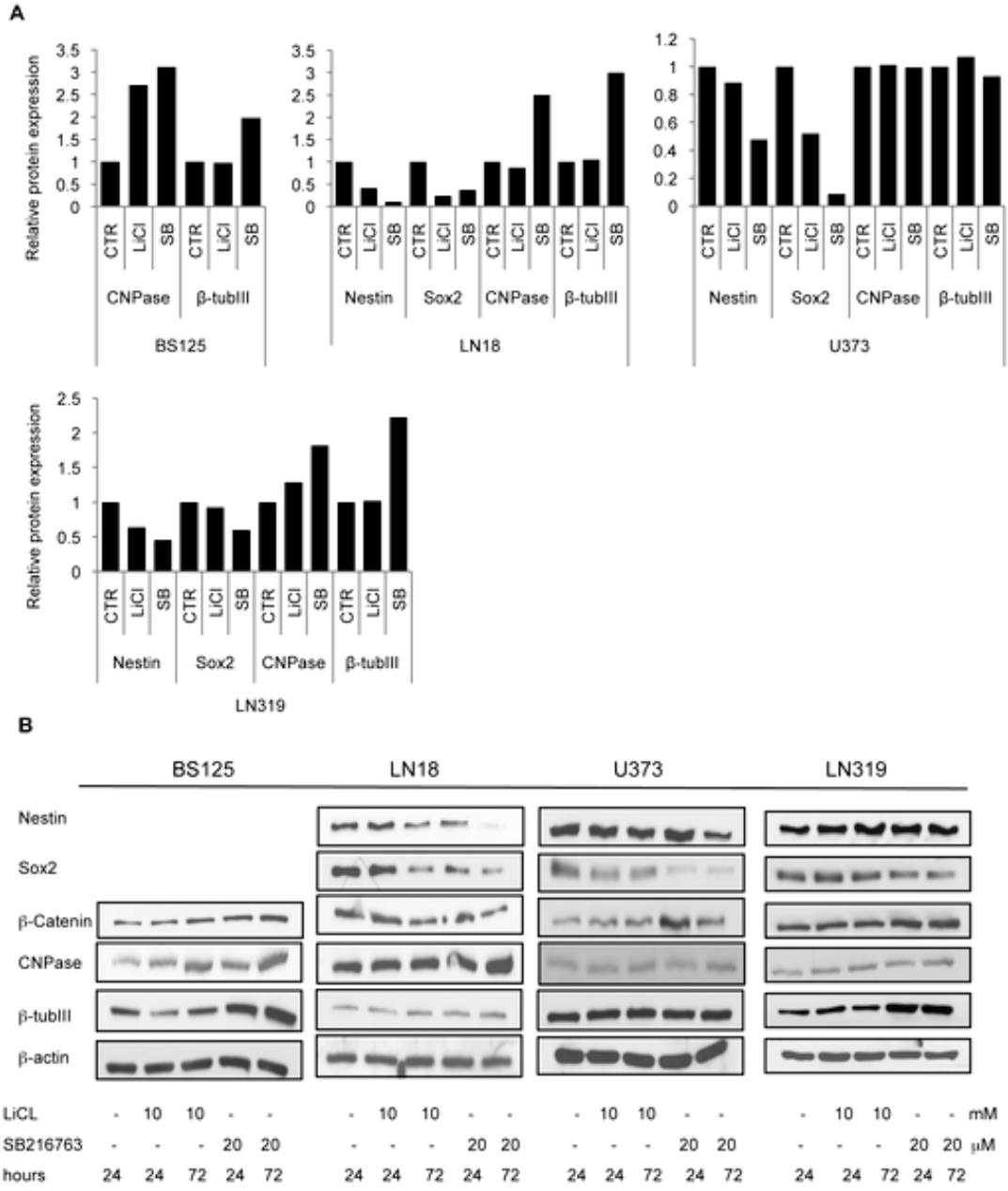

Figure 3. GSK3 inhibitors specifically induced differentiation in GBM cell lines.

Western blot analysis of Nestin, Sox2, CNPase, β -tubulin III and β -actin (loading control) protein levels after treatment of GBM cell lines with GSK3 inhibitors (10 mM LiCl; 20 μM SB216763). Each cell line showed a pro-differentiation response to GSK3β inhibitor application. (A) Protein bands quantified with ImageJ software. Protein levels were normalized to β-actin for each cell line. (B) Corresponding western blots.

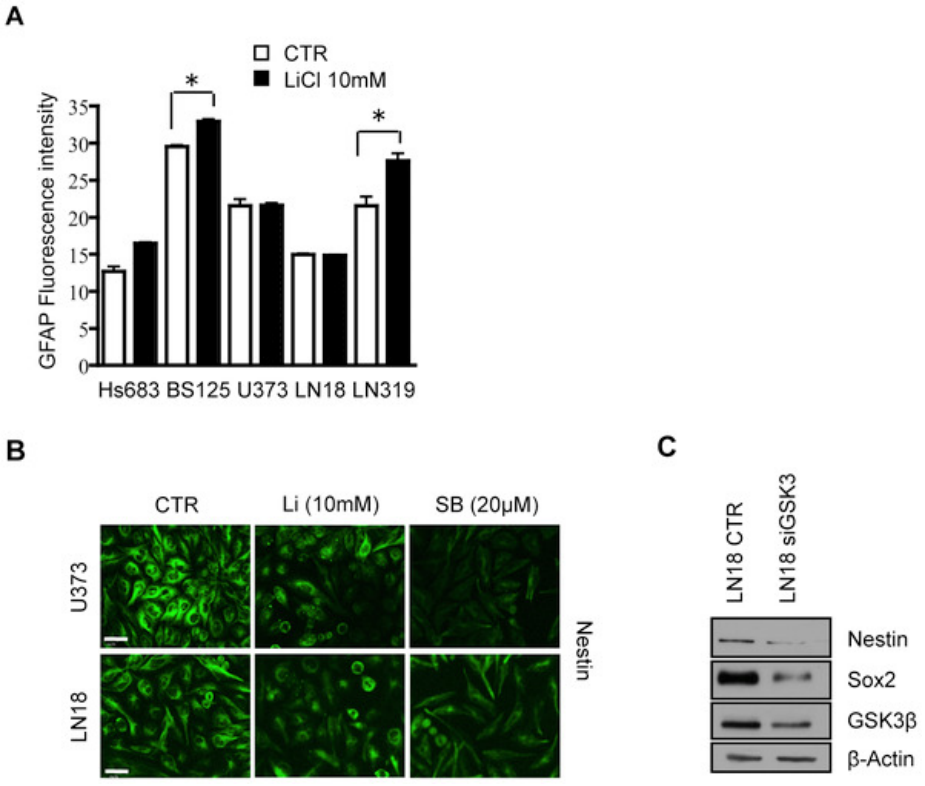

Figure 4. GSK3β downregulation by siRNA treatment induced differentiation.

(A) The intensity of GFAP, an astrocyte-specific marker, was measured by FACS analysis of GBM cell lines treated with 10 mM LiCl for 72 h. (B) Nestin immunostaining of cell lines U373 and LN18 after GSK3β inhibition by LiCl (Li) or SB216763 (SB) for 72 h. (C) GSK3β siRNA reduced Sox2 and Nestin expression in the LN18 cell line. *P<0.05; one-way ANOVA (Newman-Keuls Multiple Comparison Test). Scale bar in B is 30 μm.

Inhibition of GSK3 depletes GBM cells with a stem cell signature

The phenotypic switch towards differentiation in GBM cells following inhibition of GSK3 raises the question of whether GSK3 activity regulates cancer stem cell populations. CD133+ and CD133− cancer stem cells have been described in GBM [2], [3], [35]–[37]. In an analysis of eight different tumorigenic GBM cell lines (LN18, LN215, LN319, U373, LN229, U343, BS125 and Hs683) [34] for the presence of CD133+ cells, only LN319 contained CD133+ cells, at approximately 12%. To test whether the CD133+ population possessed a cancer stem cell-like character, the expression levels of stem cell markers were analyzed in the CD133-enriched population. Nestin, Notch2 and Bmi1 were highly expressed relative to the CD133− fraction (Figure 5C). GSK3β and β-catenin protein levels were also higher in the CD133+ population than in the control (Figure 5C). Inhibition of GSK3 in cell line LN319 with

either LiCl or SB216763 showed a selective effect on the cancer stem cell-like population. LiCl at 10 mM and SB216763 at 20 µM induced a 50–60% depletion of CD133+ cells (Figure 5A). The effects of GSK3 inhibitory drugs were found to be specific in that the epidermal growth factor receptor inhibitor (AEE788) and the γ-secretase inhibitor (DAPT) did not significantly alter the CD133+ population (data not shown). To further consolidate this observation, we enriched the LN319 CD133+ population by FACS sorting, obtaining a CD133+ cell population of approximately 80%. This was maintained for several passages and then subjected to inhibition of GSK3 by LiCl or SB216763, which depleted the CD133+ fraction (Figure 5B).

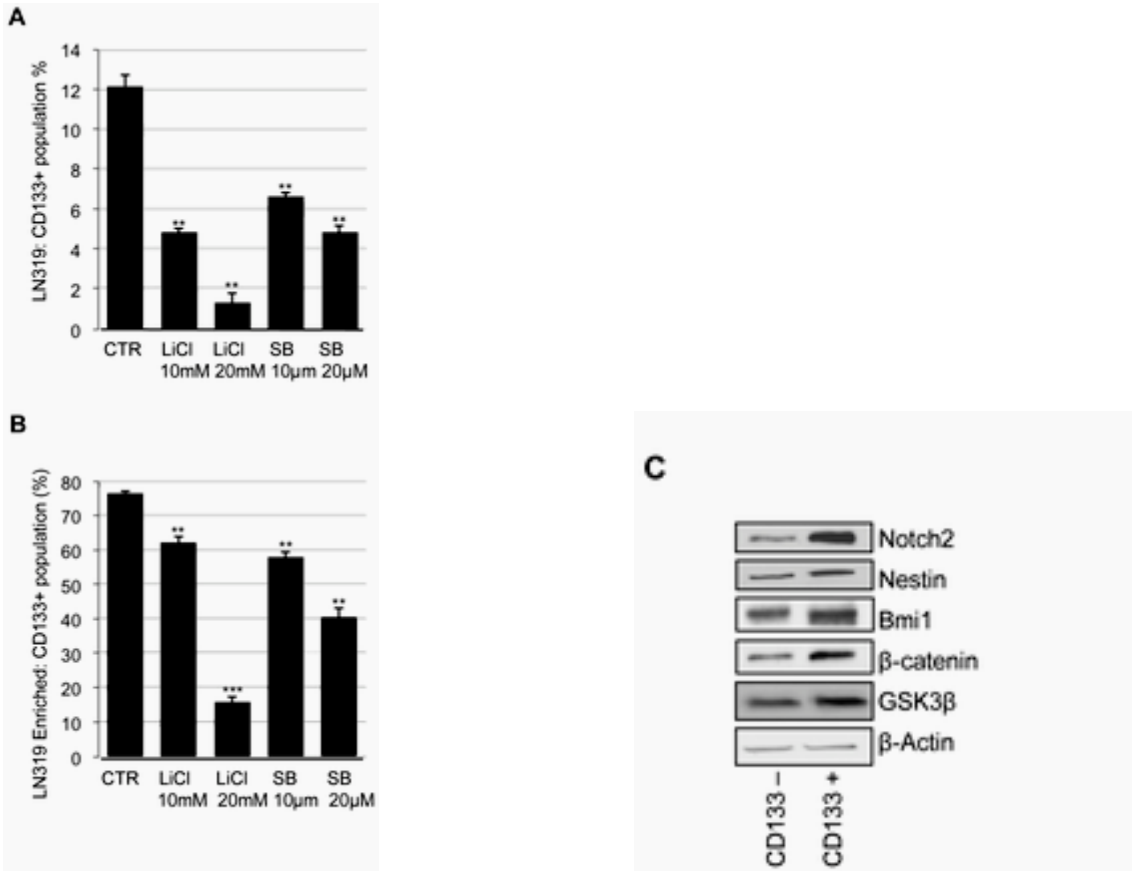

Figure 5. GSK3β inhibition reduced the CD133+ cell population of a GBM cell line.

(A) LN319 GBM cell line was treated for 72 h with 10 or 20 mM LiCl or with SB216763 at 10 or 20 µM. GSK3β inhibition reduced the CD133-positive (CD133+) population. (B) LN319 CD133+ cells were enriched to 80% purity by cell sorting. The enriched population was treated for 72 h with 10 or 20 mM LiCl or with SB216763 at 10 or 20 µM. (C) Western blot analysis of Notch2, Nestin, Bmi1, β-catenin, GSK3β and β-actin in CD133+ and CD133-negative (CD133-) enriched populations compared with the control. **P<0.01; ***P<0.001; one-way ANOVA (Newman-Keuls Multiple Comparison Test).

It has been argued that GBM cells grown for many passages in standard medium do not mirror the stem cell compartment within the original tumor [38]. To examine this, the "*ex vivo"* cell line BS287 was analyzed which had been isolated from a fresh tumor biopsy and directly grown as neurospheres in neurobasal medium supplemented with bFGF and EGF, thus favoring expansion of cancer stem cells. Interestingly, the population with a stem cell-like signature in this cell line was represented by the CD133- and not by the CD133+ population (Figure 6A–C). Only the CD133− population expressed elevated levels of Nestin, Sox2 and Bmi1 and formed neurospheres (Figure 6B, C). Inhibition of GSK3 decreased the stem cell like (CD133−) population (Figure 6D) and also altered protein levels of stem cell and differentiation markers, mainly decreased Sox2 levels (Figure S3). Induction of differentiation impairs the ability of precursor cells to form neurospheres. Inhibition of GSK3 significantly reduced the number and volume of neurospheres in BS287 cells (Figure 6E, F). The results show that inhibition of GSK3 reduces the cancer stem cell pool and that CD133 may not be a reliable cancer stem cell marker.

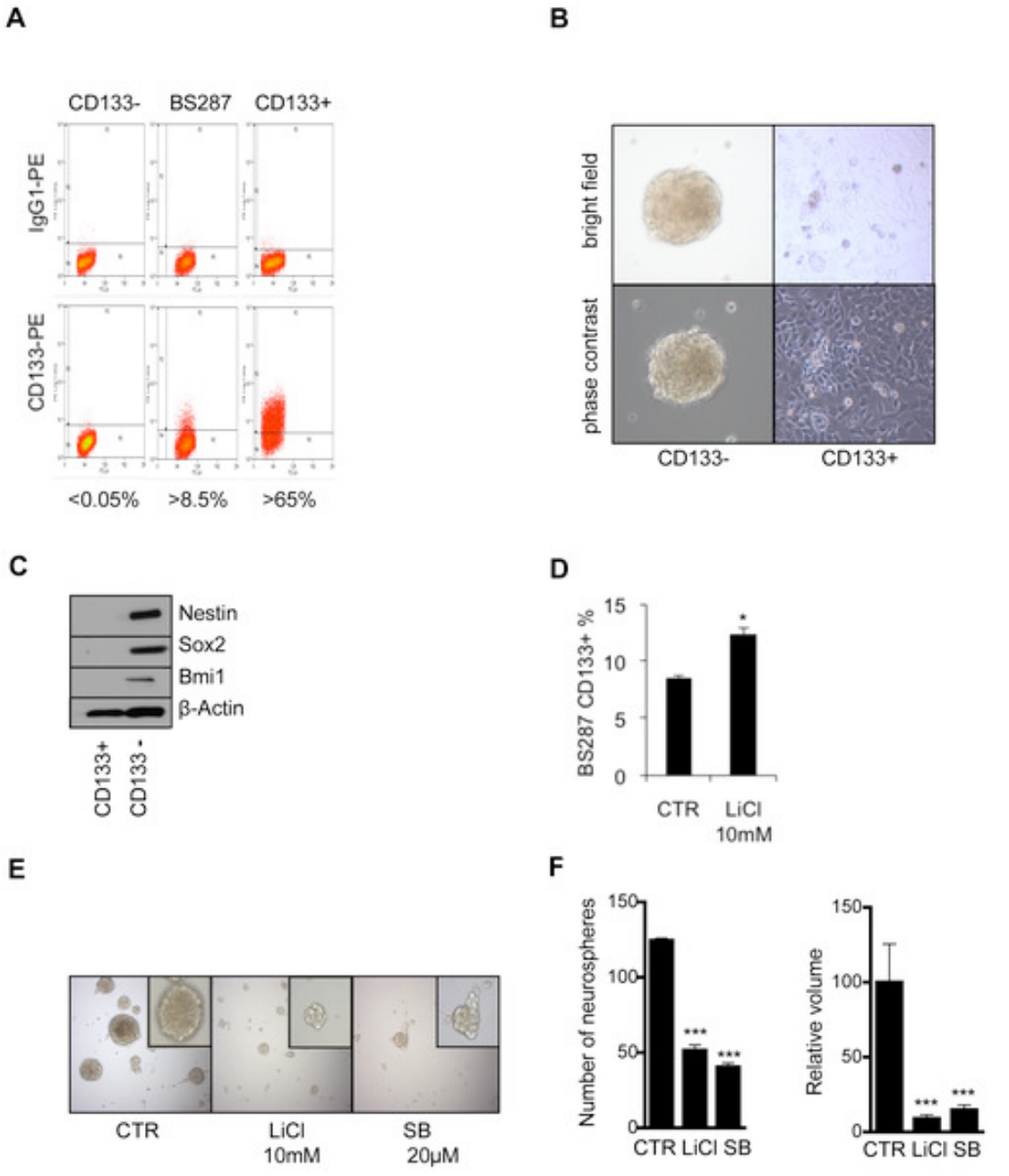

Figure 6. GSK3β inhibition reduced stem cell characteristics in an "ex vivo" GBM cell line.

(A) CD133 sorting of the BS287 "ex vivo" GBM cell line. (B) Growth characteristics of the CD133+ and CD133- populations in BS287. (C) Western blot analysis of Nestin, Sox2, Bmi1 and β-actin in BS287. The CD133- population showed stem cancer-like characteristics. (D) Cells in the CD133+ population with a more differentiated geno/phenotype increased after GSK3β inhibition. (E, F) Inhibition of GSK3β led to a reduction in the number and volume of neurospheres in the BS287 "ex vivo" cell line.

GSK3 inhibition reduces colony formation and induces apoptosis in GBM cells

The effects of GSK3 inhibition on cell proliferation and apoptosis in the GBM cell lines LN18, U373, LN215 and LN319 were analyzed using colony formation, relative cell number and cell death as readout. In a colony formation assay, both the number and size of colonies formed after 14 days of drug treatment were measured. GSK3 inhibitors significantly reduced colony formation in all GBM cell lines tested compared with the untreated control (Figure 7A). The GSK3 inhibitor concentrations used were in the non-toxic range; cell proliferation and survival of the human adipose tissue-derived progenitor cells (A111) were not negatively affected (Figure 7A). GSK3 inhibition by LiCl or SB216763 induced a slight increase in cell death for GBM cell lines LN319, LN18, U373 and BS125 after 72 h (Figure 7B). Induction of cell death was significantly elevated when GSK3 inhibitor LiCl was combined with the standard GBM therapeutic temozolomide in the LN18 cell line (Figure 7D). Cell death was dose-dependent and varied from cell line to cell line. Direct cell counting after exposure of cells to LiCl or SB216763 for 72 h showed inhibition of the proliferation of LN18, LN319, U373 and LN215 cells (Figure 7C). G2-M accumulation was recorded in LN319, LN18, U373 and G2-M arrest in LN215 (Figure S4). In a migration assay, LN319 showed a significant reduction in cell migration following GSK3 inhibition (Figure 7E). These results show that GSK3 strongly reduces colony formation and induces cell death in GBM cell-lines.

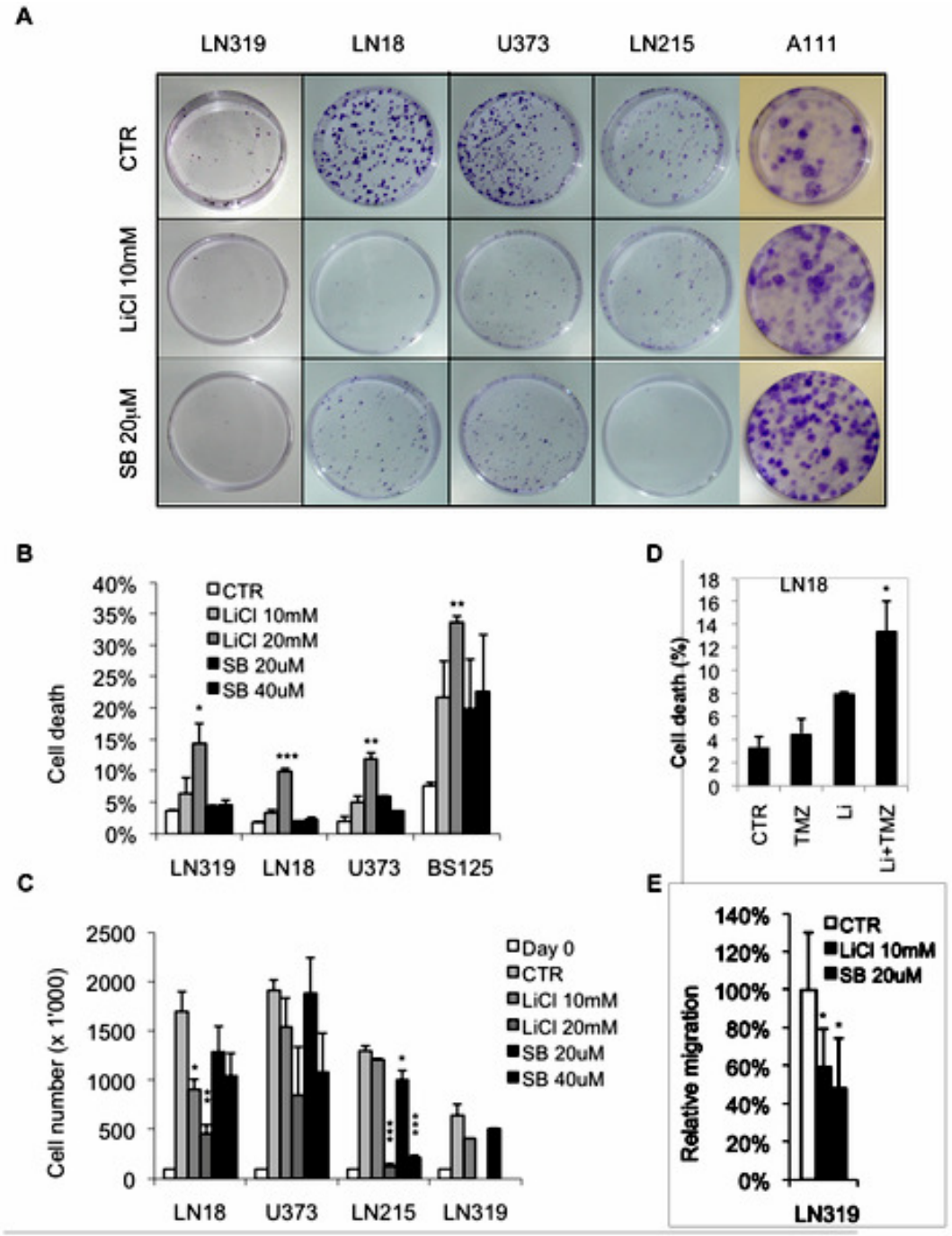

Figure 7. GSK3β inhibition reduced colony formation of GBM cells.

(A) A colony formation assay was performed on GBM cell lines treated with 10 mM LiCl or 20 µM SB216763 for 14 days. (B, C) GBM cell lines treated with LiCl or SB216763 for 72 h. (B) Percent cell death and (C) relative cell number relative to the initial seeding. (D) Cell death determined by PI staining of the LN18 cell line after treatment with 10 mM LiCl with or without 50 µg/ml temozolomide (TMZ) for 72 h. *P<0.05, for the combination of LiCl and TMZ compared with each drug alone. (E) GSK3β inhibition significantly reduced migration of the LN319 cell line. (B, C and E) Treated samples were compared to the corresponding control: *P<0.05; **P<0.01; ***P<0.001; one-way ANOVA (Newman-Keuls Multiple Comparison Test).

Discussion

Bmi1, a member of the polycomb group proteins, is required for self-renewal of neural stem cells and is upregulated in several cancers. It is also known to repress Ink4a/Arf locus inhibiting progenitor cell proliferation during neural differentiation [39]. In differentiated cells, Bmi1 levels decrease while Ink4a/Arf protein levels increase [40]. As the Ink4a/Arf locus is frequently deleted in brain tumors [41], the role of Bmi1 overexpression in GBM cells appears to be distinct from its repression of the Ink4a/Arf locus. For example, downregulation of Bmi1 did not influence Ink4a/Arf protein levels in tumor cells that retained the Ink4a/Arf locus. Thus, in GBM cells, Bmi1 targets a different pathway. Screening of several key proteins controlling cell cycle, development, metabolism, apoptosis and growth, including Erk, Akt, GSK3β, p16 and p14, Bcl-2, c-Myc, Nestin and Sox2, showed that downregulation of Bmi1 reduced GSK3β protein levels and induced differentiation in cancer cells. In addition, tumor cell proliferation, survival, migration and clonogenicity were markedly reduced.

Discovered some 25 years ago [42], GSK3 has been considered only recently as a therapeutic target for cancer [33]. It has been shown that this enzyme negatively regulates the Wnt, Hedgehog and Notch pathways, which are aberrantly activated in several cancers [33], [43]. This suggests that GSK3 inhibitors could exert a therapeutically negative, pro-survival effect on tumor cells. However, the long-term medical use of the GSK3 inhibitor LiCl for the treatment of psychiatric disorders did not lead to an increase in cancer incidence [44], arguing against an oncogenic effect of GSK3 inhibitors. On the contrary, Cohen *et al*. demonstrated that cancer prevalence in psychiatric patients on long-term LiCl medication was lower than in the general population [44], suggesting even a protective effect of LiCl. The results presented here offer a molecular explanation of this epidemiological observation: administration of LiCl induces differentiation and inhibits proliferation and, thereby, might effectively inhibit tumor formation and progression. Furthermore, the plethora of clinical data on LiCl offer solid information about potential side-effects and it appears safe to assume that normal adult stem cells are not negatively affected, even by long-term use of the drug. The very similar phenotypic and functional alterations induced by either inhibiting GSK3 or by downregulating Bmi1 in the present study points to a functional link between Bmi1 and GSK3. However, further studies are needed to analyze whether there

is a direct interaction between Bmi1 and GSK3. Downregulating GSK3 specifically decreased the subpopulation of cancer cells that contained a cancer stem cell-like signature by driving them into differentiation.

Sox2 protein is widely expressed in the early neural plate and early neural tube of several species [45]. In the developing central nervous system, Sox2 expression becomes restricted to the neuroepithelial cells of the ventricular layer, which continue to divide and exhibit an immature phenotype. Cells that leave the ventricular layer lose Sox2 expression [45]. Interestingly, Sox2 has also been implicated in GBM [46], [47] as downregulation of Sox2 reduced cell proliferation and tumorigenicity in GBM cells. Therefore, Sox2 was proposed as a new GBM therapeutic target [46]. At present, inhibitors of Sox2 are not available but the data presented here show that inhibition of GSK3 strongly downregulates Sox2 in GBM cells. This raises the possibility that LiCl or more specific GSK3-inhibitory drugs could be used to decrease the Sox2-dependent tumorigenic potential of GBM cells.

Two main strategies are currently being exploited to eradicate the cancer stem cell (CSC) pool: *i)* chemotherapeutic regimens that specifically drive CSC into apoptosis and thereby deplete the CSC reservoir of the tumor, and *ii)* strategies aiming to drive CSC into differentiation and thereby increase their susceptibility to pro-apoptotic treatments [1]. Given the high degree of drug resistance and the shared cellular and gene expression profiles of adult and cancer stem cells [48], targeting CSC has proven to be difficult. However, induction of differentiation remains a therapeutic strategy for CSC as Piccirillo *et al*. showed that bone morphogenetic proteins can induce differentiation of CD133+ GBM cells, thereby reducing their tumorigenic potential [49]. However, the use of morphogens bears the risk of interfering with the tightly regulated adult stem cell niches. Any strategy to induce differentiation in cancer stem cells must be carefully assessed for any adverse effects on the adult stem cell population.

Our results show GSK3 inhibition to be an attractive strategy for specifically targeting a subpopulation of cancer cells with stem cell-like characteristics. Expression of stem cell and differentiation markers more accurately defined the subpopulation of cells within GBM cell lines and *ex vivo* tumor cells than expression of the CD133 marker. Inactivation of both Bmi1 and GSK3 depleted precursor cells required for tumor maintenance and progression. These

data add another facet to the many effects of GSK3 as a regulator of cancer cell identity. Here, GSK3 activation is identified as a key element in maintaining stem cell-like characteristics in a subset of cancer cells, providing these cells with a higher self-renewal capacity. Recently, downregulation of GSK3 was shown to induce apoptosis in glioma cells and to have an anti-migratory effect in glioma sphreoids [50], [51]. The role of GSK3 inhibiton on differentiation was not analyzed. Optimal therapies for cancer aim to spare normal cells with minimal or no general toxicity while depleting malignant cells. The Wnt pathway is involved in regulating cell processes as proliferation, apoptosis, differentiation, mobility and stem cell self-renewal and has been described also as a major regulator of adult neurogenesis in the hippocampus [52]. In the Wnt/β-catenin pathway GSK3β mediates β-catenin degradation. Use of GSK3 inhibitors leads to the accumulation of β-catenin, which then drives cells into proliferation but this effect was not observed in the present study. This may be explained by the constitutive activation of several growth-promoting pathways, such as EGFR and PI3K, commonly found in GBM. This could lead to maximal Wnt signaling target activation masking additional activation. Conversely, differentiation- and apoptosis-inducing programs, which are low in cancer cells, could be influenced by GSK3 inhibition and are, therefore, directly detectable. On the opposite in normal system as in the A111 cells GSK3 inhibition lead to an increased cell proliferation in accordance with the previously described results in neural progenitor cells [53].

shRNA against Bmi1 downregulated not only GSK3 but also Bcl2, Nestin, Sox2 and not p16 and p14 (Figure 2A). The microarray data showed higher levels of GSK3 expression in brain tumors than in normal brain tissue, and protein was found to be expressed in the majority of the tumors analyzed indicating a role for GSK3 in GBM (Figure 2). GSK3 can thus be regarded as an important regulator of tumor cell identity in GBM.

In conclusion, we propose GSK3 inhibitory drugs, e.g. LiCl, as possible first- and/or second-line treatments complementing standard cancer therapy.

The additive effect of combining the GSK3 inhibitor LiCl and the standard GBM therapeutic temozolomide suggests possible sensitization due to the induction of differentiation by interference with GSK3 activity. In addition, the vast clinical experience of this drug with psychiatric patients indicates safe application and the lower cancer prevalence

in LiCl-treated patients than in the general population suggests a protective effect of the drug [44]. Clinically, LiCl could be tested in patients receiving standard treatments in an additional therapeutic arm, the clinical hypothesis being that long-term LiCl therapy in stabilized GBM patients may delay tumor recurrence from the residual cancer stem cell pool by driving cancer stem cells into differentiation and apoptosis.

Materials and Methods

Patients

Tumor samples obtained from patients during a neurosurgical procedure were immediately frozen and kept at −80°C. All patients gave their written consent for the neurosurgical procedure and for anonymous scientific analysis of diseased tissue according to the guidelines of the Ethics Committee of Basel, Switzerland (EKBB).

Cell culture and reagents

LN319, LN18, LN215, U373, LN229, LN401, U343, U87, BS125 and Hs683 glioma cell lines with defined genetic status of *TP53, p16/p14* and *PTEN* [34], DAOY medulloblastoma and B104 neuroblastoma cell lines were cultured in Eagle medium supplemented with 25 mM glucose, glutamine, standard antibiotics, and 10% FCS. BS287 cells were cultured in Neurobasal medium (Invitrogen) supplemented with basic fibroblast growth factor (20 ng/ml, Invitrogen), epidermal growth factor (20 ng/ml, R&D Systems), B27 (1x) and N2 supplement (0.5x) (Invitrogen). All cells were maintained at 37°C in 5% CO_2. The cell lines were seeded in 6-cm plates at 5'000–10'000 cells/cm^2 and grown for 24 h prior to treatment. For cell counting, cells were treated for 72 h as described in the figure legends and counted by hemocytometer. Lithium chloride (LiCl) was obtained from MERCK and SB216763 from Tocris. Drug concentrations used are indicated in the figure legends. LiCl was dissolved in PBS and SB216763 in DMSO and stored at −20°C. The EGFR inhibitor AEE788 was provided by Novartis Pharma. The γ–secretase inhibitor DAPT was obtained from Roche.

Colony formation assay

For each cell line, 500 cells were plated in triplicate into 94-mm Petri dishes containing 10 ml of culture medium with 10% FCS. Cells were grown for 14 days at 37°C and 5% CO_2, during which period the medium was not changed. Cells were then fixed with 4% formaldehyde in 1x PBS and stained with crystal violet.

BS287 "*ex vivo*" cell line formation and neurobasal medium

Following informed consent, a tumor sample classified as GBM based on the WHO criteria was obtained from a patient undergoing surgical treatment at the University Hospital, Basel, Switzerland. Within 1–3 h after surgical removal, the sample was treated with the Neural Tissue Dissociation Kit (Miltenyi Biotec GmbH) according to the manufacturer's protocol. Tumor cells were cultured in NBE media. Uncoated plastic dishes were used for neurosphere culture of NBE cells.

Plasmids, lentiviruses and transfection

The lentiviral vectors pLKO.1-puro-scrambled-shRNA (Addgene) and pLKO.1-puro-shRNA (Sigma, sh1061: *CCGGCCTAATACTTTCCAGATTGATCTCGAGATCAATCTG G AAAGTATTAGGTTTTT*, sh693: *CCGGCCAGACCACTACTGAATATAACTCGAGTTATA TTCAGTAGTGGTCTGGTTTT*) targeting Bmi1 were transfected into HEK293 cells together with plasmids encoding the packaging (pCMV_dr8_91) and envelope proteins (pMD2-VSV-G) using $CaCl_2$ precipitation. The concentration of infectious particles in the supernatant was titrated using HeLa cells. Glioma cells were transduced with infectious viral particles. Stably transfected clones were selected with 2 µg/ml puromycin. Bmi1 overexpression was obtained with pBABE-puro and pBABE puro-Bmi1 using $CaCl_2$ precipitation for 8 h. Stably transfected clones were selected with 2 µg/ml puromycin. siRNA transfection for GSK3 was performed using the GSK-3α/β siRNA SignalSilence Kit (Cell Signaling Technology) according to the manufacturer's instructions. Cells were transfected using the Amaxa Nucleofector device (Lonza). Cells transfected with non-specific siRNA were used as a control.

Transwell migration assays

Transwell migration assays were performed using modified Boyden chamber units with polycarbonate filters of 8-µm porosity (Costar). The lower side of the filter was coated with 10 mg/ml fibronectin for 2 h at 37°C. The bottom chamber was filled with DMEM containing 10% FCS. Cells (10^4 per well in serum-free DMEM) were plated in the upper chamber and incubated for 24 h with or without GSK3β inhibitors. After removal of the remaining cells from the upper surface of the filter, migrated cells at the bottom of the filter

were fixed with 3.7% formaldehyde in PBS and stained with 0.1% crystal violet. For each treatment, cells in 10 fields of view were counted in three independent experiments.

Western blot analysis and antibodies

Cells were washed with 1x PBS, lysed in buffer containing 2% sodium dodecyl sulfate (SDS), 50 mM Tris pH 6.8, 0.1 M dithiothreitol (DTT), boiled and used either immediately or frozen at −20°C. Protein lysates were resolved on denaturing 8–12% SDS-polyacrylamide gels and transferred to nitrocellulose membranes (iBlot Gel transfer stacks, Invitrogen). The following primary antibodies were used: anti-Bmi1 (Upstate), anti-β-catenin and anti-Nestin (Santa Cruz Biotechnology); anti-β-tubulin III and anti-GFAP (Sigma); anti-CNPase (Chemicon); anti-GSK3β (Cell Signaling); anti-Notch2 (Developmental Studies Hybridoma Bank); anti-Sox2 (R&D systems); anti-CD133 (Miltenyi Biotec); anti-Akt and phospho-Akt (Ser-473) (Millipore, Billerica MA, USA), anti-p16/p14, anti-Bcl2, anti-Erk and anti-phospho-Erk (Santa Cruz Biotechnology, Santa Cruz CA, USA), anti-Actin (Sigma-Aldrich, St. Louis, USA). Decorated proteins were revealed using horseradish peroxidase-conjugated anti-mouse, anti-rabbit, anti-rat (New England Biolabs) or anti-goat (Pierce) secondary antibodies and visualized by the chemoluminescence detection system SuperSignal West Pico (Thermo Scientific). Protein bands were quantified with ImageJ software (http://rsb.info.nih.gov/ij/). Results were normalized to actin levels.

Cell sorting and flow cytometry

Cell DNA content and apoptosis were analyzed by flow cytometry (CyAn ADP Analyzer, Beckman Coulter) and the results statistically evaluated with Summit v4.3 software. Cells were trypsinized, fixed in ice-cold 70% ethanol for 1 h and stained with 50 µg/ml propidium iodide for FACS analysis. Percent dead cells was determined from the proportion of cells in sub-G1 phase. Results are given as mean values from three independent experiments. For CD133 analysis, isolated cells were labeled with anti-CD133 antibody (1:10) for 10 min at 4°C, washed with PBS and sorted (INFLUX Cell Sorter by BD Biosciences).

For BrdU analysis, cells were pulsed with 10 µM bromodeoxyuridine for 2 h and processed with the APC-BrdU kit according to the manufacturer's instructions (BD

Pharmingen). For fluorescent labeling with GFAP, cells were fixed and permeabilized with the Cytofix/Cytoperm kit (BD Pharmingen). Permeabilized cells were incubated with anti-GFAP (1:200) or matching isotype control antibody for 30 min on ice, washed twice and incubated with the corresponding secondary antibody for 30 min on ice and analyzed by flow cytometry (CyAn ADP Analyzer, Beckman Coulter).

Immunocytochemistry

Cells were grown to 80% confluency as a monolayer as described above. Cells were then fixed in 4% PFA in PBS for 15 min at room temperature, washed with PBS and incubated with the primary antibody overnight at 4°C in PBS +1% BSA +0.1% Triton X100. After thorough washing with PBS, the secondary antibody was added for 3 h at room temperature. Cells were imaged by confocal microscopy. All tumor samples analyzed were stained with hematoxylin-eosin.

Microarray analysis of glioma

BS series are primary tumor tissues obtained from patients diagnosed with primary CNS tumors classified according to the WHO grading system. Normal brain tissue used as a template for microarray was obtained from samples of brain surgery for non-neoplastic disease. Total RNA from two normal brains, 12 GBM and eight astrocytoma samples was amplified and labeled using the Affymetrix 2-cycle amplification protocol according to the manufacturer's instructions (Affymetrix). Samples were hybridized to Affymetrix U133v2.0 GeneChips and scanned using an Affymetrix Gene Chip scanner following the manufacturer's instructions. Expression values were estimated using the GC-RMA implementation in the Genedata Refiner 4.1 (Genedata, Basel, Switzerland) package. Data-mining and visualization was performed using the Genedata Analyst 4.1 package. All samples were quantile normalized and median scaled to correct for minor variation in expression distribution. All microarray data reported in the manuscript are in accordance with the MIAME guidelines.

Supporting Information

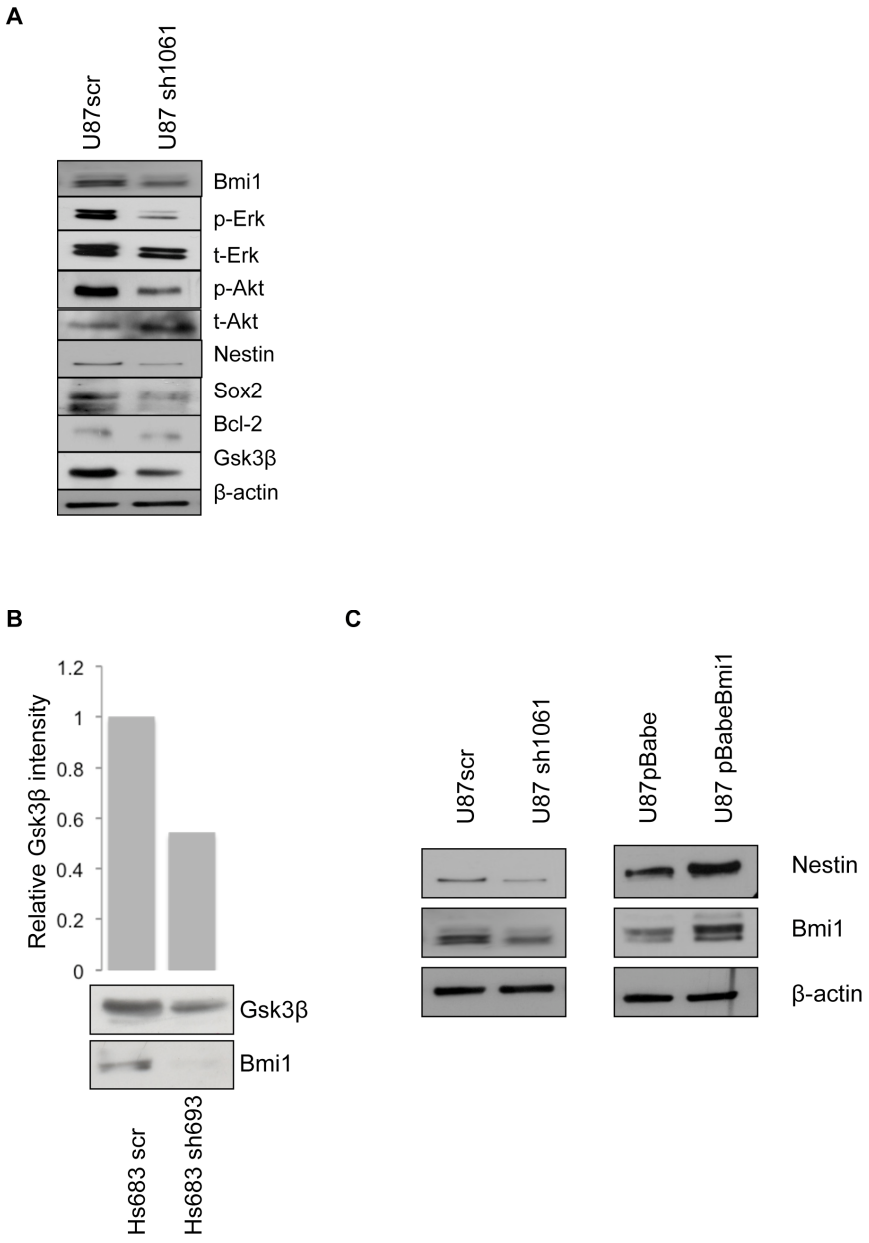

Figure S1.

Bmi1 down-regulation reduces GSK3β protein levels. (A) GBM cell line U87 is transduced with shRNA against Bmi1 (sh1061) or with scrambled shRNA (scr) (B) Bmi1 down regulation lead to GSK3β reduction in Hs683 using a different shRNA sequence. (C) Bmi1 down-regulation in U87 glioma cell line decreased nestin protein levels, whereas Bmi1 over-expression increased Nestin protein expression.

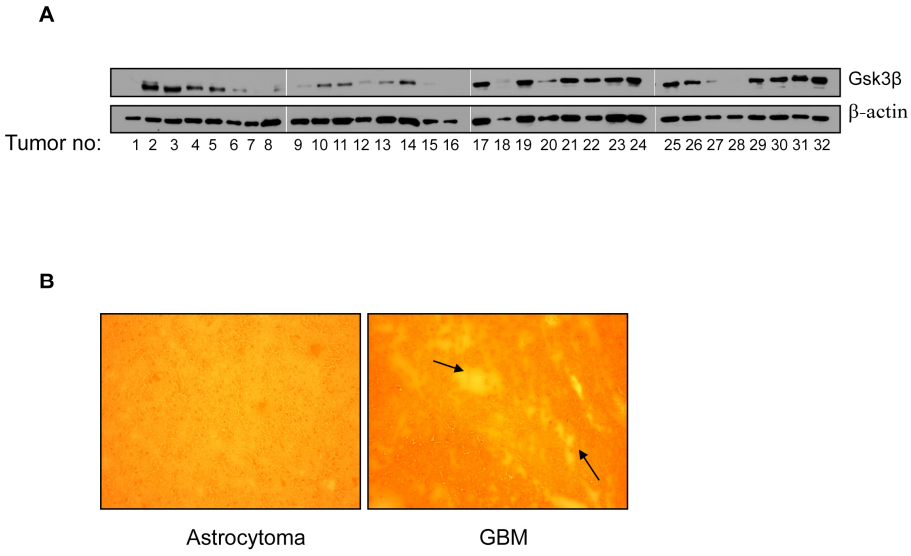

Figure S2.

GSK3β is expressed in primary brain tumors. (A) GSK3β protein expression in a series of primary GBM (1–32). (B) Photomicrograph of the immunohistochemical study showing extensive necrotic areas in GBM compared to Astrocytoma (Hematoxylin-Eosin staining). Arrows point to necrotic areas in GBM.

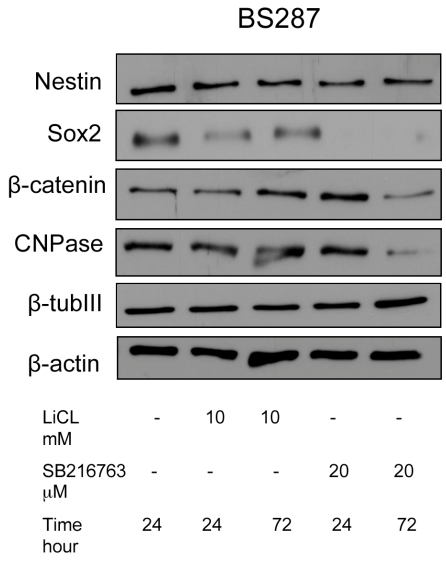

Figure S3.

GSK3 inhibition induces differentiation of the BS287 “ex vivo” cell line. Nestin, Sox2, β-catenin, CNPase, β-tubulin III and β-actin protein expression upon GSK3 inhibition (with LiCl and SB216763 for either 24 or 72 hours) on the BS287 “ex vivo” cell line.

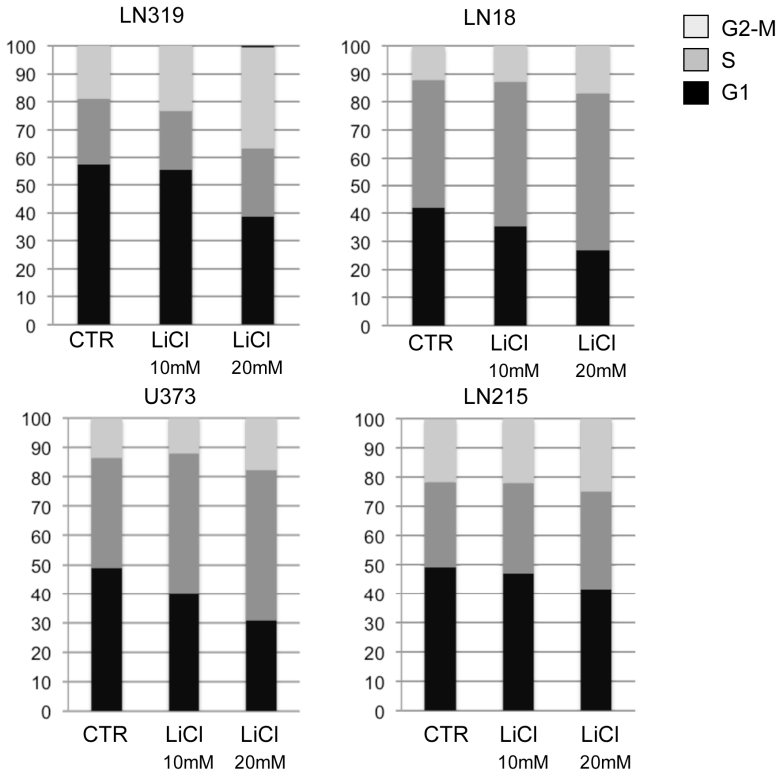

Figure S4.

Cell cycle analysis in GBM cell lines treated with LiCl. The GBM cell lines LN319, LN18, U373 and LN215 were treated with 10 or 20 mM LiCl for 24 hours. Percentage of the cells in G1, S and G2-M phase of the cell cycle were evaluated by FACS analysis.

Acknowledgments

We thank Beatrice Dolder and Dr. Elisabeth Taylor for valuable technical assistance, Emmanuel Traunecker and Verena Jäggin for cell sorting, Dr. Ivan Martin (University of Basel) for adipose tissue derived progenitor cells, Dr. Goberdhan P. Dimri (Northwestern University, Evanston, USA) for the pBabe-puro-Bmi1 vector, and Michal Grzmil (FMI, Basel) for bioinformatics. We thank Dr Patrick King (FMI) for editing the manuscript.

Author Contributions

Conceived and designed the experiments: SK AM MML. Performed the experiments: SK RH BS MP PJM MML. Analyzed the data: SK RH MP PJM AM MML. Contributed reagents/materials/analysis tools: BAH. Wrote the paper: SK RH AM MML.

References

1. Visvader JE, Lindeman GJ (2008) Cancer stem cells in solid tumours: accumulating evidence and unresolved questions. Nat Rev Cancer 8: 755–768.
2. Singh SK, Hawkins C, Clarke ID, Squire JA, Bayani J, et al. (2004) Identification of human brain tumour initiating cells. Nature 432: 396–401.
3. Singh SK, Clarke ID, Terasaki M, Bonn VE, Hawkins C, et al. (2003) Identification of a cancer stem cell in human brain tumors. Cancer Res 63: 5821–5828.
4. Dean M, Fojo T, Bates S (2005) Tumour stem cells and drug resistance. Nat Rev Cancer 5: 275–284.
5. Joo KM, Kim SY, Jin X, Song SY, Kong DS, et al. (2008) Clinical and biological implications of CD133-positive and CD133-negative cells in glioblastomas. Lab Invest 88: 808–815.
6. Merlo A (2003) Genes and pathways driving glioblastomas in humans and murine disease models. Neurosurg Rev 26: 145–158.
7. Newton HB (1994) Primary brain tumors: review of etiology, diagnosis and treatment. Am Fam Physician 49: 787–797.
8. Newton HB (2004) Molecular neuro-oncology and the development of targeted therapeutic strategies for brain tumors. Part 3: brain tumor invasiveness. Expert Rev Anticancer Ther 4: 803–821.
9. Leung C, Lingbeek M, Shakhova O, Liu J, Tanger E, et al. (2004) Bmi1 is essential for cerebellar development and is overexpressed in human medulloblastomas. Nature 428: 337–341.
10. Orlando V (2003) Polycomb, epigenomes, and control of cell identity. Cell 112: 599–606.
11. Nowak K, Kerl K, Fehr D, Kramps C, Gessner C, et al. (2006) BMI1 is a target gene of E2F-1 and is strongly expressed in primary neuroblastomas. Nucleic Acids Res 34: 1745–1754.
12. Valk-Lingbeek ME, Bruggeman SW, van Lohuizen M (2004) Stem cells and cancer; the polycomb connection. Cell 118: 409–418.
13. Park IK, Morrison SJ, Clarke MF (2004) Bmi1, stem cells, and senescence regulation. J Clin Invest 113: 175–179.
14. Molofsky AV, Pardal R, Iwashita T, Park IK, Clarke MF, et al. (2003) Bmi-1 dependence distinguishes neural stem cell self-renewal from progenitor proliferation. Nature 425: 962–967.
15. Zencak D, Lingbeek M, Kostic C, Tekaya M, Tanger E, et al. (2005) Bmi1 loss produces an increase in astroglial cells and a decrease in neural stem cell population and proliferation. J Neurosci 25: 5774–5783.
16. Park IK, Qian D, Kiel M, Becker MW, Pihalja M, et al. (2003) Bmi-1 is required for maintenance of adult self-renewing haematopoietic stem cells. Nature 423: 302–305.
17. Liu S, Dontu G, Mantle ID, Patel S, Ahn NS, et al. (2006) Hedgehog signaling and Bmi-1 regulate self-renewal of normal and malignant human mammary stem cells. Cancer Res 66: 6063–6071.
18. Jacobs JJ, Scheijen B, Voncken JW, Kieboom K, Berns A, et al. (1999) Bmi-1 collaborates with c-Myc in tumorigenesis by inhibiting c-Myc-induced apoptosis via INK4a/ARF. Genes Dev 13: 2678–2690.

19. Jacobs JJ, Kieboom K, Marino S, DePinho RA, van Lohuizen M (1999) The oncogene and Polycomb-group gene bmi-1 regulates cell proliferation and senescence through the ink4a locus. Nature 397: 164–168.
20. Vonlanthen S, Heighway J, Altermatt HJ, Gugger M, Kappeler A, et al. (2001) The bmi-1 oncoprotein is differentially expressed in non-small cell lung cancer and correlates with INK4A-ARF locus expression. Br J Cancer 84: 1372–1376.
21. Shakhova O, Leung C, Marino S (2005) Bmi1 in development and tumorigenesis of the central nervous system. J Mol Med 83: 596–600.
22. Haupt Y, Bath ML, Harris AW, Adams JM (1993) bmi-1 transgene induces lymphomas and collaborates with myc in tumorigenesis. Oncogene 8: 3161–3164.
23. Bruggeman SW, Hulsman D, Tanger E, Buckle T, Blom M, et al. (2007) Bmi1 controls tumor development in an Ink4a/Arf-independent manner in a mouse model for glioma. Cancer Cell 12: 328–341.
24. Godlewski J, Nowicki MO, Bronisz A, Williams S, Otsuki A, et al. (2008) Targeting of the Bmi-1 oncogene/stem cell renewal factor by microRNA-128 inhibits glioma proliferation and self-renewal. Cancer Res 68: 9125–9130.
25. Doble BW, Woodgett JR (2003) GSK-3: tricks of the trade for a multi-tasking kinase. J Cell Sci 116: 1175–1186.
26. Cohen P, Goedert M (2004) GSK3 inhibitors: development and therapeutic potential. Nat Rev Drug Discov 3: 479–487.
27. Hoeflich KP, Luo J, Rubie EA, Tsao MS, Jin O, et al. (2000) Requirement for glycogen synthase kinase-3beta in cell survival and NF-kappaB activation. Nature 406: 86–90.
28. Ougolkov AV, Fernandez-Zapico ME, Savoy DN, Urrutia RA, Billadeau DD (2005) Glycogen synthase kinase-3beta participates in nuclear factor kappaB-mediated gene transcription and cell survival in pancreatic cancer cells. Cancer Res 65: 2076–2081.
29. Tan J, Zhuang L, Leong HS, Iyer NG, Liu ET, et al. (2005) Pharmacologic modulation of glycogen synthase kinase-3beta promotes p53-dependent apoptosis through a direct Bax-mediated mitochondrial pathway in colorectal cancer cells. Cancer Res 65: 9012–9020.
30. Ryder J, Su Y, Liu F, Li B, Zhou Y, et al. (2003) Divergent roles of GSK3 and CDK5 in APP processing. Biochem Biophys Res Commun 312: 922–929.
31. Cline GW, Johnson K, Regittnig W, Perret P, Tozzo E, et al. (2002) Effects of a novel glycogen synthase kinase-3 inhibitor on insulin-stimulated glucose metabolism in Zucker diabetic fatty (fa/fa) rats. Diabetes 51: 2903–2910.
32. Gould TD, Manji HK (2002) The Wnt signaling pathway in bipolar disorder. Neuroscientist 8: 497–511.
33. Wang Z, Smith KS, Murphy M, Piloto O, Somervaille TC, et al. (2008) Glycogen synthase kinase 3 in MLL leukaemia maintenance and targeted therapy. Nature.
34. Ishii N, Maier D, Merlo A, Tada M, Sawamura Y, et al. (1999) Frequent co-alterations of TP53, p16/CDKN2A, p14ARF, PTEN tumor suppressor genes in human glioma cell lines. Brain Pathol 9: 469–479.
35. Beier D, Hau P, Proescholdt M, Lohmeier A, Wischhusen J, et al. (2007) CD133(+) and CD133(-) glioblastoma-derived cancer stem cells show differential growth characteristics and molecular profiles. Cancer Res 67: 4010–4015.
36. Pfenninger CV, Roschupkina T, Hertwig F, Kottwitz D, Englund E, et al. (2007) CD133 is not present on neurogenic astrocytes in the adult subventricular zone, but on embryonic neural stem cells, ependymal cells, and glioblastoma cells. Cancer Res 67: 5727–5736.

37. Galli R, Binda E, Orfanelli U, Cipelletti B, Gritti A, et al. (2004) Isolation and characterization of tumorigenic, stem-like neural precursors from human glioblastoma. Cancer Res 64: 7011–7021.
38. Lee J, Kotliarova S, Kotliarov Y, Li A, Su Q, et al. (2006) Tumor stem cells derived from glioblastomas cultured in bFGF and EGF more closely mirror the phenotype and genotype of primary tumors than do serum-cultured cell lines. Cancer Cell 9: 391–403.
39. Molofsky AV, He S, Bydon M, Morrison SJ, Pardal R (2005) Bmi-1 promotes neural stem cell self-renewal and neural development but not mouse growth and survival by repressing the p16Ink4a and p19Arf senescence pathways. Genes Dev 19: 1432–1437.
40. Molofsky AV, Slutsky SG, Joseph NM, He S, Pardal R, et al. (2006) Increasing p16(INK4a) expression decreases forebrain progenitors and neurogenesis during ageing. Nature.
41. Labuhn M, Jones G, Speel EJ, Maier D, Zweifel C, et al. (2001) Quantitative real-time PCR does not show selective targeting of p14(ARF) but concomitant inactivation of both p16(INK4A) and p14(ARF) in 105 human primary gliomas. Oncogene 20: 1103–1109.
42. Hemmings BA, Yellowlees D, Kernohan JC, Cohen P (1981) Purification of glycogen synthase kinase 3 from rabbit skeletal muscle. Copurification with the activating factor (FA) of the (Mg-ATP) dependent protein phosphatase. Eur J Biochem 119: 443–451.
43. Foltz DR, Santiago MC, Berechid BE, Nye JS (2002) Glycogen synthase kinase-3beta modulates notch signaling and stability. Curr Biol 12: 1006–1011.
44. Cohen Y, Chetrit A, Sirota P, Modan B (1998) Cancer morbidity in psychiatric patients: influence of lithium carbonate treatment. Med Oncol 15: 32–36.
45. Wegner M (1999) From head to toes: the multiple facets of Sox proteins. Nucleic Acids Res 27: 1409–1420.
46. Gangemi RM, Griffero F, Marubbi D, Perera M, Capra MC, et al. (2008) SOX2 Silencing in Glioblastoma Tumor Initiating Cells Causes Stop of Proliferation and Loss of Tumorigenicity. Stem Cells.
47. Fong H, Hohenstein KA, Donovan PJ (2008) Regulation of self-renewal and pluripotency by Sox2 in human embryonic stem cells. Stem Cells 26: 1931–1938.
48. Ben-Porath I, Thomson MW, Carey VJ, Ge R, Bell GW, et al. (2008) An embryonic stem cell-like gene expression signature in poorly differentiated aggressive human tumors. Nat Genet 40: 499–507.
49. Piccirillo SG, Vescovi AL (2006) Bone morphogenetic proteins regulate tumorigenicity in human glioblastoma stem cells. Ernst Schering Found Symp Proc 59–81.
50. Nowicki MO, Dmitrieva N, Stein AM, Cutter JL, Godlewski J, et al. (2008) Lithium inhibits invasion of glioma cells; possible involvement of glycogen synthase kinase-3. Neuro Oncol 10: 690–699.
51. Kotliarova S, Pastorino S, Kovell LC, Kotliarov Y, Song H, et al. (2008) Glycogen synthase kinase-3 inhibition induces glioma cell death through c-MYC, nuclear factor-kappaB, and glucose regulation. Cancer Res 68: 6643–6651.
52. Byfield MP, Murray JT, Backer JM (2005) hVps34 is a nutrient-regulated lipid kinase required for activation of p70 S6 kinase. J Biol Chem 280: 33076–33082.
53. Nusse R, Fuerer C, Ching W, Harnish K, Logan C, et al. (2008) Wnt signaling and stem cell control. Cold Spring Harb Symp Quant Biol 73: 59–66.

Part 4

Notch2 Signaling in Neural Stem Cells Promotes Features of Glioma Stem Cells.

submitted to 'Stem Cells', 2011

Jan S. Tchorz[1, 4], Dimitri Cloetta[1, 4], Mercedes Tome[1], Balasubramanian Sivasankaran[3], Michal Grzmil[2], **Roland M. Huber[2,3]**, Frank Kirchhoff, Nicole Schaeren-Wiemers[1], Martin Gassman[1], Brian A. Hemmings[2], Adrian Merlo[3], Bernhard Bettler[1*]

1) Department of Biomedicine, Institute of Physiology, Pharmazentrum, University of Basel, 4056 Basel, Switzerland

2) Friedrich Miescher Institute for Biomedical Research, 4056 Basel, Switzerland

3) Laboratory of Molecular Neuro-Oncology, University Hospital Basel, ZLF, 4056 Basel, Switzerland

4) these authors contributed equally to this study

Abstract

Glioblastoma multiforme (GBM) brain tumors are proposed to originate from neural stem cells (NSCs) transforming into glioma stem cells (GSCs). The underlying molecular events are poorly understood. *Notch2* is frequently amplified in GBMs and correlates with poor prognosis, possibly implicating Notch2 into gliomagenesis. Here we generated mice expressing the activated intracellular domain of Notch2 in NSCs. We found that Notch2 signaling triggers NSC differentiation into astrocytes while inhibiting oligodendrocyte and neuronal differentiation. Moreover, Notch2 signaling increases NSC proliferation, which causes a pronounced hyperplasia of the neurogenic niche. Neurospheres derived from mice expressing activated Notch2 show increased proliferation and reduced apoptosis. Likewise, high levels of Notch2 expression in GBM cell lines correlate with increased GSC proliferation and reduced apoptosis. In GBM biopsies Notch2 mRNA expression levels positively correlate with mRNA expression levels of genes controlling stemness (Sox2, Nestin) and astrocyte fate (Vimentin, GFAP) while they negatively correlate with the expression levels of genes controlling oligodendrocyte fate (Olig2, CNP, PLP1). High Notch2 mRNA expression levels also correlate with high and low expression levels of antiapoptotic (Mcl1, BclX) and proapoptotic (Bax) markers, respectively. It therefore appears that Notch2 signaling in NSCs produces key GSC features, including increased proliferation, astrocytic lineage commitment and reduced apoptosis. Aberrant Notch2 signaling may therefore contribute to malignant transformation of NSCs. Accordingly, pharmacological blockade of Notch2 signaling may represent a promising strategy for therapeutic interference with GBM formation.

Introduction

Despite advances in tumor imaging, surgery, chemo and radiation therapy, more than 70% of GBM patients die within 2 years of diagnosis [1]. The discovery of a highly tumorigenic subpopulation of stem-like GSCs in GBM biopsies [2] led to the proposal GSCs arise from developmentally stalled NSCs [3-6]. GSCs have characteristics of NSCs, such as multipotency, self-renewal capacity, high motility and robust proliferative potential [4-5]. Mutations impairing cell cycle control and apoptosis may therefore promote NSCs to become GSCs [7-8]. Intriguingly, *Notch2* was found to be amplified in most GBMs and high Notch2 mRNA levels strongly correlate with poor prognosis [9]. Moreover, the active form of Notch2 increased xenograft GBM tumor growth [10]. Notch signaling regulates proliferation, cell fate decisions and survival in various cell types, including NSCs [11-14]. Notch2 may therefore represent one of the factors contributing to malignant transformation of NSCs.

Four Notch receptors (Notch1-4) exist in mammals. Binding of ligands triggers a proteolytic processing of receptors and translocation of their intracellular domains (NotchICDs) to the nucleus. NotchICD binding to RBPjκ leads to transcriptional activation of the effector genes *Hairy* and *Enhancer of Split* homologs (e.g. *Hes1 or Hes5*), which can prevent neuronal differentiation [12, 15]. Notch1, for example, was shown to control proliferation and survival of NSCs during brain development [16-18] and to promote glial differentiation [12-14], Notch1 was also implicated in the development of a variety of tumors, including GBMs [3, 19-20]. Notch2 signaling is much less understood. Notch2 is expressed throughout the embryonic [21-22] and adult NSC niche [18, 22], regulates morphogenesis of Bergmann glia cells and inhibits granule neuron differentiation in the cerebellum [23]. Because of the strong association of Notch2 with GBMs it is also proposed that constitutive Notch2 signaling in NSCs could contribute to gliomagenesis [9]. To test this hypothesis, we now generated mice expressing activated Notch2 in NSCs and compared the properties of such NSCs with those of GSCs and GBM biopsies. Our data show that Notch2 expression during development or in adults is sufficient to induce features of GSCs and GBM in NSCs, thus further substantiating a role for Notch2 in gliomagenesis.

Results

Notch2ICD Expression in Embryos Causes Severe Hyperplasia and Inhibits Neurogenesis

To study the role of Notch2 signaling in the developing brain, we used N2ICD/Nestin-Cre mice to drive expression of myc-tagged Notch2ICD in NSCs and their progeny (Figure 1A). N2ICD/Nestin-Cre mice died at birth. Myc-immunostaining in E18.5 mice showed widespread expression of Notch2ICD in the brain (Supplementary Figure 1A). Moreover, mRNA levels not only for Notch2 but also for its direct downstream target genes Hes1 and Hey1 are highly increased in E16.5 N2ICD/Nestin-Cre mice compared to control mice (Figure 1B), showing and increase in Notch2 signaling. E18.5 N2ICD/Nestin-Cre but not single transgenic N2ICD or Nestin-Cre control embryos displayed a hyperplasia of the neurogenic region (ganglionic eminence) and enlarged ventricles in cresyl violet stainings (Figure 1C,D) when compared to wildtype embryos.. The ganglionic eminence displayed a 3-fold increase in size (Figure 1C) and an enlarged zone of Ki67+ (Figure 3E) and Nestin+ NSCs (Supplementary Figure 2A). The strata region of E18.5 N2ICD/Nestin-Cre embryos had an increased cell density and lacked the striasome, a typical porous structure (Figure 1D,F). Moreover, the striatal region lacked immunostaining for substance P and GAD67/67, which are commonly used to outline the striatum in the ventral forebrain (Figure 1F). NeuN immunostaining showed that the ventral forebrain of N2ICD/Nestin-Cre mice is not only devoid of GAD65/67+ interneurons but of mature neurons in general (Supplementary Figure 2B). It therefore appears that the striatal region is mainly populated by an increased number of Nestin+ NSCs that fail to develop into neurons (Figure 1F, Supplementary Figure 2A,B). This supports a dual role for Notch2 during embryogenesis in proliferation and inhibition of neurogenesis.

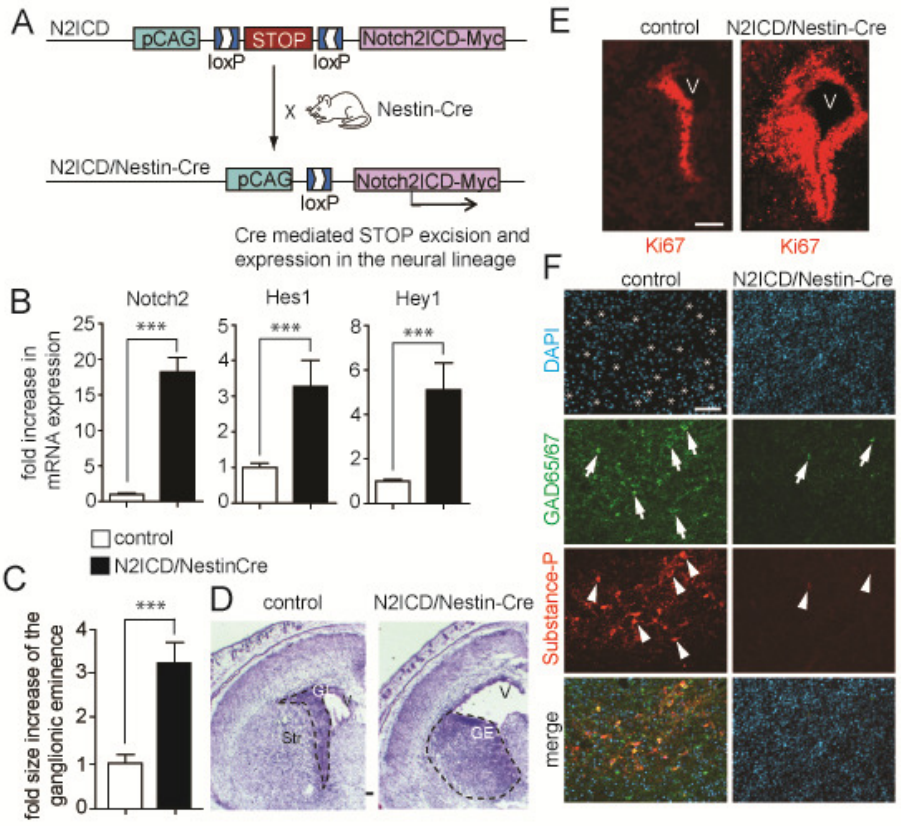

Figure 1. Activated Notch2 signaling in the developing brain results in a hyperplasia of the neurogenic zone.

(A) Transgenic expression of activated Notch2 in the developing brain. N2ICD mice contain a chicken β-actin (pCAG) promoter followed by a LoxP flanked transcriptional Stop cassette and the Notch2 intracellular domain (Notch2ICD) with a c-terminal human 5xMyc tag. Crossing N2ICD mice with Nestin-Cre mice yielded N2ICD/Nestin-Cre mice in which Nestin-Cre mediated Stop cassette excision enabled Notch2ICD expression specifically in the neural lineage. (B) Notch2 signaling is highly upregulated in N2ICD/Nestin-Cre mice. The mRNA expression levels for Notch2 and its downstream targets Hes1 and Hey1 are increased in brains from E16.5 N2ICD/Nestin-Cre mice when compared to controls mice. (C) Quantification of the ganglionic eminence revealed a more than 3-fold increase in size in E18.5 N2ICD/Nestin-Cre mice compared to E18.5 wt controls. (D) Coronal cranial sections of E18.5 control and N2ICD/Nestin-Cre mice were stained with cresylviolet. The neurogenic zone termed ganglionic eminence (GE; indicated by a dashed line in the corresponding magnified panels) showed a dramatic hyperplasia in N2ICD/Nestin-Cre mice, while it appeared normal controls. E18.5 N2ICD/Nestin-Cre mice also displayed enlarged ventricles (V) and a lack of a properly developed striatum (Str) as it was present in E18.5 wt controls.. (E) Immunostaining for the proliferation marker Ki67 reveals a highly increased population of proliferating cells in E18.5 N2ICD/Nestin-Cre mice compared to E18.5 wt controls. (F) Immunostaining for markers that are present in the striatum of E18.5 wt mice such as Gad65/67 and Substance P reveals that N2ICD/Nestin-Cre mice do not express such markers in the ventral forebrain. In addition, DAPI staining in E18.5 wt mice shows the typical porous structure of the striasome (asterisks) which was missing in N2ICD/Nestin-Cre, further indicating a lack of a properly developed striatum due to the hyperplasia of the GE. Bar diagram shows mean±SD, ***=p<0.001, students t-test). Scale bars are (A,C) = 200µm, (D) = 50 µm (D).

Notch2ICD Expression in Adult Mice Increases Proliferation and Inhibits Neuronal Differentiation in the Dentate Gyrus

GBM mostly occur in adults and therefore Notch2ICD expression in adult NSCs more accurately mimics a possible role of Notch2 in gliomagenesis. Unfortunately, perinatal lethality of N2ICD/Nestin-Cre mice precludes studying a possible role of Notch2 in malignant transformation of adult NSCs. We therefore generated triple transgenic N2ICD/YFP/GCE mice by crossing N2ICD mice with double transgenic GFAPCreERT2/R26R-YFP mice [24-25]. These mice allow for tamoxifen-induced Notch2ICD and YFP expression in adult GFAP+ NSCs and astrocytes [24] (Figure 2A). YFP/GCE mice, which express YFP but not Notch2ICD upon tamoxifen induction were used as littermate controls. N2ICD/YFP/GCE mice exhibit a 2-fold increase in Ki67+ proliferating YFP+ cells in the subventricular zone (SVZ) and the subgranular zone (SGZ), indicating that Notch2ICD increases proliferation in adult NSCs as well (Figure 2B,C,D). One year old N2ICD/YFP/GCE mice (n=8) still exhibited hyperplasia but had no tumors (data not shown). This suggests that Notch2 is not oncogenic by itself, although the number of aged mice is too small to be conclusive.

We next analyzed whether Notch2ICD prevents neuronal differentiation in the adult brain (Figure 2C). N2ICD/YFP/GCE and YFP/GCE mice were co-immunostained for YFP and NSC (GFAP, Sox2) or neuronal (Dcx, NeuN) markers. The dentate gyrus of N2ICD/YFP/GCE mice showed exhibited approximately a 2-fold increase in YFP+ cells expressing GFAP/Sox2 (Figure 2E,F). Likewise, N2ICD/YFP/GCE mice had a significantly reduced number of YFP+ cells expressing Dcx/NeuN (Figure 2E,F). This supports that Notch2 signaling inhibits neuronal differentiation in adult mice as well.

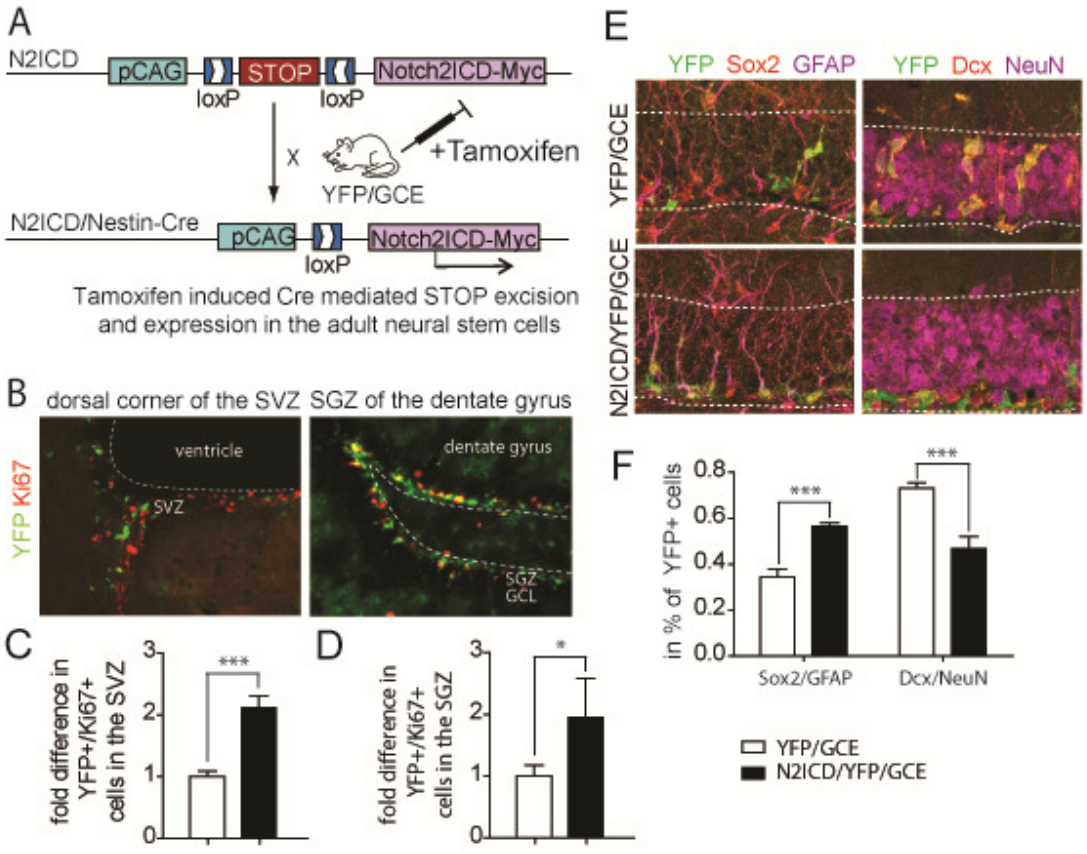

Figure 2. Notch2 regulates proliferation and differentiation in adult NSCs.

(A) N2ICD mice introduced previously in Figure 1A were mated with GFAPCreER^{T2}/Rosa26-YFP (YFP/GCE) mice, yielding N2ICD/YFP/GCE mice which allow for Stop excision in adult NSCs upon Tamoxifen injection. Upon Stop excision in N2ICD/YFP/GCE, both Notch2ICD and a YFP reporter are expressed. Tamoxifen was administered to 8 week old mice for 5 consecutive days and analysis was performed 7 days after the last injection. (B) Immunostaining for YFP and the proliferation marker Ki67 was performed on N2ICD/YFP/GCE and YFP/GCE coronal cryosections, to determine the amount of YFP+ cells that proliferate. Panels show exemplary pictures from the SVZ of the lateral ventricle and SGZ of the dentate gyrus. (C) Quantification of YFP+ cells expressing Ki67 showed a 2-fold increase of proliferating YFP+ cells in N2ICD/YFP/GCE mice compared to YFP/GCE in the SVZ and in the SGZ (D), indicating that activated Notch2ICD increased proliferation in the adult neurogenic niche. (E) Immunostaining for YFP in combination with either adult stem cell marker (Sox2, GFAP; left panels) or marker for neurons (Dcx, NeuN; right panels) was performed in the dentate gyrus to analyze the effect of activated Notch2 on adult NSC differentiation in N2ICD/YFP/GCE and YFP/GCE mice. (F) Quantification of YFP+ cells coexpressing Sox2 and GFAP revealed that N2ICD/YFP/GCE mice have almost 2-fold more YFP+ which express NSC marker compared to YFP/GCE mice, while the number of YFP+ neurons dramatically decreased. This indicates that Notch2ICD expression increased the amount of NSCs while it largely blocked neurogenesis. Bar diagrams show mean±SEM, *=p<0.05, **= p<0.01, ***= p<0.01. Statistics were performed using student's t-test.

Notch2ICD Expression in Neurospheres Increases Proliferation, Promotes Survival and Glial Differentiation

To study NSC proliferation and expansion, we made neurospheres from the ganglionic eminence of E14.5 N2ICD/Nestin-Cre and littermate control embryos (Figure 3A). Neurospheres from N2ICD/Nestin-Cre NSCs were significantly larger (73µm vs. 42µm diameter, $p<0.0001$), indicating that Notch2ICD increases NSC proliferation in neuropheres as well (Figure 3B,C). Next, we used neurospheres to study whether Notch2ICD regulates NSC fate decisions. We differentiated neurospheres from E14.5 N2ICD/Nestin-Cre embryos *in vitro* (Figure 3A) and quantified cells expressing the the neuronal marker βIII-Tubulin (Tuj1), the oligodendrocyte marker Olig2 and the astrocyte marker GFAP (Figure 3D). A significantly reduced number of Tuj1+ cells in N2ICD/Nestin-Cre cultures indicates that Notch2ICD prevents NSCs from efficiently differentiating into neurons (Figure 3E). N2ICD/Nestin-Cre NSCs efficiently developed into GFAP+ astrocytes (Figure 3F). However, no statistically significant increase in the number of GFAP+ astrocytes was observed, presumably because most cells already differentiate into astrocytes in the absence of Notch2ICD. Intriguingly, the staining intensity for GFAP in differentiated N2ICD/Nestin-Cre NSCs was visibly increased compared to control (Figure 3D). Increased GFAP protein levels and decrease Tuj1 protein levels were confirmed on immunoblots (Figure 3H). Moreover, the number of Olig2+ oligodendrocytes was significantly decreased in N2ICD/Nestin-Cre NSCs (Figure 3G). This supports that Notch2 signaling biases fate decisions in NSCs towards the astrocytic lineage by inhibiting differentiation into neurons or oligodendrocytes. Notch2 signaling in NSCs is therefore sufficient to promote and maintain the astrocytic features of GSCs.

To test the role of Notch2ICD activity on NSC survival and cell death resistance, N2ICD/NestinCre and control neurospheres were treated with etoposide to induce apoptotic cell death. Apoptosis induction was assessed by the cleavage of caspase-3 which is part of the apoptotic signaling cascade (Figure 3I). Etoposide treatment induced the cleavage of caspase-3 in control NSCs. In contrast, NSC overexpressing Notch2ICD showed low levels of cleaved caspase-3 compared to controls at the same treatment, suggesting a role of Notch2 signaling in regulating NSC survival mechanisms.

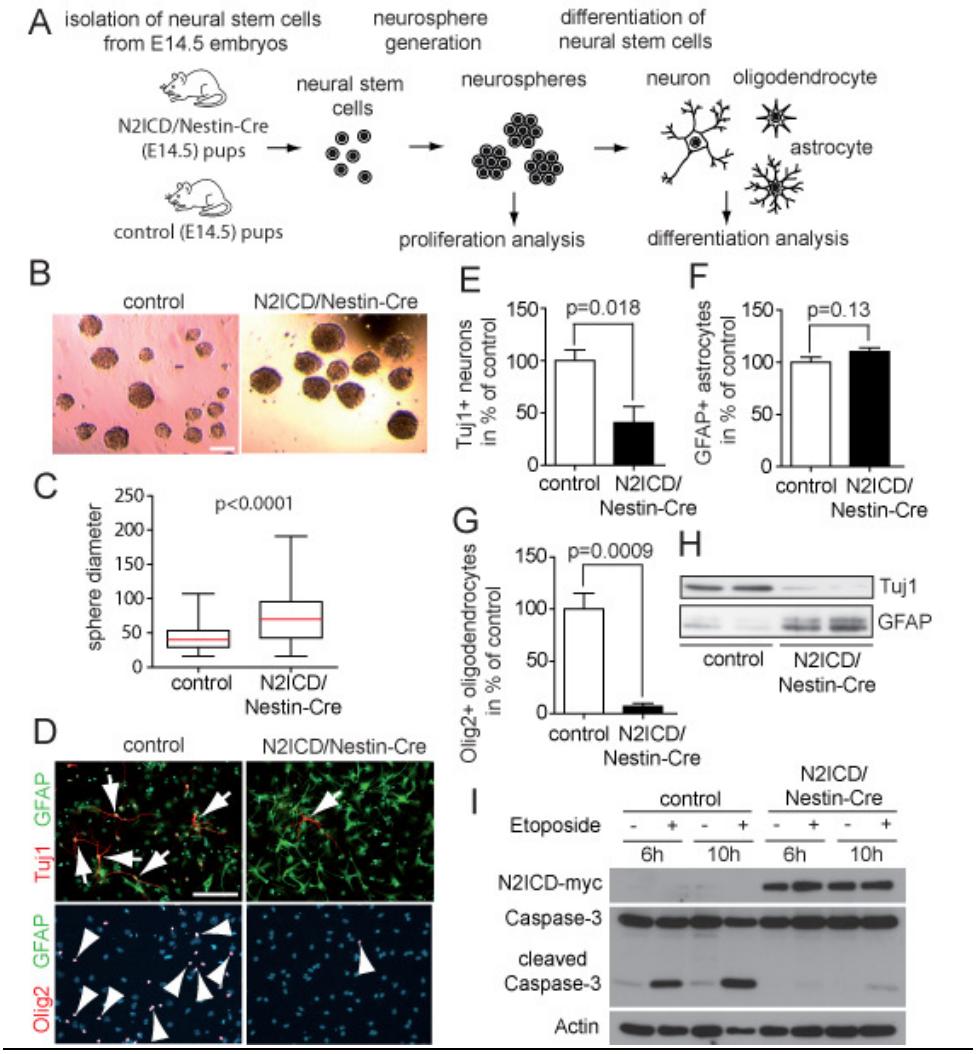

Figure 3. Notch2 signaling controls NSC proliferation and differentiation *in vitro*.

(A) Scheme depicting the experimental setup used for the analysis of activated Notch2 in NSCs. NSCs were isolated from E14.5 N2ICD/Nestin-Cre and control mice and neurospheres were cultured under non-adherent conditions in serum-free media. Neurosphere growth was determined to study NSC proliferation. In order to study NSC differentiation, neurospheres were dissociated and differentiated into neurons, astrocytes and oligodendrocytes under adherent conditions in serum-containing media. (B) Neurospheres derived from N2ICD/Nestin-Cre mice and thus overexpressing Notch2ICD showed increased sphere size when compared to control spheres. (C) Quantification of neurosphere diameters showed that the median diameter in N2ICD/Nestin-Cre spheres was increased by 75% when compared to control spheres, showing that activated Notch2 increases NSC proliferation. (D) Immunostainings on differentiated N2ICD/Nestin-Cre and control NSCs for markers defining neurons (Tuj1) (arrows), astrocytes (GFAP) and oligodendrocytes (Olig2) (arrowheads) was performed and counterstained with DAPI to study the effect of Notch2ICD on NSC fate decisions. Quantification of differentiation marker in percent of DAPI+ nuclei showed that Notch2ICD largely blocked neuronal differentiation (E) and increased the number of astrocytes (F). Furthermore, N2ICD/Nestin-Cre NSC almost completely lost their ability to differentiate into Olig2+ oligodendrocytes (G). Although the increase in GFAP+ astrocyte numbers was not statistically significant, the overall GFAP staining was more intense (D) and GFAP protein levels were highly increased in western blot analysis from differentiated NSCs, while Tuj1 levels diminished (H). (I) NSCs overexpressing Notch2ICD were protected from apoptosis. Lower levels of cleaved caspase-3 were detected in the Notch2ICD overexpressing NSCs after etoposide treatment. Box plot diagrams show median (red line), boxed 25% and 75% percentiles and whiskers marking minima and maxima, statistics were performed using Mann-Whitney test. Scale bar (B, D) = 100µm.

Notch2ICD Expression in GSCs Derived from Human Glioblastoma Cell Lines Increases Proliferation and Prevents Apoptosis

To activate and inhibit Notch2 signaling in GSCs we stably transfected U373 GBM cells with human Notch2ICD (U373-Notch2ICD cells) and dominant-negative mastermind-like I (MAML1dn) (U373-MAML1dn cells) [26-27], respectively. Transfected GBM cells were cultured in neurosphere media under non-adherent conditions, resulting sphere growth. The presence of GSC markers (Nestin, Sox2, CD133) confirmed that spheres derived from GSCs rather than non stem-like GBM cells growing under non-adherent conditions (Supplementary Figure 3).

Notch2ICD and MAML1dn expression visibly increased and reduced the size of GSC spheres, respectively (Figure 4A). Notch2ICD overexpressing GSC spheres had a significant approximately 2-fold increase in diameter compared to parental U373 (U373-wt) GSC spheres (111±2.4µm vs. 56±1.7µm; mean±SEM, $p<0.0001$) (Figure 4B). U373-MAML1dn GCS spheres had a 33% decrease in diameter when compared to U373-wt cells (41±0.5 µm vs. 56±1.7µm; mean±SEM, $p<0.0001$) (Figure 4B).

To evaluate whether Notch2 signaling plays a role on GSCs chemoresistance to cell death, U373-Notch2ICD and GFP-transfected (U373-GFP) control GBM cells were treated with etoposide. Both cell populations showed a higher resistance to apoptosis induction compared to neurospheres (data not shown) since etoposide treatment had to be prolonged to 24h to detect an effect. Similarly to the apoptosis assay on neurospheres, the GBM cells expressing Notch2ICD showed low levels of cleaved caspase-3 compared to GFP-transfected GBM cells (Figure 4C). This result supports a role for Notch2ICD activity on the chemoresistance of glioma cells to apoptosis. In addition, U373-Notch2ICD GBM cells showed increased levels of anti-apoptotic proteins such as Bcl-2 and Mcl-1 compared to U373-GFP GBM control cells, further implicating Notch2 in GBM survival (Figure 4D). Thus, Notch2 signaling not only increases GSC proliferation but also induces chemoresistance of GBM cells to etoposide treatment by upregulating antiapoptotic pathways.

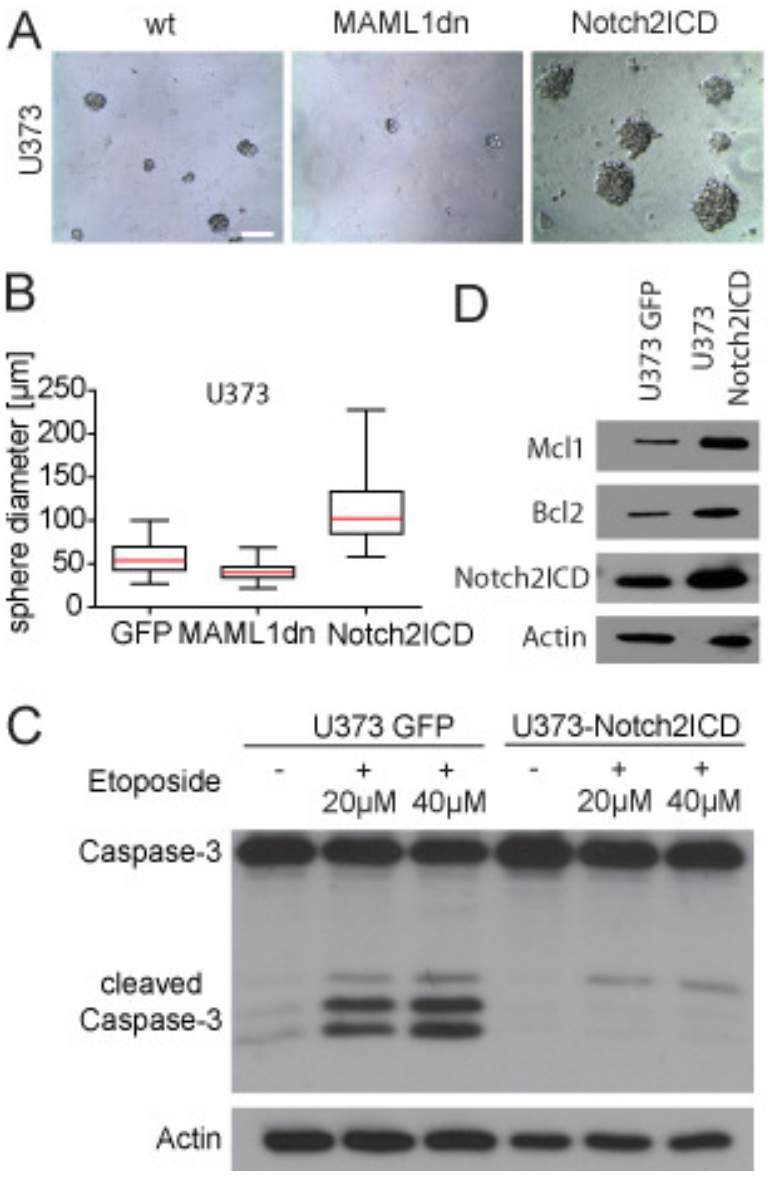

Figure 4. Notch2 signaling controls proliferation and induces survival in GSCs.

(A) U373 GBM cell were cultured for 7 days in neurospheres media under non-adherent conditions, allowing GSCs to form spheres. U373-Notch2ICD GSC spheres overexpressing Notch2ICD showed increased sphere size, indicating increased GSC proliferation, when compared to GCS spheres derived from parental (wt) U373 cells. U373-MAML1dn GSCs expressing MAML1dn and thus inhibiting canonical Notch signaling, formed only very small spheres. (B) Notch2 signaling increases GSC proliferation *in vitro*. Quantification of the GSC sphere diameters derived from U373 GSCs showed a 2-fold increase in proliferation in U373-Notch2ICD GSC spheres compared to wt U373 GSC spheres, while U373-MAML1dn GSC spheres showed a decrease. (C) Notch2 signaling induces chemoresistance to Etoposide. U373-Notch2ICD GBM cells were resistant to etoposide-induced apoptosis. Cleaved caspase-3 expression was reduced in U373-Notch2ICD GBM cells compared to U373-GFP GBM cells. (D) U373-Notch2ICD upregulate antiapoptotic proteins. U373-Notch2ICD GBM cells show an increase in Mcl1 and Bcl2 protein levels compared to U373-GFP cells, indicating that Notch2 signaling increases the resistance to apoptosis by upregulation of antiapoptotic factors. Actins controls for sample loading (C, D). Scale bar (A) = 100µm.

Notch2 Levels in Primary Human GBMs Correlate with Antiapoptotic, Stem Cell and Glial Markers

Using published microarray data [28], we investigated whether Notch2 expression in primary human GBM samples correlates with the expression of genes regulating cell differentiation and survival (Figure 5A, Supplementary Figure 4). As a control, Notch2 expression correlated highly expression of the target genes Hes1 and Hey1. Transcripts for the anti-apoptotic proteins Mcl1 and BclX exhibited moderate correlation with Notch2, while transcripts for the proapoptotic protein Bax showed a strong negative correlation. This further implicates Notch2 into GBM survival. GSC markers (Sox2, Nestin) and FABP7 (also known as BLBP) exhibited strong and moderate correlation with Notch2, respectively, supporting that Notch2 levels correlate with an increased GSC pool. The astrocyte markers vimentin and GFAP highly correlated with Notch2 expression, in line with Notch2 directing astrocyte versus oligodendrocyte fate decisions, Likewise, oligodendrocyte markers (CNP, Olig2, PLP1) showed a strong negative correlation with Notch2 transcript levels. In summary, this correlation analysis further supports that Notch2 signaling determines much of the cellular identity of GSCs.

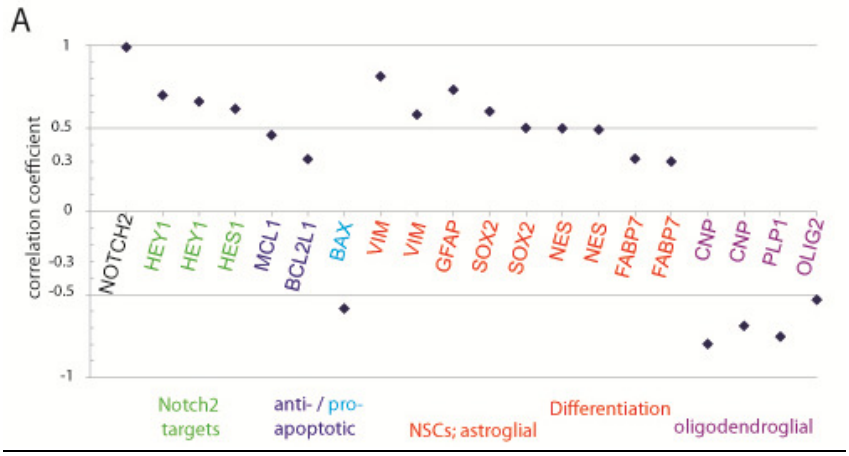

Figure 5.

Notch2 expression in primary human GBMs correlates with the expression of genes inhibiting apoptosis, promoting stemness (NSCs) and inducing astrocyte differentiation. Correlation coefficients for Notch2 and genes involved in apoptosis (blue) and differentiation (red/purple) as well as Notch2 targets (green) were calculated using Pearson's Score. Values 0.3 to 0.5 or -0.3 to -0.5 represent moderate positive or negative correlation, whereas values from 0.5 to 1 or -0.5 to -1 indicate high positive or negative correlation, respectively. Correlation coefficient (0.98) for another Notch2 probe is shown as a positive control.

Discussion

Developmentally stalled NSCs are a possible source of GSCs giving raise to GBMs [3-6]. NSCs inherently express the cellular machinery necessary for tumor formation (e.g. multipotency, self-renewal capacity, high motility and robust proliferative potential) and therefore are at risk for malignant transformation [4-5]. *Notch2* is amplified in most GBMs and high Notch2 levels correlate with poor prognosis. In contrast, loss of *Notch2* is frequently found in oligodendroglioma and low Notch 2 levels correlates with a much better prognosis. Since Notch1 is a critical regulator of neurogenesis [13-14, 29] and implicated in tumor formation, we now used a transgenic approach to study whether Notch2 signaling in NSCs potentially plays a role in GBM formation. In support of this, we found that Notch2 signaling in NSCs increases proliferation and causes severe hyperplasia of the neurogenic niche. Notch2 expression in cultured NSCs promotes astrocytic differentiation at the expense of neuronal and oligodendrocytic differentiation. Moreover, the expression of the activated form of Notch2 in NSCs increased the resistance to apoptosis of these cells, rendering them insensitive to the cytotoxic drug etoposide. Our findings therefore support that Notch2 signaling in NSCs is sufficient to induce key features of GSCs, including increased proliferation, reduced apoptosis and astrocytic lineage commitment. Given that NSCs with constitutively high Notch2 signaling acquire features akin of those of GSCs, we studied whether manipulating the level of Notch2 signaling in GSCs from cultured GBM cells influences proliferation and cell survival. We found that increasing Notch2 signaling in cultured GBM cells significantly increases proliferation, while blocking Notch2 signaling reduces proliferation. Increased Notch2 signaling in cultured GBM cells also caused an upregulation of anti-apoptotic proteins, which increases cell survival. These results are in line with activated Notch2 increasing proliferation and reducing apoptosis in HSR-GBM1 cells and xenografts thereof.

Enhanced proliferation and survival of GBM cells with elevated Notch2 levels may provide an explanation for the increased aggressiveness of GBMs with high Notch2 levels [30]. Finally, we also found that Notch2 expression levels in GBM biopsies positively correlate with the expression levels of genes controlling stemness (Sox2, Nestin) and astrocyte fate (Vimentin, GFAP) while they negatively correlate with the expression levels of

genes controlling oligodendrocyte fate (Olig2, CNP, PLP1). Notch2 expression levels in GBM biopsies positively and negatively correlate with the expression levels of antiapoptotic (Mcl1, BclX) and proapoptotic (Bax) markers, respectively. In summary, it appears that key features of GSCs, such as increased proliferation, astrocytic lineage commitment and reduced apopotosis can be induced by Notch2 signaling in NSCs. In particular, the enhanced proliferation seen in the presence of Notch2 signaling may stochastically increase the risk of NSCs to acquire somatic mutations and to transit to GSCs. It is possible that aberrant Notch2 signaling occurs after GSCs are formed. In this case high levels of Notch2 expression would promote GSCs to give rise to astrocytomas, such as GBMs. In this case, loss of Notch2 signaling in subsets of expanding GSCs with *Notch2* amplification could explain the formation of mixed oligodendroglioma. In any instance, blockade of Notch2 signaling may interfere with glioma formation and the aggressiveness of tumors and thus be of therapeutic benefit for the treatment of GBMs.

Materials and methods

Mice

Homozygous N2ICD mice [31] with a floxed STOP cassette in the chicken β-actin (pCAG) promoter were crossed with heterozygous Nestin-Cre mice [32]. Cre/LoxP-mediated activation of the pCAG promoter in double transgenic N2ICD/Nestin-Cre mice results in Notch2ICD expression in the neural lineage [32] (Figure 1A). Single transgenic N2ICD were used as littermate controls. Since E18.5 Nestin-Cre mice showed no obvious phenotype, we did not further include them as controls. Crossing of homozygous N2ICD mice with GFAPCre-ERT2 (hereafter GCE) mice [24] containing a Cre/LoxP inducible Rosa26-YFP reporter gene (hereafter YFP) [25] resulted in triple transgenic N2ICD/YFP/GCE mice expressing Notch2ICD in the adult NSC niche (Figure 2A). YFP/GCE mice were used as littermate controls. Intraperitoneal administration of tamoxifen (2 mg, Sigma) once daily for 5 consecutive days was used for Cre-mediated excision of floxed STOP cassettes in the promoters of 8-10 week old N2ICD/YFP/GCE mice or YFP/GCE mice. Mice were sacrificed 7 days after the final injection and perfused with paraformaldehyde. Genotyping was with TaqMan-PCR (YFP mice: sense 5`- ACAGCTCGTCCATGCCGA-3`, antisense 5`-ATCACATGGTCCTGCTGGAGT-3`, probe 5`-FAM-TGATCCCGGCGGCGGTCA-TAMRA-3`; N2ICD mice: sense 5`-ATATCCGCGGTGGAGATCAA-3`, antisense 5`- TAGACCAGGCTGGGCTAAA-3`, probe 5`- VIC-CGGTACCAGATCTC-MGB-3`; Nestin-Cre/GCE mice: sense 5`- GCCGCGCGAGATATGG -3`, primer antisense 5`- GCCACCAGCTTGCATGATC -3`, probe 5`- FAM-CCGCGCTGGAGTTTCAATACCGG-TAMRA -3`). Vaginal plugs correspond to embryonic day 0.5 (E0.5) in timed matings. All animal experimentation was approved by the veterinary office of Basel-Stadt.

Immunohistochemistry and Immunoblots

Embryos were fixed overnight at 4°C with 4% paraformaldehyde (PFA) in phosphate buffered saline (PBS), cryoprotected at 4°C in 30% sucrose containing PBS for 48h and frozen in TissueTEK compound (Sakura Finetec, Netherlands). Mounted cryostat sections (10µm) were washed in PBS, incubated for 1h in blocking solution (5% horse serum and 0.15% Triton

X-100 in PBS) and incubated overnight with primary antibodies in blocking solution at 4°C. Adult mice were intracardially perfused with ice-cold 0.9% saline solution, followed by ice-cold 4% PFA solution in 0.1 M phosphate buffer (PB). Brains were post-fixed with 4% PFA overnight, washed in PB, cryoprotected in 30% sucrose in PB for 48 hrs, embedded and frozen in OCT. Free floating coronal sections (30 µm) were collected in multi-well dishes and stored at -20°C in antifreeze solution. For immunostaining, sections were washed with PBS, incubated for 1 hr in blocking solution (5% horse serum and 0.3% Triton X-100 in PBS) followed by overnight incubation with primary antibodies in blocking solution at 4°C. PFA fixed cells were incubated for 1 hr in blocking solution (5% horse serum and 0.1% Triton X-100 in PBS) and incubated with primary antibodies overnight in blocking solution at 4°C. The primary antibodies were mouse anti-NeuN (MAB377; Chemicon/Millipore, Billerica, MA), rabbit anti-GFAP (ZO334; Dako, Denmark), mouse anti-GFAP (Chemicon) and rabbit anti-MAP2 (Chemicon), rat anti-Notch2 (C6551.6DbHN; Developmental Studies Hybridoma Bank, Iowa City, IA), goat anti-Myc (A-14; Santa Cruz, Santa Cruz, CA), rat anti-Substance-P (NC1/34 HL; Abcam, UK), rabbit anti-Ki67 (NCL-Ki67p; Novocastra, UK), rabbit anti-Gad65/67 (G5163; Sigma, Saint-Louis, MO), rabbit anti-Olig2 (AB9610, Chemicon) goat anti-Sox2 (AF2018; R&D Systems, Switzerland), goat anti-Dcx (SC-8066, Santa Cruz), chicken anti-GFP (Molecular Probes/Invitrogen Carlsbad, CA), mouse anti-Nestin (sc-23927, Santa Cruz), rabbit anti-CD133 (sc-30220, Santa Cruz) and mouse anti-βIII-Tubulin (Tuj1) (Sigma). After rinsing in PBS, sections were incubated with secondary antibodies in blocking solution for 1 hr and counterstained with DAPI. The secondary antibodies used were Cy3-conjugated donkey anti-rabbit, Cy3-conjugated donkey anti-mouse, Cy3-conjugated donkey anti-goat, Cy3-conjugated donkey anti-rat, Cy5-conjugated donkey anti-rabbit, Cy5-conjugated donkey anti-mouse, Cy5-conjugated donkey anti-goat and Cy2-conjugated donkey anti-chicken (Jackson Immunoresearch, UK). Imaging was with a Leica DMI6000 fluorescence microscope or a Zeiss LSM510 confocal microscope. For detection of proteins on immunoblots, whole protein lysates were prepared in lysis buffer from neurospheres or GBM cells. Protein extracts were separated by electrophoresis on SDS-PAGE gels (20ug/lane) and transferred onto polyvinylidene difluoride membranes (PVDF) (Millipore). Membranes were blocked (10 mM Tris-HCl, 150 mM NaCl, 5% milk powder and 0.5% Tween 20) for 1 hour at RT and incubated overnight at 4C with primary antibody against: GFAP (Dako), Tuj1, mouse anti-Myc (SC-40, Santa Cruz), rabbit anti-Caspase-3 (#9062, Cell Signaling), mouse anti-beta-Actin (A5316,

Sigma), anti-Bcl-2 (Santa Cruz) and anti-Mcl1 (Santa Cruz). After washing, membranes were incubated for 1 h at RT with IgG-horseradish peroxidase conjugated secondary antibodies followed by the SuperSignal chemiluminescent substrate (Pierce) to detect protein-antibody biding.

Neurosphere Cultures

NSC cultures were prepared and maintained as described [33]. Briefly, telencephali of E14.5 N2ICD/Nestin-Cre or N2ICD control mice were dissected and the tissue triturated in neurosphere medium consisting of DMEM/F12 (1:1), 0.2 mg/ml L-glutamine, 1% penicillin/streptomycin, 2% B27, 2 µg/ml Heparin, 20 ng/ml EGF and 10ng/ml FGF2. For adult neurosphere cultures, subventricular zones from N2ICD/GFP and GFP control mice were microdissected from 300 µm vibratome sections in L15 and the tissue digested with 0.05 % Trypsin. After 5 to 6 days in culture neurospheres were split plated at a density of 10^5cells/ml. For determination of neurosphere number and size, aliquots of samples were pipetted into 96 well plates. For immunoblotting, spheres were lysed in RIPA buffer supplemented with complete protease inhibitor cocktail (Roche) and phosphatase inhibitor cocktail I and II (Sigma). For *in vitro* differentiation, cells were seeded at a density of 200,000 cells/cm² on coverslips coated with 15 µg/ml poly-L-ornithin and 40 µg/ml laminin. Cells were differentiated in neurosphere medium lacking FGF2, EGF and heparin and fixed after 5 days with 4% PFA. For N2ICD or GFP expression in adult NSCs, neurosphere cultures from N2ICD/GFP or GFP mice were infected with adenovirus expressing Cre recombinase (AdCre, gift of J. Relvas) to excise the floxed STOP cassette in the promoters. For transduction of neurospheres, cell suspensions were incubated with AdCre at a multiplicity of infection (MOI = ratio of infectious virus particles to cells) of 500. Cells were infected with virus under occasional shaking for 1 h at 37°C at $5x10^3$ cells/ml and then plated at 10^5 cells/ml for neurosphere cultures.

Stable Expression of Notch2ICD in GBM Cell Lines

U373 GBM cells [34] were grown in Dulbecco's Modified Eagle Medium (DMEM, Invitrogen) supplemented with 10% (v/v) fetal bovine serum (FBS, No: S1810, Labforce,

Basel, Switzerland), 1% glutamax solution (v/v) (Invitrogen) and 1% (v/v) penicillin/streptomycin solution (Invitrogen). Cells were suspended by proteolysis with 1x trypsin-EDTA (Invitrogen) for 5 minutes at 37°C and transfected with expression plasmids using $CaCl_2$ precipitation. Stably transfected clones were selected in 100µg/ml Geneticin® or G418 (Invitrogen Corporation, California. USA) for 20 days. Notch2ICD (nucleotides 5107 to 7425 of the human Notch2 cDNA, AF308601) was expressed from pcDNA 3.0-IRES-EGFP, dominant-negative Mastermind-like I (MAML1dn) from pEGFP-N3-*MAML1dn* (kind gift of Dr. Aster). For GBM sphere culture, U373 GBM cells were cultured under the same conditions as described above for neurospheres.

RT-PCR

Total RNA was isolated from whole brain of E16.5 embryos using SV total RNA isolation system (Promega, Switzerland) and used as template to synthesize cDNA with GoScript reverse transcriptase (Promega). Relative quantitative RT-PCR was performed using Power SYBR Green PCR Master Mix (Applied Biosystems, Switzerland) according to manufacturer's protocol. Normalization was performed with GAPDH cDNA. The following primers were used for Notch2 (sense 5' CCCAAGGACTGCGAGTCAGG 3' and antisense 5' GGCAGCGGCAGGAATAGTGA 3'**)** **,** Hes1 (sense 5' CTACCCCAGCCAGTGTCAAC 3' and antisense 5' AAGCGGGTCACCTCGTTCAT 3'), Hey1 (sense 5'CTTGAGTTCGGCGCTGTGTTCC 3' and antisense 5' GATGCCTCTCCGTCTTTTCCT 3') and GAPDH (sense 5' TTAGCCCCCCTGGCCAAGG 3' and antisense 5'CTTACTCCTTGGAGGCCATG 3'.

Apoptosis assay

Neurospheres (N2ICD/NestinCre and single N2ICD control) (2-4 passages) with day in vitro (div) 6 were dissociated to obtain a single cell suspension. Cells were plated at $5x10^4$ cell/ml in a 6-well plate (Falcon) in neurosphere medium for 4 days to allow neurosphere formation. On the fourth day etoposide (Sigma) was added at 20uM for 6h or 10h or not added as a control. Neurospheres were harvested by centrifugation at 300g 5min and lysated for protein extraction. At least three independent experiments were performed.
U373-GBM cells transfected either with N2ICD or GFP were plated at $5x10^4$ cell/ml. After 2

days 20uM or 40uM etoposide was added for 24h. Protein extract were obtained as described above for neurospheres.

Correlation Analysis

To calculate correlation coefficients we used absolute expression values from published microarray data [28]}. Briefly, total RNA from two normal brains and 12 GBM samples was amplified and labeled using the Affymetrix 2-cycle amplification protocol according to the manufacturer's instructions (Affymetrix, Santa Clara, CA). Samples were hybridized to Affymetrix U133v2.0 Gene Chips and scanned using an Affymetrix Gene Chip scanner. Expression values were estimated using the GC-RMA implementation in the Genedata Refiner 4.1 (Genedata, Switzerland) package. Data-mining was performed using the Genedata Analyst 4.1 package. All samples were quantile normalized and median scaled to correct for minor variation in expression distribution.

Supplemental Material

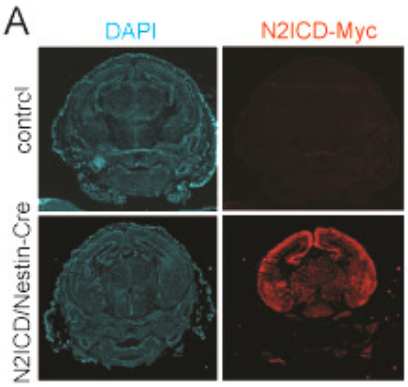

Supplementary Figure 1.

N2ICD/Nestin-Cre mice express Notch2ICD selectively in the neuronal lineage. (A) Immunostaining for the Myc tag allowed for detection of transgenic Notch2ICD expression in the developing brain. Coronal cranial sections of E18.5 N2ICD/Nestin-Cre (upper panels) and N2ICD mice (lower panels) show DAPI stained nuclei (left panels). The brain is highlighted by a dashed line. Transgenic Notch2ICD expression was detected specifically in the developing brain of N2ICD/Nestin-Cre but never in N2ICD controls, showing that the Stop cassette functionally shielded the Notch2ICD transgene and that Nestin-Cre mediated Stop excision efficiently directed Notch2ICD expression to Nestin expressing cells and their progeny. (B) Immunostaining for Neurofilament 200 (NF200) and Bungarotoxin that marks muscle innervating synapses, shows that E18.5 N2ICD/Nestin mice have a properly innervated diaphragm as seen in E18.5 wt controls.

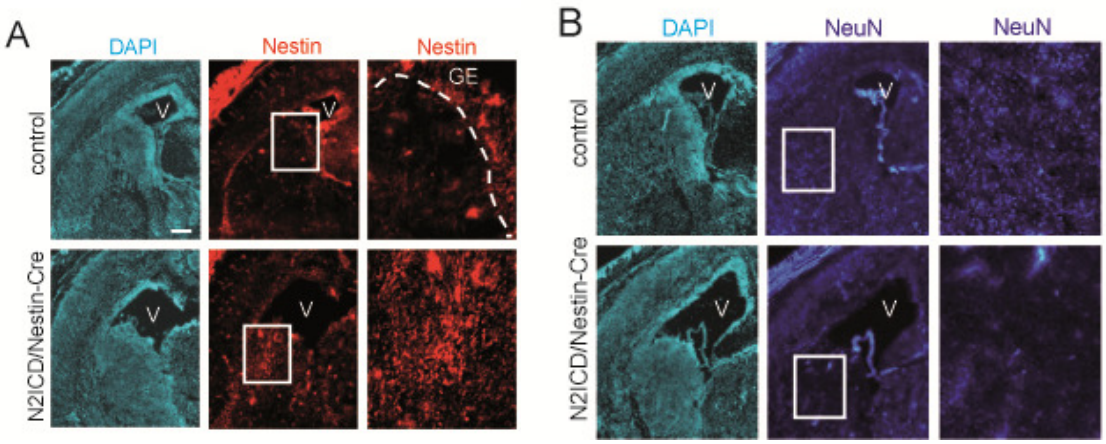

Supplementary Figure 2.

Activated Notch2 increases the NSC pool and blocks neurogenesis in the ventral forebrain. (A) Immunostaining for the NSC marker Nestin in the ventral forebrain of E18.5 N2ICD/Nestin-Cre and wt mice. N2ICD/Nestin-Cre mice show increased ventricle (V) size and a highly increased density of DAPI+ nuclei (left panels) and increased amounts of Nestin+ NSCs (middle panels) in the ventral forebrain when compared to wt mice. Magnified areas showing the Nestin+ ganglionic eminence (GE) in wt mice, which is expanded throughout most of the ventral forebrain in N2ICD/Nestin-Cre mice (right panels). (B) Immunostaining for NeuN, a marker staining mature neurons, shows that E18.5 N2ICD/Nestin-Cre mice show a dramatic decrease in neurons in the ventral forebrain when compared to E18.5 wt mice. This indicates that Notch2ICD expression in the developing brain increases the Nestin+ NSC pool at the expense of neurogenesis in the ventral forebrain. Scale bar (A,B) = 50 µm.

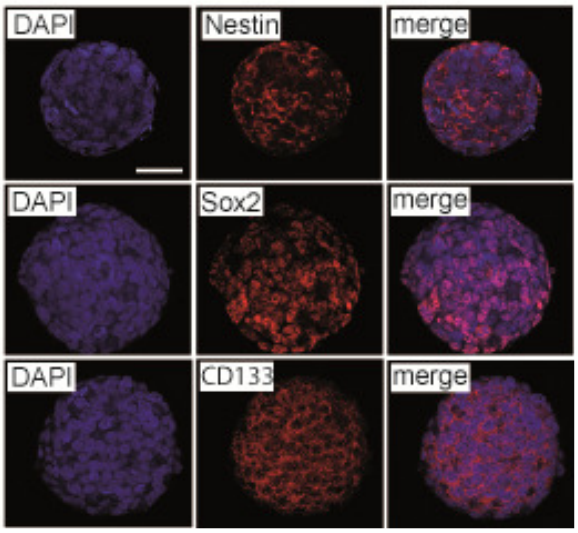

Supplementary Figure 3.

Immunostaining of U373 derived spheres overexpressing Notch2ICD for GSC markers (Nestin, Sox2, CD133) confirms that GSC spheres analyzed retain stem-like properties and represent proper GSCs. Box plot diagrams show median (red line), boxed 25% and 75% percentiles and whiskers marking minima and maxima, statistics were performed using Mann-Whitney test. (E) Western blot analysis in U373 and LN319 GBM cells shows increased levels for the antiapoptotic proteins Mcl1 and Bcl2 in GBM cells overexpressing Notch2ICD. Scale bar = 50µm.

Correlation coefficients of Notch2 (probe 202443_x_at) and selected genes in human GBMs.

Probe	Description	Gene Symbol	Correlation coefficient
212377_s_at	Notch homolog 2 (Drosophila)	NOTCH2	0.987
44783_s_at	hairy/enhancer-of-split related with YRPW motif 1	HEY1	0.698
218839_at	hairy/enhancer-of-split related with YRPW motif 1	HEY1	0.661
203394_s_at	hairy and enhancer of split 1,	HES1	0.617
200797_s_at	myeloid cell leukemia sequence 1	MCL1	0.460
1569067_at	BCL2-like 1	BCL2L1	0.314
217490_at	BCL2-associated X protein	BAX	-0.584
201426_s_at	vimentin	VIM	0.813
1555938_x_at	vimentin	VIM	0.583
229259_at	glial fibrillary acidic protein	GFAP	0.732
228038_at	SRY (sex determining region Y)-box 2	SOX2	0.601
213721_at	SRY (sex determining region Y)-box 2	SOX2	0.503
229346_at	nestin	NES	0.501
218678_at	nestin	NES	0.493
205030_at	fatty acid binding protein 7, brain	FABP7	0.317
205029_s_at	fatty acid binding protein 7, brain	FABP7	0.301
208912_s_at	2',3'-cyclic nucleotide 3' phosphodiesterase	CNP	-0.796
1557943_at	2',3'-cyclic nucleotide 3' phosphodiesterase	CNP	-0.687
210198_s_at	proteolipid protein 1	PLP1	-0.752
213825_at	oligodendrocyte lineage transcription factor 2	OLIG2	-0.530

Supplementary Figure 4.

Correlation coefficients of Notch2 (probe 202443_x_at) and selected genes in human GBMs Affymetrix probes, gene symbols, names and values for all genes illustrated in Figure 5 are summarized in this table.

Acknowledgement

We thank C. Giachino, B. Erne, J. Kinter, V. Niketopoulou and S. Frank for help with histological analysis and R. Zedi for animal caretaking. Further we thank F. Kirchhoff for providing GFAP-CreERT2 mice. We thank, N. Gakhar-Koppole, M. Lino, V. Taylor and A. Pinard for helpful discussion. This work was supported by Oncosuisse Grant to B. B., A. M. and B. H.

Author contributions

J.T.: conception and design, collection and assembly of data, data analysis and interpretation, and manuscript writing; D.C.: conception and design, collection and/or assembly of data, data analysis and interpretation; M.T.: collection and/or assembly of data, data analysis and interpretation, and manuscript writing; M.G.: data analysis and interpretation; R.M.H.: data analysis and interpretation; B.S.: data analysis and interpretation; A.M.: conception and design; B.H.: data analysis and interpretation; M.G.: conception and design, data analysis and interpretation, and manuscript writing. B.B.: conception and design, data analysis and interpretation, and manuscript writing.

References

1. Furnari, F.B., et al., Malignant astrocytic glioma: genetics, biology, and paths to treatment. Genes Dev, 2007. 21(21): p. 2683-710.
2. Tan, B.T., et al., The cancer stem cell hypothesis: a work in progress. Lab Invest, 2006. 86(12): p. 1203-7.
3. Stiles, C.D. and D.H. Rowitch, Glioma stem cells: a midterm exam. Neuron, 2008. 58(6): p. 832-46.
4. Sanai, N., A. Alvarez-Buylla, and M.S. Berger, Neural stem cells and the origin of gliomas. N Engl J Med, 2005. 353(8): p. 811-22.
5. Vescovi, A.L., R. Galli, and B.A. Reynolds, Brain tumour stem cells. Nat Rev Cancer, 2006. 6(6): p. 425-36.
6. Ignatova, T.N., et al., Human cortical glial tumors contain neural stem-like cells expressing astroglial and neuronal markers in vitro. Glia, 2002. 39(3): p. 193-206.
7. Bachoo, R.M., et al., Epidermal growth factor receptor and Ink4a/Arf: convergent mechanisms governing terminal differentiation and transformation along the neural stem cell to astrocyte axis. Cancer Cell, 2002. 1(3): p. 269-77.
8. Holland, E.C., et al., Combined activation of Ras and Akt in neural progenitors induces glioblastoma formation in mice. Nature Genetics, 2000. 25(1): p. 55-7.
9. Boulay, J.L., et al., Loss of NOTCH2 positively predicts survival in subgroups of human glial brain tumors. PLoS One, 2007. 2(6): p. e576.
10. Mullendore, M.E., et al., Ligand-dependent Notch signaling is involved in tumor initiation and tumor maintenance in pancreatic cancer. Clin Cancer Res, 2009. 15(7): p. 2291-301.
11. Artavanis-Tsakonas, S., M.D. Rand, and R.J. Lake, Notch signaling: cell fate control and signal integration in development. Science, 1999. 284(5415): p. 770-6.
12. Lewis, J., Neurogenic genes and vertebrate neurogenesis. Curr Opin Neurobiol, 1996. 6(1): p. 3-10.
13. de la Pompa, J.L., et al., Conservation of the Notch signalling pathway in mammalian neurogenesis. Development, 1997. 124(6): p. 1139-48.
14. Gaiano, N. and G. Fishell, The role of notch in promoting glial and neural stem cell fates. Annu Rev Neurosci, 2002. 25: p. 471-90.
15. Kageyama, R., et al., bHLH transcription factors and mammalian neuronal differentiation. Int J Biochem Cell Biol, 1997. 29(12): p. 1389-99.
16. Oishi, K., et al., Whole-brain voxel-based correlation analysis between regional cerebral blood flow and intelligence quotient score in Parkinson's disease. Eur Neurol, 2004. 52(3): p. 151-5.
17. Androutsellis-Theotokis, A., et al., Notch signalling regulates stem cell numbers in vitro and in vivo. Nature, 2006. 442(7104): p. 823-6.
18. Breunig, J.J., et al., Notch regulates cell fate and dendrite morphology of newborn neurons in the postnatal dentate gyrus. Proc Natl Acad Sci U S A, 2007. 104(51): p. 20558-63.
19. Allenspach, E.J., et al., Notch signaling in cancer. Cancer Biol Ther, 2002. 1(5): p. 466-76.
20. Nickoloff, B.J., B.A. Osborne, and L. Miele, Notch signaling as a therapeutic target in cancer: a new approach to the development of cell fate modifying agents. Oncogene, 2003. 22(42): p. 6598-608.

21. Higuchi, M., et al., Differential expression of Notch1 and Notch2 in developing and adult mouse brain. Brain Res Mol Brain Res, 1995. 29(2): p. 263-72.
22. Irvin, D.K., et al., Expression patterns of Notch1, Notch2, and Notch3 suggest multiple functional roles for the Notch-DSL signaling system during brain development. J Comp Neurol, 2001. 436(2): p. 167-81.
23. Solecki, D.J., et al., Activated Notch2 signaling inhibits differentiation of cerebellar granule neuron precursors by maintaining proliferation. Neuron, 2001. 31(4): p. 557-68.
24. Hirrlinger, P.G., et al., Temporal control of gene recombination in astrocytes by transgenic expression of the tamoxifen-inducible DNA recombinase variant CreERT2. Glia, 2006. 54(1): p. 11-20.
25. Srinivas, S., et al., Cre reporter strains produced by targeted insertion of EYFP and ECFP into the ROSA26 locus. BMC Dev Biol, 2001. 1: p. 4.
26. Sivasankaran, B., et al., Tenascin-C is a novel RBPJkappa-induced target gene for Notch signaling in gliomas. Cancer Res, 2009. 69(2): p. 458-65.
27. Weng, A.P., et al., Growth suppression of pre-T acute lymphoblastic leukemia cells by inhibition of notch signaling. Mol Cell Biol, 2003. 23(2): p. 655-64.
28. Korur, S., et al., GSK3beta regulates differentiation and growth arrest in glioblastoma. PLoS One, 2009. 4(10): p. e7443.
29. Artavanis-Tsakonas, S., K. Matsuno, and M.E. Fortini, Notch signaling. Science, 1995. 268(5208): p. 225-32.
30. Boulay, J.L., et al., Loss of heterozygosity of TRIM3 in malignant gliomas. BMC Cancer, 2009. 9: p. 71.
31. Tchorz, J.S., et al., Notch2 signaling promotes biliary epithelial cell fate specification and tubulogenesis during bile duct development in mice. Hepatology, 2009. 50(3): p. 871-9.
32. Tronche, F., et al., Disruption of the glucocorticoid receptor gene in the nervous system results in reduced anxiety. Nature Genetics, 1999. 23(1): p. 99-103.
33. Giachino, C., O. Basak, and V. Taylor, Isolation and manipulation of mammalian neural stem cells in vitro. Methods Mol Biol, 2009. 482: p. 143-58.
34. Ishii, N., et al., Frequent co-alterations of TP53, p16/CDKN2A, p14ARF, PTEN tumorsuppressor genes in human glioma cell lines. Brain Pathol, 1999. 9(3): p. 469-79.

Future Perspectives

Consistent with the three main therapeutic lines of attack – surgery, radiotherapy and chemotherapy – future progress is needed and can be expected in all three of them in the future. The 'magic bullet', meaning a single treatment eradicating all HGG, will probably never be found. To contemplate the future perspectives of GBM research and therapy, we will formulate 6 hypotheses which we will critically discuss; draw conclusions out of this discussion and thereby identify the fields of research key to future improvements. We will relate our work presented here to these key fields aiming at identifying promising approaches for the nearer future.

Six Hypotheses on the Future Perspectives of GBM Research and Therapy.

Hypothesis 1: Improvements in surgical methods will not substantially improve GBM patient prognosis. Intraoperative photodynamic diagnosis with 5-ALA during HGG surgery [80] is one of several approaches recently implemented aiming to improve the extent of tumor resection. Additionally, preoperative radiation or chemotherapy are also analyzed [81] trying to facilitate the discrimination of tumor versus normal brain by inducing apoptosis or necrosis in the tumor tissue. Preoperative brachy-therapy has proven to be particularly efficient at inducing tumor specific necrosis resulting in an average tumor resection of ~96% [82]. However, major limitations of resection cannot be overcome by these approaches, even if they could be further improved. GBM have a pronounced phenotype of infiltration with individual cells spreading out radially form the tumor bulk. These cells can not be removed surgically without causing inacceptable damage to the adjacent brain structures. Therefore, improved visualization and demarcation of tumors will help to remove more of the malignant tissue, but the reservoir of remaining cancer cells will always pose major therapeutic problems.

Hypothesis 2: Improvements in radio-therapeutic methods will improve patient prognosis but will not cure HGG. Radio-therapy faces similar limitations as surgery. Although molecular imaging and irradiation techniques allow highly precise application of radiation,

the issue of individual, migrating cancer cells is not resolved. Brachy-therapy with diffusible substances should at least partially overcome this limitation. Chelator-peptide constructs known to be specifically enriched in glioma cells are loaded with a radiation source (eg. the beta-emitter Yttrium-90 or most promising the alpha emitter Bi-213). After injection, these constructs distribute within in the main tumor mass including its margins and specifically bind to tumor cells via receptor-mediated internalization and then damage them by short range radiation inducing apoptosis and tumor necrosis [83]. However, it is unclear up to which distances such constructs can efficiently penetrate the brain. Furthermore, glioma initiating cells (GIC) have been attributed high radiation resistance. Recent data indicates that a considerable amount of gliomas have mutations in the DNA damage response mechanism (DDR) substantially reducing their sensitivity to radiation therapy [5]. In sum, brachytherapy in combination with advanced surgical instrumentation is an appealing strategy to improve GBM therapy and patient life expectancy. Given the advanced state of development, considerable progress can be expected from this approach in due time. However, the issue of residual cancer cells spreading throughout the brain as well as high intrinsic radio resistance remains unresolved.

Hypothesis 3: GBM will only become curable after the cell of origin has been identified. The cell of origin of HGG is still heavily disputed [20, 84]. This question is not purely academic, since the limited advances in GBM treatment are linked to the inability to precisely predict tumor behavior, which critically depends on the epigenetic status of the cell of origin, the micro-environment and the acquired mutations [20]. For example, if the cell of origin is a malignant NSC, then treatment needs to target this one cell to eradicate the tumor and to prevent recurrence. But this cell could still reside in the original location at a distance from the tumor mass and emit transformed progenitor cells even after tumor debulking and localized radio-therapy. Interestingly, the different GBM subtypes could reflect different cell-of-origin types. For example, HGG derived from neural progenitor cells could give rise to ‘proneural’ type gliomas [8]. This concept would stratify HGG cases into treatment subgroups based on their molecular and epigenetic identity, an achievement long sought after in the clinic. If the cell of origin and therefore the precise cause of tumor formation are not identified, any treatment is prone to target secondary effects rather than the true source. This will inevitably lead to tumor recurrence and treatment failure. However, recurrence and

treatment resistance can also be explained by the clonal evolution of tumor cell populations [1]. We need a profound understanding of the GBM biology and tumor-ontogeny before this question can be answered.

Hypothesis 4: No single treatment or regimen will be effective in all GBM cases. Surgical resection will not be able to remove single cells which have migrated away from the tumor bulk, even if the advances made in this field are further improved (see above). Radio-therapy faces similar limitations, particularly when it comes to far migrating cells. Furthermore, the pronounced mutator phenotype described in GBM [85, 86] and the ability to survive high radiation doses, particularly of glioma inducing cells (GIC) [87], will limit this treatment option. Additionally, the lack of effectiveness of single compound regimens so far [12] indicates that GBM will probably not show sufficient response to individual drugs. It therefore becomes apparent, that only an adept combination of available treatments – including surgery, radio- and chemo/bio-therapy – has the potential to substantially improve progression free survival as well as overall survival in GBM and other HGG patients.

Hypothesis 5: Without improved detection and characterization methods GBM will remain lethal in the majority of all cases. The central nervous system is excellent at compensating for lost functions or structures. Exemplary therefore is the famous case of Phineas Gage who suffered massive brain damage in 1848. After recovery, his brain was able to compensate for the lost prefrontal cortex enabling a relatively normal life despite massive changes in his personality. However, the ability to compensate poses a major problem in brain tumor diagnosis: the HGG has already reached a considerable size and tumor grade until it is finally diagnosed [12, 86, 88, 89]. The generalized symptoms (eg. headache, vomiting, dizziness, or papilloedema) of brain tumors are so unspecific that they do not immediately point to a neoplastic lesion in the CNS, a problem discussed since decades [88]. Furthermore, specific symptoms critically depend on the tumor location rather then on the tumor itself, making early detection based on “key” symptoms almost impossible. Together, this usually leads to the detection of brain tumors at late disease stages. No easy and safe early detection method is currently available for HGG. Ionizing radiation is the only known risk factor for gliomas [90], questioning the rational of certain imaging methods (eg. hole body CT scans) as an early detection method. Reliable detection methods which do not expose the patient to

risk factors (eg. blood levels of free, mutated DNA; serum concentration of CSF factors, etc.) are urgently needed.

Modern imaging methods are still not capable of displaying a true representation of a glioma, making localized therapies and adequate planning of resection difficult. Mostly, the tumor induced edema rather then the actual tumor mass is represented. Novel molecular imaging methods are needed which show the actual tumor rather then secondary effects. This will improve not only radiological approaches, but also surgical resection and tumor monitoring, a key feature for the evaluation of new treatments.

Glioma, and GBM in particular, are a highly heterogenic disease. The diagnosis GBM does not represent a single, well described condition but rather a compilation of stage IV brain tumors with glial characteristics [91]. Even within a single tumor, different areas can show distinct properties. Recent data is indicative of how different subtypes of GBM require different treatment strategies and how they correlate with patient prognosis [92]. Even if a highly effective treatment is found, it remains doubtful if it would be effective in more than few particular subtypes. In sum, if no early detection method for brain tumors can be established, diagnosis will likely occur at late stages of disease, when prognosis and treatment chances are already poor. Detected lesions then need to be characterized individually in order to decide on the most promising regimen. If not, treatment will remain a blindfolded fight against a neoplastic Hydra.

Hypothesis 6: Novel chemo/bio-therapeutic strategies will significantly improve patient prognosis. Currently, more than 37 compounds are in clinical development for HGG. More than 16 different targets are evaluated, ranging from EGFR, HSP-90 and HDAC to mTOR and PKC [12]. In the past 10 years the FDA has solely granted approval to Bevacizumab (a humanized anti-VEGF antibody, Roche) for the treatment of recurrent GBM (which was not followed by the EMEA). MRI based data suggests that treatment of HGG with anti-VEGF therapies could promote tumor cell infiltration along existing blood vessels [15] further aggravating one of the main problems in HGG treatment. The difficulty of developing targeted glioma therapies is further highlighted by the fact that only 10-15% (but often less) of the patients show at least partial response to new drugs and no prolongation of overall

survival has been observed so far [89]. Except for Bevacizumab, only a handful of other compound has made it past phase II clinical trials for HGG treatment. Several modes of resistance have been described explaining the lack of efficacy of targeted strategies. For example, the inhibition of PI3K can lead to increased RTK expression compensating the inhibitory effect on PI3K or bypassing it via the Ras/Raf/MEK/Erk pathway [93]. Another example is the relief of feedback inhibition when signaling components are blocked. PKB inhibition, for example, relieves the negative feedback on RTK expression through FOXO transcription factors and thereby induces PI3K activation compensating for the primary inhibitory effect. The same holds true for the inhibition of mTORC1 which is counteracted by increased PI3K activation [94]. Therefore, we postulate that single target strategies will not lead to a significant improvement in glioma treatment. However, combination strategies have a much bigger potential. The combinatorial use of inhibitors to different targets or of compounds with multiple targets has already proven to be effective *in vitro* [95] and we are currently evaluating the potential of such strategies *in vivo* (Chapter 2).

The inhibition of hyper-active survival and growth promoting signaling pathways in HGG in combination with the inhibition of resistance mechanisms could become available within few years. If no additional resistance mechanisms appear, this might reduce tumor growth significantly. However, given the heterogeneity of HGG and of the clones within a single tumor, it might not lead to a complete block of glioma growth for a prolonged period of time in clinical settings. However, this is by far the most promising approach in the near future.

Main Conclusions and Open Questions.

Conclusion A: Only multi-target therapies will significantly improve patient prognosis.

Surgery and radio-therapy, even in combination, will not cure GBM. Single agent therapies are likely to face the same fate as the ~40 compounds which have been evaluated so far. Therefore, a major breakthrough in GBM therapy can only be achieved by targeting several, non-redundant pathways thereby blocking evasion and resistance mechanisms. A successful strategy will also need to include surgical resection and improved radio-therapy.

Conclusion B: We need to improve our understanding of GBM sub-types, the cell of origin and glioma biology in general in order to be able to develop successful treatments.

a) Different GBM sub-types show different responses to treatment [92]. Therefore, we need to have a better understanding of the individual sub-types as well as reliable ways to define the specific type of a given tumor. GBM is not a single condition but only the end stage of different initial lesions.

b) The cell of origin of HGG defines the epigenetic background of the tumor and the cellular context in which the tumor initially develops. The sub-types of gliomas could be a representation of different cells of origin. A clear identification thereof including the underlying mutations of particular GBM types will allow to design personalized, combinatorial strategies and also to evaluate novel chemo/bio-therapies within specified tumor sub-groups.

c) Only a profound understanding of the biology of GBM will allow tailoring treatments according to the underlying mutations and epigenetic state of the cancer cells in complex *in vivo* setting. It will be of key importance to understand the underlying signaling networks operative in an individual tumor and their unique interactions which need to be targeted.

Our Results in Perspective.

We have extensively discussed the need of systemic GBM treatments above. Only an approach reaching the majority of all cancer cells can have a major impact on progression free and overall survival in GBM patients. Our work has focused on the understanding of GBM biology in general and non-canonical Notch signaling in particular (Figure 1). In parallel, we have set up an animal model in which we can test systemic strategies aiming to bridge the gap between tissue culture and the clinical bedside by using an orthotopic animal model.

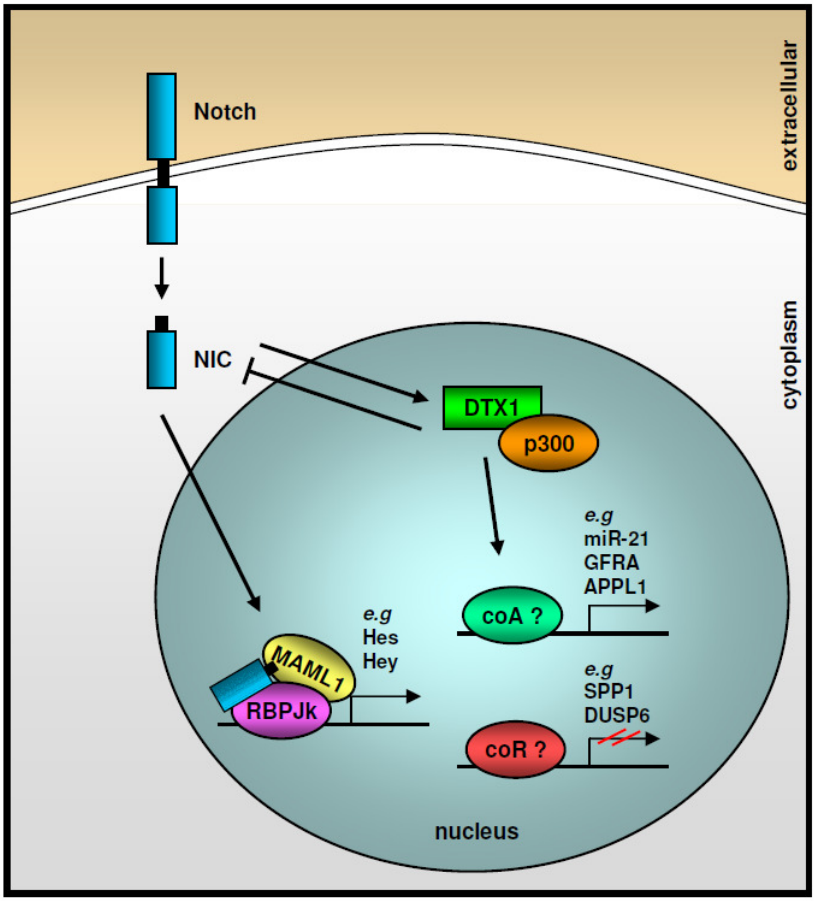

Figure 1. Model of DTX1 signaling in GBM cells.

A schematic drawing of the signaling events and interactions observed in chapter 1 of this thesis. In short, activated Notch signaling leads 1) to the expression of DTX1 and the activation thereof; 2) DTX1 has a negative feedback role on NIC and forms a protein complex with p300, presumably in the nucleus; 3) the DTX1/p300 complex changes gene expression, eventually with additional co-factors. Examples of DTX1 down stream targets are indicated (a full list can be found in chapter 1 of this thesis).

Notch signaling plays a fundamental role during cell-fate specification in the developing mammalian CNS. During neocortical development, the active Notch pathway inhibits neuronal differentiation and maintains the NSC and progenitor cell status permitting continuous waves of progenitor cells to emerge followed by neurogenesis and gliogenesis [96]. Notch signaling is not used in all proliferating neural precursors. Canonical Notch signaling is only active in NSC but not in neural progenitor cells. Recent data also implies Notch signaling in glioma biology [20, 25, 27, 97]. Several Notch receptor isoforms are over-expressed in brain tumors and the Notch2 status is predictive for patient survival in oligodendroglioma and GBM [25]. We have analyzed the role of Notch2 in GBM and it appears that Notch2 signaling triggers NSC differentiation into astrocytes. Moreover, it increases NSC proliferation, which causes a pronounced hyperplasia of the neurogenic niche in mice. Neurospheres derived from mice expressing N2IC show increased proliferation and reduced apoptosis. Likewise, high levels of Notch2 expression in GBM cells correlates with increased glioma stem-like cell proliferation and reduced apoptosis. In GBM-biopsies Notch2 mRNA levels positively correlate with expression levels of genes controlling stemness and astrocyte fate. High Notch2 mRNA levels also correlate with high and low expression levels of anti-apoptotic and pro-apoptotic markers, respectively (Chapter 4). Aberrant Notch2 signaling may therefore contribute to a malignant transformation of NSCs.

It remains to be determined if the effects described above are induced by canonical Notch signaling via MAML1 and RBPJκ since we have also found that the non-canonical Notch pathway via DTX1 has an oncogenic role in gliomas, aggravating key features of gliomas (Chapter 1). DTX1 increased tumor aggressiveness, seen by an increased clonogenic potential, elevated both migration and invasion of glioma cells and activated several signaling pathways protecting cancer cells form apoptosis and stimulating cell survival and proliferation. DTX1 mRNA levels correlate with patient prognosis in grade IV gliomas. These effects were linked to a set of genes specifically controlled by non-canonical Notch signaling. Interestingly, miR-21, a well described oncomir, is also controlled by DTX1 in GBM cells, linking Notch signaling to the expression of specific micro-RNA species. Therefore, Notch canonical and non-canonical signal pathways play important, only partially overlapping roles in glioma biology.

How do these results help to answer the main questions at hand in GBM research depicted above? DTX mediates MEKK1 degradation [50] and activates PI3K/PKB signaling via $p56^{Lck}$ [98]. Our results confirm these results in GBM cells and also demonstrate a link between Notch signaling and miR-21 expression highlighting the tight interaction of multiple signaling pathways within individual cells. This will help to further unravel the molecular programs within GBMs and offers a better understanding of its general biology. These results can now be used for improved or novel therapies. For example, pharmacological blockade of Notch signaling may represent a promising strategy (or better part of a multi-target strategy) for therapeutic interference with GBM of the 'classical' sub-type [12], particularly because it would block both the canonical and the DTX1 mediated pathway branches. Furthermore, γ-secretase inhibitors are already available and in clinical use for Alzheimer's disease therapy. It remains to be seen if Notch is important in more than one type of GBM, but the data presented here for DTX1 could point to a more general mechanism. Furthermore, Notch has been described to play critical roles not only in different leukemias, but also in many solid tumors (eg. cervical, head and neck, endometrial, renal, lung, ovarian, pancreatic, breast and prostate cancer [99]) and DTX1 was related to cell invasion in osteosarcoma [100]. Additionally, our own results demonstrate a correlation between DTX1 expression and survival in early breast cancer patients (Chapter 1). It is tempting to speculate that DTX1 has an oncogenic role in several of these solid tumors or eventually also in Leukemia. Therefore, tumor patients of all of these diseases could profit from such refined chemotherapeutic regimens.

Our results could also hint to a possible cell of origin of GBM, again, one of the main questions at hand. NSC proliferation is Notch driven [101] and NSC and glioma inducing cells share several key features (self-renewal and long term proliferation, ability to differentiate into neurons, astrocytes, and oligodendrocytes [12]). Radio-necrosis after brachy-therapy is found in a trail from the tumor mass towards the SVC where NSC reside (personal communication A. Merlo). Therefore, several lines of evidence point to the SVC and therefore to NSC as the source of GBM. In line with these observations is the fact that GBM cells show elevated levels of stem-cell marker expression (Chapert 1, 3, 4) also found in NSC (eg. Nestin). However, in a clonal evolution of cancer it could also be the case that stem cell marker expressing cells are more competitive then others and that the expression is rather a

reason for fast growth and resistance rather than a remnant of the cell of origin. Never the less, canonical and non-canonical Notch signaling are involved both in NSC control as well as in GBM, a link which needs to be further analyzed.

One of the main problems in GBM research is the lack of a reliable and relevant animal model. Only such a model will allow testing of novel therapies in a setting as close to the patient situation as possible. Without such a system, future approaches are prone to face the same fate as the ~36 compounds tested before [12]. But such a model, based on defined genetics, can only be established once the cell of origin has been identified. However, other *in vivo* models can be used to evaluate promising candidates until such a model becomes available, even if they are limited in terms of representing a true GBM case *in vivo*.

In vivo evidence on the efficacy of a treatment still is a prerequisite to any clinical trial. We have established an orthotopic xeno-transplantation model of GBM using Luciferase transfected human U87MG cells which were implanted into the brains of immuno-compromised 'nude' mice of various genetic backgrounds. Using this model, we were able to show the anti-tumor efficacy of HDI + 2DG on gliomas *in vivo* (Chapter 2). The HDI + 2DG combination therapy prolonged overall survival of the experimental animals and significantly reduced tumor growth after only four days of treatment for up to additional 19 days. Single drug treatments were significantly less effective, and only HDI had a tumor reducing effect when administered alone. Therefore, the epigenetic status of glioma cells is a key determinant to treatment susceptibility. Again, this emphasizes the importance the cell of origin has on our understanding of GBM biology. It will be interesting to see if these results can be further optimized by more specific HDIs and refined dosing regimens or schedules. More importantly, this model will allow us to systematically screen novel inhibitor compounds *in vivo* based on *in vitro* findings already available in our labs. Ongoing experiments in the lab are currently evaluating some of these possible drug combinations *in vivo*. However, the results are preliminary and not suited for publication in this thesis at this time.

We hope and believe that the results presented here help answering the two main questions defined above. Epigenetic remodeling forms part of a promising therapeutic approach in our GBM animal model. This underlines the importance of the epigenetic status a GBM cells has, which is the result of the epigenetic status of the cell of origin in combination with the acquired mutations and modifications. Our results on the role of both canonical and non-canonical Notch signaling offer a possible explanation for the previous observation correlating Notch status and survival as well as indicate Notch driven cells as a possible source of GBMs.

References

(w/o results section)

1. Nowell, P.C., *The clonal evolution of tumor cell populations.* Science, 1976. **194**(4260): p. 23-8.
2. Hanahan, D. and R.A. Weinberg, *The hallmarks of cancer.* Cell, 2000. **100**(1): p. 57-70.
3. *Comprehensive genomic characterization defines human glioblastoma genes and core pathways.* Nature, 2008. **455**(7216): p. 1061-8.
4. Schutte, M., et al., *DPC4 gene in various tumor types.* Cancer Res, 1996. **56**(11): p. 2527-30.
5. Ashkenazi, A. and V.M. Dixit, *Apoptosis control by death and decoy receptors.* Curr Opin Cell Biol, 1999. **11**(2): p. 255-60.
6. Harris, C.C., *p53 tumor suppressor gene: from the basic research laboratory to the clinic--an abridged historical perspective.* Carcinogenesis, 1996. **17**(6): p. 1187-98.
7. Hayflick, L., *Mortality and immortality at the cellular level. A review.* Biochemistry (Mosc), 1997. **62**(11): p. 1180-90.
8. Wright, W.E., O.M. Pereira-Smith, and J.W. Shay, *Reversible cellular senescence: implications for immortalization of normal human diploid fibroblasts.* Mol Cell Biol, 1989. **9**(7): p. 3088-92.
9. Shay, J.W. and S. Bacchetti, *A survey of telomerase activity in human cancer.* Eur J Cancer, 1997. **33**(5): p. 787-91.
10. Hynes, R.O. and D.D. Wagner, *Genetic manipulation of vascular adhesion molecules in mice.* J Clin Invest, 1996. **98**(10): p. 2193-5.
11. Ohgaki, H. and P. Kleihues, *Epidemiology and etiology of gliomas.* Acta Neuropathol, 2005. **109**(1): p. 93-108.
12. Van Meir, E.G., et al., *Exciting new advances in neuro-oncology: the avenue to a cure for malignant glioma.* CA Cancer J Clin, 2010. **60**(3): p. 166-93.
13. Ohgaki, H. and P. Kleihues, *Population-based studies on incidence, survival rates, and genetic alterations in astrocytic and oligodendroglial gliomas.* J Neuropathol Exp Neurol, 2005. **64**(6): p. 479-89.
14. Ohgaki, H., *Genetic pathways to glioblastomas.* Neuropathology, 2005. **25**(1): p. 1-7.
15. Huse, J.T. and E.C. Holland, *Targeting brain cancer: advances in the molecular pathology of malignant glioma and medulloblastoma.* Nat Rev Cancer, 2010. **10**(5): p. 319-31.
16. Stiles, C.D. and D.H. Rowitch, *Glioma stem cells: a midterm exam.* Neuron, 2008. **58**(6): p. 832-46.
17. Zhu, Y., et al., *Early inactivation of p53 tumor suppressor gene cooperating with NF1 loss induces malignant astrocytoma.* Cancer Cell, 2005. **8**(2): p. 119-30.
18. Persson, A.I., et al., *Non-stem cell origin for oligodendroglioma.* Cancer Cell, 2010. **18**(6): p. 669-82.
19. Becher, O.J. and E.C. Holland, *Evidence for and against regional differences in neural stem and progenitor cells of the CNS.* Genes Dev, 2010. **24**(20): p. 2233-8.
20. Sanai, N., A. Alvarez-Buylla, and M.S. Berger, *Neural stem cells and the origin of gliomas.* N Engl J Med, 2005. **353**(8): p. 811-22.
21. Furnari, F.B., et al., *Malignant astrocytic glioma: genetics, biology, and paths to treatment.* Genes Dev, 2007. **21**(21): p. 2683-710.

22. Labuhn, M., et al., *Quantitative real-time PCR does not show selective targeting of p14(ARF) but concomitant inactivation of both p16(INK4A) and p14(ARF) in 105 human primary gliomas.* Oncogene, 2001. **20**(9): p. 1103-9.
23. Brennan, C., et al., *Glioblastoma subclasses can be defined by activity among signal transduction pathways and associated genomic alterations.* PLoS One, 2009. **4**(11): p. e7752.
24. Phillips, H.S., et al., *Molecular subclasses of high-grade glioma predict prognosis, delineate a pattern of disease progression, and resemble stages in neurogenesis.* Cancer Cell, 2006. **9**(3): p. 157-73.
25. Boulay, J.L., et al., *Loss of NOTCH2 positively predicts survival in subgroups of human glial brain tumors.* PLoS One, 2007. **2**(6): p. e576.
26. Kageyama, R. and S. Nakanishi, *Helix-loop-helix factors in growth and differentiation of the vertebrate nervous system.* Curr Opin Genet Dev, 1997. **7**(5): p. 659-65.
27. Allenspach, E.J., et al., *Notch signaling in cancer.* Cancer Biol Ther, 2002. **1**(5): p. 466-76.
28. Nickoloff, B.J., B.A. Osborne, and L. Miele, *Notch signaling as a therapeutic target in cancer: a new approach to the development of cell fate modifying agents.* Oncogene, 2003. **22**(42): p. 6598-608.
29. Nicolas, M., et al., *Notch1 functions as a tumor suppressor in mouse skin.* Nature Genetics, 2003. **33**(3): p. 416-421.
30. Fan, X., et al., *Notch1 and Notch2 have opposite effects on embryonal brain tumor growth.* Cancer Research, 2004. **64**(21): p. 7787-7793.
31. Ronchini, C. and A.J. Capobianco, *Induction of cyclin D1 transcription and CDK2 activity by Notch(ic): implication for cell cycle disruption in transformation by Notch(ic).* Mol Cell Biol, 2001. **21**(17): p. 5925-34.
32. Rangarajan, A., et al., *Notch signaling is a direct determinant of keratinocyte growth arrest and entry into differentiation.* EMBO J, 2001. **20**(13): p. 3427-36.
33. Ge, W., et al., *Notch signaling promotes astrogliogenesis via direct CSL-mediated glial gene activation.* J Neurosci Res, 2002. **69**(6): p. 848-60.
34. Artavanis-Tsakonas, S., M.D. Rand, and R.J. Lake, *Notch signaling: cell fate control and signal integration in development.* Science, 1999. **284**(5415): p. 770-6.
35. Somasundaram, K., et al., *Upregulation of ASCL1 and inhibition of Notch signaling pathway characterize progressive astrocytoma.* Oncogene, 2005. **24**(47): p. 7073-83.
36. Sriuranpong, V., et al., *Notch signaling induces rapid degradation of achaete-scute homolog 1.* Mol Cell Biol, 2002. **22**(9): p. 3129-39.
37. Stockhausen, M.T., K. Kristoffersen, and H.S. Poulsen, *The functional role of Notch signaling in human gliomas.* Neuro Oncol, 2010. **12**(2): p. 199-211.
38. Kanamori, M., et al., *Contribution of Notch signaling activation to human glioblastoma multiforme.* J Neurosurg, 2007. **106**(3): p. 417-27.
39. Hulleman, E., et al., *A role for the transcription factor HEY1 in glioblastoma.* J Cell Mol Med, 2009. **13**(1): p. 136-46.
40. Fitzgerald, K., A. Harrington, and P. Leder, *Ras pathway signals are required for notch-mediated oncogenesis.* Oncogene, 2000. **19**(37): p. 4191-8.
41. Stockhausen, M.T., J. Sjolund, and H. Axelson, *Regulation of the Notch target gene Hes-1 by TGFalpha induced Ras/MAPK signaling in human neuroblastoma cells.* Exp Cell Res, 2005. **310**(1): p. 218-28.
42. Weijzen, S., et al., *Activation of Notch-1 signaling maintains the neoplastic phenotype in human Ras-transformed cells.* Nat Med, 2002. **8**(9): p. 979-86.

43. Miyamoto, Y., et al., *Notch mediates TGF alpha-induced changes in epithelial differentiation during pancreatic tumorigenesis.* Cancer Cell, 2003. **3**(6): p. 565-76.
44. Zeng, Q., et al., *Crosstalk between tumor and endothelial cells promotes tumor angiogenesis by MAPK activation of Notch signaling.* Cancer Cell, 2005. **8**(1): p. 13-23.
45. Shih, A.H. and E.C. Holland, *Notch signaling enhances nestin expression in gliomas.* Neoplasia, 2006. **8**(12): p. 1072-82.
46. Rajasekhar, V.K., et al., *Oncogenic Ras and Akt signaling contribute to glioblastoma formation by differential recruitment of existing mRNAs to polysomes.* Mol Cell, 2003. **12**(4): p. 889-901.
47. Sang, L., H.A. Coller, and J.M. Roberts, *Control of the reversibility of cellular quiescence by the transcriptional repressor HES1.* Science, 2008. **321**(5892): p. 1095-100.
48. Matsuno, K., et al., *Deltex acts as a positive regulator of Notch signaling through interactions with the Notch ankyrin repeats.* Development, 1995. **121**(8): p. 2633-44.
49. Mukherjee, A., et al., *Regulation of Notch signalling by non-visual beta-arrestin.* Nat Cell Biol, 2005. **7**(12): p. 1191-201.
50. Liu, W.H. and M.Z. Lai, *Deltex regulates T-cell activation by targeted degradation of active MEKK1.* Mol Cell Biol, 2005. **25**(4): p. 1367-78.
51. Hu, Q.D., et al., *F3/contactin acts as a functional ligand for Notch during oligodendrocyte maturation.* Cell, 2003. **115**(2): p. 163-75.
52. Hu, Q.D., et al., *Axoglial interaction via the notch receptor in oligodendrocyte differentiation.* Ann Acad Med Singapore, 2004. **33**(5): p. 581-8.
53. Eiraku, M., et al., *DNER acts as a neuron-specific Notch ligand during Bergmann glial development.* Nat Neurosci, 2005. **8**(7): p. 873-80.
54. Brennan, K. and P. Gardner, *Notching up another pathway.* Bioessays, 2002. **24**(5): p. 405-10.
55. Martinez Arias, A., V. Zecchini, and K. Brennan, *CSL-independent Notch signalling: a checkpoint in cell fate decisions during development?* Curr Opin Genet Dev, 2002. **12**(5): p. 524-33.
56. Dotto, G.P., *Crosstalk of Notch with p53 and p63 in cancer growth control.* Nat Rev Cancer, 2009. **9**(8): p. 587-95.
57. Dai, C. and E.C. Holland, *Glioma models.* Biochim Biophys Acta, 2001. **1551**(1): p. M19-27.
58. Yoshida, J. and H. Cravioto, *Nitrosourea-induced brain tumors: an in vivo and in vitro tumor model system.* J Natl Cancer Inst, 1978. **61**(2): p. 365-74.
59. Lee, J., et al., *Tumor stem cells derived from glioblastomas cultured in bFGF and EGF more closely mirror the phenotype and genotype of primary tumors than do serum-cultured cell lines.* Cancer Cell, 2006. **9**(5): p. 391-403.
60. Doblas, S., et al., *Glioma morphology and tumor-induced vascular alterations revealed in seven rodent glioma models by in vivo magnetic resonance imaging and angiography.* J Magn Reson Imaging, 2010. **32**(2): p. 267-75.
61. Tan, B.T., et al., *The cancer stem cell hypothesis: a work in progress.* Lab Invest, 2006. **86**(12): p. 1203-7.
62. Lapidot, T., et al., *A cell initiating human acute myeloid leukaemia after transplantation into SCID mice.* Nature, 1994. **367**(6464): p. 645-8.
63. Ignatova, T.N., et al., *Human cortical glial tumors contain neural stem-like cells expressing astroglial and neuronal markers in vitro.* Glia, 2002. **39**(3): p. 193-206.

64. Galli, R., et al., *Isolation and characterization of tumorigenic, stem-like neural precursors from human glioblastoma.* Cancer Res, 2004. **64**(19): p. 7011-21.
65. Hemmati, H.D., et al., *Cancerous stem cells can arise from pediatric brain tumors.* Proc Natl Acad Sci U S A, 2003. **100**(25): p. 15178-83.
66. Singh, S.K., et al., *Identification of a cancer stem cell in human brain tumors.* Cancer Res, 2003. **63**(18): p. 5821-8.
67. Clement, V., et al., *Marker-independent identification of glioma-initiating cells.* Nat Methods, 2010. **7**(3): p. 224-8.
68. Korur, S., et al., *GSK3beta regulates differentiation and growth arrest in glioblastoma.* PLoS One, 2009. **4**(10): p. e7443.
69. Kelly, P.N., et al., *Tumor growth need not be driven by rare cancer stem cells.* Science, 2007. **317**(5836): p. 337.
70. Singec, I., et al., *Defining the actual sensitivity and specificity of the neurosphere assay in stem cell biology.* Nat Methods, 2006. **3**(10): p. 801-6.
71. Wernig, M., et al., *In vitro reprogramming of fibroblasts into a pluripotent ES-cell-like state.* Nature, 2007. **448**(7151): p. 318-24.
72. Nakagawa, M., et al., *Generation of induced pluripotent stem cells without Myc from mouse and human fibroblasts.* Nat Biotechnol, 2008. **26**(1): p. 101-6.
73. Okita, K., T. Ichisaka, and S. Yamanaka, *Generation of germline-competent induced pluripotent stem cells.* Nature, 2007. **448**(7151): p. 313-7.
74. Bachoo, R.M., et al., *Epidermal growth factor receptor and Ink4a/Arf: convergent mechanisms governing terminal differentiation and transformation along the neural stem cell to astrocyte axis.* Cancer Cell, 2002. **1**(3): p. 269-77.
75. Maher, E.A., et al., *Malignant glioma: genetics and biology of a grave matter.* Genes Dev, 2001. **15**(11): p. 1311-33.
76. Kondo, T. and M. Raff, *Oligodendrocyte precursor cells reprogrammed to become multipotential CNS stem cells.* Science, 2000. **289**(5485): p. 1754-7.
77. Belachew, S., et al., *Postnatal NG2 proteoglycan-expressing progenitor cells are intrinsically multipotent and generate functional neurons.* J Cell Biol, 2003. **161**(1): p. 169-86.
78. Xiong, J., et al., *NG2 proteoglycan increases mesangial cell proliferation and extracellular matrix production.* Biochem Biophys Res Commun, 2007. **361**(4): p. 960-7.
79. Vescovi, A.L., R. Galli, and B.A. Reynolds, *Brain tumour stem cells.* Nat Rev Cancer, 2006. **6**(6): p. 425-36.
80. Maruyama, T., *[Intraoperative photodynamic diagnosis using 5-ALA for glioma surgery].* Nippon Rinsho, 2005. **63 Suppl 9**: p. 380-8.
81. Boiardi, A., et al., *Neoadjuvant chemotherapy in the treatment of recurrent glioblastomas (GBM).* Ital J Neurol Sci, 1992. **13**(7): p. 583-8.
82. Cordier, D., et al., *Neoadjuvant targeting of glioblastoma multiforme with radiolabeled DOTAGA-substance P--results from a phase I study.* J Neurooncol, 2010. **100**(1): p. 129-36.
83. Kneifel, S., et al., *Local targeting of malignant gliomas by the diffusible peptidic vector 1,4,7,10-tetraazacyclododecane-1-glutaric acid-4,7,10-triacetic acid-substance p.* Clin Cancer Res, 2006. **12**(12): p. 3843-50.
84. Schiffer, D., et al., *On the origin and growth of gliomas.* Anticancer Res, 2010. **30**(6): p. 1977-98.

85. Misra, A., et al., *Clonal mutations in primary human glial tumors: evidence in support of the mutator hypothesis.* BMC Cancer, 2007. **7**: p. 190.
86. Merlo, A., *Genes and pathways driving glioblastomas in humans and murine disease models.* Neurosurg Rev, 2003. **26**(3): p. 145-58.
87. Fischer, U. and E. Meese, *Glioblastoma multiforme: the role of DSB repair between genotype and phenotype.* Oncogene, 2007. **26**(56): p. 7809-15.
88. Rowbotham, G.F., et al., *The problem of glioma of the brain.* Br Med J, 1955. **1**(4928): p. 1445-8.
89. Wen, P.Y. and S. Kesari, *Malignant gliomas in adults.* N Engl J Med, 2008. **359**(5): p. 492-507.
90. Prasad, G. and D.A. Haas-Kogan, *Radiation-induced gliomas.* Expert Rev Neurother, 2009. **9**(10): p. 1511-7.
91. Burger, P.C., et al., *Glioblastoma multiforme and anaplastic astrocytoma. Pathologic criteria and prognostic implications.* Cancer, 1985. **56**(5): p. 1106-11.
92. Verhaak, R.G., et al., *Integrated genomic analysis identifies clinically relevant subtypes of glioblastoma characterized by abnormalities in PDGFRA, IDH1, EGFR, and NF1.* Cancer Cell, 2010. **17**(1): p. 98-110.
93. Serra, V., et al., *PI3K inhibition results in enhanced HER signaling and acquired ERK dependency in HER2-overexpressing breast cancer.* Oncogene, 2011.
94. Chandarlapaty, S., et al., *AKT inhibition relieves feedback suppression of receptor tyrosine kinase expression and activity.* Cancer Cell, 2011. **19**(1): p. 58-71.
95. Failly, M., et al., *Combination of sublethal concentrations of epidermal growth factor receptor inhibitor and microtubule stabilizer induces apoptosis of glioblastoma cells.* Mol Cancer Ther, 2007. **6**(2): p. 773-81.
96. Pierfelice, T.J., et al., *Notch, neural stem cells, and brain tumors.* Cold Spring Harb Symp Quant Biol, 2008. **73**: p. 367-75.
97. Fan, X., et al., *Notch1 and notch2 have opposite effects on embryonal brain tumor growth.* Cancer Res, 2004. **64**(21): p. 7787-93.
98. Sade, H., S. Krishna, and A. Sarin, *The anti-apoptotic effect of Notch-1 requires p56lck-dependent, Akt/PKB-mediated signaling in T cells.* J Biol Chem, 2004. **279**(4): p. 2937-44.
99. Miele, L., T. Golde, and B. Osborne, *Notch signaling in cancer.* Curr Mol Med, 2006. **6**(8): p. 905-18.
100. Zhang, P., et al., *Regulation of NOTCH signaling by reciprocal inhibition of HES1 and Deltex 1 and its role in osteosarcoma invasiveness.* Oncogene, 2010. **29**(20): p. 2916-26.
101. Lathia, J.D., M.P. Mattson, and A. Cheng, *Notch: from neural development to neurological disorders.* J Neurochem, 2008. **107**(6): p. 1471-81.

Appendices

Appendix I

ETS Transcription Factor Erm Controls Subsynaptic Gene Expression in Skeletal Muscles

'Neuron', 2007

Simon Hippenmeyer,[1,2,4,5] **Roland M. Huber**,[1,2,4] David R. Ladle,[1,2] Kenneth Murphy,[3] and Silvia Arber[1,2,*]

1) Biozentrum, Department of Cell Biology, University of Basel, Klingelbergstrasse 70, 4056 Basel, Switzerland

2) Friedrich Miescher Institute, Maulbeerstrasse 66, 4058 Basel, Switzerland

3) Department of Pathology and Immunology, Howard Hughes Medical Institute, Washington University School of Medicine,St. Louis, MO 63110, USA

4) These authors contributed equally to this work.

5) Present address: Howard Hughes Medical Institute, Department of Biological Sciences, 385 Serra Mall, Stanford University, Stanford, CA 94305, USA.

Neuron
Article

ETS Transcription Factor *Erm* Controls Subsynaptic Gene Expression in Skeletal Muscles

Simon Hippenmeyer,[1,2,4,5] Roland M. Huber,[1,2,4] David R. Ladle,[1,2] Kenneth Murphy,[3] and Silvia Arber[1,2,*]
[1]Biozentrum, Department of Cell Biology, University of Basel, Klingelbergstrasse 70, 4056 Basel, Switzerland
[2]Friedrich Miescher Institute, Maulbeerstrasse 66, 4058 Basel, Switzerland
[3]Department of Pathology and Immunology, Howard Hughes Medical Institute, Washington University School of Medicine, St. Louis, MO 63110, USA
[4]These authors contributed equally to this work.
[5]Present address: Howard Hughes Medical Institute, Department of Biological Sciences, 385 Serra Mall, Stanford University, Stanford, CA 94305, USA.
*Correspondence: silvia.arber@unibas.ch
DOI 10.1016/j.neuron.2007.07.028

SUMMARY

Accumulation of specific proteins at synaptic structures is essential for synapse assembly and function, but mechanisms regulating local protein enrichment remain poorly understood. At the neuromuscular junction (NMJ), subsynaptic nuclei underlie motor axon terminals within extrafusal muscle fibers and are transcriptionally distinct from neighboring nuclei. In this study, we show that expression of the ETS transcription factor *Erm* is highly concentrated at subsynaptic nuclei, and its mutation in mice leads to severe downregulation of many genes with normally enriched subsynaptic expression. *Erm* mutant mice display an expansion of the muscle central domain in which acetylcholine receptor (AChR) clusters accumulate, show gradual fragmentation of AChR clusters, and exhibit symptoms of muscle weakness mimicking congenital myasthenic syndrome (CMS). Together, our findings define *Erm* as an upstream regulator of a transcriptional program selective to subsynaptic nuclei at the NMJ and underscore the importance of transcriptional control of local synaptic protein accumulation.

INTRODUCTION

The alignment of presynaptic and postsynaptic elements of chemical synapses represents an important step in wiring neuronal circuits for function. This process involves the spatially coordinated enrichment and assembly of presynaptic neurotransmitter release machinery and postsynaptic structures at nascent synaptic sites. Despite the recognized importance of subcellular protein accumulation to synaptic sites, regulatory mechanisms orchestrating local accumulation of synaptic proteins to these highly specialized cellular compartments remain poorly defined (McAllister, 2007).

The vertebrate neuromuscular junction (NMJ) has been at the forefront of studies to define the cellular and molecular mechanisms of synaptogenesis. Presynaptic motor axon terminals align precisely with postsynaptic acetylcholine receptor (AChR) clusters within the central domain of extrafusal skeletal muscle fibers (Arber et al., 2002; Burden, 2002; Kummer et al., 2006; Sanes and Lichtman, 2001). Specialized transcriptional programs expressed from subsynaptic nuclei within extrafusal muscle fibers underlying presynaptic motor axon terminals play an important role in the enrichment of proteins required locally at the NMJ (Burden, 2002; Sanes and Lichtman, 2001; Schaeffer et al., 2001). These transcriptional mechanisms ensure spatial separation of multinucleated extrafusal muscle fibers into extrasynaptic and synaptic domains and allow local enrichment of synaptic proteins. Despite the fact that many genes are expressed subsynaptically at the NMJ (Burden, 2002; Schaeffer et al., 2001), the transcription factors involved in regulation of subsynaptic gene expression in vivo remain to be identified.

A series of studies suggests that transcriptional regulation through ETS transcription factors might contribute to subsynaptic gene expression (Schaeffer et al., 2001). Several genes expressed subsynaptically, including the *AChRε* subunit, contain a conserved ETS binding site (N-box) in their respective promoter regions (Duclert et al., 1996; Koike et al., 1995). The in vivo relevance of this N-box element in the regulation of *AChRε* expression is underscored by the observation that mutation of this binding site in humans leads to congenital myasthenic syndrome (CMS) (Nichols et al., 1999; Ohno et al., 1999), a broad class of diseases characterized by a dysfunction of neuromuscular transmission due to either presynaptic or postsynaptic NMJ abnormalities (Engel et al., 2003). The ETS-related transcription factor GABPα has been shown to bind in vitro to elements containing the N-box motif, and it is thought to activate subsynaptic gene transcription (Fromm and Burden, 1998; Schaeffer et al., 1998). Supporting the view for a role of GABPα in

Neuron
Erm Controls Subsynaptic Gene Expression

subsynaptic gene transcription in vivo, expression of a dominant-negative GABPβ subunit known to heterodimerize with GABPα led to reduced *AChR*ε promoter induction in innervated muscle fibers (Briguet and Ruegg, 2000).

Nevertheless, at least two lines of evidence argue against a major role for *GABPα* in the regulation of subsynaptically restricted gene expression. First, *GABPα* is expressed broadly throughout extrafusal muscle fibers with only a minor enrichment in the subsynaptic domain (Schaeffer et al., 1998). Second, two recent studies have analyzed mice with a conditional mutation of *GABPα* in skeletal muscles (Jaworski et al., 2007; O'Leary et al., 2007). These mutant mice survive to adulthood without any overt signs of muscle weakness or motor behavioral phenotypes to be expected from mice with severely compromised subsynaptic gene expression. In a detailed analysis of NMJs, one study observed no changes in the level or pattern of subsynaptic gene expression at NMJs (Jaworski et al., 2007), and in the other study, only mild alterations in AChR cluster morphology for a fraction of NMJs were detected (O'Leary et al., 2007). Both of these recent in vivo studies thus strongly argue against a dominant role of the ETS-related transcription factor *GABPα* in subsynaptic gene expression, a hypothesis previously proposed mainly on the basis of in vitro assays.

These recent findings suggest that other ETS transcription factors function in the regulation of subsynaptic gene expression in skeletal muscles. *Pea3* subfamily members share a highly conserved DNA binding domain structure (Sharrocks, 2001) and have been demonstrated to exhibit in vitro DNA binding preferences similar to GABPα (Mo et al., 1998), thus making them plausible candidates as potential regulators of subsynaptic gene expression in skeletal muscles. The *Pea3* subfamily of ETS transcription factors comprises three members (*Pea3*, *Er81*, and *Erm*), all of which are expressed in intrafusal muscle fibers within muscle spindles (Arber et al., 2000; Hippenmeyer et al., 2002). *Pea3* and *Er81* are not expressed in a selective way within extrafusal muscle fibers, whereas *Erm* is expressed within a centralized domain of skeletal muscles, reminiscent of subsynaptic localization (Hippenmeyer et al., 2002). In addition, while both *Pea3* and *Er81* are expressed in distinct motor neuron pools in the spinal cord, *Erm* is not expressed by motor neurons (Arber et al., 2000; Lin et al., 1998; Livet et al., 2002). Functionally, both *Pea3* and *Er81* play important and selective neuronal roles in the assembly of neuromuscular circuitry (Arber et al., 2000; Lin et al., 1998; Livet et al., 2002; Vrieseling and Arber, 2006), but a role for *Erm* in this system remains to be determined.

In this study, we provide evidence that within extrafusal muscle fibers, the ETS transcription factor *Erm* is expressed selectively from subsynaptic nuclei. *Erm* mutant mice display a broader endplate (EP) domain and gradual fragmentation of AChR clusters, but alignment of presynaptic and postsynaptic structures is not affected. Moreover, *Erm* mutant mice develop muscle weakness and show functional neuromuscular transmission defects. Mechanistically, we provide genome-wide evidence that *Erm* is required for transcriptional regulation of many genes normally expressed subsynaptically. Taken together, these results demonstrate that the ETS transcription factor *Erm* is essential to enhance subsynaptic gene expression at the NMJ, and they emphasize the importance of transcriptional regulatory programs in synaptic protein enrichment.

RESULTS

Erm Expression by Subsynaptic Nuclei in Extrafusal Muscle Fibers

In previous experiments, we found that the ETS transcription factor *Erm* is expressed by intrafusal muscle fibers, but also in a restricted central domain within extrafusal muscle fibers (Hippenmeyer et al., 2002). This domain correlated with the location of presynaptic motor innervation in mouse hindlimb muscles. To study a putative role of *Erm* in NMJ development and maintenance, we first conducted a detailed analysis of *Erm* expression in skeletal muscles of the mouse at different developmental stages.

Using in situ hybridization on serial sections, we analyzed the expression pattern of *Erm* in relation to a transcript known to be subsynaptically expressed, the AChR delta subunit (*AChR*δ) (Simon and Burden, 1993). In mouse hindlimb muscles, we first detected *Erm* expression in a diffuse but centralized domain within muscles at embryonic day 14.5 (E14.5) (Figure 1A). *Erm* expression contrasted with the widespread expression of the basic helix-loop-helix transcription factor *MyoD* throughout extrafusal muscle fibers (Figure 1C). To selectively visualize motor axons and the forming neuromuscular EP band, we performed these experiments in *Hb9*^{GFP} transgenic embryos, a strain of mice expressing GFP in motor neurons (Wichterle et al., 2002). We found that *Erm* expression coincided with GFP$^+$ axons in the muscle (Figure 1B), thus demonstrating restricted expression to the neuromuscular EP domain even at these early stages. By E16.5, *Erm* and *AChR*δ expression were detected in a narrow band within muscles (Figures 1D–1F) and found in tight association with GFP$^+$ motor axons also containing Neurofilament (NF) (Figures 1E and 1F). We observed the same restricted expression pattern of *Erm* at postnatal day 1.5 (P1.5) (Figures 1G and 1I), at P8 (Figure 1M), and in the adult (Figures S1I and S1J in the Supplemental Data available with this article online). Together, these findings show that extrafusal *Erm* expression is restricted to the position of the neuromuscular EP band.

To determine more precisely the site of *Erm* expression at the level of individual NMJs of an EP band, we performed high-resolution analysis of NMJs at P1.5 and P8 (Figures 1J–1L, 1N, and 1O). We found that *Erm* expression in individual extrafusal muscle fibers is associated with presynaptic motor nerve terminals, as revealed by Synaptophysin and NF immunohistochemistry (Figures

Neuron
Erm Controls Subsynaptic Gene Expression

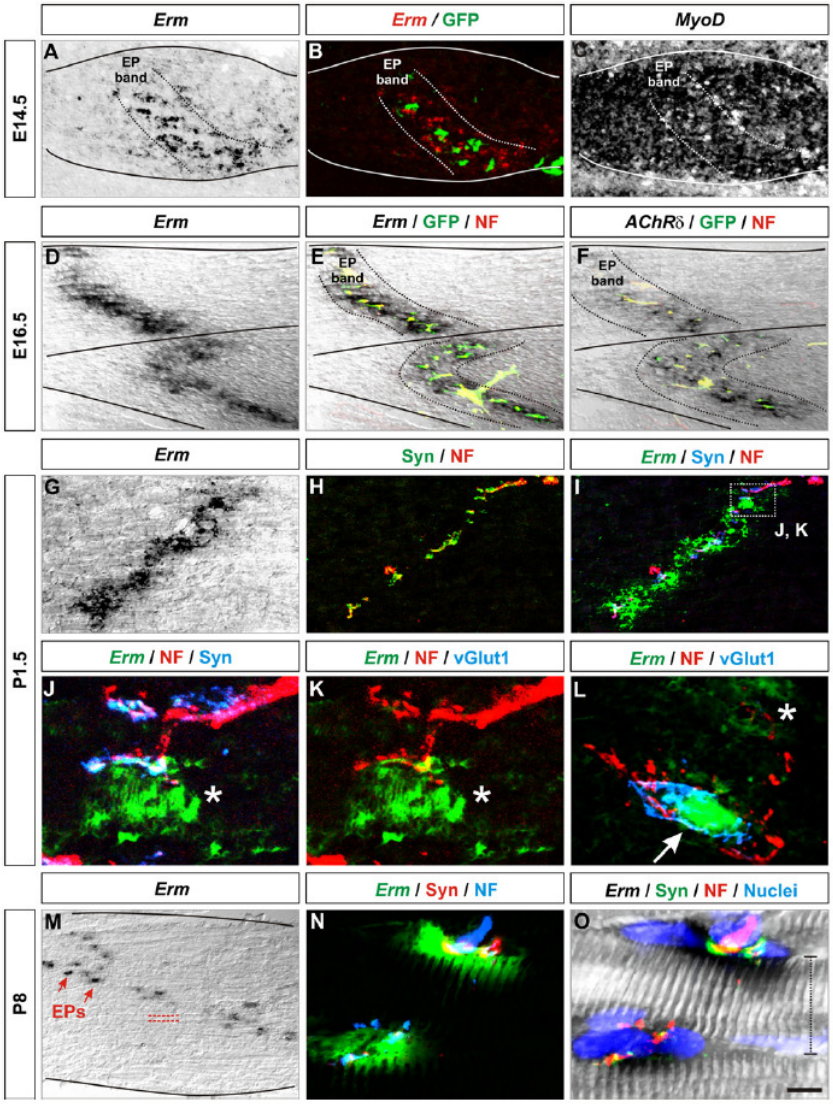

Figure 1. *Erm* Expression by Subsynaptic Nuclei in Extrafusal Muscle Fibers

(A–C) In situ hybridization to *Erm* (A and B) and *MyoD* (C) on consecutive longitudinal sections of E14.5 tibialis anterior muscle (muscle outline: solid lines) in an $Hb9^{GFP}$ embryo. Neuromuscular endplate (EP) band (dotted lines in [A]–[C]) was identified by antibodies to GFP (green) (B).

(D–F) Expression of *Erm* (D and E) and *AChR*δ (F) on consecutive longitudinal sections of hindlimb muscles of an E16.5 $Hb9^{GFP}$ embryo detected by in situ hybridization (black) in combination with immunocytochemistry to GFP and NF (E and F). Boundaries of muscles are shown as solid lines, outline of EP band in (E) and (F) as dotted lines.

(G–L) In situ hybridization to *Erm* ([G], black; [I–L], green) on P1.5 hindlimb muscles combined with immunohistochemical detection of Synaptophysin (H–J), NF (H–L), and vGlut1 (present at intrafusal [(L), arrow], but not extrafusal [(K) and (L), asterisk], muscle fibers). High-resolution images of (I) (box) are shown in (J) and (K).

(M–O) *Erm* expression on P8 hindlimb muscles by in situ hybridization in combination with Synaptophysin, NF, and nuclei. (M) Low-resolution image reveals EP band; arrows point to individual EPs; dashed lines outline individual muscle fibers. (N and O) High-resolution images of individual NMJs; dotted line depicts diameter of individual muscle fiber.

Scale bar, 40 μm in (A)–(C); 90 μm in (D)–(F); 50 μm in (G)–(I); 5 μm in (J) and (K); 10 μm in (L); 120 μm in (M); 6.5 μm in (N) and (O).

Neuron
Erm Controls Subsynaptic Gene Expression

1J, 1N, and 1O). Moreover, we also found a tight association of *Erm* expression with nuclear clusters (Figure 1O) known to accumulate preferentially underneath individual NMJs (Grady et al., 2005; Schaeffer et al., 2001). *Erm* expression was also detected in intrafusal muscle fibers, which could clearly be distinguished from extrafusal muscle fibers by their association with vGlut1$^+$ group Ia proprioceptive afferent terminals (Figures 1K and 1L) (Pang et al., 2006).

Taken together, these findings show that *Erm* expression in skeletal muscles is initiated in a centralized domain in alignment with ingrowing motor axons. As NMJs mature, *Erm* expression is refined to precisely underlie the neuromuscular EP band, and its expression in individual extrafusal muscle fibers eventually matches the presynaptic innervating motor EP.

Motor Innervation Does Not Regulate *Erm* Expression from Subsynaptic Nuclei

Since we found that the onset of *Erm* expression paralleled the ingrowth of motor axons into the muscle, these findings raised the question of whether its expression is influenced by motor-neuron-derived signals. To directly address this question, we made use of a previously generated mouse strain in which motor neurons are ablated selectively before their axons reach skeletal muscles; this is done by the expression of diphtheria toxin A (DTA) in motor neurons through a binary genetic system ($Isl2^{DTA}/Hb9^{Cre}$) (Pun et al., 2002).

In E16.5 $Isl2^{DTA}/Hb9^{Cre}$ embryos, muscles were devoid of both presynaptic motor axons and S100$^+$ Schwann cells (Figures S1G and S1H) (Pun et al., 2002), thus confirming the absence of motor innervation in $Isl2^{DTA}/Hb9^{Cre}$ embryos. In contrast, AChR clusters visualized by the fluorescently labeled snake venom α-Bungarotoxin (BTX) still accumulated in the central domain (Figure S1F), in agreement with previous observations (Yang et al., 2001). Since the position of the neuromuscular EP band can be followed easily on consecutive sections, we next compared the position of *Erm* in situ hybridization signal (Figures S1A and S1E) to the location of AChR clusters on consecutive sections (Figures S1B and S1F). We found that in both wild-type and $Isl2^{DTA}/Hb9^{Cre}$ embryos, *Erm* expression was confined to the position of AChR clusters (Figures S1A, S1B, S1E, and S1F). These findings thus demonstrate that the onset of *Erm* expression and its confinement to a centralized domain within extrafusal muscle fibers is not regulated by motor-axon-derived factors.

The lack of responsiveness of *Erm* expression to the absence of motor axons during early NMJ development left open the possibility that *Erm* expression might be regulated by nerve-derived signals at later stages, in particular after nerve lesion in the adult. Several genes including *AChR*δ are upregulated prominently in denervated extrafusal muscle fibers upon peripheral nerve lesion, whereas the expression of *AChR*ε remains largely unaffected (Moss et al., 1987; Witzemann et al., 1991). To directly address the question of whether *Erm* expression is influenced by the presence of motor axons in adult mice, we performed denervation experiments in which the sciatic nerve was cut ipsilaterally and animals were allowed to survive for 7 days subsequent to lesion. To confirm successful lesion of the sciatic nerve, we analyzed Synaptophysin immunoreactivity (Figures S1I, S1M, S1Q, and S1U). Similar to the method employed for the embryonic analysis (Figures S1A–S1H), we next used analysis of gene expression on consecutive sections in the EP band region. We found that expression of *AChR*δ was extensively upregulated throughout the denervated triceps surae muscle group, whereas nearly undetectable levels were found in contralateral muscles (Figures S1L, S1P, S1T, and S1X). Moreover, we found that independent of innervation, *Erm* expression was confined to a central domain within triceps surae muscles (Figures S1J, S1N, S1R, and S1V). Finally, denervation experiments in P2 mice did not lead to changes in the expression pattern of *Erm* 3 days subsequent to denervation (Figure S2). The response properties of *Erm* are thus similar to *AChR*ε, whose expression is also not strongly changed by denervation (Figures S1K, S1O, S1S, and S1W) (Witzemann et al., 1991). Together, these findings suggest that *Erm* expression in skeletal muscles is not influenced by the state of innervation, in contrast to other genes also expressed subsynaptically, such as the *AChR*δ subunit.

Erm Mutation Results in Progressive Muscle Weakness

The confined domain of *Erm* expression to subsynaptic extrafusal muscle fiber nuclei raised the question of the role of this transcription factor in NMJ development and maintenance. We therefore examined whether *Erm* mutant mice exhibit defects in the neuromuscular system. *Erm* mutant mice were born at normal Mendelian frequencies (Chen et al., 2005) (unpublished data), but already shortly after birth showed significant differences in body weight when compared with wild-type littermates (~82% of wild-type body weight at P1.5, $n \geq 3$; Figure S3A). In a postnatal developmental time course, we found that *Erm* mutants showed severe deficits in weight gain when compared with control littermates. By 1 month of age, *Erm* mutant mice exhibited only ~60% of the body weight of control littermates (Figure S3A). These defects in body weight acquisition observed in *Erm* mutant mice were paralleled by a reduction in weight acquisition at the level of individual muscle groups over time (quadriceps: P10, ~70% / 10 weeks, ~45% of wild-type; triceps surae: P10, ~76% / 10 weeks, ~46% of wild-type; Figures S4E and S4F). Nevertheless, *Erm* mutant mice did not exhibit obvious defects in muscle patterning, insertion points of muscles to tendons, pattern of striation in individual extrafusal muscle fibers, establishment of sensory organs within muscles, or expression levels of many structural and metabolic genes (Figures S4–S6), arguing against a role of *Erm* in the process of general muscle patterning and differentiation.

Neuron
Erm Controls Subsynaptic Gene Expression

In addition to severe deficits in weight gain, *Erm* mutant mice showed behavioral anomalies reminiscent of NMJ defects. *Erm* mutant mice exhibited a strong hunchback with 100% phenotypic penetrance and striking differences in movement when compared with their control littermates, characterized by slow movement and periods of immobility (Figures S3C and S3D, and data not shown). Moreover, between P10 and P20, *Erm* mutant mice developed fast, irregular breathing and an unusual vocalization pattern characterized by uncoordinated whistling sounds never observed in wild-type mice. Finally, median life expectancy of *Erm* mutant mice was only 2.3 months (n = 12) compared to over 2 years for control littermates (n = 9), and no *Erm* mutant mouse survived past 9 months of age (Figure S3B). Together, these findings suggest that *Erm* mutant mice exhibit gross phenotypic behavioral deficits similar to those described to occur in CMS (Engel et al., 2003).

Erm Mutation Results in Postsynaptic AChR Cluster Fragmentation

To begin to assess whether *Erm* mutation in mice leads to morphologically detectable defects at NMJs, we first assayed the appearance of individual AChR clusters in 6- to 8-month-old *Erm* mutant mice (Figures 2A–2F). Whereas the shape of postsynaptic specializations of AChR cluster accumulations at wild-type NMJs exhibited a typical "pretzel-like" appearance (Figures 2A–2C), we found that AChR clusters in *Erm* mutant mice showed a highly disrupted pattern (Figures 2D–2F). To assay these differences quantitatively, we assessed the number of uninterrupted, fluorescently BTX-labeled AChR cluster fragments at individual NMJs (Figure 2G) and measured the length of the longest fragment of these clusters (Figure 2H). Moreover, we also determined the surface area covered by the total NMJ and the area covered by individual fragments (Figures 2I and 2J). Whereas the number of uninterrupted AChR fragments at wild-type NMJs averaged two with a maximal fragment length of ~45 μm (n = 27), *Erm* mutant AChR clusters were frequently disrupted, reaching an average of approximately seven fragments per NMJ, with a maximal cluster length of only ~15 μm (n = 32) (Figures 2G and 2H). Moreover, we found a significant decrease in the surface area covered by AChR clusters at NMJs of *Erm* mutant mice when compared with that of wild-type littermates (Figures 2I and 2J).

We also assayed whether AChR clusters in *Erm* mutant mice show normal morphologies at earlier stages. We found that at 2 months of age, most AChR clusters in *Erm* mutant mice already exhibited a fragmented appearance, but ~20% of clusters showed an immature "plaque-like" configuration (Figures 2L and 2M), never observed in wild-type mice of this age (Figure 2K and data not shown). Together, these data show that the morphology of individual postsynaptic NMJs in the adult is severely affected in *Erm* mutant mice and suggest that a mature pretzel-like appearance of AChR clusters never develops in diaphragm muscles of these mice.

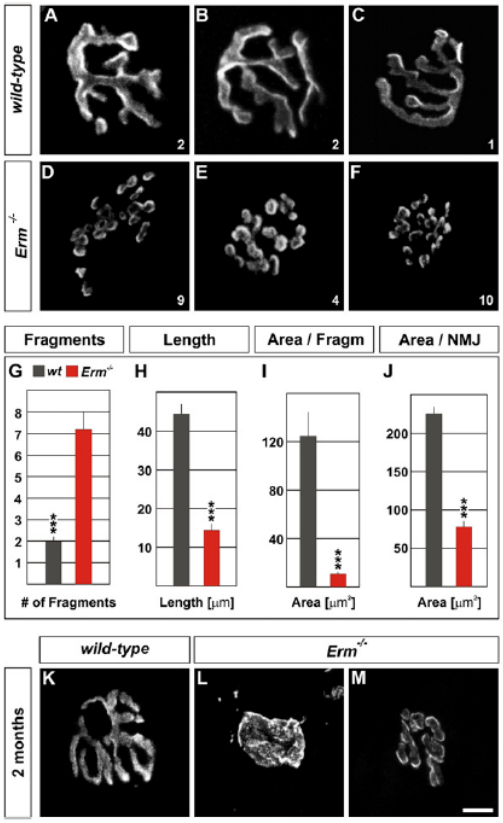

Figure 2. Fragmentation of AChR Clusters in Adult *Erm* Mutant Mice

(A–F) AChR clusters visualized using fluorescent BTX in diaphragm muscle of 6- to 8-month-old wild-type (A–C) and *Erm* mutant (D–F) mice (lower right corner: number of fragments for AChR cluster shown).

(G–J) Quantification of BTX^+ AChR clusters in diaphragm muscles of wild-type (gray) and *Erm* mutant (red) mice. Average number of fragments (G), longest individual fragment per NMJ (H), area occupied by individual fragment (I), and area occupied by entire NMJ (J) are illustrated. Values are derived from the analysis of 32 *Erm* mutant and 27 wild-type AChR clusters (from $n \geq 2$ animals). ± SEM: ***$p \leq 0.001$.

(K–M) AChR clusters visualized using fluorescent BTX in diaphragm muscle of 2-month-old wild-type (K) and *Erm* mutant ([L], plaque-like configuration; [M], fragmentation) mice.

Scale bar, 8 μm in (A)–(F); 9 μm in (K)–(M).

Erm Mutant Mice Exhibit Early Defects in NMJ Positioning within the Muscle

Since the expression pattern of *Erm* demarcates the central domain of extrafusal muscle fibers, we next determined whether *Erm* mutation affects the positioning of NMJs with respect to the central domain. In order to be able to evaluate quantitatively the width of the synaptic domain in which NMJs accumulate, we focused our

analysis on the diaphragm muscle and intercostal muscles, two muscle types with relatively flat anatomy that are easily accessible for whole-mount analysis.

At E14.5, no difference in the width of AChR cluster accumulation was detected in *Erm* mutants (Figure 3E, Figures S7A–S7D; data not shown). However, by E16.5, when the width of subsynaptic gene expression is normally refined to match motor axon terminals, we observed a significant difference between wild-type and *Erm* mutant mice (Figures 3A–3E; Figures S7E–S7H). To compare quantitatively the width of the domain in which AChR clusters accumulate between wild-type and *Erm* mutant mice, we used the entry point of the phrenic nerve into the left hemidiaphragm as an anatomical reference point (Figures 3A–3D). At E16.5, we observed an ~60% increase in broadening of the domain in which AChR clusters were detected in diaphragm muscles of *Erm* mutant mice when compared with the domain in wild-type (Figures 3C and 3D), and this value remained similar at P1.5 and P10 (Figure 3D). Together, these findings suggest that at early developmental stages, AChR clusters in *Erm* mutant mice already distribute over a broader central domain than in wild-type mice.

Normal Alignment of Presynaptic and Postsynaptic Structures in *Erm* Mutant Mice

Several mouse mutants with defects in postsynaptic AChR cluster differentiation also exhibit defects in presynaptic alignment of motor axon terminals (Sanes and Lichtman, 2001). Our findings that *Erm* mutant mice exhibit a broadened positioning of AChR clusters therefore raised the question of whether presynaptic alignment of motor axons with these clusters is also affected. We therefore first compared the alignment of presynaptic $Hb9^{GFP+}$ motor axon terminals with postsynaptic AChR clusters in wild-type and *Erm* mutant diaphragm muscles at the gross anatomical level. We found that AChR clusters were consistently associated with nerve terminals in both mouse strains from E16.5 onward (Figures 3F–3I and data not shown). In particular, even AChR clusters positioned at a far distance from the central ingrowth point of motor nerves in *Erm* mutant mice were innervated (Figure 3I).

We next monitored NMJs in *Erm* mutant mice at high resolution. We performed immunohistochemistry with antibodies to presynaptic proteins on P10 hindlimb muscles, but found no differences in presynaptic and postsynaptic alignment in *Erm* mutants when compared with that of wild-type (Figure S8). At 6 months of age, when *Erm* mutant AChR clusters exhibit a high degree of fragmentation (Figures 2D–2F and Figures 4D and 4J), presynaptic Synapsin/Synaptophysin^{+} motor axons nevertheless precisely followed individual AChR cluster fragments (Figures 4A–4L). Finally, we also determined whether *Erm* mutation affects aggregation of subsynaptic nuclei (Grady et al., 2005), but we found no difference in the clustering of these nuclei at individual NMJs in *Erm* mutants in comparison with that of wild-type (Figures 4M–4R). We conclude that the absence of *Erm* does not affect the alignment of presynaptic and postsynaptic structures at NMJs or clustering of subsynaptic nuclei.

Erm Mutant Mice Show Deficiencies in Neuromuscular Transmission

To determine whether the anatomical defects observed at NMJs of *Erm* mutant mice correlate with defects in neuromuscular synaptic transmission, we performed intracellular recordings from individual diaphragm muscle fibers in wild-type and *Erm* mutant mice.

We first analyzed the frequency of miniature EP potentials (MEPPs), events of spontaneous neurotransmitter release that are a reflection of the number of release sites at a given NMJ. We found a highly significant reduction in the frequency of MEPPs in *Erm* mutant mice to ~35% of wild-type levels (Figure 5E). This finding is in agreement with our anatomical analysis, in which we found the total area covered by synaptic structures at individual NMJs in *Erm* mutant mice to be reduced by approximately the same degree (Figure 2J). Moreover, the average MEPP amplitude was reduced by ~33% in *Erm* mutant mice, indicative of postsynaptic defects in these animals (Figures 5A–5D and 5F).

We also found deficits in response to nerve stimulation in *Erm* mutant mice. We used low extracellular calcium concentration to reduce the number of quanta released upon nerve stimulation and thus prevent action potential responses in muscle fibers. Under these conditions, phrenic nerve stimulation in wild-type mice elicited no postsynaptic response in ~58% of trials. In contrast, an average of ~75% of trials failed to evoke responses in *Erm* mutant mice (Figure 5K). Also, the average amplitude corresponding to the first quantal peak of the evoked EP potentials (EPPs) was reduced in *Erm* mutants to a similar degree as the amplitude of MEPPs (Figures 5G–5J and 5L). Together, these findings show that defects observed at the anatomical level in *Erm* mutant mice are also manifested as functional deficiencies in synaptic transmission at the NMJ.

Transcriptional Broadening in Subsynaptic Gene Expression in *Erm* Mutant Mice

The observation that accumulation of AChR clusters is detected in a broadened central domain in *Erm* mutant muscles raised the question of whether a similar phenotype can also be observed at the level of transcripts, which are selectively expressed subsynaptically. To address this issue, we analyzed the expression of the *AChRα* subunit in intercostal muscles of wild-type and *Erm* mutant mice using whole-mount in situ hybridization. We found that at E16.5 and P1.5, the width of the *AChRα* expression domain is significantly increased in *Erm* mutant mice when compared with that of wild-type (Figures 6A–6D and 6G). Furthermore, we also made use of the fact that *Erm* mutant mice still express truncated *Erm* transcript (Chen et al., 2005), and found similar changes for the expression domain of *Erm* (Figures 6E–6G). Together, these findings

Neuron
Erm Controls Subsynaptic Gene Expression

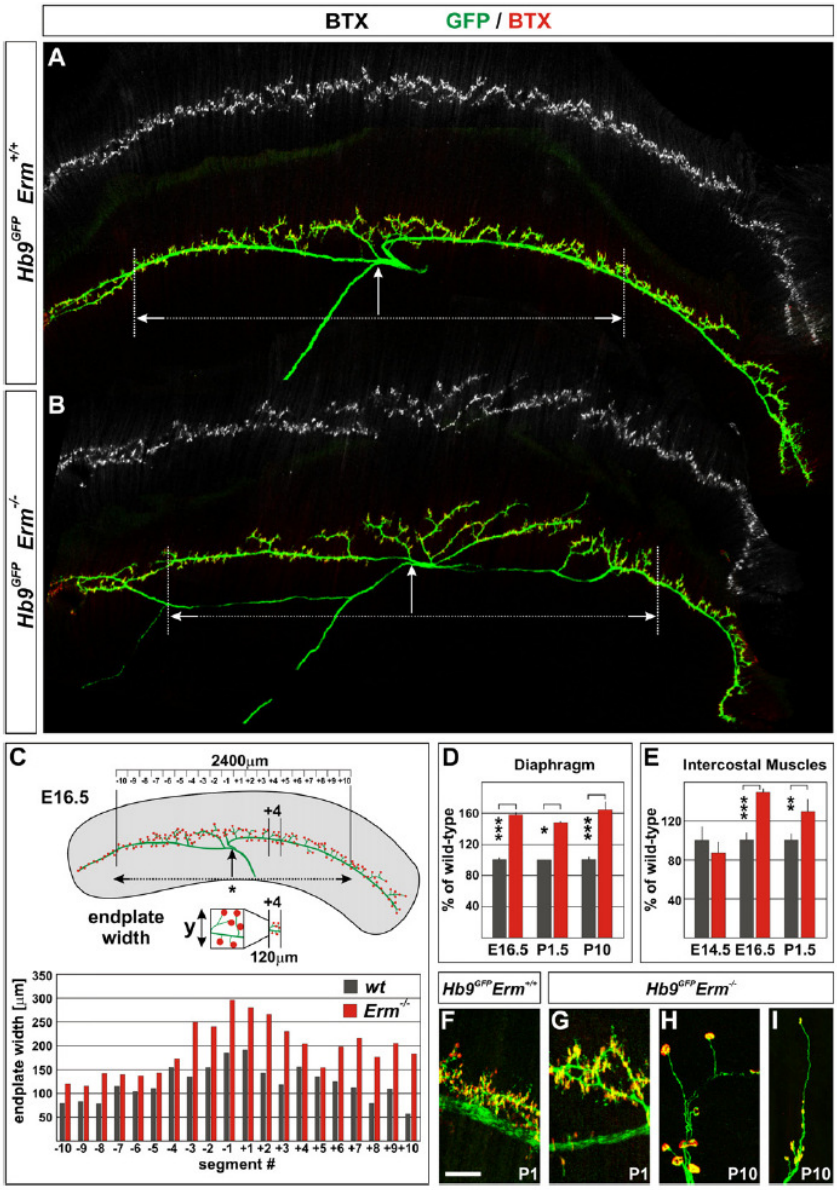

Figure 3. *Erm* Mutant Mice Exhibit Defects in AChR Cluster Positioning

(A and B) Analysis of AChR cluster distribution (BTX) and motor nerve ingrowth ($Hb9^{GFP}$) into diaphragm muscles of E16.5 wild-type (A) and *Erm* mutant (B) mice. Both BTX signals, as well as overlay with GFP, are shown in each panel. Arrows indicate the area used for quantification (C and D).

(C and D) Quantification of domain in which AChR clusters accumulate in diaphragm muscles (left hemidiaphragm used for analysis). Ten bins to the left and right of phrenic nerve entry point were analyzed, in bins of 120 µm at E16.5. Example for bin number +4 is shown schematically and quantitative analysis of all bins is displayed below. (D) Averages of this analysis over all bins and as a percentage of wild-type at E16.5, P1.5, and P10 for wild-type (gray) and *Erm* mutants (red). ±SEM: $^*p \leq 0.05$, $^{**}p \leq 0.01$, and $^{***}p \leq 0.001$.

(E) Analysis of AChR cluster accumulation domain for intercostal muscles relative to muscle width at E14.5, E16.5, and P1.5 detected as a percentage of wild-type. ±SEM: $^*p \leq 0.05$, $^{**}p \leq 0.01$, and $^{***}p \leq 0.001$.

(F–I) Alignment analysis of presynaptic and postsynaptic differentiation at P1 (F and G) and P10 (H and I) in wild-type (F) and *Erm* mutant (G–I) mice by visualization of GFP (green: $Hb9^{GFP}$) and BTX (red: AChR clusters).

Scale bar, 200 µm in (A) and (B); 60 µm in (F) and (G); 45 µm in (H); 100 µm in (I).

Neuron
Erm Controls Subsynaptic Gene Expression

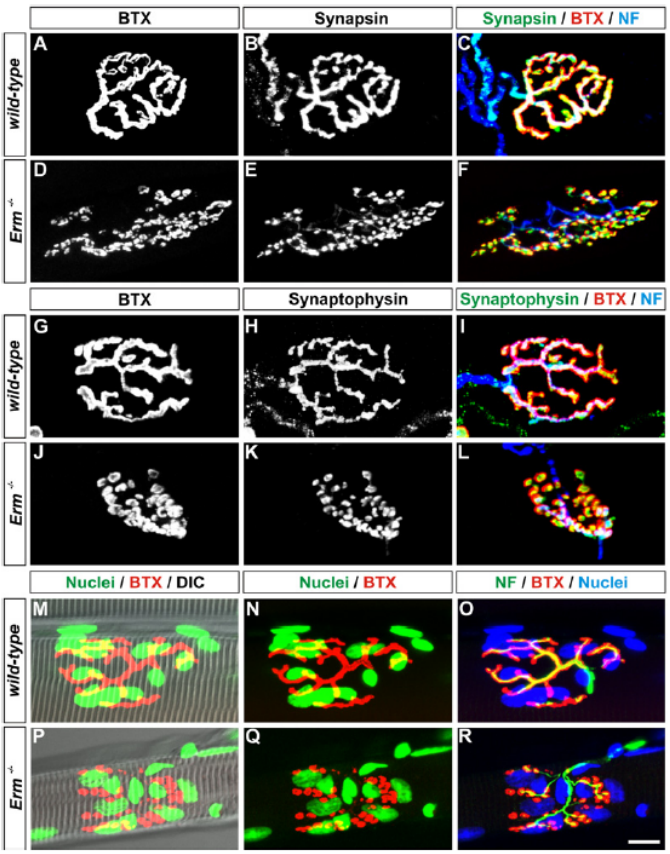

Figure 4. Alignment of Synaptic Structures of NMJs in *Erm* Mutant Mice

(A–L) BTX$^+$ AChR clusters in single teased tibialis anterior muscle fibers of 6-month-old wild-type ([A–C] and [G–I]) and *Erm* mutant ([D–F] and [J–L]) mice align with presynaptic structures as revealed by antibodies to Synapsin (B, C, E, and F) or Synaptophysin (H, I, K, and L). NF immunohistochemistry visualizes motor axons in (C), (F), (I), and (L), and occasional NF$^+$ axons extending to neighboring removed muscle fibers are visible ([L], bottom). (M–R) Analysis of subsynaptic nuclear clusters in extrafusal muscle fibers of 6-month-old wild-type (M–O) or *Erm* mutant (P–R) mice revealed by DRAQ5 fluorescence. Note that DRAQ5 labels all nuclei (including those of Schwann cells and fibroblasts), but in both wild-type and *Erm* mutant mice, subsynaptic nuclei accumulate and cluster underneath AChR clusters.

Scale bar, 10 μm in (A)–(L); 13 μm in (M)–(R).

show that *Erm* is required to define the width of the transcriptionally specialized central region within extrafusal muscle fibers.

Downregulation of a Subset of Genes Expressed Subsynaptically in *Erm* Mutants

The pronounced defects in postsynaptic NMJ differentiation in *Erm* mutant mice raise the question of the consequences of *Erm* mutation at the transcriptional level. We first analyzed several genes whose expression is known to be selectively regulated at the transcriptional level within the subsynaptic domain and which have previously been linked to regulation by ETS transcription factor binding sites (Briguet and Ruegg, 2000; de Kerchove D'Exaerde et al., 2002; Fromm and Burden, 1998). Specifically, we determined expression of *AChR*ε and *AChR*δ by in situ hybridization at P10, a time point at which expression of *AChR*ε is upregulated in wild-type mice. We used consecutive sections probed for *Erm* as a positive control for in situ hybridization and determined the presence of presynaptic motor nerves on all sections by combinatorial immunohistochemical detection of NF. While expression levels of *Erm* and *AChR*α were not affected in *Erm* mutant hindlimb muscles (Figures 7A–7D, data not shown), we found that both *AChR*ε and *AChR*δ expression were reduced considerably when compared with wild-type (Figures 7E–7L). To evaluate expression levels of the muscle-specific tyrosine kinase receptor *MuSK*, we used quantitative real-time PCR, since expression levels of *MuSK* are rapidly downregulated in muscles at late embryonic stages of wild-type mice (Valenzuela et al., 1995). In *Erm* mutants, we found an ~35% reduction of *MuSK* levels detected in wild-type littermates at E16.5 and an ~65% reduction at P1.5 (Figures 7Y and 7Z). These findings suggest that the expression of a subset of subsynaptically expressed genes was affected in *Erm* mutant muscles.

To evaluate the fraction of synaptically expressed genes whose expression is affected by absence of *Erm* at a genome-wide level, we next conducted a screen based on Affymetrix chip technology. To isolate muscle tissue enriched in subsynaptic or extrasynaptic nuclei, we used visually guided manual microdissection of muscle tissue at P1.5 and P9.5. To validate the isolation procedure of our samples, we first identified genes selectively enriched in subsynaptic areas of wild-type mice when compared with extrasynaptic samples (synaptic enrichment

Neuron
Erm Controls Subsynaptic Gene Expression

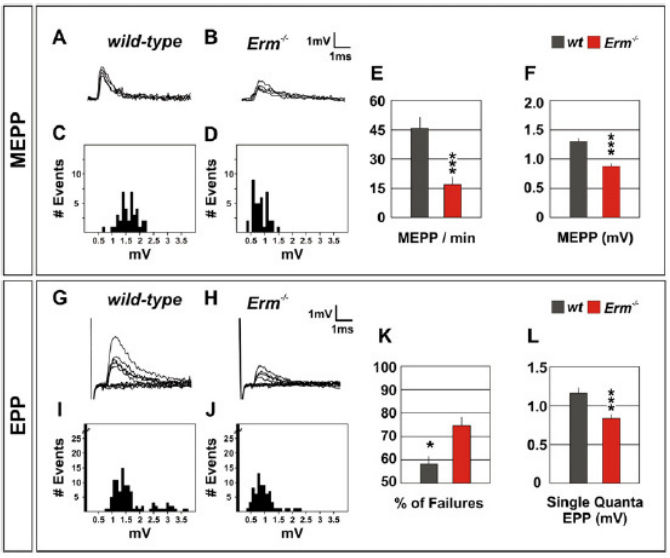

Figure 5. Defects in Synaptic Transmission at NMJs of *Erm* Mutant Mice

Analysis of MEPPs (A–F) and EPPs (G–L) at NMJs of diaphragm muscle fibers of 10-week-old wild-type and *Erm* mutant mice using intracellular recording techniques. (A)–(D) and (G)–(J) depict analysis of a single muscle fiber for wild-type (A, C, G, and I) and *Erm* mutant (B, D, H, and J). (A) and (B) show four representative MEPPs, and (G) and (H), ten sequential evoked traces, including some failed responses (flat traces). (C), (D), (I), and (J) show frequency histograms for MEPPs (C and D) and EPPs (I and J). Note that in EPP histograms, failures are scored at 0mV (wild-type: 206 of 307 trials; *Erm* mutant: 238 of 311 trials for fibers shown). Total analysis includes 16 muscle fibers each from wild-type and *Erm* mutant mice, and averaged MEPP frequency (wild-type 45.8 ± 5.8, mutant 16.8 ± 4.2 MEPP events/min [E]), MEPP amplitude (wild-type 1.31 ± 0.06, mutant 0.87 ± 0.06mV [F]), EPP failure rate (wild-type 58.1% ± 3.4%, mutant 74.7% ± 3.5% of trials [K]) and first quantal peak EPP amplitude (wild-type 1.16 ± 0.07, mutant 0.84 ± 0.05mV [L]) for all recordings are shown. The average resting membrane potentials of fibers recorded were −55.9 ± 1.4mV for wild-type and −61.0 ± 1.9mV for *Erm* mutant mice. ±SEM: *$p \leq 0.05$ and ***$p \leq 0.001$.

factors ≥2.5-fold: P1.5, 71 genes; P9.5, 64 genes; Tables S1–S3 in the Supplemental Data available with this article online). This analysis revealed that most genes previously known to be expressed subsynaptically or isolated in similar screens (Chakkalakal and Jasmin, 2003; Jevsek et al., 2006; Kishi et al., 2005) were recovered by our approach (Tables S1–S3).

Using the list of genes expressed in a synaptically enriched pattern in wild-type, we next evaluated how many of these genes were misregulated in *Erm* mutant mice. We found that at P1.5, ~48% of all synaptically enriched genes were downregulated in *Erm* mutant subsynaptic muscle preparations by at least 1.5-fold when compared with wild-type levels (34/71 genes; Table S1). At P9.5, ~69% of all genes were downregulated in *Erm* mutants (44/64 genes; Table S2). No synaptically enriched genes recovered in the wild-type analysis were upregulated in synaptic regions of P9.5 *Erm* mutants by ≥1.5-fold. A combined analysis of lists derived from both developmental stages identified 38 genes with synaptic enrichment of ≥2.5-fold at both stages; of these, 17 genes (~45%) were downregulated by >1.5-fold in *Erm* mutants (Table S3). Interestingly, we noticed a population of genes transiently upregulated by >1.5-fold in *Erm* mutants at P1.5 (8/71), but most of these genes corresponded to genes known to be expressed by Schwann cells (Table S1), indicating that Schwann cells might be transiently affected in *Erm* mutant mice. Moreover, since genes expressed by Schwann cells also score as synaptically enriched in our screen, we are likely to underestimate the number of genes directly or indirectly regulated by *Erm* in extrafusal muscle fibers.

We next verified a number of genes isolated by our Affymetrix screen using in situ hybridization experiments on P1.5 thigh muscles of wild-type and *Erm* mutant mice. In particular, we confirmed downregulation of two genes recently identified as subsynaptically expressed in wild-type mice: dual specificity phosphatase 6 (*Dusp6*) and *Cd24*, the latter of which encodes a GPI-anchored sialoglycoprotein (Jevsek et al., 2006; Nazarian et al., 2005) (Figures 7M–7P; data not shown). Moreover, our analysis also identified a number of genes previously not described to be expressed subsynaptically, among them a putative potassium channel accessory protein (*Kcne1-like*) and the voltage-gated sodium channel subunit *Scn3b*, the expression of both of which is dramatically downregulated to nearly undetectable levels in *Erm* mutant thigh muscles (Figures 7Q–7X). High levels of functional sodium channels at NMJs have been observed many years ago (Caldwell et al., 1986), but regulatory mechanisms of synaptic enrichment of sodium channel subunits have remained elusive. Our findings suggest that at least part of this regulation may be controlled by *Erm*-dependent transcriptional mechanisms.

In summary, these findings show that the gene expression changes identified in our Affymetrix gene chip experiments were confirmed by in situ hybridization experiments and matched the degree of downregulation detected in *Erm* mutant muscles. We conclude that *Erm* is essential to enhance expression levels of a large fraction

Neuron
Erm Controls Subsynaptic Gene Expression

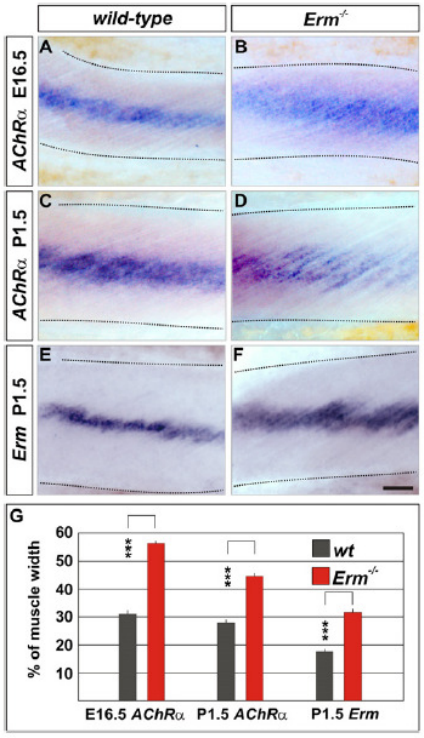

Figure 6. Broadened Subsynaptic Gene Expression Domain in *Erm* Mutant Mice

Analysis of *AChRα* (A–D) and *Erm* (E and F) expression by whole-mount in situ hybridization experiments in intercostal muscles of E16.5 (A and B) and P1.5 (C–F) wild-type (A, C, and E) and *Erm* mutant (B, D, and F) mice. Note broadening of expression domain in *Erm* mutant mice, as quantified in (G) (wild-type: gray bars; *Erm* mutant: red bars). ±SEM: ***$p \leq 0.001$. Scale bar, 175 μm in (A) and (B); 145 μm in (C)–(F).

of genes confined to subsynaptic nuclei in skeletal muscle fibers.

DISCUSSION

Local protein accumulation is important to regulate availability of specific proteins at synapses, but mechanisms contributing to this subcellular specificity remain poorly defined. At the developing NMJ, a transcriptionally specialized region within nascent myotubes delineates the postsynaptic domain where NMJs form. In this study, we provide evidence that the expression of the ETS transcription factor *Erm* plays an important role in controlling the selective subsynaptic accumulation of many transcripts at NMJs. Its mutation in mice has severe consequences for NMJ maintenance and function at multiple levels of analysis. We discuss our findings in the context of mechanisms regulating local protein accumulation at synapses, signaling pathways involved in NMJ differentiation, and the role of *Erm* in these processes.

Molecular Mechanisms Controlling Protein Accumulation at the Subcellular Level

Which molecular mechanisms act to restrict, target, and accumulate proteins to defined subcellular sites? Local availability of proteins can be regulated at many different levels. Classical studies on mechanisms of protein targeting have revealed the existence of dedicated peptide sequences responsible for guiding proteins to sites of action such as secretory pathways or mitochondria. In addition to these posttranslational targeting mechanisms, regulation at the level of local protein synthesis is a relatively recently discovered mechanism which has been studied intensely at synapses (Sutton and Schuman, 2006) and allows highly selective production of distinct proteins at defined synapses. The multinuclear structure of muscle fibers adds additional mechanistic flexibility for accumulation of synaptic transcripts and proteins at the NMJ. Our study provides evidence that *Erm* is essential to regulate accumulation of mRNAs at subsynaptic nuclei in extrafusal muscle fibers and thereby contributes to synaptic protein enrichment through transcriptional mechanisms.

ETS Transcription Factor Signaling at Subsynaptic Nuclei

The elucidation of transcriptional mechanisms regulating gene expression within the subsynaptic domain of extrafusal muscle fibers has been a topic of many investigations (Burden, 2002; Sanes and Lichtman, 2001; Schaeffer et al., 2001). In particular, mapping studies for transcription factor binding sites in AChR subunit promoter elements have led to the suggestion that the ETS transcription factor *GABPα* might play a key role in the regulation of subsynaptic gene expression (Duclert et al., 1996; Koike et al., 1995; Schaeffer et al., 1998). However, the absence of overt behavioral abnormalities resembling CMS after conditional *GABPα* mutation (Jaworski et al., 2007; O'Leary et al., 2007) argues against a role of *GABPα* as the major transcriptional regulator involved in enhancing subsynaptic gene expression.

Our findings from analyses of *Erm* mutant mice suggest instead that the ETS transcription factor *Erm* plays an essential role in subsynaptic gene expression. We found the expression of *Erm* to be subsynaptically restricted within extrafusal muscle fibers, and *Erm* mutation leads to pronounced changes in subsynaptic transcription. Our study does not provide biochemical evidence that Erm interacts with ETS consensus site regulatory elements of genes whose expression levels are affected in *Erm* mutant skeletal muscles. However, due to the relative promiscuity of promoter binding assays to test for ETS transcription factor binding in reduced systems (Mo et al., 1998), interaction of Erm with the same binding sites that have been described to interact with GABPα is to be expected. In support of this, within the relatively broadly defined ETS transcription factor consensus binding site, a more

Neuron
Erm Controls Subsynaptic Gene Expression

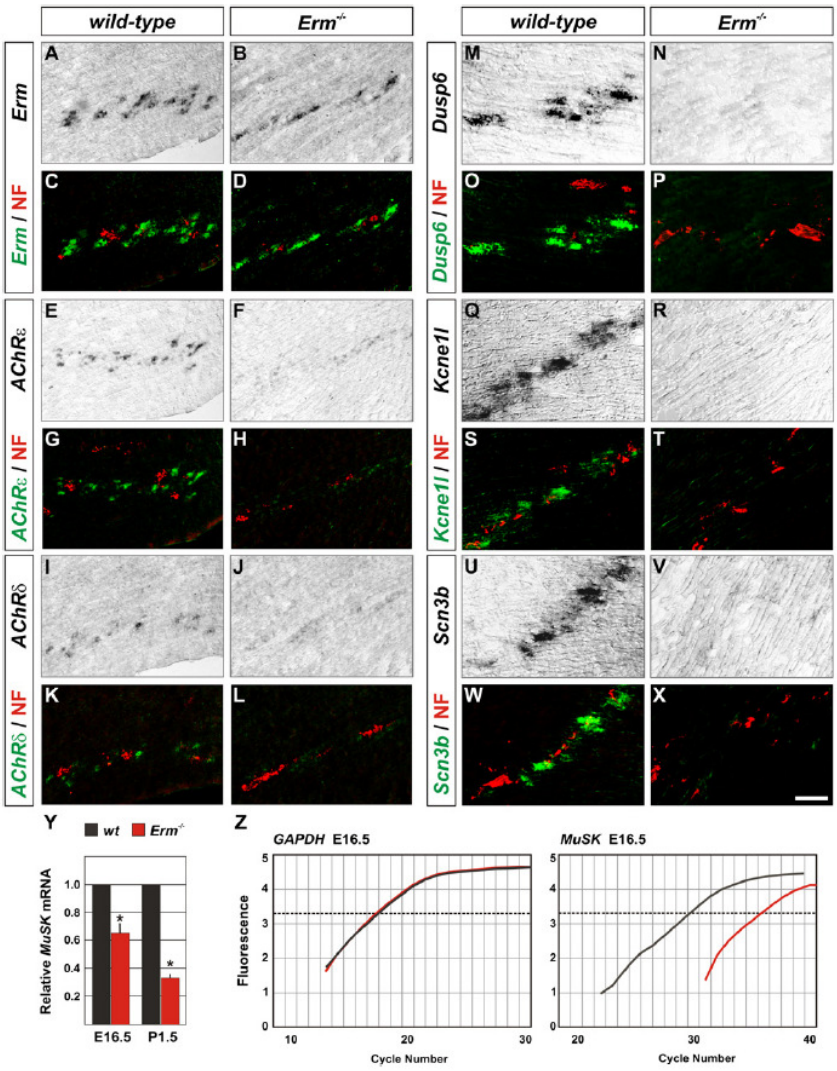

Figure 7. Selective Downregulation of a Fraction of Subsynaptic Genes in *Erm* Mutant Mice

(A–L) Analysis of *Erm* (A–D), *AChRε* (E–H), and *AChRδ* (I–L) expression by in situ hybridization experiments on hindlimb muscles of P10 wild-type (A, C, E, G, I, and K) and *Erm* mutant (B, D, F, H, J, and L) mice. (M–X) Analysis of *Dusp6* (M–P), *Kcne1l* (Q–T), and *Scn3b* (U–X) expression by in situ hybridization experiments on hindlimb muscles of P1.5 wild-type (M, O, Q, S, U, and W) and *Erm* mutant (N, P, R, T, V, and X) mice. In situ hybridization (false color images in green) was combined with immunocytochemical detection of NF (red) to visualize presynaptic motor nerve terminals.

(Y and Z) Quantitative analysis of *MuSK* expression levels determined by real-time PCR on cDNA derived from E16.5 (Y and Z) and P1.5 (Y) gastrocnemius muscles of wild-type and *Erm* mutant mice. *MuSK* reactions were normalized against *GAPDH*, and (Z) depicts a representative example of amplification at E16.5. Relative fluorescent units are plotted against cycle number. Dashed line indicates signal intensity used for quantitative assessment of differences. ±SEM: $^*p \leq 0.05$

Scale bar, 60 μm in (A)–(L); 40 μm in (M)–(X).

restricted consensus site known as the N-box element has been implicated in GABPα-mediated responses of subsynaptic gene expression (Briguet and Ruegg, 2000; Fromm and Burden, 1998; Schaeffer et al., 1998). This N-box consensus site also matches the binding site observed for *Pea3* ETS transcription factor subfamily members including *Erm* in a study analyzing DNA sequence discrimination by ETS proteins (Mo et al., 1998).

Could there be interplay between Erm- and GABP-mediated signaling pathways in the control of subsynaptic

Neuron
Erm Controls Subsynaptic Gene Expression

gene expression? ETS transcription factors interact with a variety of cofactors in order to control cell-type-specific downstream responses (Sharrocks, 2001), raising the possibility that Erm could interact with some of the same cofactors as GABPα—most importantly, its high-affinity binding partner GABPβ. Against this possibility, GABPβ does not augment DNA-binding activity of Er81, a Pea3 ETS family member closely related to Erm (Brown and McKnight, 1992). Moreover, domains required for interaction between GABPα and GABPβ have been mapped and it appears unlikely that Erm would associate with GABPβ (Rosmarin et al., 2004). Whether and how GABP and Erm signaling pathways interact in skeletal muscles remains to be determined. Most likely, possible convergence would be at the level of overlapping target genes, where *GABPα* only plays a minor role in vivo (Jaworski et al., 2007; O'Leary et al., 2007).

Molecular Pathways Regulated by *Erm* in Subsynaptic Nuclei

Our genome-wide estimate of the fraction of genes whose expression levels are affected by *Erm* mutation would predict that at least half of the genes expressed in a subsynaptically enriched pattern in wild-type diaphragm muscles are regulated either directly or indirectly through this pathway. However, while we detect strong downregulation of many of these genes, *Erm* can clearly not be the sole determinant for their expression within extrafusal muscle fibers. Against such a dominant role, a low level of expression for some downregulated genes can still be detected in a centralized domain by in situ hybridization. Our observations are compatible with detailed analysis of regulatory pathways involved in *AChRδ* expression that reveal multiple *cis*-acting elements involved in control of expression. In these studies, in addition to an ETS transcription factor binding site implicated in subsynaptic expression (Fromm and Burden, 1998), an E-box element defines skeletal muscle expression as such (Simon and Burden, 1993). Further support against an "all-or-none" trigger role of *Erm* comes from our observations that the phenotype of *Erm* mutant mice is clearly less severe than the additive phenotypes of mutation in individual genes with downregulated expression levels in *Erm* mutants. For example, *Erm* mutant mice show a phenotype highly distinct from *MuSK* mutants, which exhibit a complete lack of transcriptional patterning and AChR clustering as well as extensive motor axon sprouting (DeChiara et al., 1996), suggesting that even reduced levels of *MuSK* in *Erm* mutant mice are sufficient to support AChR clustering, alignment of presynaptic and postsynaptic structures of NMJs, and survival of mice beyond birth. We propose that *Erm* acts to boost gene expression levels selectively at subsynaptic nuclei rather than being an all-or-none trigger for the expression of these genes in extrafusal muscle fibers. As such, *Erm* controls an essential subprogram in subsynaptic gene expression involved in NMJ maturation and maintenance (Figure 8E). In addition, our findings support the existence of at least one *Erm*-independent pathway controlling subsynaptic gene expression (Figure 8E).

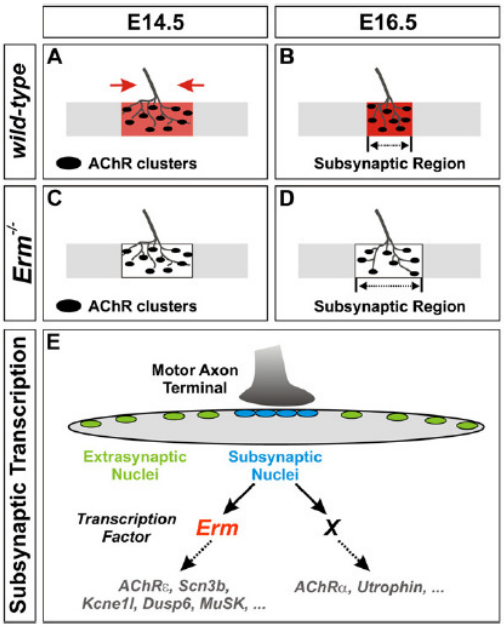

Figure 8. *Erm* Controls Subsynaptic Gene Expression
(A–D) Schematic model figure depicting developmental time course of NMJ formation in wild-type (A and B) and *Erm* mutant (C and D) mice at E14.5 and E16.5. In wild-type, AChR clusters are confined to a centralized domain within extrafusal muscle fibers. By E16.5, presynaptic motor axons align with postsynaptic AChR clusters overlying the transcriptionally defined subsynaptic region (B). *Erm* mutant mice show a broadened domain in which AChR clusters already accumulate within extrafusal fibers at E16.5, but no defects in alignment of presynaptic and postsynaptic structures are detected (D).
(E) Schematic diagram illustrating the existence of at least two alternative transcriptional pathways involved in the regulation of subsynaptic gene expression. *Erm* is essential to enhance subsynaptic gene expression of a major fraction of the genes expressed subsynaptically within extrafusal muscle fibers. The remaining set of genes is hypothesized to be regulated through one or more other transcriptional pathways (X).

Erm and the Establishment of an AChR-Cluster-Rich Central Domain

The restricted expression of *Erm* to the subsynaptic domain of extrafusal muscle fibers raises the question of whether *Erm* itself defines the domain competent for NMJ formation before motor axons arrive. We found that *Erm* fulfills at least one of the criteria required to qualify as such a gene: its expression is not regulated by motor-nerve-derived signals. But what are the consequences of *Erm* mutation for setting the width of the domain in which NMJs form? At the transcriptional level, genes with maintained expression levels in *Erm* mutants exhibit

a significant broadening compared with wild-type but nevertheless preserve central patterning. These findings strongly argue against *Erm* being an upstream transcription factor involved in setting up the transcriptionally specialized central domain within extrafusal muscle fibers. Since in the absence of *Erm*, this transcriptionally defined domain is significantly broader than in wild-type mice, our results raise the possibility that the primary cause resulting in the formation of a broadened NMJ domain in *Erm* mutants could be a defect in refining the width of the central transcriptional specialization. The accumulation of AChR clusters in a broadened domain and the subsequent association with presynaptic terminals within the limits of this domain would thus be a secondary consequence of an initially broadened transcriptional domain (Figures 8A–8D). In support of this view, in *Erm* mutants analyzed at E16.5, we observed transcriptional broadening and a wider domain in which AChR clusters accumulate. This stage corresponds to the stage at which a sharpened transcriptionally defined central domain is normally first observed in wild-type embryos. In such a model, the broadening of AChR cluster accumulation would be a consequence of a disturbed transcriptional territory in *Erm* mutants.

We cannot, however, exclude a model in which the broadening of the transcriptional expression is a secondary consequence of a less efficient process of NMJ differentiation, perhaps due to weakened activity of postsynaptic elements in response to signals derived from ingrowing motor axons. Similarly, broadening of the synaptic EP band in *Erm* mutants could equally well reflect a weakening in a MuSK-dependent feedback loop. In support of such a model, *MuSK* heterozygous mutant mice in the absence of motor innervation essentially fail to form AChR clusters (Lin et al., 2001), and lower MuSK activity could thus contribute to the lack of refinement of the AChR-rich central domain in *Erm* mutant mice.

By which cellular and molecular mechanisms is the establishment of the transcriptionally specialized central domain controlled in wild-type mice? The fact that *Erm* is regulated by motor-nerve-independent mechanisms raises the question of what mechanisms are regulating the expression domain of *Erm* in the muscle. Lineage tracing experiments have provided convincing evidence that myoblast clones do not become restricted to particular muscles, but can spread out between different muscles (Kardon et al., 2002). These studies suggest that muscles are patterned by mechanisms not primarily residing within immigrating myoblasts, but instead suggest that this information is superimposed onto nascent myotubes by signaling interactions from underlying mesenchyme tissue (Kardon et al., 2003). Furthermore, the developmental progression of muscle cleavage is a process driven by mesenchymal signals and future muscle endpoint domains have been suggested to be important upstream regulators in this process. These observations make it most plausible that signals from within the mesenchyme pattern nascent myotubes.

In developing somites, recent work has established a molecular link between FGF signaling and the induction of *Erm* expression acting at a certain distance (Brent and Tabin, 2004). Interestingly, *FGF6* is one of only a few genes observed to be selectively expressed by primary myotube endcompartments and prospective tendon mesenchyme (deLapeyriere et al., 1993). In analogy to the work in developing somites (Brent and Tabin, 2004), FGF signaling from the tendon region may therefore act to induce the expression of *Erm* in the central domain of forming myotubes. In an alternative model, the establishment of the prepatterning domain has been suggested to be a consequence of enhanced initial MuSK signaling and associated kinase activation in this central region (Yang et al., 2001). Indeed, *MuSK* mutant mice lack subsynaptically enriched gene expression, and ectopic expression of MuSK outside this domain is sufficient to trigger postsynaptic differentiation (DeChiara et al., 1996; Sander et al., 2001).

A Link between *Erm* and CMS?

Perhaps the most striking phenotype we observed in *Erm* mutant mice is the progressive development of muscle atrophy, accompanied by severe movement deficits and premature death. These deficits are highly reminiscent of the clinical symptoms described for patients with CMS, characterized by dysfunction of neuromuscular transmission as a consequence of either presynaptic or postsynaptic NMJ defects (Engel et al., 2003). To our knowledge, no *Erm* mutation has been linked to CMS in humans to date. Strikingly, however, mutation of an N-box consensus ETS binding site in the *AChRε* promoter region in humans leads to a form of CMS (Ohno et al., 1999), highlighting the clinical relevance of ETS transcription-factor-mediated signaling pathways. The *Erm* mutant mouse model analyzed in this study may thus shed light on signaling pathways whose disruption leads to symptoms of CMS in humans.

EXPERIMENTAL PROCEDURES

Mouse Genetics, Immunohistochemistry, and In Situ Hybridization

$Erm^{+/-}$ (Chen et al., 2005), $Hb9^{GFP}$ (Wichterle et al., 2002), $Isl2^{DTA}$, and $Hb9^{Cre}$ (Yang et al., 2001) mouse strains have been described previously. Immunohistochemistry and in situ hybridization experiments were essentially performed as described (Arber et al., 2000). Images were collected on an Olympus confocal microscope or an MVX10 stereo dissection microscope and analyzed as described in the Supplemental Data. For all experiments, significance was determined performing an ANOVA single-factor test and defined as $^{*}p \leq 0.05$, $^{**}p \leq 0.01$, and $^{***}p \leq 0.001$.

Gene Expression Analysis

For Affymetrix microarray gene expression analysis (U74Av2/U74Bv2 gene chip arrays), total RNA was isolated from BTX-labeled synaptic EP band and BTX-negative extrasynaptic region of the diaphragm muscles at P1.5 and P9.5 from wild-type and *Erm* mutant littermates, similar to a method described previously (Kishi et al., 2005). Data analysis was performed using Expressionist Pro 3.1 software (GeneData). Details on chip and quantitative real-time PCR are described in the Supplemental Data.

Neuron

Erm Controls Subsynaptic Gene Expression

Intracellular Muscle Fiber Electrophysiology

Intracellular muscle fiber recordings were performed from diaphragm muscle fibers of wild-type and *Erm* mutants according to previously published procedures (Knight et al., 2003) further described in the Supplemental Data.

Supplemental Data

The Supplemental Data for this article can be found online at http://www.neuron.org/cgi/content/full/55/5/726/DC1/.

ACKNOWLEDGMENTS

We are very grateful to Pico Caroni for advice and discussions throughout the project. Furthermore, we would like to thank Chen Chen for initial interactions in our studies of *Erm* mutant mice, Edward Oakeley and Herbert Angliker for expert technical assistance with processing and analysis of Affymetrix microarrays, Thomas Jessell and Hynek Wichterle for providing $Hb9^{GFP}$ transgenic mice, Steve Burden and Alexander Jaworski for advice on quantitative PCR to determine *MuSK* levels, Thomas Jessell and Steve Burden for helpful comments on the manuscript, and John Hassell for discussions and interactions on ETS gene function. S.H., R.M.H., D.R.L, and S.A. were supported by a grant from the Swiss National Science Foundation, by the Kanton of Basel-Stadt, and by the Novartis Research Foundation.

Received: March 8, 2007
Revised: June 22, 2007
Accepted: July 24, 2007
Published: September 5, 2007

REFERENCES

Arber, S., Ladle, D.R., Lin, J.H., Frank, E., and Jessell, T.M. (2000). ETS gene Er81 controls the formation of functional connections between group Ia sensory afferents and motor neurons. Cell *101*, 485–498.

Arber, S., Burden, S.J., and Harris, A.J. (2002). Patterning of skeletal muscle. Curr. Opin. Neurobiol. *12*, 100–103.

Brent, A.E., and Tabin, C.J. (2004). FGF acts directly on the somitic tendon progenitors through the Ets transcription factors Pea3 and Erm to regulate scleraxis expression. Development *131*, 3885–3896.

Briguet, A., and Ruegg, M.A. (2000). The Ets transcription factor GABP is required for postsynaptic differentiation in vivo. J. Neurosci. *20*, 5989–5996.

Brown, T.A., and McKnight, S.L. (1992). Specificities of protein-protein and protein-DNA interaction of GABP alpha and two newly defined ets-related proteins. Genes Dev. *6*, 2502–2512.

Burden, S.J. (2002). Building the vertebrate neuromuscular synapse. J. Neurobiol. *53*, 501–511.

Caldwell, J.H., Campbell, D.T., and Beam, K.G. (1986). Na channel distribution in vertebrate skeletal muscle. J. Gen. Physiol. *87*, 907–932.

Chakkalakal, J.V., and Jasmin, B.J. (2003). Localizing synaptic mRNAs at the neuromuscular junction: it takes more than transcription. Bioessays *25*, 25–31.

Chen, C., Ouyang, W., Grigura, V., Zhou, Q., Carnes, K., Lim, H., Zhao, G.Q., Arber, S., Kurpios, N., Murphy, T.L., et al. (2005). ERM is required for transcriptional control of the spermatogonial stem cell niche. Nature *436*, 1030–1034.

de Kerchove D'Exaerde, A., Cartaud, J., Ravel-Chapuis, A., Seroz, T., Pasteau, F., Angus, L.M., Jasmin, B.J., Changeux, J.P., and Schaeffer, L. (2002). Expression of mutant Ets protein at the neuromuscular synapse causes alterations in morphology and gene expression. EMBO Rep. *3*, 1075–1081.

DeChiara, T.M., Bowen, D.C., Valenzuela, D.M., Simmons, M.V., Poueymirou, W.T., Thomas, S., Kinetz, E., Compton, D.L., Rojas, E., Park, J.S., et al. (1996). The receptor tyrosine kinase MuSK is required for neuromuscular junction formation in vivo. Cell *85*, 501–512.

deLapeyriere, O., Ollendorff, V., Planche, J., Ott, M.O., Pizette, S., Coulier, F., and Birnbaum, D. (1993). Expression of the Fgf6 gene is restricted to developing skeletal muscle in the mouse embryo. Development *118*, 601–611.

Duclert, A., Savatier, N., Schaeffer, L., and Changeux, J.P. (1996). Identification of an element crucial for the sub-synaptic expression of the acetylcholine receptor epsilon-subunit gene. J. Biol. Chem. *271*, 17433–17438.

Engel, A.G., Ohno, K., and Sine, S.M. (2003). Congenital myasthenic syndromes: A diverse array of molecular targets. J. Neurocytol. *32*, 1017–1037.

Fromm, L., and Burden, S.J. (1998). Synapse-specific and neuregulin-induced transcription require an ets site that binds GABPalpha/GABP-beta. Genes Dev. *12*, 3074–3083.

Grady, R.M., Starr, D.A., Ackerman, G.L., Sanes, J.R., and Han, M. (2005). Syne proteins anchor muscle nuclei at the neuromuscular junction. Proc. Natl. Acad. Sci. USA *102*, 4359–4364.

Hippenmeyer, S., Shneider, N.A., Birchmeier, C., Burden, S.J., Jessell, T.M., and Arber, S. (2002). A role for neuregulin1 signaling in muscle spindle differentiation. Neuron *36*, 1035–1049.

Jaworski, A., Smith, C.L., and Burden, S.J. (2007). GA-binding protein is dispensable for neuromuscular synapse formation and synapse-specific gene expression. Mol. Cell. Biol. *27*, 5040–5046.

Jevsek, M., Jaworski, A., Polo-Parada, L., Kim, N., Fan, J., Landmesser, L.T., and Burden, S.J. (2006). CD24 is expressed by myofiber synaptic nuclei and regulates synaptic transmission. Proc. Natl. Acad. Sci. USA *103*, 6374–6379.

Kardon, G., Campbell, J.K., and Tabin, C.J. (2002). Local extrinsic signals determine muscle and endothelial cell fate and patterning in the vertebrate limb. Dev. Cell *3*, 533–545.

Kardon, G., Harfe, B.D., and Tabin, C.J. (2003). A Tcf4-positive mesodermal population provides a prepattern for vertebrate limb muscle patterning. Dev. Cell *5*, 937–944.

Kishi, M., Kummer, T.T., Eglen, S.J., and Sanes, J.R. (2005). LL5beta: a regulator of postsynaptic differentiation identified in a screen for synaptically enriched transcripts at the neuromuscular junction. J. Cell Biol. *169*, 355–366.

Knight, D., Tolley, L.K., Kim, D.K., Lavidis, N.A., and Noakes, P.G. (2003). Functional analysis of neurotransmission at beta2-laminin deficient terminals. J. Physiol. *546*, 789–800.

Koike, S., Schaeffer, L., and Changeux, J.P. (1995). Identification of a DNA element determining synaptic expression of the mouse acetylcholine receptor delta-subunit gene. Proc. Natl. Acad. Sci. USA *92*, 10624–10628.

Kummer, T.T., Misgeld, T., and Sanes, J.R. (2006). Assembly of the postsynaptic membrane at the neuromuscular junction: paradigm lost. Curr. Opin. Neurobiol. *16*, 74–82.

Lin, J.H., Saito, T., Anderson, D.J., Lance-Jones, C., Jessell, T.M., and Arber, S. (1998). Functionally related motor neuron pool and muscle sensory afferent subtypes defined by coordinate ETS gene expression. Cell *95*, 393–407.

Lin, W., Burgess, R.W., Dominguez, B., Pfaff, S.L., Sanes, J.R., and Lee, K.F. (2001). Distinct roles of nerve and muscle in postsynaptic differentiation of the neuromuscular synapse. Nature *410*, 1057–1064.

Livet, J., Sigrist, M., Stroebel, S., De Paola, V., Price, S.R., Henderson, C.E., Jessell, T.M., and Arber, S. (2002). ETS gene Pea3 controls the central position and terminal arborization of specific motor neuron pools. Neuron *35*, 877–892.

McAllister, A.K. (2007). Dynamic aspects of CNS synapse formation. Annu. Rev. Neurosci. *30*, 425–450.

Mo, Y., Vaessen, B., Johnston, K., and Marmorstein, R. (1998). Structures of SAP-1 bound to DNA targets from the E74 and c-fos promoters: insights into DNA sequence discrimination by Ets proteins. Mol. Cell *2*, 201–212.

Moss, S.J., Beeson, D.M., Jackson, J.F., Darlison, M.G., and Barnard, E.A. (1987). Differential expression of nicotinic acetylcholine receptor genes in innervated and denervated chicken muscle. EMBO J. *6*, 3917–3921.

Nazarian, J., Bouri, K., and Hoffman, E.P. (2005). Intracellular expression profiling by laser capture microdissection: three novel components of the neuromuscular junction. Physiol. Genomics *21*, 70–80.

Nichols, P., Croxen, R., Vincent, A., Rutter, R., Hutchinson, M., Newsom-Davis, J., and Beeson, D. (1999). Mutation of the acetylcholine receptor epsilon-subunit promoter in congenital myasthenic syndrome. Ann. Neurol. *45*, 439–443.

O'Leary, D.A., Noakes, P.G., Lavidis, N.A., Kola, I., Hertzog, P.J., and Ristevski, S. (2007). Targeting of the ETS factor GABPalpha disrupts neuromuscular junction synaptic function. Mol. Cell. Biol. *27*, 3470–3480.

Ohno, K., Anlar, B., and Engel, A.G. (1999). Congenital myasthenic syndrome caused by a mutation in the Ets-binding site of the promoter region of the acetylcholine receptor epsilon subunit gene. Neuromuscul. Disord. *9*, 131–135.

Pang, Y.W., Li, J.L., Nakamura, K., Wu, S., Kaneko, T., and Mizuno, N. (2006). Expression of vesicular glutamate transporter 1 immunoreactivity in peripheral and central endings of trigeminal mesencephalic nucleus neurons in the rat. J. Comp. Neurol. *498*, 129–141.

Pun, S., Sigrist, M., Santos, A.F., Ruegg, M.A., Sanes, J.R., Jessell, T.M., Arber, S., and Caroni, P. (2002). An intrinsic distinction in neuromuscular junction assembly and maintenance in different skeletal muscles. Neuron *34*, 357–370.

Rosmarin, A.G., Resendes, K.K., Yang, Z., McMillan, J.N., and Fleming, S.L. (2004). GA-binding protein transcription factor: a review of GABP as an integrator of intracellular signaling and protein-protein interactions. Blood Cells Mol. Dis. *32*, 143–154.

Sander, A., Hesser, B.A., and Witzemann, V. (2001). MuSK induces in vivo acetylcholine receptor clusters in a ligand-independent manner. J. Cell Biol. *155*, 1287–1296.

Sanes, J.R., and Lichtman, J.W. (2001). Induction, assembly, maturation and maintenance of a postsynaptic apparatus. Nat. Rev. Neurosci. *2*, 791–805.

Schaeffer, L., de Kerchove d'Exaerde, A., and Changeux, J.P. (2001). Targeting transcription to the neuromuscular synapse. Neuron *31*, 15–22.

Schaeffer, L., Duclert, N., Huchet-Dymanus, M., and Changeux, J.P. (1998). Implication of a multisubunit Ets-related transcription factor in synaptic expression of the nicotinic acetylcholine receptor. EMBO J. *17*, 3078–3090.

Sharrocks, A.D. (2001). The ETS-domain transcription factor family. Nat. Rev. Mol. Cell Biol. *2*, 827–837.

Simon, A.M., and Burden, S.J. (1993). An E box mediates activation and repression of the acetylcholine receptor delta-subunit gene during myogenesis. Mol. Cell. Biol. *13*, 5133–5140.

Sutton, M.A., and Schuman, E.M. (2006). Dendritic protein synthesis, synaptic plasticity, and memory. Cell *127*, 49–58.

Valenzuela, D.M., Stitt, T.N., DiStefano, P.S., Rojas, E., Mattsson, K., Compton, D.L., Nunez, L., Park, J.S., Stark, J.L., Gies, D.R., et al. (1995). Receptor tyrosine kinase specific for the skeletal muscle lineage: expression in embryonic muscle, at the neuromuscular junction, and after injury. Neuron *15*, 573–584.

Vrieseling, E., and Arber, S. (2006). Target-induced transcriptional control of dendritic patterning and connectivity in motor neurons by the ETS gene Pea3. Cell *127*, 1439–1452.

Wichterle, H., Lieberam, I., Porter, J.A., and Jessell, T.M. (2002). Directed differentiation of embryonic stem cells into motor neurons. Cell *110*, 385–397.

Witzemann, V., Brenner, H.R., and Sakmann, B. (1991). Neural factors regulate AChR subunit mRNAs at rat neuromuscular synapses. J. Cell Biol. *114*, 125–141.

Yang, X., Arber, S., William, C., Li, L., Tanabe, Y., Jessell, T.M., Birchmeier, C., and Burden, S.J. (2001). Patterning of muscle acetylcholine receptor gene expression in the absence of motor innervation. Neuron *30*, 399–410.

Curriculum Vitae

Personal Information

Last Name:	Huber
First Name:	Roland Martin
Address:	Meltingerstrasse 3, Basel CH-4053, Switzerland
Phone:	+41 79 357 10 14
e-mail:	roland.huber@fmi.ch
Nationality:	Swiss
Date of Birth:	25.03.1981
Marital Status:	unmarried
Military:	Captain, Company Commander

Education

01/87-11/87	Grammar School Greensboro (NC, USA)
12/87-07/94	Grammar School Hochwald
08/94-07/97	Bezirksschule Büren
08/97-12/00	Gymnasium Münchenstein, Matura

University Studies

10/02-09/05	Bachelor of Science, Major in Molecular Biology; University of Basel
10/05-10/06	Master of Science, Major in Neurobiology; University of Basel
11/06- 06/11	Philosophical Doctor, Major in Cell Biology; University of Basel

Research Experience:

- Experimental MSc thesis and continuing research on the neuro-muscular junction and the *Erm* transcription factor in NMJ maturation in the laboratory of Prof. S. Arber at the Biozentrum, University of Basel and at the Friedrich Miescher Institute (FMI, Basel); 2005 – 2007

- Experimental PhD thesis on *Deltex-1* function in glioblastoma multiforme in the laboratory of molecular neuro-oncology of Prof. A. Merlo, University of Basel; 2008 – 2010

- Experimental PhD Thesis and continuing postdoctoral research on an orthotopic *in vivo* model of glioblastoma multiforme in the laboratory of Dr. B.A. Hemmings, FMI, Basel; 2011 – present

Publications

- Simon Hippenmeyer*, **Roland M. Huber***, David R. Ladle, Kenneth Murphy, and Silvia Arber. (2007) *ETS transcription factor Erm controls subsynaptic gene expression in skeletal muscle.* Neuron 55 (5), 726-740.
  **These authors contributed equally to this work.*

- Serdar Korur, **Roland M. Huber**, Balasubramanian Sivasankaran, Michael Petrich, Pier Morin Jr, Brian A. Hemmings, Adrian Merlo and Maria Maddalena Lino. (2009) *GSK3β Regulates Differentiation and Growth Arrest in Glioblastoma.* PLoS ONE 4(10): e7443. doi:10.1371/journal.pone.0007443

- Jan Tchorz, Dimitri Cloetta, Mercedes Tome, Balasubramanian Sivasankaran, Michal Grzmil, **Roland M. Huber**, Frank Kirchhoff, Nicole Schaeren-Wiemers, Martin Gassmann, Brian A. Hemmings, Adrian Merlo and Bernhard Bettler. (2011) *Notch2 Signaling in Neural Stem Cells Promotes Features of Glioma Stem.* submitted.

- **Roland M. Huber**, Balasubramanian Sivasankaran, Michal Rajski, Brian A. Hemmings, Maria Maddalena Lino, Adrian Merlo. (2011) *The alternative Notch pathway via Deltex-1 is an oncogenic factor in malignant glioma.* In Preparation.

Fellowships and Awards

- Boehringer Ingelheim PhD Scholarship (personal grant for 24 months)
  2007 – 2009 (grant gratefully declined)

Teaching Experience

- Undergraduate teaching in general biology in their 1st semester, University of Basel, 2009

- Undergraduate teaching in neurobiology, lab course and lectures for 5th and 6th semester students, University of Basel, 2007-2008

- Technical supervision of an experimental MD thesis in molecular oncology, University of Basel, 2009-2011

Additional Education in Animal Experimentation

- Education and Training as “Expert Carrying out Animal Experiments”; 2005 and 2007 (equivalent to the FELASA category B)

- Education and Training as “Director of Animal Experiments”; 2009 (equivalent to the FELASA category C)

Language Skills

German:	native language
English:	fluent
French:	fair